Investigating mechanisms of anti-cancer drug resistance in breast cancer cells and extracellular vesicles

A thesis submitted to the University of Dublin, Trinity College

towards a degree of Doctor of Philosophy

January 2019

Michelle C. Lowry, M.Sc.

Based on research carried out under supervision of

Prof. Lorraine O'Driscoll

School of Pharmacy & Pharmaceutical Sciences,

Trinity Biomedical Sciences Institute,

Trinity College Dublin.

Trinity College Dublin
Coláiste na Tríonóide, Baile Átha Cliath
The University of Dublin

Declaration

I declare that this thesis has not been submitted as an exercise for a degree at this or any other university and it is entirely my own work, unless where otherwise indicated. I agree to deposit this thesis in the University's open access institutional repository or allow the Library to do so on my behalf, subject to Irish Copyright Legislation and Trinity College Library conditions of use and acknowledgement.

Signed: _____

Acknowledgments

Firstly, I wish to thank my supervisor, Prof. Lorraine O'Driscoll. Thank you for giving me the opportunity to do this PhD. Thank you for encouraging me to present my research at conferences and to apply for grants and awards throughout my PhD. I have learned so much from a great team of scientists, so thank you Vanesa, Susan, Sadhbh and Melissa. A special thank you to Vanesa, you are the most intelligent and the most fantastic scientist I know. Thankfully, I get to call you a very good friend too, thanks for always checking in on me and looking out for me during my PhD. Thank you to Niamh and Delva, I've loved getting to know you both. Thank you for asking all the questions, it's been an absolute pleasure to show you the ropes in the lab, not that you needed much help in that respect. You are both extremely intelligent, I have no doubt that you will both complete fantastic PhDs.

To Caoimhe and Mohammed, we all started at the same time and the office has not been the same since you left. I know you will both have fantastic careers in the future. To Nadhim, a true friend right from the start. Thanks for all the laughs and I will even thank you for all the frights that you gave me in the last year too. To Maria, thank you for always looking after us all in the office and in the lab too. You are the best teacher and its been a pleasure getting to know you. I wish you all the best in your career and I will seriously miss your tiramisu skills.

Thank you to the Department of Surgery, especially to Jacintha. You have been a mentor to me before I even started my PhD and you continued to be one even during it. Your lab is a fantastic place to work; it has always been so welcoming and supportive. I wish you and all the Surgery gang all the best in the future and I appreciate all your help and for kick-starting my research career.

To everyone in BREAST-PREDICT, thank you for being an exceptional group to work with. Special thank you to Amelia, you've been the best friend to have during a PhD, thanks for all the fun and always being right next to me in all the stressful situations. Special thanks to Michelle C too, you always lightened the mood and kept us smiling and laughing! Thank you to the Irish Cancer Society for funding such an amazing program. Firstly, thank you for giving me the opportunity to go to media training, for giving me the opportunity to present my research to everyone and for allowing me to get involved in outreach work. The outreach work made my PhD so fulfilling. To the current Irish Cancer Society research team (Rob, Claire, Rachel, Chris, Zita and Michael), thank you for your

trust, your patience and your advice in the final few months of my PhD. I have thoroughly enjoyed working with you all. To Bella, thank you wholeheartedly for being a mentor to me. You gave me the best advice, you gave me confidence when I needed it, gave me the opportunity to present my research to the public and to patients. All of which were invaluable and I greatly appreciate all the support you've given me. To all the members of the public and especially to all the patients that I have met along the way, thank you! Thank you for being so strong and thank you for sharing your stories with me. I have learned more from you than I ever could in a book or journal.

To Ita and Siobhan, thank you for always being there for me (in everything, not just in terms of my PhD). You have no idea how thankful I am to you both for being so patient when I spent too much time away from home. To the immuno gang, I am very grateful that we always meet up and still keep in touch, especially to Deborah, Grace and Jay. You are the best friends, the best gang for a laugh and a great support group.

To Aileen, thank you for being my rock. You were right beside me when I was offered this PhD and you have always been right there next to me ever since. Thanks for always listening to my rants, for having my back, for taking my mind off the PhD, for always cheering me up and for always knowing when I need a hug. I couldn't have done it without you.

Finally, to my family, to Amanda and James, I always know I can rely on you both no matter what. Thank you for always being there for me when I needed you both, especially for the weekends of catch ups and for always looking after the "forever" student of the family. To my parents, Jim and Mary. I owe you both the biggest thank you.Thank you for always being there for me, at every single step of the way. Thank you for always encouraging me even when I kept telling you I was going back to college for another degree. Thank you for pushing me to do my best and for always supporting me in my education, my career and in life in general. I would not have been able to do any of it without having you both by my side, you have encouraged me every step of the way. For that, I am forever grateful.

Table of Contents

Table of Figures

List of Tables

Summary

In Ireland, breast cancer is the most commonly diagnosed cancer in women. Breast cancer accounts for approximately 3,141 cases each year. Of which, 15-25% of breast cancers are HER2-overexpressing. HER2-overexpressing breast cancers are typically characterised by high levels of cell proliferation, high grade, lymph node involvement and metastasis to distant organs. There are many HER2-targeted treatment options. Trastuzumab has dramatically changed response rates and progression-free survival in metastatic HER2+ breast cancer. In the adjuvant setting, disease-free survival and overall survival are also improved. Innate resistance, acquired resistance (*de-novo*) and cross-resistance to anticancer therapies are the main reasons that anti-cancer drugs fail in the clinic. It is imperative that we investigate the mechanisms of drug resistance, find ways to overcome this resistance and find predictive and/or prognostic biomarkers for breast cancer treatments.

The focus of this project is neratinib. Neratinib is a small tyrosine kinase inhibitor that irreversibly binds to EGFR (HER1), HER2 and HER4, thus preventing HER2 dimerisation and therefore preventing HER2-mediated signalling. Neratinib was approved for extended adjuvant treatment of early stage HER2-positive breast cancer by the Food and Drug Administration (FDA) in July 2017. Neratinib is showing promise in the clinic but, like most therapies, the issue of resistance prevails.

Using our novel neratinib-resistant cell line variants, we have identified CAIX as playing a role in acquired neratinib-resistance. In both normoxic and hypoxic conditions, using ELISAs, CAIX levels were found to be increased in neratinib-resistant cell line variants compared to neratinib-sensitive cell line variants. Similarly, when investigating other HER2-targeted drug-resistant cell line variants (lapatinib-resistant, trastuzumab-resistant and trastuzumab- and lapatinib-resistant), the CAIX levels were increased in all drug-resistant cell line variants (except the HCC1954-NR cell line variant) compared to drug-sensitive cell line variants. We sought to re-sensitise the neratinib-resistant cell line variants to neratinib by using a sulfamate small molecule CAIX inhibitor, S4. Using immunoblots and ELISAs, CAIX was found to be initially inhibited in cell line variants using this inhibitor. However, overtime, unlike the drug-sensitive cell line variants (in which CAIX was continuously inhibited by S4), the neratinib-resistant cell line variants

had the ability to overcome the inhibitory effects, this effect correlated with increasing neratinib-resistance. Using acid phosphatase assays and Compusyn software, the combination treatment of the sulfamate CAIX inhibitor with neratinib was found to be synergistic in all neratinib-resistant cell lines. The level of synergy for the combination therapy directly correlated with increased neratinib-resistance *i.e.* the neratinib-resistant cell line variants with the highest levels of resistance responded better to the combination of S4 with neratinib than the cell line variants with lower levels of neratinib-resistance. Although S4 originally blocked CAIX expression in other HER2-targeted therapy-resistant cell line variants (lapatinib-resistant, trastuzumab-resistant and lapatinib plus trastuzumab-resistant), synergism did not result from the combination of S4 with lapatinib or TDM-1.

The discovery of predictive biomarkers is essential to improving personalised medicine for all cancer patients. EVs are described as mini-maps of their cell-of-origin. EV-cargo from cancer cells can contain DNA, RNA, miRNAs and proteins associated with cancer. They may provide a minimally-invasive liquid biopsy analytical tool. Thus, we isolated EVs from plasma specimens from the TCHL neo-adjuvant clinical trial to determine the potential of EVs to carry CAIX and their potential use as predictive biomarkers for HER2-targeted therapies. CAIX was investigated on both the surface of EVs and encapsulated inside the EVs by ELISA. EV-surface CAIX was only detectable in 25% and 42% of pre- and post-treatment samples. It was therefore deemed that EV-surface CAIX was not a reliable test for detecting CAIX. This may in part be due to CAIX being degraded/destroyed during the EV isolation process of ultracentrifugation. It was determined that investigating CAIX levels encapsulated inside the EVs was an improved method for detecting EV-derived CAIX (CAIX was undetected in 4% of pre-treatment samples and 25% of all post-treatment samples). However, CAIX was not detectable in all samples. The method of ultracentrifugation was deemed unsuitable for EV-derived CAIX analysis, this may be due to the force of the ultracentrifugation steps or degradation of CAIX due to the length of time required to complete the isolation steps. Next, we aimed to investigate the potential of CAIX in raw plasma specimens as a predictive biomarker for resistance to HER2-targeted therapy. We used ELISAs to test the raw plasma specimens from this neo-adjuvant clinical trial to investigate if the levels of CAIX in plasma specimens correlated with response to therapies. CAIX was found to be significantly increased in plasma specimens from HER2+ breast cancer patients that had no response to therapy compared to those who experiences a complete response or partial response.

To conclude, our results suggest that CAIX plays a role in the mechanism of neratinib-resistance. We have evidence to suggest that the combination of S4 with neratinib may overcome this resistance in HER2+ breast cancer cell lines. CAIX levels are elevated in HER2-targeted drug-resistant cell line variants. We clinically validated our findings in plasma specimens from patient's who did not respond to HER2-targeted therapies. The results highlighted in this PhD project are promising for overcoming neratinib-resistance in the future. This work sets a premise for future pre-clinical breast cancer models such as *in vivo* models to investigate the efficacy of S4 with neratinib for overcoming neratinib-resistance. Associated with further trials with neratinib, investigating the levels of CAIX in patient's plasma specimens is warranted to further investigate the potential of CAIX as a predictive biomarker for neratinib.

Abbreviations

4E-BP1	Eukaryotic translation initiation factor 4E-binding protein 1
5’NT	5'-nucleotidase
ABL1	Tyrosine-protein kinase ABL1
ADA	Adenosine Deaminase
ADAM-TS 15	A disintegrin and metalloproteinase with thrombospondin motifs 15.
ADC	Antibody-drug conjugate
Adr	Adriamycin
AKT	Protein kinase B
ALIX	Apoptosis-linked gene-2-interacting protein X
ALK	Anaplastic lymphoma kinase
ALTTO	Adjuvant Lapatinib and/or Trastuzumab Treatment Optimisation
ANGPTL4	Angiopoietin-like 4
ANXA1	Annexin A1
APC	Annexin-V-allophycocyanin
AR	Amphiregulin
ARTN	Artemin
AXIN1	Axin-1
BCA	Bicinchoninic acid assay
BDNF	Brain-derived neurotrophic factor
Beta-NGF	Beta-nerve growth factor binding buffer (BB).
BL1	Basal-like 1
BRAF	Proto-oncogene B-Raf
BSA	Bovine serum albumin
CAIX	Carbonic anhydrase IX
CASP-8	Caspase-8
CCL11	Eotaxin-1
CCL19	C-C motif chemokine 19
CD207	C-type lectin domain family 4 member K
CD244	Natural killer cell receptor 2B4
CD5	T-cell surface glycoprotein CD5
CD6	T cell surface glycoprotein CD6 isoform
CDCP1	CUB domain-containing protein 1
CDK4	Cyclin-dependent kinase 4

CDKN1A	Cyclin-dependent kinase inhibitor 1
CDKN1B	Cyclin-dependent kinase inhibitor 1B
cDNA	Complementary DNA
CEA	Carcinoembryonic antigen
CEACAM1	Carcinoembryonic antigen-related cell adhesion molecule 1
CM	Conditioned media
CPE	Carboxypeptidase E
CR	Complete response
CRNN	Cornulin
CSF-1	Macrophage colony-stimulating factor-1
CST5	Cystatin D
CT	Cycle threshold
ctDNA.	Circulating tumour DNA
CTSV	Cathepsin L2
CTNNB1	Catenin beta-1
CX3CL1	Fractalkine
CXCL1	C-X-C motif chemokine 1
CXL17	VEGF-co regulated chemokine 1
CYP3A4	Cytochrome P450 3A4
DDR2	Discoidin domain receptor 2
dFBS	EV-depleted-FBS
DFO	Deferoxamine mesylate
DFS	Disease-free survival
DLK1	Delta like non-canonical notch ligand 1
DLL1	Delta-like protein 1
DM	Distant metastases
DMEM	Dulbecco’s Modified Eagles Medium
DMOG	Dimethyloxalylglycine
DNA	Deoxyribonucleic acid
dNTP	Deoxyribonucleotide triphosphate
Doc	Docetaxel
dsDNA	Double-stranded DNA
DSS	Disease-specific survival
ECM	Extracellular matrix
EGF	Pro-epidermal growth factor

EGFR/HER1	Epidermal growth factor receptor 1
ELISA	Enzyme-linked immunosorbent assay
EMA	European Medicines Agency
EMT	Epithelial–mesenchymal transition
EPHA2	Ephrin type-A receptor 2
ER	Estrogen-receptor
ERBB2	Erythroblastic oncogene B 2
ERK	Extracellular signal-regulated kinase
ERK	Extracellular Signal-Regulated Kinases
ESCRT	Endosomal sorting complex required for transport
ESM-1	Endothelial cell-specific molecule 1
EVs	Extracellular vesicles
FADD	FAS-associated death domain protein
FasL	Fas antigen ligand
FBS	Fetal bovine serum
FBXO4	Human F box only protein 4
FBXW7	F-box and WD repeat domain-containing 7
FCRLB	Fc receptor-like B
FDA	Food and Drug Administration
FGF-19	Fibroblast growth factor 19
FGF-BP1	Fibroblast growth factor-binding protein 1
FGFR1	Fibroblast growth factor receptor 1
Flt3L	Fms-related tyrosine kinase 3 ligand
FR-alpha	Folate receptor alpha
FUR	Furin
Gal-1	Galectin-1
GDNF	Glial cell line-derived neurotrophic factor
GNAQ	Guanine nucleotide-binding protein G(q) subunit alpha
GPC1	Glypican-1
GPNMB	Transmembrane glycoprotein NMB
GRP94	Glucose-regulated protein 94
GZMB	Granzyme B
HB-EGF	Heparin-binding EGF-like growth factor
HDAC1	Histone deacetylase 1
HER2	Human epidermal growth factor

HGF	Hepatocyte growth factor
HIFs	Hypoxia inducible factors
hK11	Kallikrein-11
HRAS	Transforming protein p21
IC_{50}	The half maximal inhibitory concentration
ICORG	All-Ireland Cooperative Oncology Research Group
ICOSLG	ICOS ligand
IDH1	Isocitrate dehydrogenase 1
IFN-gamma	Interferon gamma
IGF1R	Insulin-like growth factor 1 receptor
IL-8	Interleukin 8
ILVs	Intraluminal vesicles
IM	Immunomodulatory
ITGAV	Integrin alpha-V
ITGB5	Integrin beta-5
LAR	Luminal androgen receptor
LIF	Leukemia inhibitory factor
LIF-R	Leukemia inhibitory factor receptor
LN-	Lymph node negative
LR	Lapatinib-resistant
LRR	Loco-regional recurrence
LTBP1	Latency-associated peptide transforming growth factor beta-1
LY9	T-lymphocyte surface antigen Ly-9
LYN	Tyrosine-protein kinase Lyn
LYPD3	Ly6/PLAUR domain-containing protein 3
M	Mesenchymal-like
MAD homolog 5	Mothers against decapentaplegic homolog 5
MALDI-TOF	Matrix Assisted Laser Desorption/Ionization
MAP2K1	Mitogen-activated protein kinase kinase 1
MAPK	Mitogen-activated protein kinase
MCP-1	Monocyte chemotactic protein 1
MEG3	Maternally expressed 3
MetAP2	Methionine aminopeptidase 2
MIA	Melanoma-derived growth regulatory protein
MIC-A/B	MHC class I polypeptide-related sequence A/B

miR-630	microRNA 630
MK	Midkine
MLH1	MutL homolog 1
MMP-9	Matrix metallopeptidase 9
NmU	Neuromedin U
MS	Mass spectrometry
MSL	Mesenchymal stem-like
MSLN	Mesothelin
MUC-16	Mucin-16
MVEs	Multivesicular endosomes
MVs	Microvesicles
NC	Negative control
NCOR1	Human Nuclear receptor corepressor 1
ncRNA	Non-coding RNA
NF-κB	Nuclear factor kappa-light-chain-enhancer of activated B cells
NoR	No response
NPX	Normalised protein expression
NR	Neratinib-resistant
NRAS	Neuroblastoma ras viral oncogene homolog
NRTN	Neurturin
NT-3	Neurotrophin-3
NTA	Nanoparticle tracking analysis
OPG	Osteoprotegerin
OS	Overall survival
OSM	Oncostatin-M
PAMPs	Pathogen-associated molecule patterns
PBS	Phosphate buffered saline
PBST	PBS/0.01 % Tween 20
PCR	Polymerase chain reaction
PDGFRA	Platelet-derived growth factor receptor A
PD-L1	Programmed death-ligand 1
PDX	Patient-derived xenografts
PEA	Proximity extension assay
PFS	Progression-free survival
PGE2	Prostaglandin E2

P-gp	P-glycoprotein
PHLPP2	PH domain leucine-rich repeat protein phosphatase 2
PI	Propodium iodide
PI3K	Phosphoinositide 3-kinase
PODXL	Podocalyxin
Poly (I:C)	Polyinosinic:polycytidylic acid
PPY	Pancreatic prohormone
PR	Partial response
PR	Progesterone receptor
PTEN	Phosphatase and tensin homolog
PTPN11	Protein-tyrosine phosphatase Shp2
PVDF	Polyvinylindene fluoride
PVRL4	Nectin-4
Q8NFT8	Delta and Notch-like epidermal growth factor-related receptor
qRT-PCR	Quantitative real-time polymerase chain reaction
Rab	Ras-associated binding
RB1	Retinoblastoma protein 1
RET	Proto-oncogene tyrosine-protein kinase receptor Ret
RNA	Ribonucleic acid
RNAi	RNA interference
RPMI	Roswell Park Memorial Institute medium
RSPO3	R-spondin-3
S100A11	S100 Ca2+-binding protein A1
SAP	Shrimp alkaline phosphatase
SCAMP3	Secretory carrier-associated membrane protein 3
SCF	Stem cell factor
SDS-PAGE	Sodium Dodecyl Sulfate PolyAcrylamide Gel Electrophoresis
SEM	Standard error of the mean
SEZ6L	Seizure 6-like protein
siRNA	Short interfering RNA
SIRT2	SIR2-like protein 2
SLAMF1	Signaling lymphocytic activation molecule
SOS1	Son of Sevenless 1
SPARC	Secreted protein acidic and rich in cysteine
ST1A1	Sulfotransferase 1A1

STAMBP	STAM-binding protein
STK11	Serine/threonine-protein kinase 11
SYND1`	Syndecan-1
TAMs	Tumour-associated macrophages
TANCE	TNF-related activation-induced cytokine
TBST	Tris-buffered saline with tween 20
TBX3	T-box transcription factor 3
TCH	Docetaxel, Carboplatin and Trastuzumab
TCHL	Docetaxel, Carboplatin, Trastuzumab and Lapatinib
TCL	Docetaxel, carboplatin and lapatinib
TCL1A	T-cell leukemia / lymphoma protein 1A
TEM	Transmission electron microscopy .
TF	Tissue factor
TFPI2	Tissue factor pathway inhibitor 2
TGF-alpha	Transforming growth factor alpha
TGFR-2	Transforming growth factor-beta receptor type-2
TGF-β	Transforming growth factor-Beta
TKI	Tyrosine kinase inhibitor
TLR	Trastuzumab and lapatinib-resistant
TLR3	Toll-like receptor 3
TMA	Tissue microarray
TNBC	Triple-negative breast cancer
TNFB	Tumour necrosis factor-beta
TNFSF14	Tumour necrosis factor ligand superfamily member 14
TP53	Tumour protein 53
TR	Trastuzumab-resistant
TRAIL	TNF-related apoptosis-inducing ligand
TSG101	Tumour susceptibility gene 101
TSLP	Thymic stromal lymphopoietin
TWEAK	Tumour necrosis factor (Ligand) superfamily, member 12
TXLNA	Alpha-taxilin
uPA	Urokinase-type plasminogen activator
VEGF	Vascular endothelial growth factor
VHL	Von Hippel–Lindau
VIM	Vimentin

WFDC2	WAP four-disulfide core domain protein 2
WHO	World Health Organisation
WIF-1	Wnt inhibitory factor 1
WISP-1	WNT1-inducible-signaling pathway protein 1
Wnt	Wingless/Integrated
XONPEP2	Xaa-Pro aminopeptidase 2

CHAPTER ONE: Introduction

Parts of this chapter are published in the following review articles:

- The Role of Exosomes in Breast Cancer. Lowry M.C, Gallagher W.M, O'Driscoll L Clinical Chemistry. 2015 Dec;61(12):1457-65.
- Can hi-jacking hypoxia inhibit extracellular vesicles in cancer. Lowry MC, O'Driscoll L. Drug Discovery Today. 2018 Jun;23(6):1267-1273.

1. Introduction

1.1. Hallmarks of cancer

Cancer is a highly heterogeneous disease. Cancer is not just one disease, but a multitude of diseases (over 200 types of cancer) that can affect any part of the body. In 2018 alone, the World Health Organisation (WHO) estimates that 9.6 million people worldwide are estimated to die from cancer (https://www.who.int/cancer/en/).

Hanahan and Weinberg proposed that there were 6 hallmarks of cancer; evading apoptosis, sustained angiogenesis, tissue invasion and metastasis, limitless replicative potential, self-sufficiency in growth signals and insensitivity to anti-growth signals (1). Later they noted that cancer was not just composed of proliferating cancer cells but complex tissues composing of many distinct types of cells all interacting together (2). With this complexity came the emergence of newer hallmarks; deregulating cellular energetics, genome instability and mutation, avoiding immune destruction and tumour-promoting inflammation (2).

1.2. Breast cancer

1.2.1. Breast cancer statistics

Despite the screening programs, early diagnosis and the availability of many treatments, breast cancer is still a major health problem in Ireland and worldwide. According to the National Cancer Registry Ireland (www.ncri.ie, statistics correct as of 3rd November 2018), after non-melanoma skin cancer, in Ireland, breast cancer is the most common cancer diagnosed in women and the second most common cause of cancer deaths. The annual percent change (from 2015-2017) for all cancers in men and women was -2% and -0.1%, respectively. On average there are 22,321 new cancer cases per year, with female breast cancer accounting for 3,141 (3,141 invasive and 375 *in situ* diagnoses) of all cancer cases. Female breast cancer accounts for 709 deaths per year, with an 83.1% 5-year net survival rate (statistics from 2009-2013). Of note, breast cancer is not restricted to the female population, with approximately 1% of these cancers occurring in males.

Primary breast tumours typically do not kill; this occurs due to cancer spread/metastasis to secondary sites in the body. In fact, the 5-year survival rate for localised breast cancer is

99.4%, 86.4% for regional stage (nearby lymph nodes) and 27.9% for metastases (distant organs and lymph nodes) (3).

1.2.2. Breast cancer subtypes

Breast cancer is a highly heterogeneous disease. The identification of the cellular and molecular tumour signatures is fundamental for advancing the area of targeted personalised medicine and, therefore, improving clinical outcome from this disease. Breast cancer classification can be performed based on the presence or absence of extracellular receptors, such as the hormone receptors estrogen-receptor (ER), progesterone receptor (PR) and human epidermal growth factor (HER2). These hormone receptors play a role in the development and progression of breast cancer. In 2000, Perou *et al.* (4) made a fundamental contribution to defining breast cancer sub-classifications, using DNA microarrays. From this, hierarchal clustering analysis revealed various sub-types based on the gene expression patterns *i.e.* basal-like (mostly classified as triple-negative breast cancer (TNBC)), although basal-like and TNBC are not synonymous (5), HER2/neu-overexpressing, normal-like and luminal epithelial/ER. Subsequent to this study, the luminal sub-class was further sub-divided to luminal A and luminal B. All subtypes are summarised in Table 1.1.

Subgroup	**Associated Molecular Signature**	**4-year survival rate (6)**
Luminal A	ER^+ and/or PR^+, HER2-, low Ki67	92.5%
Luminal B	ER^+ and/or PR^+, $HER2^+$ (or HER2- with high Ki67)	90.3%
$HER2^+$	ER-, PR-, $HER2^+$	82.7%
*Basal-like/TNBC***	ER-, PR-, HER2-	77.0%
Claudin-low	ER-, PR-, HER2-, low expression of E-cadherin	-

Table 1.1: Breast cancer subtypes and molecular signatures
* 4 year overall survival rates (6). **Basal-like is mostly classified as TNBC, although basal-like and TNBC are not synonymous.

1.2.3. Breast cancer disease management

Breast cancer is conventionally diagnosed by mammography (but for middle-aged women only), magnetic resonance imaging and breast biopsies. Blood-based biomarkers (protein, DNA, RNA, miRNAs and circulating tumour cells) are currently being investigated in breast cancer. Genomic and proteomic testing of tissue have been developed in breast cancer, MammaPrint assays and Oncotype DX test. MammaPrint predicts early risk of metastastis by investigating 70 genes associated with breast cancer invasion, metastasis, invasion and angiogenesis (7). Oncotype DX determines the rescurrence score by investigating the RNA from tumour tissue. It uses qRT-PCR to investigate mRNA transcribed by five reference genes and 16-related genes (7). Using Onctoype DX, the Trial Assigning Individualised Options for Treatment (Rx) (TAILORx) trial found no benefit of chemotherapy for early stage breast cancer patients (n=10,273) with hormone receptor-positive, HER2-negative and lymph node-negative breast cancer (8).

The main treatment types for breast cancer are surgery, radiation therapy, chemotherapy, hormone therapy and targeted therapy. In Ireland (2013-2015), within one year of diagnosis 68% of cases receive radiation therapy, 54% receive hormone therapy, 45% receive chemotherapy and 82% have breast cancer surgery (www.ncri.ie).

1.2.4. Current breast cancer treatments

Without treatment being considered, the poorest breast cancer survival rates have been associated with basal-like and HER2-overexpressing tumours (9, 10). Due to its heterogeneous nature and different stages of diagnosis from individual-to-individual, breast cancer treatment typically involves multimodality approaches with surgery, chemotherapy, radiation therapy, hormone therapy and other newer targeted treatments, including monoclonal antibodies, small molecules and antibody-drug conjugates. The current targeted treatments for breast cancer patients include those summarised in Table 1.2. However, several of these patients (~20-30%) will relapse despite targeted therapies and optimal adjuvant therapies.

Target	**Monoclonal Antibody**	**Small molecule inhibitor**
HER2 inhibitors	Trastuzumab Pertuzumab T-DM1 MM-111	Lapatinib Neratinib Afatinib
ER^+/PR^+ treatments	MM-121/SAR256212	Tamoxifen Aromatase inhibitors Fulvestrant Cabozantinib
TNBC treatment	Cetuximab	PARP inhibitors Anti-Hsp90 compounds

Table 1.2: Current breast cancer targeted therapies

1.2.5. HER2+ Breast Cancer

Human epidermal growth factor (HER/ErbB) tyrosine kinase family consists of HER1 (Epidermal growth factor receptor 1 (EGFR)), HER2, HER3 and HER4. They comprise of transmembrane, intracellular and extracellular membranes. Activation of HER family kinases comes about by homo- or heterodimerisation resulting from ligand binding, receptor mutations or overexpression of receptors. Dimerisation results in downstream signalling through phosphoinositide 3-kinase (PI3K) and the mitogen-activated protein kinase (MAPK) pathways (Figure 1.1). HER2 is a receptor tyrosine kinase with no known ligand. HER2 is amplified in 15-25% of breast cancer cases, however, normal tissues express low levels of HER2. HER2 overexpressing breast cancers are characterised by high levels of cell proliferation, high grade, lymph node involvement and metastasis to distant organs (4). In 1998, the monoclonal antibody, trastuzumab, was developed for the treatment of HER2+ metastatic breast cancer (11). Trastuzumab has dramatically changed response rates and progression-free survival in metastatic disease. In the adjuvant setting, disease-free survival and overall survival were also improved (12). Innate resistance, acquired resistance and cross-resistance to anticancer therapies are the main reasons that anti-cancer drugs fail in the clinic (13). Continued efforts to decipher the mechanism(s) of resistance are necessary to predict and circumvent this problem. Other HER2 targeting agents have been developed such as lapatinib, pertuzumab, T-DM1 and neratinib.

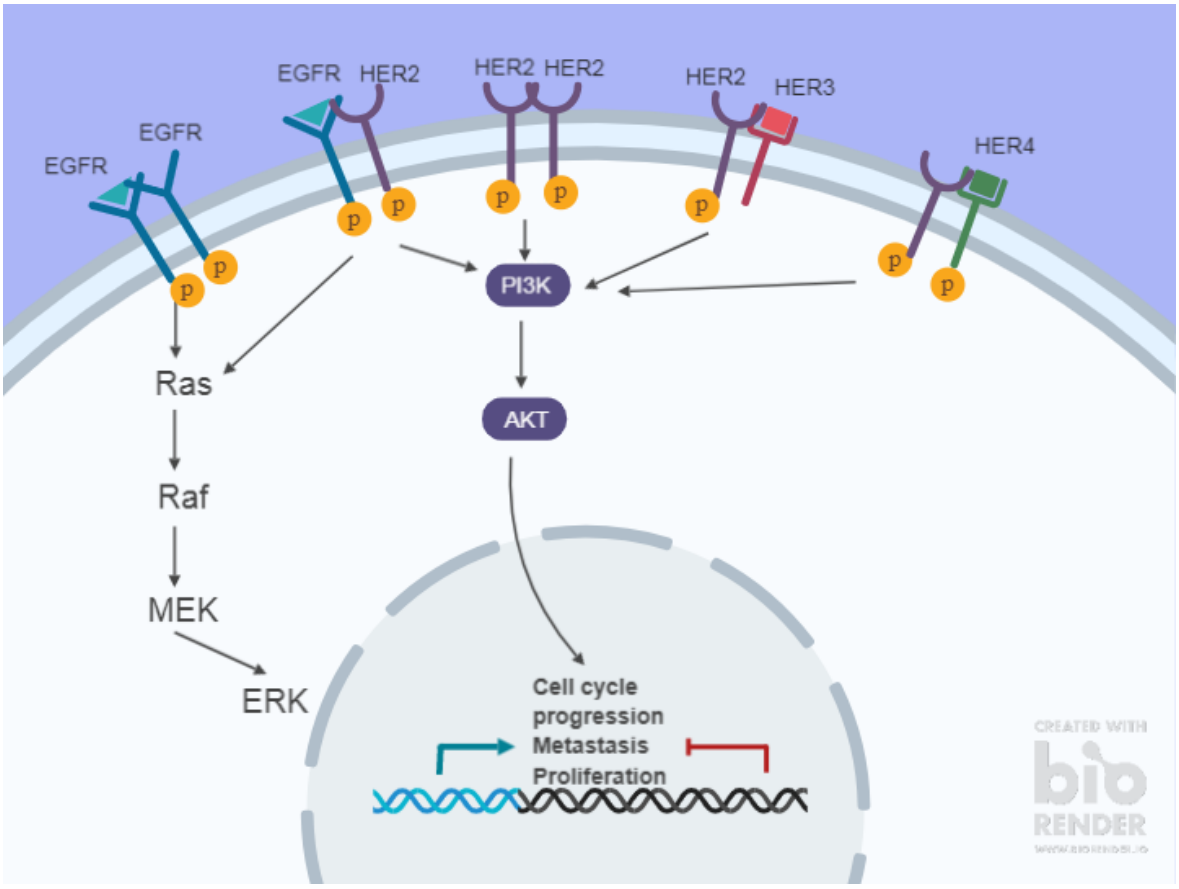

Figure 1.1 HER2 signalling pathway
HER2 signalling through homo- and heterodimerisation with other HER family members. Dimerisation and subsequent phosphorylation leads to activation of the HER2 signalling pathways (PI3K/AKT and RAF/MEK/MAPK). Activation of the PI3K/AKT and RAF/MEK/MAPK pathways leads to enhanced survival, cell cycle progression, proliferation and metastasis.

1.3. Neratinib

Neratinib is an oral, irreversible tyrosine kinase inhibitor (TKI) of HER1 (EGFR), HER2 and HER4 (14) (Figure 1.2). In July 2017, Neratinib was approved by the Food and Drug Administration for adjuvant treatment of patients with early-stage HER2+ breast cancer (15). In July 2018, the European Medicines Agency (EMA) recommended granting the marketing authorisation of Neratinib for adjuvant treatment of breast cancer patients. The EMA committee recommended that Neratinib use should be restricted to HER2+ and hormone receptor positive breast cancer. Since its approval, neratinib is currently in many

clinical trials (summarised in Table 1.3).

NCT no.	**Condition**	**Interventions**
NCT00878709	Early-Stage HER2+ Breast Cancer	Drug: neratinib
NCT01042379	Invasive Breast Cancer (all subtypes)	I-SPY 2 TRIAL: Neoadjuvant and personalised adaptive novel agents to treat breast cancer. new drug agents including neratinib
NCT01494662	HER2+ Breast Cancer with brain metastasis	Drug: HKI-272 (neratinib) procedure: surgical resection, drug: capecitabine
NCT01670877	Metastatic HER2-mutant Breast Cancer	Drug: neratinib, drug: fulvestrant, drug: trastuzumab, procedure: tumour biopsy, procedure: research blood sample
NCT01808573	HER2+ Metastatic Breast Cancer	Drug: neratinib, drug: capecitabine, drug: lapatinib
NCT02236000	HER2+ Metastatic Breast Cancer	Drug: neratinib, drug: T-DM1
NCT02400476	Early Stage HER2+ Breast Cancer	Drug: neratinib, drug: loperamide, drug: colestipol, drug: budesonide
NCT02396108	HER2+ Breast Cancer (Stage I-III)	Drug: Paclitaxel + carboplatin + ASLAN001
NCT02673398	HER2+ Metastatic Breast Cancer	Laboratory biomarker analysis, drug: neratinib, other: pharmacological study
NCT03182634	HER2+ Metastatic Breast Cancer	Drug: Fulvestrant, drug: neratinib, drug: AZD5363
NCT03094052	HER2+ Breast Cancer (Stage II/III)	Drug: Neratinib, drug: trastuzumab, drug: crofelemer, drug: loperamide
NCT03289039	HER2+, ER+ Metastatic Breast Cancer	Drug: Neratinib, drug: fulvestrant
NCT03065387	HER2+ Breast Cancer	Drug: neratinib, drug: everolimus, drug: palbociclib, drug: trametinib
NCT03377387	HER2+ Metastatic Breast Cancer	Drug: capecitabine, drug: neratinib
NCT03101748	HER2+/HR+ HER2- Metastatic Breast Cancer	Drug: neratinib, paclitaxel, pertuzumab, trastuzumab, doxorubicin, cyclophosphamide

Neratinib has undergone Phase I, II and III clinical trials to date. Phase I results indicated that neratinib had anti-tumour efficacy in patients with metastatic or advanced-stage HER2+ breast cancer (n=73) (16). In a phase II study, two cohorts of HER2+ breast cancer patients were enrolled, trastuzumab pre-treated patients (n=66) and trastuzumab naïve patients (n=77). The results from this study showed neratinib to have substantial clinical activity in both cohorts of patients (17). A phase II monotherapy trial was conducted to determine the efficacy of neratinib treatment compared to lapatinib plus capecitabine (18). HER2+, trastuzumab pre-treated, locally advanced or metastatic breast cancer patients were enrolled in the study. Neratinib was administered to patients (n=117) and lapatinib plus capecitabine was administered to the other arm of patients (n=116) (18). The results from this non-inferiority trial were considered inconclusive due to the fact that neratinib was not regarded as non-inferior to lapatinib plus capecitabine. However, neratinib showed relevant clinical activity and acceptable tolerability among patients and may be an option for patients unable to receive lapatinib and capecitabine combination therapy. Further to these trials, a phase III, multicentre, randomised, double-blind, placebo-controlled trial was established (ExteNET trial) (19). The aim of this study was to investigate the efficacy of neratinib on disease-free survival when compared to placebo on patients who had completed trastuzumab therapy up to 1 year previously. 2840 patients were randomly assigned neratinib or placebo for 12 months following adjuvant treatment with chemotherapy and trastuzumab (19). Patients in the neratinib group had fewer invasive disease-free survival events than the placebo group of patients. Disease-free survival significantly improved in the patients on neratinib after 2yrs *vs* placebo (94.2% vs. 91.9%, respectively). At the 5-year follow up of this trial, it was determined that after chemotherapy and trastuzumab, adjuvant treatment with neratinib for 1 year significantly reduced breast cancer relapses (20). A recent meta-analysis study was conducted to evaluate the safety and efficacy of neratinib in 23 prospective clinical trials (21). This study analysed 23 trials, which included 4,896 patients. The most frequently occurring adverse events were diarrhoea (25.1%), nausea (37.9%) and abdominal pain (28.4%). Diarrhoea was mitigated by prophylactic loperamide. This meta-analysis concluded that neratinib therapy led to a high frequency of adverse events, although most were tolerable. Neratinib was found to provide survival benefit and may hold promise when combined with other anticancer agents (21).

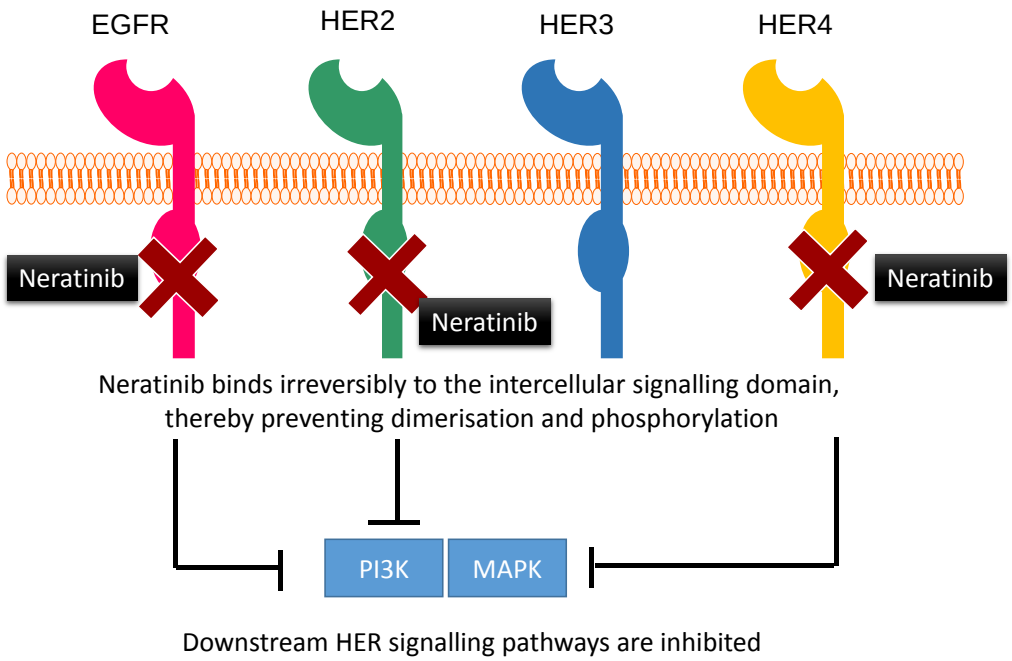

Figure 1.2: Mode of action of neratinib and other HER2 targeted therapies
The tyrosine kinase inhibitor, neratinib, targets EGFR,, HER2, HER2 and HER4. Preventing dimerisation and therefore downstream signalling. Neratinib binds irreversibly to the intercellular signaling domain and inhibits phosphorylation and thus prevents HER downstream signaling pathways.

1.4. Neratinib-resistance

Despite neratinib being a very newly approved drug for breast cancer patients, studies have commenced investigating neratinib-resistance in breast cancer cell lines and in patient specimens.

Using a pool-based lentiviral genome-wide functional RNAi screen, Seyhan *et al.* discovered genes that associated with neratinib-resistance (22). The genes discovered by this group were associated with oncogenesis, transcription factors, cell cycle, cellular ion transporters, protein ubiquitination and with the interaction of breast cancer associated

genes. Similarly, our group have shown that neuromedin U (NmU) overexpression is associated with neratinib-resistance (23). Low levels of miR-630 were also associated with neratinib-resistance (24). These studies show that neratinib is both associated with innate and acquired resistance. The molecular mechanisms of resistance to this drug, therefore, need to be fully elucidated to facilitate improving the efficacy of neratinib and to identify biomarkers for predicting response to neratinib and treatment outcome for patients. We have shown that neratinib-resistant cell lines are cross-resistant to other HER2-targeted therapies and increased CYP3A4 activity may be involved in increasing the metabolism of neratinib in these cell line variants (25). In a recent study of HER2+ breast cancer cell lines (SKBR3, MDA-MB-453 ad HCC1569), the combination of pertuzumab with lapatinib enhanced the response to trastuzumab in SKBR3 cell lines, however, this was not observed for the combination of pertuzumab with neratinib (26).

Investigations into HER2 mutations and neratinib-resistance have commenced. In $HER2^{L869R}$-mutant (L869R mutation is located within the activation loop of the HER2 kinase domain, leucine replaced by arginine at position 869) breast cancer (one patient case study), neratinib had the ability to block HER2-mediated signalling in a tumour. However, if the cells express $HER2^{L869R/T798}$, neratinib is unable to block HER2-mediated signalling (27). In that study, the $HER2^{T798I}$ mutation (on protein, threonine replaced by isoleucine) was found to promote neratinib-resistance in lentivirally-transduced cells. Following the benefits of neratinib in the ExteNET trial, *in vivo* studies were established using a mouse model of ER+/HER2+ MDA-MB-361 tumours. The mice were treated with paclitaxel plus trastuzumab ± pertuzumab for 4 weeks and then randomised to fulvestrant (estrogen receptor (ER) antagonist) ± neratinib treatment (28). The extended adjuvant therapy with neratinib and fulvestrant maintained a complete response (CR), however, those treated with fulvestrant alone relapsed immediately. From this study, it was concluded that extended HER2 blockade was necessary to achieve complete response *in vivo*. ER blockade alone did not prevent relapse (28). A recent study investigated neratinib efficacy in association with HER2 mutations in HER2+ breast cancer patients, HER2+ breast cancer cell lines (BT474 and SKBR3) and patient-derived xenograft models (PDXs) (29). In this study, it was found that amplification and mutation of HER2 (L755S, gain-of-function mutation, resulting in an amino acid substitution at position 755 in HER2, from a leucine to a serine) was associated with poor response to trastuzumab and lapatinib in cell lines. Neratinib however, was found to be effective in breast cancer cells (BT474 and

SKBR3) bearing both HER2 amplification and mutation (L755S). Neratinib was found to be more potent than lapatinib against breast cancers with HER2 amplification and the L755S mutation. PDX models from HER2+ breast cancer patients with lung metastatic lesions harbouring HER2 amplification and the D769Y HER2 mutation (results in an amino acid substitution at position 769 in HER2, from an aspartic acid to a tyrosine) were treated with vehicle control, trastuzumab, lapatinib or neratinib for 5 weeks (29). The xenografts were found to have resistance to both trastuzumab and lapatinib, neratinib statistically significantly inhibited tumour growth. A pilot study was preformed to establish response to neratinib in patients harbouring HER2 mutations (n=6). 4 patients experienced substantial reduction in tumour volume following neratinib treatment (30% reduction). This study indicates that neratinib may have clinical benefit in patients with both HER2 amplification and mutation.

NCT no.	**Condition**	**Interventions**
NCT00878709	Early-Stage HER2+ Breast Cancer	Drug: neratinib
NCT01042379	Invasive Breast Cancer (all subtypes)	I-SPY 2 TRIAL: Neoadjuvant and personalised adaptive novel agents to treat breast cancer. new drug agents including neratinib
NCT01494662	HER2+ Breast Cancer with brain metastasis	Drug: HKI-272 (neratinib) procedure: surgical resection, drug: capecitabine
NCT01670877	Metastatic HER2-mutant Breast Cancer	Drug: neratinib, drug: fulvestrant, drug: trastuzumab, procedure: tumour biopsy, procedure: research blood sample
NCT01808573	HER2+ Metastatic Breast Cancer	Drug: neratinib, drug: capecitabine, drug: lapatinib
NCT02236000	HER2+ Metastatic Breast Cancer	Drug: neratinib, drug: T-DM1
NCT02400476	Early Stage HER2+ Breast Cancer	Drug: neratinib, drug: loperamide, drug: colestipol, drug: budesonide
NCT02396108	HER2+ Breast Cancer (Stage I-III)	Drug: Paclitaxel + carboplatin + ASLAN001
NCT02673398	HER2+ Metastatic Breast Cancer	Laboratory biomarker analysis, drug: neratinib, other: pharmacological study
NCT03182634	HER2+ Metastatic Breast Cancer	Drug: Fulvestrant, drug: neratinib, drug: AZD5363
NCT03094052	HER2+ Breast Cancer (Stage II/III)	Drug: Neratinib, drug: trastuzumab, drug: crofelemer, drug: loperamide
NCT03289039	HER2+, ER+ Metastatic Breast Cancer	Drug: Neratinib, drug: fulvestrant
NCT03065387	HER2+ Breast Cancer	Drug: neratinib, drug: everolimus, drug: palbociclib, drug: trametinib
NCT03377387	HER2+ Metastatic Breast Cancer	Drug: capecitabine, drug: neratinib
NCT03101748	HER2+/HR+ HER2- Metastatic Breast Cancer	Drug: neratinib, paclitaxel, pertuzumab, trastuzumab, doxorubicin, cyclophosphamide

Table 1.3: Current clinical trials of neratinib in breast cancer

Current clinical trials that are active or recruiting. Information as on https://clinicaltrials.gov (information correct as of 3rd November 2018).

1.5. Extracellular vesicles

Exosomes, cell-derived vesicles, were initially described as vesicles released during the maturation process of reticulocytes (30). Exosomes and microvesicles (MVs; See Section 1.5.1) are typically differentiated based on size, origin (endosomal or cell membrane), markers and contents (31). Collectively these vesicles are termed extracellular vesicles (EVs), throughout this project, the terms used for EVs/exosomes/microvesicles are indicative of the terms used by the authors in the publications. Two distinct processes of vesicle release from the cells have been described, *i.e.* cell membrane shedding produces MVs, while EVs originate from multivesicular endosomes (MVEs) (summarised in Figure 1.3). EVs are mediators of intercellular communication (32-34).

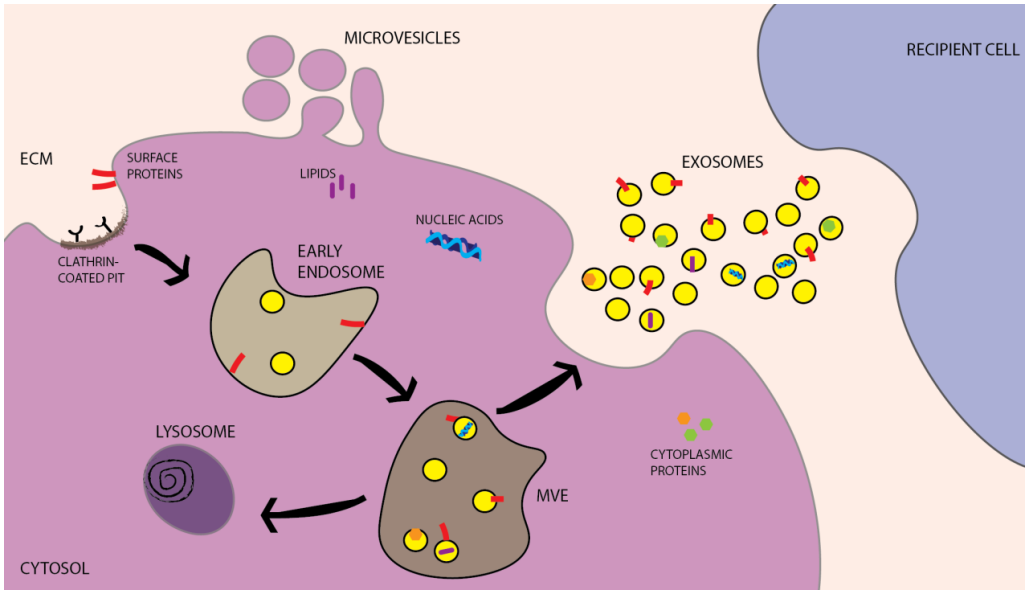

Figure 1.3: Biogenesis of extracellular vesicles
Microvesicles are formed by direct budding off from the cell membrane. The initial steps in exosome formation involve the clathrin-coated pits and cell membrane invagination and form early endosomes. Following on from this ILVs are formed following a second invagination and are called MVEs. Upon fusion with the cell membrane, exosomes are released.

1.5.1. Microvesicle formation

MVs/ectosomes are often described as 120-1000 nm (35). MVs are formed and released into the extracellular milieu *via* direct budding and fission of the cell membrane (36). MV cargo does not contain all membrane proteins from the cells in which they originate (37). Cholesterol-enrichment of MVs has been shown and MV generation was found to be reduced by depleting cholesterol with a methyl-beta-cyclodextrin, an inhibitor of lipid raft formation (38). MV release has been shown to involve the GTP-binding protein, ARF6,

extracellular signal-regulated kinase (ERK) and myosin light chain kinase (37). To distinguish between MVs and apoptotic bodies, apoptotic bodies contain cytosolic organelles and/or nuclear fragments, whereas, MVs do not (39). MVs have been shown to be present in peripheral blood, urine and ascitic fluids (40).

1.5.2. Exosome formation

Exosomes are typically described as less than 150nm in diameter (41). Primary endocytic vesicles are formed through the process of cell membrane invagination, the fusion of the endocytic vesicle results in early endosomes. Late endosomes are formed from early endosome maturation processes which include Rab5 to Rab7 exchange, endocytosed cargo retention and interactions with membrane components and lysosomal hydrolases (42, 43). Intraluminal vesicles (ILVs) accumulate following a second invagination. The ILVs are contained within the late endosomes and are called MVEs. MVE formation is a multistep process involving endosomal sorting complex required for transport (ESCRT), membrane lipid domains and many other processes (44). Upon fusion with lysosomes, MVEs and its cargo are degraded. However, upon fusion with the cell membrane, ILVs are released and are termed exosomes. Exosomes have been found to be secreted in bodily fluids such as blood, urine, saliva, breast milk, amniotic fluid, ascites, cerebrospinal fluid, bile, and semen (44).

1.5.3. Extracellular vesicle composition

EVs contain proteins, nucleic acids and lipids. Publically available datasets such as Exocarta (http://www.exocarta.org/) and Vesiclepedia (http://www.microvesicles.org/) provide additional information on the magnitude of EV contents. A recent database update collated data from 10 different species, showing 7540 RNA, 41,860 proteins and 1116 lipids in EVs across all studies (45).

EVs carry nucleic acids. Most EV studies focused predominantly on mRNAs and miRNAs as well as carrying coding and non-coding RNA (ncRNA), cDNA, single-stranded DNA and double-stranded DNA (46, 47). EVs containing nucleic acids have been shown to transport nucleic acids to induce phenotypic changes in recipient cells (48, 49). It has been suggested that RNAs are sorted into EVs *via* cellular RNA interactions with the surface of MVEs and subsequent uptake of RNAs into ILVs (50). Additionally, it is suggested that

post-transcriptional modifications such as 3' end adenylation and uridylation play a role in ncRNA sorting (51). Exosomes have been found to carry siRNA for Huntingtin mRNA silencing (52).

EV cargo includes proteins such as endosomal proteins such as Rab GTPases, annexins and flotillin (53, 54), tetraspanins including CD63, CD81, CD82, CD53, and CD37 (55, 56), and proteins involved in their biogenesis such as tumour susceptibility gene 101 (TSG101) and apoptosis-linked gene-2-interacting protein X (ALIX); some of which are considered to be measured on EVs or their sub-populations (53). Although not fully elucidated, EV cargo may also result from specific sorting mechanisms, such as CD63-dependent-ESCRT-independent sorting and sorting of the ESCRT complex (57, 58). The specific microenvironment and/or pathology may influence the specific proteins sorted into EVs. For example, Harris *et al.* (59) concluded that metastatic breast cancer cell (MDA-MB-231) derived-exosomes contain specific protein signatures compared to non-metastatic breast cancer cell (MCF-7)-derived exosomes. Proteomic analysis is being used to identify the heterogeneous nature of EV populations (60). This study defined subtypes of EVs based on proteomic analysis: large EVs pelleting at low speed, medium-sized EVs pelleting at intermediate speed and small EVs pelleting at high speeds.

The lipid content of EVs comprises of phospholipids, sphingomyelin, ganglioside GM3, cholesterol, glycosphingolipids and phosphatidylserine (61, 62). A study to investigate lipid content in prostate cancer cells (PC-3) and their exosomes demonstrated that exosomes are enriched with specific lipid classes, notably glycosphingolipids. It was calculated that there is an 8.4-fold higher amount of lipids per mg protein in exosomes than in the parent cells (61). This study suggested that lipids may have potential as biomarkers of prostate cancer, however, comparisons with normal cells would need to be performed and following on from this more lipidomic studies should be performed on more cancer types. Exosomal lipids may be important for future biomarker discovery and in optimising exosomes for drug delivery (reviewed by (63).

1.5.4. Extracellular vesicles in breast cancer

Exosomes/EVs have been described as a means of communication between tumour cells and other cell types including those of the microenvironment and beyond; in breast, as well as other cancer types (64). Dysregulation in this cell-to-cell communication and thus undesirable cellular cross-talk is understood to contribute to cancer development and

progression. The multi-roles of exosomes/EVs in breast cancer are reviewed (65) and summarised in Figure 1.4. The roles of EVs in hypoxia, and drug resistance will be discussed.

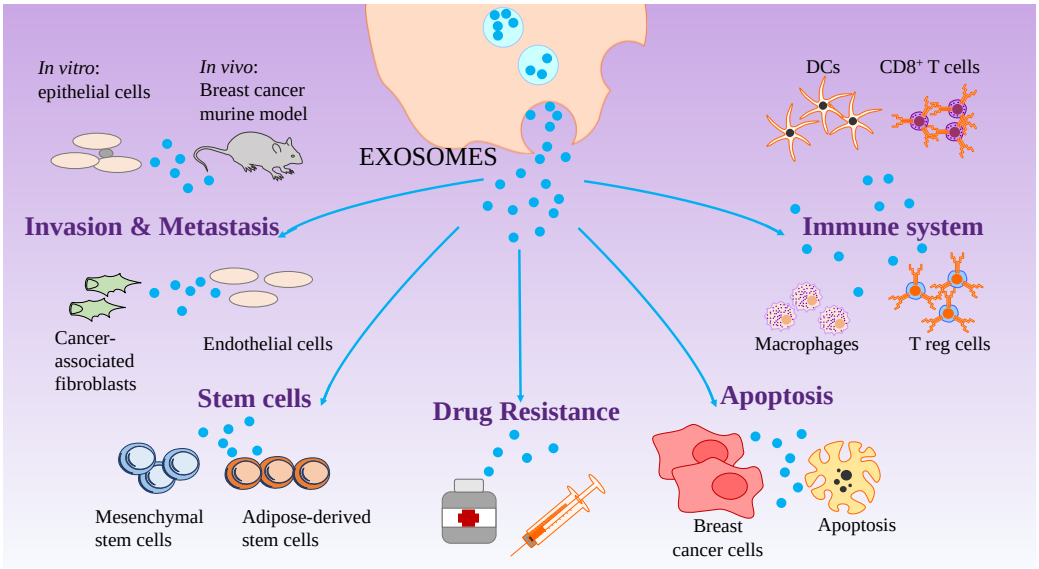

Figure 1.4: The multiple roles of exosomes/EVs in breast cancer
In breast cancer exosomes/EVs have been shown to influence invasion and metastasis, stem cells, the immune system, apoptosis and drug resistance (65).

1.5.4.1.Hypoxia and EVs

Lack of oxygen (hypoxia) is a prominent component of tumour progression and is associated with poor prognosis in many cancer types (66) (Table 1.4). The hypoxic microenvironment initiates many pathways involved in tumour progression, such as, angiogenesis, migration, invasion, metastasis, epithelial–mesenchymal transition (EMT), influencing the immune system and is involved in chemotherapy-resistance (reviewed by (67)). Hypoxia inducible factors (HIFs) are central to hypoxia (reviewed by (68)), for example, in breast cancer HIF-1α is associated with promoting tumour growth, vascularization, metastasis and bone colonization (69). In addition to promoting tumour progression, hypoxia influences EV secretion and their downstream effects.

Many studies investigating exosomes in hypoxic conditions have been completed in different cancer types. These studies should be further expanded in to other cancer types including breast cancer. Hypoxia has been shown to increase microvesicle secretion in lung cancer cells (70). Microvesicles derived from murine (LL-2) or human (A549) lung cancer cell lines were also shown to increase the expression of interleukin 8 (IL-8), VEGF, Leukaemia inhibitory factor (LIF), OSM, IL-11, and MMP-9 in fibroblast cells. MVs may

have potential as antiangiogenic therapeutics in lung cancer and should also be investigated in other cancers including breast cancer (70). Under hypoxic conditions, the squamous carcinoma cell line (A431), exhibited enhanced metastatic and angiogenic potential (71). Proteomic analysis of the secretome revealed that 50% of the proteins isolated from A431 cells were presumed to be from the exosome preparation, further analysis of the exosome preparation is warranted, with proteomic studies being imperative for the discovery of novel exosomal biomarkers for many cancers (71). Under hypoxic conditions, GBM cells have been shown to release microvesicles bearing TF/VIIa which up-regulate PAR-2 on endothelial cells, thereby increasing the levels of proangiogenic growth factor heparin-binding EGF-like growth factor (HB-EGF) (72). HB-EGF has been previously shown to be involved in the development of TNBC (73). HB-EGF regulates VEGFA and ANGPTL4 through ERK-mediated and AKT-mediated HIF-1α and NF-κB activation in a TNBC cell line (MDA-MB-231). The vascular permeability of the endothelial cell line (HUVECs) was increased in the presence of HB-EGF, VEGFA and ANGPTL4 (73). Inhibitors against HB-EGF have now been brought forward into clinical trials for various cancer types. Angiogenesis was promoted by exosomes derived from hypoxic colorectal cancer cells (HT29 and HCT116) (74). Under hypoxic conditions, the colorectal cancer cells promoted angiogenesis in endothelial cells (HUVECs) through exosome-mediated Wnt/β-catenin signalling. Exosomes derived from hypoxic conditions were found to have increased levels of MMP-13 in nasopharyngeal cancer patients tissue samples (n=126), which could be potentially associated with increased migration and invasion (75).

During hypoxia (0.1% O_2, 24hr), exosome release from breast cancer cells (MCF7, SKBR3 and MDA-MB-231) was significantly increased when compared to normoxic conditions (76). The HIF pathway was also investigated in this study; MDA-MB-231 cells were treated with the HIF hydroxylase inhibitor (1mM Dimethyloxalylglycine (DMOG)) for 24hr. DMOG, ultimately prevents HIF-1α degradation and it was found that treatment of MDA-MB-231 cells with this inhibitor significantly increased exosome release (76). miR-210 expression was increased in MCF7 cells under hypoxic conditions (1% O_2, 48hr), this suggests that this miRNA may play a role in angiogenesis and tumour progression. Exosomal Cav-1 was significantly increased following treatment of MDA-MB-231 cells with decorin (represses HIF-1α and VEGFA) (77). This study suggests that decorin triggers exosome release.

Under hypoxic conditions (1% O_2), breast cancer cell (MDA-MB-231 and BT-474)-derived exosome secretion was significantly increased and the isolated exosomes displayed

potent immunosuppressive traits through TGF-β and IL-10 secretion (78). IL-10 is a potent anti-inflammatory cytokine whereas TGF-β is both a pro- and anti-inflammatory protein, greater insight into these proteins in breast cancer-mediated immune suppression is required. Rong *et. al* suggested looking at the immunosuppressive properties of PGE_2 (reviewed by (79)) also (78). In hypoxic conditions, prostate cancer cells (PANC-1, BxPC-3) were found to generate exosomes with high levels of miR-301a-3p, the exosomes were found to polarize M2 macrophages by the PTEN/PI3Kγ pathway (80). When polarised by the exosomes, the macrophages were found to promote *in vivo* metastasis. The metastatic potential was evident in BALB/c nude mice following tail-vein injection of PANC-1 mixed with macrophages treated with PANC-1-hypoxic-exosomes (80).

Type of Cancer	**Hypoxic Factors**	**Reference**
Breast	HIF-1α HIF-2α	(81-87) (88)
Colorectal	HIF-1α HIF-2α	(89, 90) (91)
Gastric	HIF-1α	(92-98)
Hepatocellular carcinoma	HIF-1α	(99-103)
Lung	HIF-1α HIF-2α HIF hydroxylases HIF-1α and HIF-2α	(104-107) (108) (109) (110, 111)

Table 1.4: List of cancers with hypoxic-factor-related poor prognosis
Details of hypoxic factors associated with poor clinical prognosis in the top 5 cancers (most common causes of cancer deaths as stated in the World Health Organisation's World Cancer Report 2014).

1.5.4.2. Drug resistance and EVs

Drug resistance is a major obstacle in breast cancer treatment and exosomes/EVs are of substantial interest in drug resistance studies. Exosomes, cell-derived vesicles, were initially described as vesicles released during the maturation process of reticulocytes (30). Exosomes and microvesicles are typically differentiated based on size, origin (endosomal or cell membrane), markers and contents (31). Collectively these vesicles are termed EVs, throughout this project, the terms used are indicative of the terms used by the authors in the

publications. It was hypothesised that the EV-induced transfer of chemoresistance was linked to the transfer of miR-19b and miR-20a. Exosomal transport of P-glycoprotein (P-gp) has been described as a possible mechanism in exosome-mediated drug resistance. Our research group initially showed this in relation to prostate cancer (112) and, more recently, exosomes from docetaxel-resistant MCF-7 cells have been shown to transfer drug resistance to docetaxel-sensitive MCF-7 cells. The suggested mechanism of resistance is *via* exosomal delivery of P-gp, since P-gp concentrations are higher in exosomes derived from drug-resistant cells compared to the drug-sensitive cells. P-gp was also successfully transferred by exosomes from drug-resistant cells to drug-sensitive cells (113). Advancing on what we believe to be the first study associating exosomes/EVs with drug resistance, where we reported a transfer of docetaxel-resistance in prostate cancer (114), exosomes/EVs have more recently been shown to play roles in mediating drug resistance in many cancer types (reviewed by (115, 116)). In synovial sarcoma cell-derived EVs were found to release miR-761 and it was found to be associated with pazopanib-resistance (117). miR-761 directly targeted and decreased the levels of TRIP6, LMNA and SIRT3 in synovial sarcoma cell lines (SYO-1 and 1273/99), all genes were previously described to be associated with increased drug resistance. Similarly, drug-resistant leukemic cells transferred chemoresistance *via* EVs (118).

The bystander effect was originally described as a radio-biological effect whereby unexposed neighbouring cells exhibit phenotypic and biochemical changes as a consequence of local cells being irradiated (119). The effect was reported to be gap-junction-mediated or caused by the secretion of extracellular factors. In 2014, our group showed EVs to be involved in in mediating radiation-induced bystander signalling in human keratinocyte cells (120). Asur *et. al* have shown that the bystander effect is not limited to radiation, but can also be chemically-induced (121). They showed treatment of human B normal lymphoblastoid cells with mitomycin C and phleomycin induced a bystander effect through secreted soluble factors. Similarly, Testi *et. al* (122) found that both vincristine and mitomycin C induced a bystander effect in cells, in a dose-dependent manner. In a recent study, EVs derived from cisplatin-treated ovarian cancer cells (A2780) were reported to cause increased invasion and cisplatin drug resistance in local cells (123). Upon heparin treatment of recipient cells (to prevent EV uptake), this drug induced resistant effect was decreased, suggesting that preventing EV uptake -if possible in a targeted manner *in vivo*- during chemotherapy treatment may help improve outcome for

patients. Thus, the targeted prevention of EV communication should be considered when investigating the effect of hypoxia on drug resistance/response.

Stromal cells play important roles in the microenvironment of the bone marrow. They were found to initiate crosstalk with breast cancer cells (MDA-MB-231) *via* exosomes. In that study, exosomes were transferred from stromal cells to breast cancer cells, thereby activating antiviral RIG-I signalling and in parallel activating NOTCH3 pathways to regulate the expansion of therapy-resistant tumour-initiating cells. It has been proposed that this mechanism of exosomal transfer is regulated through the stromal cell-induced increase in RAB27B and the activation of RIG-I signalling *via* the transfer of exosomal 5'tripohosphate RNA. Further to these findings, MDA-MB-231 xenograft female nude mice were co-injected with non-transformed MRC5 human diploid fibroblasts (as stromal cells), STAT1 expression was increased, with reduced cell death and increased tumour growth evident in this model (124).

Adriamycin (Adr) and docetaxel (Doc) have been shown to have therapeutic efficacy in breast cancer patients, but drug resistance limits their clinical benefits. The drug-sensitive (MCF-7/S) and drug-resistant human breast cancer cell lines (MCF-7/Adr and MCF-7/Doc) were used to investigate possible exosomal transfer of resistance. Upon co-culture of MCF-7/Adr exosomes with MCF-7/S cells, reduced levels of proliferation and high levels of drug resistance were observed. Similarly, this effect was seen for MCF-7/Doc-derived exosomes. Microarray analysis identified miRNA profiles for both MCF-7/Adr and MCF-7/Doc resistant cells in which possible common pathways of resistance were observed, suggesting that the transfer of miRNAs plays a role in this exosomal transfer of resistance (125, 126). In relation to tamoxifen, exosomes from tamoxifen-resistant MCF-7 cells were found to promote proliferation of MCF-7 wild-type cells. Functional assays (cell viability, apoptosis and colony formation) assessed the involvement of miR-221 and miR-222 in the transfer of this tamoxifen-resistance, the phenotypic effects were found to be significantly blocked using anti-miR-221/anti-miR-222 (127).

HER2 is found on exosomes from breast cancer cell lines, SKBR3 and BT474 and $HER2^{+}$-exosomes have been shown to bind to and interfere with trastuzumab's activity in *in vitro* studies (128). In a study of specimens from HER2-overexpressing breast cancer patients (n=22), higher exosome-trastuzumab binding capacity was evident in advanced disease stage serum (n=11) compared to serum from the early-stage cohort (n=11). In contrast, exosomes did not interfere with the *in vitro* anti-proliferative activity of the small molecule lapatinib that targets EGFR as well as HER2 (128). It is possible that, *in vivo*, $HER2^{+}$-

exosomes will modulate trastuzumab availability and so adversely affect patient outcome. While *in vivo* studies and more extensive analysis of relevant patients' specimens are necessary to further investigate this activity, this study supports a broad range of important roles held by exosomes in breast cancer and highlights their potential in a diagnostic and therapeutic setting.

1.6. Project aims

The hypothesis of the existing research framework was that protein and DNA alterations are key drivers of acquired drug resistance in breast cancer cell lines. The overall aim of this project was to investigate HER2-targeted drug resistance using HER2+ breast cancer cell lines.

1. To investigate acquired neratinib-resistance in EFM19.2A, HCC1954 and SKBR3 cell line variants and EVs using sequenom and proteomic analysis. DNA mutations and protein expression levels between neratinib-sensitive cell line variants (EFM19.2A-Par, HCC1954-Par and SKBR3-Par) and neratinib-resistance cell line variants (EFM19.2A-NR, HCC1954-NR and SKBR3-NR) will be investigated.
2. From Aim 1, carbonic anhydrase IX (CAIX) was identified as the strongest candidate protein for further investigation. We aimed to validate the overexpression of CAIX in HER2-targeted therapy resistant cell lines. We aimed to inhibit CAIX expression in drug-resistant cell line to invesitgate if this would re-sensitise the cell line variants to neratinib.
3. Our next aim was to investigate the potential of CAIX as a predictive biomarker for resistance to therapy. We aimed to use plasma specimens from the TCHL neo-adjuvant clinical trial to test if the levels of CAIX in plasma specimens correlate with response to therapies. We also sought to use plasma specimens to isolate EVs to determine the potential of EVs to carry CAIX and their potential use as predictive biomarkers for HER2-targeted therapies.
4. To progress the investigation of miR-134 in TNBC. Previous PhD student, Dr. Keith O'Brien, determined that miR-134 acts as a tumour suppressor in $Hs578Ts(i)_8$ cells. To progress this work further, a panel of TNBC cell lines (BT-549, HCC1143 and HCC1937) will be used to determine to strengthen this observation.

CHAPTER TWO: Materials and Methods

2. Materials and Methods

2.1. Cell culture

2.1.1. Cell lines

A total of sixteen cell lines and cell line variants were used in this PhD project; 5 TNBC cell lines and 11 HER2+ cell line variants.

HER2+ parent cell lines (BT474-Par, EFM19.2A-Par, HCC1954-Par and SKBR3-Par) and their representative HER2-targeted therapy-resistant (lapatinib-resistant (LR), neratinib-resistant (NR), trastuzumab-resistant (TR) and trastuzumab and lapatinib-resistant (TLR)) cell line variants (BT474-TR, EFM19.2A-NR, HCC1954-LR, HCC1954 NR, SKBR3-NR, SKBR3-TR and SKBR3 TLR,) were used in this study. All HER2+ cell line variants were cultured in RPMI-1640 (Sigma-Aldrich, Cat #: R0883) containing 10% fetal bovine serum (FBS) (Gibco; Cat. #: 10270-106) and 2mM L-Glutamine (Sigma-Aldrich; Cat. #: G7513), summarised in Table 2.1. Dr. Dennis Slamon's laboratory (UCLA, California) established the BT474-TR cell line variant. Dr Martina McDermott (NICB, Dublin) established the HCC1954-LR cell line variant. Dr Brigit Browne (NICB, Dublin) established the SKBR3-TR and SKBR3-TLR cell line variants. As detailed in Section 2.2, Dr Susan Breslin established the HCC1954-NR and EFM19.2A-NR cell line variants. The SKBR3-NR cell line variants were established in this project.

TNBC isogenic cell line variants Hs578T and its more aggressive clonal variant Hs578Ts(i)$_8$ were gifts from Dr Lynda Hughes and Dr Susan McDonnell (University College Dublin). The BD Matrigel™ Invasion Chamber assay system was used to isolate isogenic subclones of Hs578T cells (129). Briefly, the most invasive cells which passed through the chamber were isolated and cultured in a 75cm^2 flask and labelled Hs578Ts(i)$_8$. This process was repeated 7 times to give Hs578Ts(i)$_8$ cells which were shown to have a 3-fold more invasive potential and 2.5-fold more migratory potential when compared to parent cells. Both cell lines were cultured in Dulbecco's Modified Eagles Medium (DMEM) (Sigma-Aldrich; Cat. #: D5671) containing 10% FBS (Gibco; Cat. #: 10270-106), 2mM L-Glutamine (Sigma-Aldrich; Cat. #: G7513), and 10μg/mL of insulin (Sigma-Aldrich; CAT#: I0516). TNBC cell lines: HCC-1937 (ATCC, Cat. #: CRL-2336) and HCC-1143 (ATCC, Cat. #: CRL-2321) were cultured in RPMI-1640 (Sigma-Aldrich, Cat #: R0883) with 10% FBS. MDA-MB-231 (ATCC, Cat. #: HTB-26) were cultured in

DMEM containing 10% FBS and 2mM L-Glutamine. All culture conditions are summarised in Table 2.1.

All cell lines and variants were grown in 37ºC, 5% CO_2. For normoxic conditions, all cell lines were grown at 37ºC, 5% CO_2 and 21% O_2. For hypoxic conditions, all cell lines were grown at 37ºC, 5% CO_2 and 1% O_2. Two hypoxia chambers were used throughout this study, the ProOx hypoxia chamber (Biospherix, Model C21) and the H35 hypoxystation (Don Whitley Scientific, Model H35). It will be detailed in further Sections where each chamber was used. For all text throughout, 21% O_2 will be referred to as normoxic conditions and 1% O_2 will constitute hypoxic conditions.

Cells were routinely tested for *Mycoplasma* contamination every three months using the PCR *Mycoplasma* Test Kit I/C (PromoKine; Cat. #: PK-CA91-1048)/Universal *Mycoplasma* Detection kit (ATCC; Cat. #: 30-1012K) and were found to be negative. As the SKBR3 neratinib-resistant cell line variant was established in this project, the Mycoplasma Detection Lab Service was used to check for *Mycoplasma* contamination prior to any experiments (Fisher Scientific, Cat. #: 13408049).

Cell lines/cell line variants	*Breast Cancer Subtype*	*Cell culture medium*	*Culture conditions*
BT474-Par	Luminal B	RPMI-1640, 10% FBS,2mM L-Glutamine	37°C, 5% CO_2
BT474-TR	Luminal B	RPMI-1640, 10% FBS,2mM L-Glutamine	37°C, 5% CO_2
EFM19.2A-Par	Luminal B	RPMI-1640, 10% FBS,2mM L-Glutamine	37°C, 5% CO_2
EFM19.2A-NR	Luminal B	RPMI-1640, 10% FBS,2mM L-Glutamine	37°C, 5% CO_2
HCC1954-Par	HER2+	RPMI-1640, 10% FBS,2mM L-Glutamine	37°C, 5% CO_2
HCC1954-LR	HER2+	RPMI-1640, 10% FBS,2mM L-Glutamine	37°C, 5% CO_2
HCC1954-NR	HER2+	RPMI-1640, 10% FBS,2mM L-Glutamine	37°C, 5% CO_2
SKBR3-Par	HER2+	RPMI-1640, 10% FBS,2mM L-Glutamine	37°C, 5% CO_2
SKBR3-NR	HER2+	RPMI-1640, 10% FBS,2mM L-Glutamine	37°C, 5% CO_2
SKBR3-TR	HER2+	RPMI-1640, 10% FBS,2mM L-Glutamine	37°C, 5% CO_2
SKBR3-TLR	HER2+	RPMI-1640, 10% FBS,2mM L-Glutamine	37°C, 5% CO_2
Hs578T	TNBC	DMEM, 10% FBS,2mM L-Glutamine, 10µg/mL insulin	37°C, 5% CO_2
Hs578Ts(i)$_8$	TNBC	DMEM, 10% FBS,2mM L-Glutamine, 10µg/mL insulin	37°C, 5% CO_2
HCC1937	TNBC	RPMI-1640, 10% FBS	37°C, 5% CO_2
HCC1143	TNBC	RPMI-1640, 10% FBS	37°C, 5% CO_2
MDA-MB-231	TNBC	DMEM, 10% FBS,2mM L-Glutamine	37°C, 5% CO_2

Table 2.1: Cellular breast cancer subtypes and cell culture conditions for all cell lines and cell line variants used in this project

2.2. Establishment of neratinib-resistant cell lines

[HCC1954-NR and EFM19.2A-NR were previously developed by Dr Susan Breslin, School of Pharmacy and Pharmaceutical Sciences, Trinity College Dublin]

Neratinib-resistant (NR) cell line variants (HCC1954-NR and EFM19.2A-NR) were developed over a 6-month period by Dr. Susan Breslin *et al.* (130). These cell line variants were developed by stepwise increased concentrations of neratinib. Using the same methods, the SKBR3-NR cell line was developed over a period of 6 months. Cells were continuously maintained in neratinib, with treatments beginning at 4nM neratinib (IC_{10}) for the SKBR3 parent cell lines. Medium containing neratinib was changed every 2-3 days. As cells developed resistance to treatments of neratinib, the drug concentration was subsequently increased with final treatment doses of 80nM. Resistance was evaluated based on decreased cell death and increased proliferation of cells (see Section 2.3). Un-treated parent cells were aged alongside these cells as an appropriate control for all experiments. All experiments on acquired-resistant cells and corresponding aged controls were performed within 10 passages in culture. Cytotoxicity assays (acid phosphatase assays Section 2.3) were performed to determine the IC_{50} values for the cell line variants acquiring resistance to neratinib. All HER2-targeted treatment-resistant cell line variants were maintained in their associated drug as described in Table 2.2. All drug-resistant cell line variants were cultured in drug-free medium 24hr prior to all assays. Similarly, all drug-resistant cell line variants were seeded and cultured in drug-free medium for the duration of the assays.

Cell line variant	*Drug*	*Concentration*
BT474-TR	Trastuzumab (Herceptin, Roche, obtained from St James's Hospital, Dublin)	10µg/mL
EFM19.2A-NR	Neratinib (Sequoia Research Products, Cat. #: SRP06000n)	80nM
HCC1954-LR	Lapatinib (Sequoia Research Products, Cat. #: SRP01211I)	1µM
HCC1954-NR	Neratinib (Sequoia Research Products, Cat. #: SRP06000n)	80nM
SKBR3-NR	Neratinib (Sequoia Research Products, Cat. #: SRP06000n)	80nM
SKBR3-TR	Trastuzumab (Herceptin, Roche, obtained from St James's Hospital, Dublin)	10µg/mL
SKBR3-TLR	Trastuzumab (Herceptin, Roche, obtained from St James's Hospital, Dublin), Lapatinib (Sequoia Research Products, Cat. #: SRP01211I)	5µg/mL 100nM

Table 2.2: Drug concentration for maintenance of drug-resistant cell line variants

2.3. Cytotoxicity Assays

Cells were seeded in 96-well plates (Corning, Cat. #: 101-46810) and allowed to attach overnight. Cell line densities are detailed in Table 2.3. Cells were treated with the selected drug the next day and cultured for 5 days. Cell culture medium was removed and cells were subsequently washed in 100µl PBS (twice) (Sigma-Aldrich, Cat. #: P8537). 1M sodium acetate buffer was prepared (500 mL dH20, 4.1g sodium acetate (Sigma Aldrich, Cat. #: S5636), 500µl triton X (Sigma-Aldrich, Cat. #: T8787), pH to 5.5) and subsequently used for the phosphatase substrate buffer. Fresh phosphatase substrate buffer was prepared prior to use using 0.27g of 10mM p-nitrophenol phosphate (VWR chemicals, Cat. #: 27963.101) per 100mL sodium acetate buffer. 100µL of phosphatase substrate was added to each well. The plates were wrapped in aluminium foil and placed in an incubator at 37ºC/5% CO_2 for 1.5hr. After the incubation period, 50µL 1M NaOH (Sigma Aldrich, Cat. #: S5881) was added to each well to stop the reaction. The absorbance was read at

405nm using the FlouStar Optima microplate reader (BMG Labtech, serial #: 413-2103). Acid phosphatase assays were cultured at normoxic or hypoxic conditions (1% O_2/5% CO_2).

Cell line	*Seeding density for 1 day assay*	*Seeding density for 3 day assay (96-well)*	*Seeding density for 5 day assay (96-well)*
EFM19.2A-Par	13,000	8000	5000
EFM19.2A-NR	13,000	8000	5000
BT-474-Par	-	8000	5000
BT-474-TR	-	8000	5000
HCC1954-Par	8000	5000	3000
HCC1954-LR	-	5000	3000
HCC1954-NR	8000	5000	3000
SKBR3-Par	8000	5000	3000
SKBR3-NR	8000	5000	3000
SKBR3-TR	-	5000	3000
SKBR3-TLR	-	5000	3000

Table 2.3: Seeding densities for all assays performed in 96-well plates

2.3.1. Neratinib cytotoxicity assays

For establishment of SKBR3-NR cell line variants, cells were treated with neratinib concentrations ranging 0-300nM for 5days. SKBR3-Par cell line variants were treated from 0-120nM neratinib. Acid phosphatase assays were performed as previously described.

2.3.2. DFO cytotoxicity assays

To determine if CAIX is detectable in HER2+ cell line variants in response to hypoxic conditions, the hypoxia mimic (deferoxamine mesylate (DFO)) was used. Cells were seeded according to Table 2.3 for a one day assay. EFM19.2A, HCC1954 and SKBR3 cell line variants were treated with DFO concentrations ranging from 0-400µM. Acid phosphatase assays were performed as previously described.

2.3.3. S4 cytotoxicity assays

To determine the efficacy of S4 (Tocris, Cat. #: 5577) as an inhibitor of CAIX, prior to CAIX immunoblots, cytotoxicity assays were set up to determine a suitable concentration of S4 for protein isolation. EFM19.2A, HCC1954 and SKBR3 cell line variants were treated with S4 (0-100µM) for 3 days.

To determine any variation in S4 toxicity between the normoxic and hypoxic conditions BT474, EFM19.2A, HCC1954 and SKBR3 cell line variants were treated with S4 (0-100µM) for 5 days under normoxic (21% O_2) and hypoxic conditions (1% O_2). Acid phosphatase assays were performed as previously described in Section 2.3.

2.3.4. Combination cytotoxicity assays: S4 and neratinib

Combination assays were set up to determine if the addition of S4 to neratinib was synergistic in all cell line variants. Cytotoxicity assays were first set up with S4 and neratinib alone for all cell line variants to determine the IC_{50} values. All BT474, EFM19.2A, HCC1954 and SKBR3 cell line variants were treated with S4 concentrations ranging from 0-100µM for 5 days. For neratinib treatments, BT474 cell line variants were treated with neratinib ranging from 0-200nM. SKBR3 cell line variants were treated with a 0-1000nM range of neratinib. EFM19.2A and HCC1954 cell line variants were treated with neratinib concentrations ranging from 0-2000nM. Acid phosphatase assays were performed as previously described.

Once the IC_{50} values were calculated for each drug treatment, combination assays were set up, with fixed ratio concentrations. Combination concentrations for each drug in each cell line variant are detailed in Table 2.4.

Cell line variant	*S4 concentration (µM)*	*Neratinib concentration (nM)*
BT474-Par	0-154	0-14.3
BT474-TR	0-154	0-14.3
EFM19.2A-Par	0-154	0-32
EFM19.2A-NR	0-222	0-1922
HCC1954-Par	0-50.6	0-318
HCC1954-LR	0-222	0-570.5
HCC1954-NR	0-101.25	0-1053
SKBR3-Par	0-222	0-72
SKBR3-NR	0-154	0-570.5
SKBR3-TR	0-222	0-72
SKBR3-TLR	0-154	0-570.5

Table 2.4: Drug concentrations for S4 and neratinib combination cytotoxicity assays
All cell line variants with 8 different drug concentrations, the highest concentration was halved for each consecutive dose.

2.3.5. Combination cytotoxicity assays: S4 and lapatinib

Combination assays were set up to determine if the addition of S4 to lapatinib was synergistic in all lapatinib-resistant cell line variants and matched lapatinib-sensitive cell line variants. Cytotoxicity assays were first set up with S4 as previously described. For lapatinib treatments, SKBR3 cell line variants were treated with a 0-500nM range of lapatinib. HCC1954 cell line variants were treated with lapatinib concentrations ranging from 0-2000nM. Acid phosphatase assays were performed as previously described.

Once the IC_{50} values were calculated for each drug treatment, combination assays were set up, with fixed ratio concentrations. Combinations concentrations for each drug in each cell line variant is detailed in Table 2.5.

Cell line variant	*S4 concentration (µM)*	*Lapatinib concentration (nM)*
HCC1954-Par	0-68.3	0-987
HCC1954-LR	0-154	0-3800
SKBR3-Par	0-154	0-570
SKBR3-TLR	0-154	0-685

Table 2.5: Drug concentrations for S4 and lapatinib combination cytotoxicity assays
All cell line variants with 8 different drug concentrations, the highest concentration was halved for each consecutive dose.

2.3.6. Combination cytotoxicity assays: S4 and TDM-1

Combination assays were set up to determine if the addition of S4 to TDM-1 was synergistic in all trastuzumab-resistant cell line variants and matched trastuzumab-sensitive cell line variants. Cytotoxicity assays were first set up with S4 as previously described. For TDM-1 treatments, SKBR3 cell line variants were treated with a 0-0.08µg/mL range of TDM-1. BT474 cell line variants were treated with TDM-1 concentrations ranging from 0-5µg/mL. Acid phosphatase assays were performed as previously described.

Once the IC_{50} values were calculated for each drug treatment, combination assays were set up, with fixed ratio concentrations. Combinations concentrations for each drug in each cell line variant is detailed in Table 2.6.

Cell line variant	*S4 concentration (µM)*	*TDM-1 concentration (µg/mL)*
BT474-Par	0-240	0-0.15
BT474-TR	0-240	0-5
SKBR3-Par	0-154	0-0.08
SKBR3-TR	0-154	0-0.08
SKBR3-TLR	0-154	0-0.08

Table 2.6: Drug concentrations for S4 and TDM-1 combination cytotoxicity assays
All cell line variants with 8 different drug concentrations, the highest concentration was halved for each consecutive dose.

2.3.7. TNBC cells treated with cisplatin

Cells ($Hs578Ts(i)_8$, MDA-MB-231, HCC1143 and HCC1937) were seeded in 6-well plates (Corning, Cat. #: 101-46810) and treated with cisplatin (Hospira UK Limited, Cat. #: PA437/4/7) and mock transfections (see Section 2.16, using all reagents and protocols but miR-134 mimic was not added) were set up to determine the equivalent IC_{50} values Cell culture medium was removed and cells were subsequently washed in PBS (Sigma-Aldrich, Cat. #: P8537). 2.97mLof phosphatase substrate was added to each well. The plates were wrapped in aluminium foil and placed in the incubator at 37ºC/5% CO_2 for 1.5hr. After incubation, 1.485mL of 1M NaOH (Sigma Aldrich, Cat. #: S5881) was added to each well to stop the reaction. The absorbance was read at 405nm using the FlouStar Optima microplate reader (BMG Labtech, serial #: 413-2103).

2.4. Immunoblotting

2.4.1. Protein extraction

For all protein extraction in this project, cellular protein was obtained directly from cell culture flasks. CM was removed and 1mL of ice-cold PBS was added to wash the cells. 1mL of PBS was added to the cells and scraped using a sterile cell scraper (Fisher Scientific, Cat. #: 08-100-241). The cell suspension was centrifuged at 13,000g at 4ºC for 5min. The supernatant was removed and 50µL of cell lysis buffer (Invitrogen, Cat. #: FNN0011) including protease inhibitors (Roche, Cat. #:05892970001) was added. Cell

lysate pellets were incubated on ice for 30min with 15sec vortexing every 10min. Samples were centrifuged at 13,000g at 4ºC for 10min and the protein lysate supernatant was collected and stored at -20ºC for further analysis. EV pellets were lysed using this exact protocol for all cell-derived EVs and plasma specimen-derived EVs. EVs were lysed for EV characterisation immunoblotting and ELISAs (detailed in Section 2.9.1, 2.10.1 and 2.12). Intact EVs were used for the CAIX ELISA (detailed in Section 2.12.2)

2.4.2. Protein quantification

Bio-Rad protein assay Dye reagent (Bio-Rad, Cat. #: 500-0006) was used to quantify protein levels in cell line samples, lysed EVs and intact EV samples. Bovine serum albumin (BSA) standards were prepared (800µg/mL, 400µg/mL, 200µg/mL, 100µg/mL, 50µg/mL, 25µg/mL and 0µg/mL). A 10µL sample of a 1:50 dilution of cellular protein lysate in dH_2O was placed in a 96-well plate. Each lysed EV sample and each intact EV sample were diluted 1:10 and 1:5, respectively, in dH_2O. Bio-Rad dye was diluted 1:5 with dH_2O and 200µL was added to each sample and standard. Following a 5min incubation at room temperature, the absorbance was read at 595nm on a FlouStar Optima microplate reader (Serial #: 08-100-241).

2.4.3. Immunoblotting protocol

For all immunoblotting performed in this project, total protein (30µg of cellular protein and 10µg of EV protein) was resolved on 10% bis-acrylamide gels for Protein SDS-PAGE electrophoresis, along with a molecular weight marker, SeeBlue Plus2 Pre-stained standard (Invitrogen; Cat. #: LC5925). Separated proteins were transferred to polyvinylindene fluoride (PVDF) membranes (BioRad, Cat. #: 162-0177) using semi-dry transfer at 20V for 1hr. Following transfer, blots were incubated in blocking buffer (5% Bovine Serum Albumin (BSA) (Sigma-Aldrich, Cat. #: A9413) in PBS) at room temperature for 1hr. Blots were then washed in PBS/0.01 % Tween 20 (PBST) for 5min (x3 times). Primary antibodies were prepared in 3% BSA in PBST/TBST. Membranes were incubated in primary antibodies overnight at 4°C under constant rocking. Membranes were subsequently washed in PBST (x3 times) and incubated in secondary horseradish peroxidase-conjugated secondary antibodies for 1hr at room temperature under constant rocking. Membranes were again washed in PBST (x3 times) and proteins were visualised

by Super Signal® West Pico chemiluminescence substrate (Thermofisher, Cat. #: 34080) or Super Signal® West Femto maximum sensitivity substrate (Thermofisher, Cat. #: 3409s). Proteins were detected using a chemidoc exposure system (BioRad laboratories). All

antibody conditions and catalogue numbers, positive controls and conditions are detailed in

Antibody	*Company, Cat. #*	*Dilution*	*Antibody conditions*	*Secondary ab*	*Company, Cat. #*	*Dilution*	*Blot conditions*
CYP3A4	Santa Cruz, sc-53850	1:1000	3% BSA in PBST	Anti-mouse	Cell Signalling; 7074	1:1000	3% BSA in PBST
β-actin	Sigma-Aldrich, A5316	1:1000	3% BSA in PBST	Anti-mouse	Cell Signalling; 7074	1:1000	3% BSA in PBST
GRP-94	Cell Signalling, 2104S	1:1000	3% BSA in PBST	Anti-rabbit	Cell Signalling, 7074s	1:1000	3% BSA in PBST
ALIX	Abcam, ab76608	1:1000	3% BSA in PBST	Anti-rabbit	Cell Signalling, 7074s	1:1000	3% BSA in PBST
TSG101	Abcam, ab83	1:1000	3% BSA in PBST	Anti-mouse	Cell Signalling; 7074	1:1000	3% BSA in PBST
TLR3	Abcam, ab12085	1:50	3% Milk in TBST	Anti-mouse	Cell Signalling; 7074	1:1000	3% BSA in PBST
TLR3	Santa Cruz, sc-32232	1:500	3% Milk in TBST	Anti-mouse	Cell Signalling; 7074	1:1000	3% BSA in PBST
CSF-1	Abcam, 52864	1:1000	3% Milk in TBST	Anti-rabbit	Cell Signalling, 7074s	1:1000	3% BSA in PBST
CSF-1	Santa Cruz, sc-365779	1:1000	3% Milk in TBST	Anti-mouse	Cell Signalling; 7074	1:1000	3% BSA in PBST
CAIX	Abcam, ab107257	1:1000	3% BSA in PBST	Anti-mouse	Cell Signalling; 7074	1:1000	3% BSA in PBST
CAIX	Biosciences Slovakia, M75	1:1000	3% BSA in PBST	Anti-mouse	Cell Signalling; 7074	1:1000	3% BSA in PBST
GAPDH	Sigma-Aldrich, ab8245	1:1000	3% BSA in PBST	Anti-mouse	Cell Signalling; 7074	1:1000	3% BSA in PBST

Table 2.7. HEPG2 and mouse spleen lysates for positive controls were obtained from Dr Sadhbh O'Neill and Dr. Keith O'Brien. A549 cell lysate was obtained from Dr. Carsten Ehrhardt, School of Pharmacy, Dublin. HeLa lysates were obtained from Dr James Murray, School of Biochemistry with Immunology, TCD, Dublin.

2.4.4. Stripping buffer protocol

PVDF membrane stripping was performed using a mild stipping buffer (15g glycine, 1g SDS, 10 mL Tween 20, 800mL distilled water, pH to 2.2 and made up to 1 litre with distilled water. The stripping procedure was as follows: the membrane was covered and incubated at room temperature for 5–10 min, this step was repeated, the membrane was wased for 10min in PBS twice followed by two 5min washes in TBST.

Table 2.7: Conditions and antibody dilutions for immunoblotting

Antibody	*Company, Cat. #*	*Dilution*	*Antibody conditions*	*Secondary ab*	*Company, Cat. #*	*Dilution*	*Blot conditions*
CYP3A4	Santa Cruz, sc-53850	1:1000	3% BSA in PBST	Anti-mouse	Cell Signalling; 7074	1:1000	3% BSA in PBST
β-actin	Sigma-Aldrich, A5316	1:1000	3% BSA in PBST	Anti-mouse	Cell Signalling; 7074	1:1000	3% BSA in PBST
GRP-94	Cell Signalling, 2104S	1:1000	3% BSA in PBST	Anti-rabbit	Cell Signalling, 7074s	1:1000	3% BSA in PBST
ALIX	Abcam, ab76608	1:1000	3% BSA in PBST	Anti-rabbit	Cell Signalling, 7074s	1:1000	3% BSA in PBST
TSG101	Abcam, ab83	1:1000	3% BSA in PBST	Anti-mouse	Cell Signalling; 7074	1:1000	3% BSA in PBST
TLR3	Abcam, ab12085	1:50	3% Milk in TBST	Anti-mouse	Cell Signalling; 7074	1:1000	3% BSA in PBST
TLR3	Santa Cruz, sc-32232	1:500	3% Milk in TBST	Anti-mouse	Cell Signalling; 7074	1:1000	3% BSA in PBST
CSF-1	Abcam, 52864	1:1000	3% Milk in TBST	Anti-rabbit	Cell Signalling, 7074s	1:1000	3% BSA in PBST
CSF-1	Santa Cruz, sc-365779	1:1000	3% Milk in TBST	Anti-mouse	Cell Signalling; 7074	1:1000	3% BSA in PBST
CAIX	Abcam, ab107257	1:1000	3% BSA in PBST	Anti-mouse	Cell Signalling; 7074	1:1000	3% BSA in PBST
CAIX	Biosciences Slovakia, M75	1:1000	3% BSA in PBST	Anti-mouse	Cell Signalling; 7074	1:1000	3% BSA in PBST
GAPDH	Sigma-Aldrich, ab8245	1:1000	3% BSA in PBST	Anti-mouse	Cell Signalling; 7074	1:1000	3% BSA in PBST

2.5. CYP3A4 study

2.5.1. Wound healing assay

Dr Susan Breslin previously performed migration assays with EFM19.2A, EFM19.2A variants did not migrate through transwell chamber inserts (BD Bioscience, Cat. #: 353097). As an alternative, in this project the cells were seeded at $5x10^5$ cells/well in 24-well plates and wound-scratch assays were performed as previously described (131). For the equivalent wound healing assay with the HCC1954-Par and HCC1954-NR cell variants, cells were seeded at $2x10^4$ cells/well and this assay was carried out as described for the EFM19.2A cells.

2.5.2. CYP3A4 Ketoconazole treatments

Following completion of the P450-Glo CYP3A4 (Promega, Cat. #: V8801) assay in HCC1954-Par, HCC1954-NR, EFM19.2A-Par and EFM19.2A-NR cell line variants performed by Dr Breslin, it was decided to try to block CYP3A4 activity. To block CYP3A4 activity, HCC1954-NR cells were seeded at $3x10^3$ cells/well and EFM19.2A-NR cells were seeded at $5x10^3$ cells/well in 96-well plates. After 24hr, cells were exposed to 40nM ketoconazole alone or in combination with the IC_{50} concentrations of neratinib (325nM for HCC1954-NR cells and 46.7nM for EFM19.2A-NR cells) treatments for 5 days. The assay was evaluated using acid phosphatase (Section 2.3.3).

2.6. Extracellular vesicle isolation

2.6.1. Cell line-derived EVs

Cells were seeded at $1x10^6$ per T175cm^2 flasks for HCC1954 and SKBR3 cell line variants and at $2x10^6$ for EFM19.2A cell line variants. Cells were seeded in 5xT175cm^2 flasks (Corning, Cat. #: 431466) in complete medium and allowed to attach overnight. Media was replaced with medium containing 10% EV-depleted-FBS (dFBS), 2mM L-Glutamine and 1% penicillin/streptomycin. 1% penicillin/streptomycin was only used for dFBS media for EV isolations. To obtain dFBS, FBS was ultracentrifuged at 110,000g at 4ºC for 16hr. Due to the increased handling involved in EV-depletion of FBS, penicillin/streptomycin was used for the EV collection incubation period to prevent bacterial infections. Cells were grown in dFBS for 4/5 days. Once confluency reached 80%, cells were counted, cell

pellets were washed in PBS then stored at -80ºC for later DNA/RNA isolations, protein pellets were collected and stored at -20ºC for later use and conditioned media (CM) was collected from all flasks to isolate EVs using the ultracentrifugation method (Flow diagram, Figure 2.1). A preclearing step (centrifuge 200g, 4ºC, and 10min, followed by a second centrifugation at 2,000g 4ºC, 15min) was performed to remove cells and cellular debris. To further remove cells and debris, CM was then filtered (0.45µm filter, Pall Corporation, Cat. #: 4654) and transferred into polyallomer Bell-Top Quick-seal centrifuge tubes (Beckman Coulter, Cat. #: 344623). Using the SW 32 Ti swinging rotor (Beckman Coulter, Cat. #: 369650), CM was ultracentrifuged at 110,000g at 4ºC for 75min. EV pellets were washed in PBS, resuspended and placed in new UC tubes and ultracentrifuged again (110,000g at 4ºC for 75min). The EV pellet was re-suspended in 200µL PBS and stored in Protein LoBind tubes (Eppendorf®, Cat. #: 0030 108.116) at -80ºC for later analysis. For EV-protein isolation, EV pellets were resuspended in 30µL lysis buffer (Invitrogen, Cat. #: FNN0011) including protease inhibitors (Roche, Cat. #:05892970001). The EV sample was placed on ice for 30min with quick vortexing every 10min, the sample was centrifuged at 13,000g, 4ºC for 10min, the supernatant was removed and the protein pellets were stored at -20ºC, for future use. We have submitted all relevant data of our experiments to the EV-TRACK knowledgebase (EV-TRACK ID: EV180066) (132).

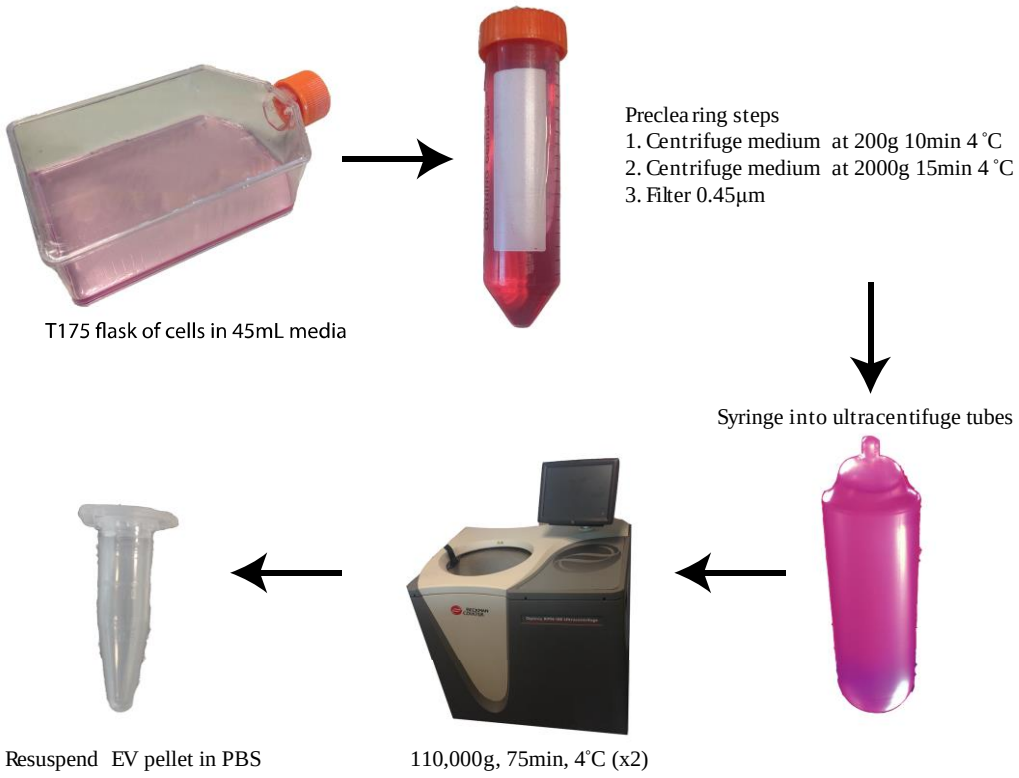

Figure 2.1 Flow diagram illustrating the EV isolation protocol from cell conditioned medium

2.6.2. Plasma specimen-derived EVs

Plasma specimens (200µL) were diluted in 5mL of ice-cold PBS. The plasma sample was then filtered (0.45µm filter, Pall Corporation, Cat. #: 4654) and transferred into polyallomer Bell-Top Quick-seal centrifuge tubes, ice-cold PBS was used to fill the up the remaining tubes (8mL tubes) (Beckman Coulter, Cat. #: 344621). Using the SW 32 Ti swinging rotor (Beckman Coulter, Cat. #: 369650), the plasma samples were ultracentrifuged at 110,000g at 4ºC for 75min. EV pellets were washed in PBS, resuspended and placed in new UC tubes and ultracentrifuged again (110,000g at 4ºC for 75min). The EV pellet was re-suspended in 200µL PBS and stored in Protein LoBind tubes (Eppendorf®, Cat. #: 0030 108.116) at -80ºC for later analysis.

2.7. EV quantification and characterisation

2.7.1. Nanoparticle tracking analysis (NTA)

Nanoparticle tracking analysis (NTA) was performed using the NTA NS300 system (NanoSight, Nanosight, Amesbury, UK). EV size distribution and concentration can be determined using NTA system which measures nanoparticles from 10nm to 2000nm. The concept the NTA system uses includes both light scattering and Brownian motion, upon nanoparticle impact on laser beams, the beams are scattered and visualized by 20X magnification. Brownian motion of the particles is observed by capturing 30 frames/sec. Filtered PBS (0.45µm filter, Pall Corporation, Cat. #: 4654) was used as a negative control. EV samples were diluted appropriately using filtered PBS, loaded onto the NTA using a NanoSight syringe pump and five 60sec videos were taken. The size of the particles was determined using the NTA software.

2.7.2. EV Immunoblotting

Total protein extraction, quantification and immunoblotting of EVs was performed as described in Section 2.4. 10µg total of cellular and EV protein was resolved on 10% bis-

acrylamide gels using the antibody conditions as described in

Antibody	*Company, Cat. #*	*Dilution*	*Antibody conditions*	*Secondary ab*	*Company, Cat. #*	*Dilution*	*Blot conditions*
CYP3A4	Santa Cruz, sc-53850	1:1000	3% BSA in PBST	Anti-mouse	Cell Signalling; 7074	1:1000	3% BSA in PBST
β-actin	Sigma-Aldrich, A5316	1:1000	3% BSA in PBST	Anti-mouse	Cell Signalling; 7074	1:1000	3% BSA in PBST
GRP-94	Cell Signalling, 2104S	1:1000	3% BSA in PBST	Anti-rabbit	Cell Signalling, 7074s	1:1000	3% BSA in PBST
ALIX	Abcam, ab76608	1:1000	3% BSA in PBST	Anti-rabbit	Cell Signalling, 7074s	1:1000	3% BSA in PBST
TSG101	Abcam, ab83	1:1000	3% BSA in PBST	Anti-mouse	Cell Signalling; 7074	1:1000	3% BSA in PBST
TLR3	Abcam, ab12085	1:50	3% Milk in TBST	Anti-mouse	Cell Signalling; 7074	1:1000	3% BSA in PBST
TLR3	Santa Cruz, sc-32232	1:500	3% Milk in TBST	Anti-mouse	Cell Signalling; 7074	1:1000	3% BSA in PBST
CSF-1	Abcam, 52864	1:1000	3% Milk in TBST	Anti-rabbit	Cell Signalling, 7074s	1:1000	3% BSA in PBST
CSF-1	Santa Cruz, sc-365779	1:1000	3% Milk in TBST	Anti-mouse	Cell Signalling; 7074	1:1000	3% BSA in PBST
CAIX	Abcam, ab107257	1:1000	3% BSA in PBST	Anti-mouse	Cell Signalling; 7074	1:1000	3% BSA in PBST
CAIX	Biosciences Slovakia, M75	1:1000	3% BSA in PBST	Anti-mouse	Cell Signalling; 7074	1:1000	3% BSA in PBST
GAPDH	Sigma-Aldrich, ab8245	1:1000	3% BSA in PBST	Anti-mouse	Cell Signalling; 7074	1:1000	3% BSA in PBST

Table 2.7. The markers used in this project are as per the MISEV guidelines ((133) (134)): GRP94 should be absent or under-represented in EV samples as it associated with the endoplasmic reticulum, TSG101 should be present or enriched in EVs as it is associated with the endosome and ALIX should be present or enriched in EVs as it is part of the ESCRT protein complex and CD63 (tetraspanin) should be present or enriched in EVs. The updated MISEV 2018 guidelines were submitted for publication to the Journal of Extracellular Vesicles in September 2018. Upon successful publication, all future EV work must coincide with the recommendations provided in this updated article.

2.7.3. Transmission electron microscopy (TEM) (EVs derived from cell line variants)

[TEM imaging of cell-derived EVs was performed in the Centre for Microscopy and Analysis in Trinity College Dublin, with the help of Neal Leddy, Chief Technical Officer]

A 10µL sample of EV suspension was placed onto parafilm (Sigma-Aldrich; Cat. #: P7793). A formvar carbon-coated nickel grid (Ted Pella Inc, Cat. #: 01813) was placed on top (coated-side facing the droplet) of the EV suspension droplet. The grid was incubated for 60min at room temperature, washed in 30µL of PBS (x3 times) on parafilm for 5min. Absorbent paper was used to remove excess PBS from the washing steps. A droplet of paraformaldehyde (2%) was placed on parafilm and the grid was placed on top and fixed for 10min. The PBS washing steps were repeated. The grid was then contrasted in 2% uranyl acetate (BDH, Cat. #: 230550) and all images were taken using the JEOL JEM-2100 transmission electron microscope at 120kV.

2.7.4. Transmission electron microscopy (TEM) (EVs derived from plasma specimens)

[Sample preparation was performed in the Centre for Microscopy and Analysis in Trinity College Dublin, with the help of Neal Leddy, Chief Technical Officer]

[TEM imaging of plasma specimen-derived EVs was performed in The CRANN Advanced Microscopy Laboratory, Trinity Technology and Enterprise Campus with the help of Dr Eoin K. McCarthy]

The TEM grids were prepared as described in Section 2.7.3. All images were taken using the JEOL JEM-2100 transmission electron microscope at 200kV.

2.7.5. Bicinchoninic acid assay (BCA)

Due to the limited volume of plasma available for this study and thus the limited amount of EV sample for analysis, the bicinchoninic acid assay (BCA) assay was used to determine the quantity of EVs by using EV protein as a surrogate marker for EV quantity. 10µL of EV samples were added to the BCA assay in duplicate. The assay was performed as previously described in Section 2.4.2.

2.8. Sequenom

[Sequenom was performed by Dr Sinead Toomey, Sequenom Core Facility, RSCI, Beaumont hospital, Dublin]

Sequenom is a mass spectrometry based-single nucleotide polymorphisms (SNPs) detection tool. Analysis of 284 genes was performed (list of genes in Appendix I).

2.8.1. DNA isolation

DNA was isolated from EFM19.2A, HCC1945 and SKBR3 cell line variants and their EVs using the QIAamp DNA mini kit (Qiagen, Cat #: 51304), according to the manufacturer's protocol. Cells were trypsinised and washed twice with 1 mL PBS and collected by centrifugation at 13,000g for 5min. The respective EVs were isolated as described in Section 2.6. 50µL of the EV suspension was added to 150µL of PBS, 400µL of PBS was added to the cell pellet from one T175 flask and 200µL of this was used for DNA isolation. 20µL of proteinase K solution was added to each sample, 200µL of Buffer AL was subsequently added and pulse-vortexed for 15sec. Samples were incubated at 56 ºC for 10min then briefly centrifuged. 200µL of ethanol (96%-100%) (Sigma, Cat. #: E7148) was added and pulse-vortexed for 15sec, samples were briefly centrifuged and carefully added to the QIAamp Mini spin column and centrifuged at 6000g for 1min. The filtrate was discarded and 500µL of Buffer AW1 was added and centrifuged again at 6000g for 1min. The filtrate was discarded and 500µL of Buffer AW2 was added and centrifuged at

20,000g for 3min. This step was repeated. The QIAamp Mini spin column was placed in a clean 1.5mL microcentrifuge tube and 50µL and 200µL of Buffer AE was added to EVs and cells respectively and incubated at room temperature for 5min to increase DNA yield. The columns were centrifuged at 6000g for 1min and the filtrate was collected, quantified by Qubit® 2.0 fluorometer (Invitrogen) (Section 2.8.2) and stored at -20ºC.

2.8.2. DNA quantification by Qubit

The Qubit was used to quantify dsDNA in the cells and their respective EVs. The Qubit dsDNA HS assay kit (Life Technologies, Cat. #: Q32851) was used as per manufacturer's protocol. The working solution was prepared by diluting the Qubit reagent (1:200) in Qubit buffer. The standards (Standard #1: 0ng/µl and Standard #2: 10ng/µl) were prepared, 10µL of each standard was diluted in 190µL working solution. 1µL of each sample was diluted in 199µL of working solution. Standards and samples were vortexed for 2-3sec and incubated at room temperature for 2min. Qubit calibration was first completed with the standards. Readings were then taken for all samples.

2.8.3. Sequenom protocol

The Sequenom MassARRAY® system is a DNA analysis platform that uses MALDI-TOF mass spectrometry to analyse DNA. Detection by MALDI-TOF mass spectrometry (MS) offers high sensitivity and accuracy.

In the first step an allele-specific PCR reaction takes place. The PCR primers are designed in a region of approximately 100 base pairs around the SNP of interest and an extension primer is designed immediately adjacent to the SNP.

Following the PCR, treatment with shrimp alkaline phosphatase (SAP) is performed in order to remove remaining, nonincorporated dNTPs from amplification products. SAP dephosphorylates unincorporated dNTPs by cleaving the phosphate groups from the 5′ termini.

The next step is a locus-specific primer extension reaction (iPLEX assay) in which an oligonucleotide primer anneals immediately upstream of the polymorphic site being genotyped. During the iPLEX reaction, the primer is extended by one mass-modified nucleotide depending on the allele and the design of the assay. Such a reaction mixture generates 55 allele specific products of different lengths, which allows easy interrogation by MALDI-TOF MS.

The primer extension reaction is then desalted, as cations are known to interfere with MALDI. This clean-up step is important to optimise mass spectrometry analysis of the extended reaction products. A slurry of resin is added directly to primer extension reaction products to remove salts such as Na+, K+, andMg2+ ions. If not removed, these ions can result in high background noise in the mass spectra. The analyte mixture is transferred to a SpectroCHIP® Array. The SpectroCHIP® Array is coated with a matrix which allows crystallization of the PCR product on its surface. The chip is placed into the mass spectrometer and a laser is fired at the crystal which ionizes the molecules. These ions travel through a vacuum tube to an ion detector based on their mass. Smaller molecules travel faster than larger ones. Time of flight measures the difference in time different molecules hit the detector and the software calculates the mass of the fragments. The primer's mass indicates the sequence and, therefore, the alleles present at the polymorphic site of interest. Sequenom supplies software (SpectroTYPER) that automatically translates the mass of the observed primers into a genotype for each reaction. A summary of the protocol is represented in Figure 2.2.

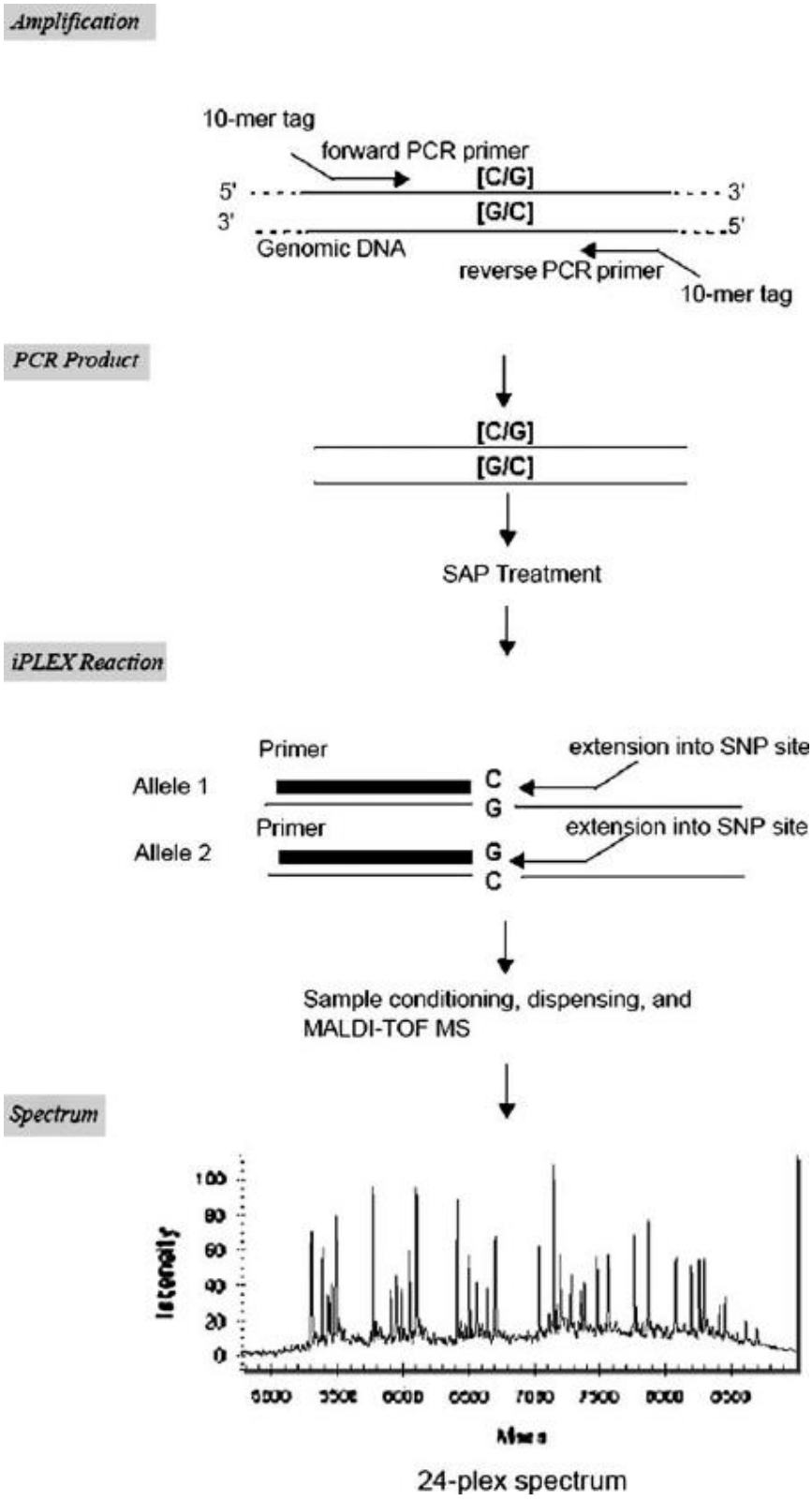

Figure 2.2: iPLEX Assay (The scheme depicts a single assay).
The starting point of the iPLEX assay is PCR amplification, followed by the addition of Shrimp Alkaline Phosphatase (SAP) to inactivate remaining nucleotides in the reaction. Following a brief incubation, the primer mixture is added and conducted using a standardised cycling programme, placed on a SpectroChip and analysed by MALDI-TOF MS.

2.9. Olink Proteomics

[Olink analysis was performed by Olink Proteomics AB, Uppsala, Sweden]

Olink proteomics provides a biomarker discovery service. This company uses high-quality multiplex immunoassay panels to identify multiple proteins. Each biomarker is identified by a matched pair of antibodies that are coupled to partially complementary oligonucleotides and then measured by real-time PCR. Cross-reactivity of antibodies is therefore excluded by the unique coupling of antibodies and oligonucleotides.

Protein extraction and quantification was performed as described in Section 2.4.1 and Section 2.4.2, respectively. 22µL of protein samples from both cells and their respective EVs were used per assay at a protein concentration of 0.5µg/µL. Protein samples were transported using a 96-well PCR plate (Sarstedt; Cat. #: 72.1980.202) with plate seal (Life Technologies, Cat. #: 4306311). Protein analysis was performed using the Inflammation and Oncology II multiplex panels (see Appendix I).

2.9.1. Olink multiplex protocol

All samples, the incubation stabilizer and the interpolate controls were thawed, vortexed, briefly centrifuged and incubated at room temperature for 1min. The incubation mix was prepared according to Table 2.8.

Incubation mix	**Per 96-well plate (µL)**
Incubation solution	280
Incubation stabilizer	40
A-probes	40
B-probes	40
TOTAL	400

Table 2.8 Incubation mix for Olink multiplex

Using a multichannel pipette, 3µL of the incubation mix was transferred to a 96-well plate. 1µL of each sample was added to the incubation mix in each well. 1µL of negative control and 1µL of interpolate control were added to control wells. The plate was sealed and centrifuged at 150g for 1min at room temperature. The plate was incubated overnight at

4ºC. The next day the PEA solution and the incubation plate were thawed, vortexed and briefly centrifuged. The extension mix was prepared according to Table 2.9.

Extension mix	**Per 96-well plate (µL)**
High purity water	9385
PEA solution	1100
PEA enzyme	55
PCR polymerase	22
TOTAL	10562

Table 2.9 Extension mix for Olink multiplex

Using a multichannel pipette, 96µL of the extension mix was added to each well of the incubation plate, the plate was sealed and centrifuged at 150g for 1min at room temperature. The plate was placed in the thermal cycler and the PEA program was performed according to Table 2.10.

PEA program	**Temperature (ºC)**	**Time**
Extension	50	20min
Hot start	95	5min
PCR cycle (x17)	95 54 60	30sec 1min 1min
Maintain reaction	10	∞

Table 2.10 PEA program for Olink multiplex

For the detection step, 96.96 Dynamic Array IFC was prepared and primed according to manufacturer's instructions. The primer plate and detection solutions were thawed, vortexed and briefly centrifuged. The detection solution was prepared according to Table 2.11.

Detection mix	**Per 96-well plate (µL)**
Detection solution	550
High purity water	230
Detection enzyme	7.8
PCR polymerase	3.1
TOTAL	790.9

Table 2.11 Detection mix for Olink multiplex

7.2µL of the detection mix was added to each well of a new 96-well plate (sample plate). 2.8µL of each sample from the incubation plate was added to the sample plate. The plate was sealed, vortexed and centrifuged at 150g for 1min at room temperature. 5µL from each well of the primer plate was added to the primed 96.96 Dynamic Array IFC. Primers and samples were loaded according to the Olink multiplex loading manual (Appendix I) and the Olink Protein Expression 96x96 Program was run on the chip (Table 2.12). Results are represented at Normalised Protein expression (NPX), an arbitrary unit on Log2 scale. Data pre-processing (normalisation) is performed to minimize both intra- and inter-assay variation.

Protein expression program	**Temperature (ºC)**	**Time**
Thermal Mix	50 70 25	120sec 1800sec 600sec
Hot start	95	300sec
PCR cycle (x40)	95 60	15sec 1min

Table 2.12 Protein expression program for Olink multiplex

2.10. Protein Validation (CAIX, CSF-1 and TLR3)

Cell pellets from EFM19.2A, HCC1954 and SKBR3 cell variants were collected, lysed and quantified as previously described in Sections 2.4.1 and 2.4.2 Immunoblotting for CAIX, macrophage colony-stimulating factor-1 (CSF-1) and toll-like receptor (TLR3) was carried out as described in Section 2.4.3 using 30µg of protein for each cell line in triplicate. Protein

samples were separated using 10% SDS-PAGE electrophoresis gels for CAIX and CSF-1 proteins. Protein samples for TLR3 analysis were separated on 8% gels.

2.10.1. CSF-1 ELISA

All cell line variants were seeded in dFBS media in T175 flasks and placed in normoxic conditions for 5days. Seeding densities were as follows; HCC1954 and SKBR3 cell line variants were seeded at $1x10^6$ cells/flask. Protein lysates were collected and quantified as described in Sections 2.4.1 and 2.4.2. Conditioned media was collected and EVs were isolated as in Section 2.7.

CSF-1 was quantified in all cell line variants and EVs by ELISA (Abcam, Cat. # ab100590) which was performed according to the manufacturers' instructions using 10µg of total cellular protein and 10µg of total EV protein diluted in PBS to bring total volume to 100µl.

2.10.2. Poly (I:C) treatment to activate TLR3

Poly(I:C) (Tocris Bioscience, Cat.#: 4287) was prepared freshly in RPMI media. HCC1954-Par and HCC1954-NR cell line variants were treated with Poly(I:C) for 24hr at 50 and 100µg/mL. Protein lysates were prepared and quantified as detailed in Section 2.4.

2.11. Bioinformatics

2.11.1. Heatmaps

Sample relationship and variability were assessed using hierarchical clustering and principle component analysis. This analysis was performed using R (http://www.r-project.org). Heatmap image production and analysis was performed on Olink protein expression data using the code displayed in Figure 2.3.

```
HEATMAP CODE (R-package)
# load libraries required
>library(ggplot2)
>library(gplots)
>library(heatmap.plus)
>library(RColorBrewer)
>pinkgreen<-brewer.pal(11, "PiYG")

# load data (df=data frame/data table)
df<-read.csv("onchccellsevs.csv", + header=TRUE, + row.names=1)

# change data to data matrix for analysis
df_matrix <- data.matrix(df)

# draw heatmap with visualization parameters
df_heatmap <- heatmap(df_matrix, Rowv=TRUE, Colv=TRUE, col = pinkgreen, scale="column", margins=c(5,10),
main="Oncology: HCC1954 samples", xlab="Sample", ylab= "Protein", cexCol=0.6, cexRow=0.6)

# Add heatmap colours and histogram
df_heatmap.2 <- heatmap.2(df_matrix, Rowv=TRUE, Colv=TRUE, col = pinkgreen, scale="column", margins=c(5,10),
main="Inflammation: SKBR3 samples", xlab="Sample", ylab= "Protein", cexCol=0.6, cexRow=0.6, key=TRUE,
density.info="none", keysize=1, tracecol=NA, symkey=TRUE)
```

Figure 2.3 Heatmap code used for R software
Code used for R software. This code was used to create a graphical representation of the Olink data using Heatmaps.

2.11.2. Volcano plots

Image and data analyses were computed and performed under R environment (http://www.r-project.org). The libraries used for this analyses were “ggplot2”, “dplyr” and “ggrepel”. The results were adjusted for multiple testing by Benjamini and Hochberg method to control false discovery rate. The list of differentially expressed proteins was obtained by the following criteria; adjusted *p-value* (represents the smallest family error rate at which a particular null hypothesis will be rejected) (calculated using the Benjamini and Hochberg test) and fold changes in protein levels between variants, and visualized by volcano plots. The code for the following analysis is displayed in Figure 2.4.

```
VOLCANO PLOT CODE (R-package)
# load libraries required
>library(ggplot2)
>library(dplyr)
>library(ggrepel)

# load sample excel file, named res for "results"
>res<-read.csv("hcccells.csv", header=TRUE)

# View res file to ensure correct headings etc
> print(res)

# Identify significant and non-significant entries based on pvalue and fold change
>results = mutate(res, sig=ifelse(res$pvalue<0.05, "log2FoldChange>0.27", "Not Sig"))

# Use ggplot to draw volcano plot of log2foldchange vs –log10(pvalue), colour various data points
>p = ggplot(results, aes(log2FoldChange, -log10(pvalue))) + geom_point(aes(col=sig)) + scale_color_manual(values=c("red",
"black"))

# perform Benjamini and Hochberg (BH) test on samples
>res$BH=p.adjust(res$pvalue, method="BH")

# Edit volcano plot of log2foldchange vs adjusted pvalue based on BH, with data points coloured as previously
>p+geom_text(data=filter(results, adjp<0.05 & log2FoldChange>0.27), aes(label=Protein))

# Use ggrepel to repel data names to avoid overlap
>p+geom_text_repel(data=filter(results, adjp<0.05 & log2FoldChange>0.27), aes(label=Protein))
```

Figure 2.4 Volcano plot code used for R software
Code used for R software. This code was used to create a graphical representation of the Olink data using Volcano plots.

2.12. CAIX ELISA

2.12.1. CAIX Duoset ELISA

CAIX was quantified in all cell line variants by ELISA (Carbonic Anhydrase IX DuoSet) (R&D systems, Cat. # DY2188) which was performed according to the manufacturers' instructions using 10µg of total cellular protein diluted in PBS to bring total volume to 100µl. All cell line variants were seeded in T75 flasks and placed in normoxic or hypoxic conditions (whitley H35 hypoxystation) for 24, 48 or 72hr. Seeding densities were as follows; BT474 and EFM19.2A cell line variants were seeded at $2x10^6$ cells/flask, $3x10^6$ cells/flask and $4.5x10^6$ cells/flask for 72, 48 and 24hr respectively. For all HCC1954 and SKBR3 cell line variants, cells were seeded at $1x10^6$ cells/flask, $1.5x10^6$ cells/flask and $2.25x10^6$ cells/flask for 72, 48 and 24hr respectively. For S4-treated cells, all cell line variants were seeded at the same densities and treated with 25µM S4 for 24, 48 or 72hr under hypoxic conditions, similarly for BT474-TR and SKBR3-TR, flasks were set up and also placed under both normoxic and hypoxic conditions.

CAIX expression was tested in CM of HCC1954-Par and HCC1954-NR. CM was collected from T75 flasks, centrifuged at 1500 rpm for 10min at 4°C, then aliquoted and stored at -80°C immediately.

2.12.2. CAIX Quantikine ELISA

CAIX was quantified in all plasma patient samples by ELISA (Carbonic Anhydrase IX Quantikine) (R&D systems, Cat. # DCA900) which was performed according to the manufacturers' instructions using 20µL of plasma diluted in 80µL PBS to bring total volume to 100µl.

For plasma-derived EVs, 100µL of EV suspension was added to each well. To test the quantity of CAIX in EV lysates, 30µL of EV suspension was lysed with 30µL lysis buffer containing protease inhibitors. Lysis procedure was carried out as described in Section 2.4.1. BCA assay was performed on EV lysates to determine CAIX levels per mg of protein as described in Section 2.4.2.

For cell-derived EV suspension, 50µL of EVs (from 200µL) was added to PBS so make up to 100µL and added to the ELISA. For EV lysates, 10µg EV lysates, diluted in PBS were added to the ELISA.

2.13. RNA extraction

Total RNA was isolated from pelleted cells in one T75 flask by extracting with TriReagent™ (Sigma Aldrich, Cat. #: T9424). In brief, 200µL of chloroform (Sigma-Aldrich, Cat. #:C4342) was added to each sample and this was shaken vigorously for 15secs, followed by incubation at room temperature for 10mins. This was then centrifuged at 13,200g for 15min at 4ºC and the aqueous phase containing RNA (upper layer) was removed and transferred into a fresh 1.5mLEppendorf tube (Sigma-Aldrich, Cat. #:Z606340). Ice-cold isopropanol (Sigma-50Aldrich, Cat. #: I9516) (0.5ml) and glycogen (Sigma-Aldrich Cat. #:G8751) (final concentration 120µg/ml) were added, incubated overnight at –20ºC, to ensure maximum RNA precipitation. Eppendorf tubes were then centrifuged at 13,200g for 30mins at 4ºC to pellet the precipitated RNA. The supernatant was removed and the pellet was subsequently washed by the addition of 750µl of 70% ethanol (Sigma-Aldrich, Cat. #: E7418) and vortexing. Following centrifugation at 7,500g for 5mins at 4ºC, supernatant was removed (this wash step was repeated). The RNA pellet was then allowed to air-dry for 5-20mins and subsequently was re-suspended in 30µl (for cell-derived RNA) of DEPC-treated H_2O (Ambion, Cat. #: AM9916). Quantity and quality of RNA isolated was assessed on the Nanodrop-ND 1000 spectrophotometer.

2.14. cDNA synthesis

2.14.1. miR-134

Synthesis of single stranded cDNA from total RNA samples (10ng of total RNA) was performed using the TaqMan MicroRNA Reverse Transcription (RT) Kit (Applied Biosystems, Cat. #: 4366597) and according to the Applied Biosystems protocol. In brief, each 15µL reaction (per single RNA sample) consisting of the components of the TaqMan MicroRNA Reverse Transcription Kit as outlined in Table 2.13 was prepared with the addition of 3µl RT Primer (TaqMan miRNA assays, miR-134 Cat. #: 001186) and 5µl (10ng) total RNA.

Reaction Mix	**Volume (µL)**
10x RT Buffer	1.5
RNase inhibitor	0.19
dNTP (100mM)	0.15
Nuclease-free water (Ambion, Cat. #: AM9920)	4.16
Multiscribe RTase (50U/µL)	1
5x RT primer	3

Table 2.13: Volumes of components used for RT Reaction for Taqman miRNA assays.

All components except for water were part of TaqMan MicroRNA Reverse Transcription Kit (Applied Biosystems, Cat. #: 4366597). The reactions were dispensed into a MicroAmp Fast Optical 96-well Reaction Plate (Applied Biosystems, Cat. #: 4346906). The plate was sealed with MicroAmp clear adhesive film (Applied Biosystems, Cat. # 4306311) and incubated on ice for 5mins. The reverse transcription was conducted in the ABI 9700 thermal cycler using standard ramp speed and the thermal cycling conditions indicated in Table 2.14.

Step	Time (min)	Temperature (ºC)
Hold	30	16
Hold	30	42
Hold	5	85
Hold	∞	4

Table 2.14: Thermal cycling conditions used for RT Reaction for Taqman miRNA assays.

2.14.2. MEG3/DLK1

Synthesis of single stranded cDNA from total RNA samples was performed. 1µl of Oligo dT primer (Eurofins MWG Operon) was added to 4µl of RNA (500ng) and incubated on ice for 10min. 15µl reaction (per single RNA sample) consisting of the components of the Reverse Transcription Kit as outlined in Table 2.15 was prepared and added to the RNA samples. Another RT reaction was set up without MMLV-RT as a negative control. Reverse transcription was performed for 1hr at 37ºC in the BIO-RAD DNA engine Peltier Thermal cycler.

Reaction Mix	Volume (µL)
10x Buffer Sigma (Sigma-Aldrich, Cat. #: B8559)	2
RNasin (40U/µL) (Sigma-Aldrich, Cat. #: R2520)	1
dNTP (10mM) (Invitrogen, Cat. #: 18427-013)	1
Nuclease-free water (Ambion, Cat. #: AM9920)	10
MMLV-RT (200U/µL) (Sigma-Aldrich, Cat. #: M1427)	1

Table 2.15: Volumes of components used for cDNA synthesis reaction

2.15. PCR Amplification

2.15.1. miR-134

PCR amplification was performed according to the Applied Biosystems protocol for TaqMan MicroRNA Assays. In brief, each 20µl reaction (per single cDNA sample) consisted of 10µl TaqMan 2X Universal PCR Master Mix, No AmpErase UNG (Applied Biosystems, Cat. #: 4440040), 7.67µl Nuclease-free water (Ambion, Cat. #: AM9920), 1µl 20X Taqman microRNA Assay mix, 1.33µl RT product. The reaction was mixed and dispensed into a single well (per reaction) of a MicroAmp Fast Optical 96-well Reaction

Plate (Applied Biosystems, Cat. #: 4346906). The plate was sealed with MicroAmp optical adhesive cover (Applied Biosystems, Cat. #: 4311971) and centrifuged briefly to spin down contents and eliminate any air bubbles. The PCR reaction was conducted in the ABI 9700 thermal cycler using standard ramp speed, 9600 emulation run mode and the thermal cycling conditions indicated in Table 2.16. Taqman miRNA assay (Applied Biosystems) was used to quantify miR-134 (Assay ID #: 001186;). miR-134 was quantified using the cycle threshold (CT) adjusting to the levels of RNU44 (Assay ID #:PN4427975) used as an endogenous control.

Step	**Temperature (ºC)**	**Time (min)**	
Hold	50	2	
Hold	95	10	
Denature *Anneal*	95 60	15 60	40 cycles

Table 2.16: Thermal cycling conditions used for real time PCR for Taqman miRNA assays.

2.15.2. MEG3/DLK1

PCR amplification was performed according to the Applied Biosystems protocol. In brief, each 20µl reaction (per single cDNA sample) consisted of 10µl TaqMan 2X Universal PCR Master Mix, No AmpErase UNG (Applied Biosystems, Cat. #: 4440048), 7µl Nuclease-free water (Ambion, Cat. #: AM9920), 1µl 20X Taqman mRNA Assay, 2µl RT product. Delta like non-canonical notch ligand 1 (DLK1) (Applied Biosystems, Cat. #: 4453320) and maternally expressed 3 (MEG3) (Applied Biosystems, Cat. #: 4448892) were quantified using the cycle threshold (CT) adjusting to the levels of GAPDH (Applied Biosystems, Cat. #: Hs03929097-g1). The PCR reaction was conducted using the ABI 9700 thermal cycler using standard ramp speed, 9600 emulation run mode and the thermal cycling conditions were as described in Table 2.17.

Step	**Temperature (ºC)**	**Time (min)**	
Hold	95	10	
Denature	95	15	40 cycles
Anneal	60	60	

Table 2.17: Thermal cycling conditions used for real time PCR for Taqman mRNA assays.

2.16. miR-134 transfection

TNBC cells (Hs578Ts(i)$_8$, HCC-1937 and HCC-1143) were seeded in 6-well plates according to Table 2.18 and allowed to adhere overnight. All cells were transfected with 30nM of miR-134 (Applied Biosystems, Cat. #: 4464066, ID: MC10341) or negative control (NC) (Applied Biosystems, Cat. #: 4464058, ID: Negative Control #1). The following day, 5µl of lipofectamine 2000 (Invitrogen, Cat #: 11668027) was diluted in 250µl of opti-MEM medium (Invitrogen, Cat #: 11058021) per well, inverted and incubated at room temperature for 5min. Similarly, miRNA mimic was diluted in 250µl of opti-MEM medium to a final concentration of 30nM, inverted and incubated for 5min. Following the incubation time, the lipofectamine/opti-MEM solution was added dropwise to the miRNA/opti-MEM solution and allowed to incubate for 20min. 500µl/per well of this solution was added dropwise to cells and incubated for 4hr at 37ºC/5% CO_2. Medium was then removed and cells were washed gently with fresh medium. Fresh medium was added to the cells and 24hr later cells were treated with Cisplatin (7.75µM-15µM) (Hospira UK Limited, Cat. #: PA437/4/7)) for 24hr. Toxicity was measured as described in Section 2.3 and the apoptosis assay was performed as described in Section 2.17.

Cell line	**Cell seeding density (cells/per well/2mLmedium)**
Hs578Ts(i)$_8$	$1.5x10^5$
HCC-1937	$1.0x10^5$
HCC-1143	$1.5x10^5$

Table 2.18: Seeding densities for miR-134 transfections

2.17. Apoptosis assay (Annexin/PI)

To analyse the effects of miR-134 on the induction of apoptosis in TNBC cell lines following 24hr cisplatin treatment, flow cytometric analysis using annexin-V-allophycocyanin (APC) (BD Biosciences, Cat #: 550474) and propodium iodide (PI)

staining solution (BD Biosciences, Cat #: 556463). CM (containing apoptotic cells/debris) was collected and used to neutralise trypsinised cells. Cells were pelleted and resuspended in 2mL of 1X binding buffer (BB) (0.1M HEPES (Sigma, Cat. #: H3375), 1.4M NaCl (MP Biomedicals LLC, Cat. #: 194848), 25mM $CaCl_2$ (Sigma, Cat. #: C5080), adjusted to pH 7.4), centrifuged at 200g and resuspended in 30µl 1X BB solution. 20µl of cell suspension was added to 5mL polystryrene round-bottomed tubes (Falcon, Cat #: 352054). 5µl of annexin and 5µl of PI was added to each tube. 70µl of 1X BB solution was added and incubated in the dark for 15min. 400µl of 1X BB solution was added and apoptosis was analysed on $2x10^4$ events/cells using BD Accuri™ C6 flow cytometer.

2.18. Clinical Trial Design (TCHL)

The TCHL trial was initially facilitated by All-Ireland Cooperative Oncology Research Group (ICORG) and completed by Cancer Trials Ireland in 2016. This trial was titled "A Phase II Neo-adjuvant Study Assessing TCH (Docetaxel, Carboplatin and Trastuzumab) and TCHL (Docetaxel, Carboplatin, Trastuzumab and Lapatinib) in HER-2 Positive Breast Cancer Patients. (TCHL Phase II)" (NCT01485926). This trial has completed its recruitment and is in the follow-up stage.

The primary objective of this trial was to assess the efficacy of TCH (docetaxel, carboplatin and trastuzumab), TCL (docetaxel, carboplatin and lapatinib) and TCHL (docetaxel, carboplatin, trastuzumab and lapatinib) in neo-adjuvant treatment of HER2+ breast cancer. This trial used pathological CR as the primary endpoint (Phase II). The secondary objectives of this trial were as follows; to assess the clinical response rate and overall response rate for docetaxel and carboplatin with trastuzumab or lapatinib alone or trastuzumab combined with lapatinib in HER-2 positive breast cancer, to assess the relationship between drug exposure and adverse events, to examine potential molecular and pharmacological markers of response to trastuzumab and lapatinib, to assess disease-free survival (DFS) and overall survival (OS) and to determine if prophylactic loperamide significantly reduces the number of diarrhoea -related adverse events.

Patients received 6 cycles of treatment. CR was defined as the absence of invasive carcinoma in breast tissue and lymph nodes. Partial response (PR) was defined as the presence of carcinoma in either or both the tumour and lymph nodes. No response (NoR) was defined as no change in the tumour or lymph nodes when compared to pre-treatment analysis.

Plasma specimens available for this study were taken at pre- and post-treatment time points. 88 patients were enrolled on this trial, 33 of which consented to blood specimens being taken for research purposes. 28 of which were available for this study. All details are outlines in Table 2.19.

Ethics approval to perform the translational studies described here was obtained from the Ethics Committees of each of the individual hospitals part-taking in this clinical trial. This included St. Vincent's University Hospital Ethics Committee, Beaumont Hospital Ethics Committee, Tallaght University Hospital/St. James's Hospital Joint Research Ethics Committee, and Cork University Hospital Ethics Committee.

Patient No.	*Age*	*Arm*	*Response to therapy*	*Primary tumour*	*Lymph nodes (regional)*	*Distant metastasis*	*Overall stage*	*Histological (hormone type)*
3	49.	TCL	NoR	T2	N0	MX	Stage IIA	HER2+, ER+, PR+
4	58.	TCHL	PR	T2	N0	M0	Stage IIA	HER2+, ER+, PR+
8	87.	TCL	CR	T2	N0	M0	Stage IIA	HER2+, ER+, PR-
9	46.	TCH	CR	T2	N1	M0	Stage IIB	HER2+, ER+, PR+
12	76.	TCL	NoR	T1	N1	M0	Stage IIA	HER2+, ER+, PR+
14	76.	TCH	CR	T3	N1	M0	Stage IIIA	HER2+, ER-, PR-
15	60.	TCL	CR	T4d	N1	M0	Stage IIIB	HER2+, ER-, PR-
17	62.	TCL	NoR	T2	N1	M0	Stage IIB	HER2+, ER+, PR-
18	57.	TCHL	PR	T2	N1	M0	Stage IIB	HER2+, ER-, PR-
20	75.	TCH	CR	T2	N0	M0	Stage IIA	HER2+ ER- PR-
26	58.	TCH	CR	T3	N2	M0	Stage IIIA	HER2+, ER+, PR+
29	52.	TCL	PR	T4d	N1	M0	Stage IIIB	HER2+, ER+, PR+
32	56.	TCH	CR	T3	N0	M0	Stage IIB	HER2+, ER-, PR-
34	55.	TCH	NoR	T2	N1	M0	Stage IIB	HER2+, ER-, PR-
39	59.	TCH	NoR	T2	N1	M0	Stage IIB	HER2+, ER+, PR+
42	49.	TCHL	NoR	T2	N1	M0	Stage IIB	HER2+ ER- PR-
44	60.	TCHL	CR	T3	N0	M0	Stage IIB	HER2+ ER+ PR+
45	52.	TCH	CR	T2	N0	M0	Stage IIA	HER2+ ER+ PR+
47	48.	TCHL	CR	T4b	N1	M0	Stage IIIB	HER2+ ER- PR-
48	45.	TCH	CR	T2	N1	M0	Stage IIB	HER2+ ER- PR-
49	46.	TCHL	CR	T3	N0	M0	Stage IIB	HER2+ ER- PR-
50	52.	TCH	CR	T2	N0	M0	Stage IIA	HER2+ ER- PR-
54	*51.*	*TCHL*	*PR*	*T2*	*N0*	*MO*	*Stage IIA*	*HER2+ ER- PR-*
61	47.	TCHL	CR	T2	N0	M0	Stage IIA	HER2+ ER- PR-
66	58.	TCHL	CR	T2	N0	M0	Stage IIA	HER2+ ER- PR+
72	69.	TCH	NoR	T1	N1	M0	Stage IIA	HER2+ ER+ PR+
87	45.	TCHL	PR	T2	N1	M0	Stage IIB	HER2+ ER+ PR+
88	70.	TCHL	PR	T1	N0	M0	Stage IA	HER2+ ER+ PR+

Table 2.19: Age and tumour details for patient samples used in this study

2.19. Statistical analysis

Statistical analysis of data was performed using GraphPad Prism. *P-values* were generated by Student's t-tests (paired, unless otherwise stated) or *ANOVA* (performed using Tukey's post hoc test) (tests stated in every Figure), where $p<0.05$ was considered as statistically significant. Results are displayed as n=3 ± standard error of the mean (SEM). Graphs were generated using GraphPad Prism 5.00.

The Benjamini–Hochberg test (as part of the SPSS software program) was used to discover type I errors (rejection of a true null hypothesis (also known as a "false positive" finding), type II error is failing to reject a false hypothesis (also known as a "false negative" finding)) to control for false discoveries (135).

Grubbs' test is part of the Graphpad software and is used to detect a single outlier in a univariate data set that follows an approximately normal distribution.

Spearman correlation values and *p*-values were calculated using the Spearman Rank two-tailed Spearman rank test using GraphPad Prism 5.00. An r value of 1 indicates a perfect correlation. Values >0 but <1 indicates two variable tend to increase or decrease together. A value of 0 indicates that the two variables do not vary together at all. R value of -1 to <0 indicates that one variable increases as the other decreases and a value of -1.0 indicates a perfect negative or inverse correlation.

Compusyn (ComboSyn Inc, www.combosyn.com) analysis was performed to determine the effects of combination therapies. A fixed ratio was used for drug combinations. The synergy quantification is performed using the Chou-Talalay method (136). The combination index levels were calculated and defined according to Table 2.20 as described by Chou (137).

Range of Combination Index	*Description*
<0.1	Very strong synergism
>0.1-0.3	Strong synergism
>0.3-0.7	Synergism
>0.7-0.85	Moderate synergism
>0.85-0.9	Slight synergism
>0.9-1.1	Nearly additive
>1.1-1.2	Slight antagonism
>1.2-1.45	Moderate antagonism
>1.45-3.3	Antagonism
>3.3-10	Strong antagonism
>10	Very strong antagonism

Table 2.20: Compusyn synergy value definitions

CHAPTER THREE: TLR3, CSF-1 and CAIX: Potential mechanisms of acquired neratinib-resistance in HER2+ breast cancer cells and in their EVs

Parts of this chapter are published in the following peer-reviewed article and reviews:

- Neratinib-resistance and cross-resistance to other HER2-targeted drugs due to increased activity of metabolism enzyme cytochrome P4503A4. Breslin S*, Lowry MC*, O'Driscoll L. British Journal of Cancer. 2017 Feb 28;116(5):620-625.
- Can hi-jacking hypoxia inhibit extracellular vesicles in cancer. Lowry MC, O'Driscoll L. Drug Discovery Today. 2018 Jun;23(6):1267-1273.
- The Role of Exosomes in Breast Cancer. Lowry MC, Gallagher WM, O'Driscoll L. Clinical Chemistry. 2015 Dec;61(12):1457-65.

3. Abstract

Neratinib is a small tyrosine kinase inhibitor that irreversibly binds to EGFR, HER2 and HER4, thus preventing HER2 dimerisation and therefore preventing HER2-mediated signalling. Neratinib was approved for extended adjuvant treatment of early stage HER2-positive breast cancer by the Food and Drug Administration (FDA) in July 2017. Here, we sought to investigate the potential mechanisms of neratinib drug resistance in HER2+ breast cancer cell lines.

In this study, to investigate the mechanisms of acquired neratinib-resistance in cell line variants (EFM19.2A, HCC1954 and SKBR3), we have sequenced the DNA and profiled the protein of cell line variants and their derived EVs. Three SNPs were identified in the cell line variants, but were determined to be cell line-specific. Following proteomic profiling of 181 proteins in neratinib-sensitive and neratinib-resistant cell line variants, three proteins (TLR3, CSF-1 and CAIX) were identified as possible candidates to be involved in the mechanisms of drug resistance.

Following bioinformatics analysis and immunoblotting validation of the three proteins of interest, we identified CAIX as the lead protein to be further tested to elucidate if it is likely to be causally involved in the mechanisms of neratinib-resistance in HER2+ breast cancer.

3.1. Introduction

3.1.1. Mechanisms of neratinib drug resistance

As discussed in Section 1.4, drug resistance is a major obstacle in breast cancer treatment; patients can be innately resistant to therapies or acquire resistance to therapies over time. Neratinib was approved by the FDA for extended adjuvant treatment of early stage HER2-positive breast cancer in 2017 and recommended for marketing by the EMA in June 2018. Resistance has, however, been observed in clinics and we have shown acquired neratinib-resistance in our cell lines. EVs have been studied with respect to drug resistance (as discussed in Section 1.5.4), however, to our knowledge this is the first study investigating EVs in neratinib-resistant cell lines.

3.1.2. Aims

In this study, we aimed to develop a HER2+ neratinib-resistant cell line. We aimed to investigate the differences between neratinib-sensitive cell line variants and neratinib-resistant cells line variants, notably to investigate the DNA and protein-content of these cell line variants. The overall aim of this study was to determine a potential target associated with mechanisms of neratinib-resistance in HER2+ breast cancer cell lines. Similarly, the targets would be investigated in EVs derived from neratinib-sensitive cell line variants and neratinib-resistant cell line variants.

3.2. Results

3.2.1. Increased cell aggression

[Dr Susan Breslin has previously established HCC1954-NR (6.5 fold more resistant than HCC1954-Par) and EFM19.2A-NR (note: results as per publication, EFM192A cell are also termed EFM19.2A) (6.8 fold more resistant than EFM19.2A-Par). It was shown that HCC1954-NR cells were more resistant to anoikis with only 2.8±0.2% of HCC1954-NR cell death, compared to 12±1.7% of HCC1954-Par cells. HCC1954-NR cells were significantly more migratory than HCC1954-Par by 1.3-fold (when assessed using transwell assays). Similarly, for EFM19.2A-NR cells, where only 24.7±1.1% of EFM19.2A-NR cells died compared to 33.7±0.8% of EFM19.2A-Par cells. Using the wound healing assay, EFM19.2A-NR demonstrated 17% increased wound closure after 48hr compared to EFM19.2A Par cells.]

To follow-up on this work, in this thesis, using the wound healing assay, at 48hr, HCC1954-NR cells demonstrated 21% increased wound closure (*i.e.* migration) when compared to HCC1954-Par (Figure 3.1) (*p-value*=0.0481).

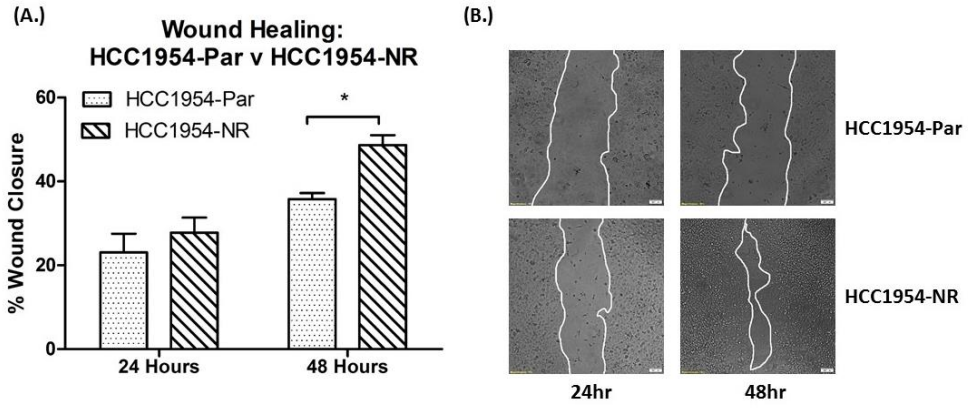

Figure 3.1: Wound healing assay of HCC1954-Par and HCC1954-NR cells
Graphical representation of wound healing assays for 24hr- and 48hr-post scratch (A.). Wound closure images are shown for 24 and 48hr in both cell lines (B.) n=3±SEM, *p<0.05. (Student's t-test).

3.2.2. CYP3A4 analysis

[Dr Susan Breslin had established that CYP3A4 activity was significantly increased in both the HCC1954-NR and EFM19.2A-NR cell line variants compared to their drug-sensitive counterparts. Specifically, the HCC1954-NR cells had 2.9±0.3-fold increased CYP3A4 activity when compared to HCC1954-Par cells ($p<0.01$). Similarly, EFM19.2A-NR cells displayed 1.5±0.2-fold increased CYP3A4 activity compared to EFM19.2A-Par control cells ($p<0.05$)].

In this thesis, ketoconazole was found to have little to no toxic effects on HCC1954-NR and EFM19.2A-NR cell line variants (Figure 3.2). CYP3A4 protein expression levels were found not to change significantly between the drug-resistant and drug-sensitive counterparts (Figure 3.3 (A.)). Blocking CYP3A4 activity was performed using CYP3A4 inhibitor, ketoconazole at 40nM (as selected as per previous results published by (138) and as per cytotoxicity assays (Figure 3.2)). To establish if blocking CYP3A4 could help to at least partially restore neratinib sensitivity, HCC1954-NR and EFM19.2A-NR were treated with neratinib IC_{50} values and 40nM ketoconazole and showed a small (4.4% for HCC1954-NR and 17.4% for EFM19.2A-NR, respectively) but significant restoration of neratinib sensitivity (Figure 3.3 (B.)).

(A.) **EFM192A-NR cells with ketoconazole treatment**

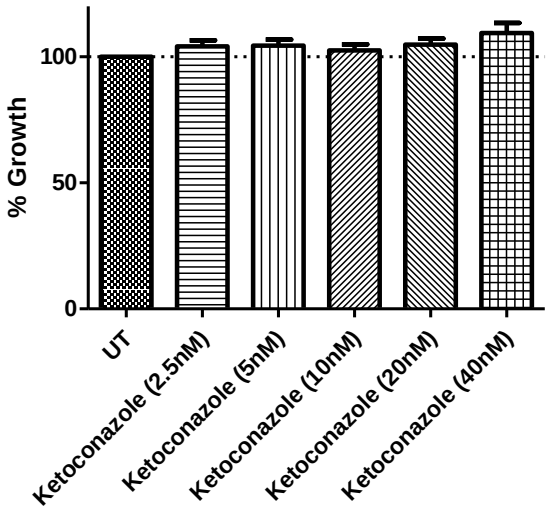

(B.) **HCC1954 NR cells with ketoconazole treatment**

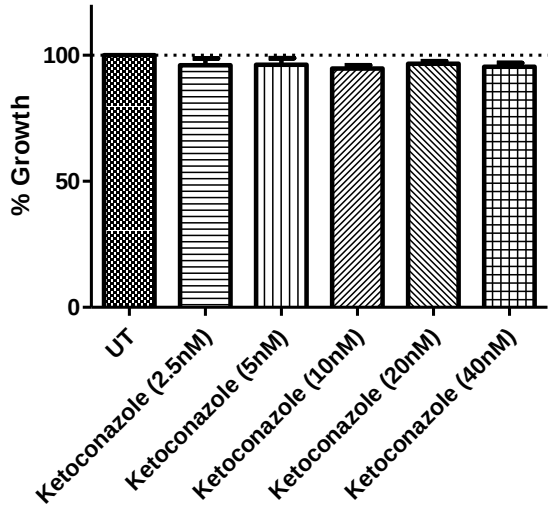

Figure 3.2: In vitro cytotoxicity results for ketoconazole treatment of HCC1954-NR and EFM19.2A-NR cell line variants

Acid phosphatase assay was used to determine the level of ketoconazole toxicity in HCC1954-NR (A.) and EFM19.2A-NR (B.) cell line variants (n=3±SEM) (*ANOVA*, Tukey's post hoc test).

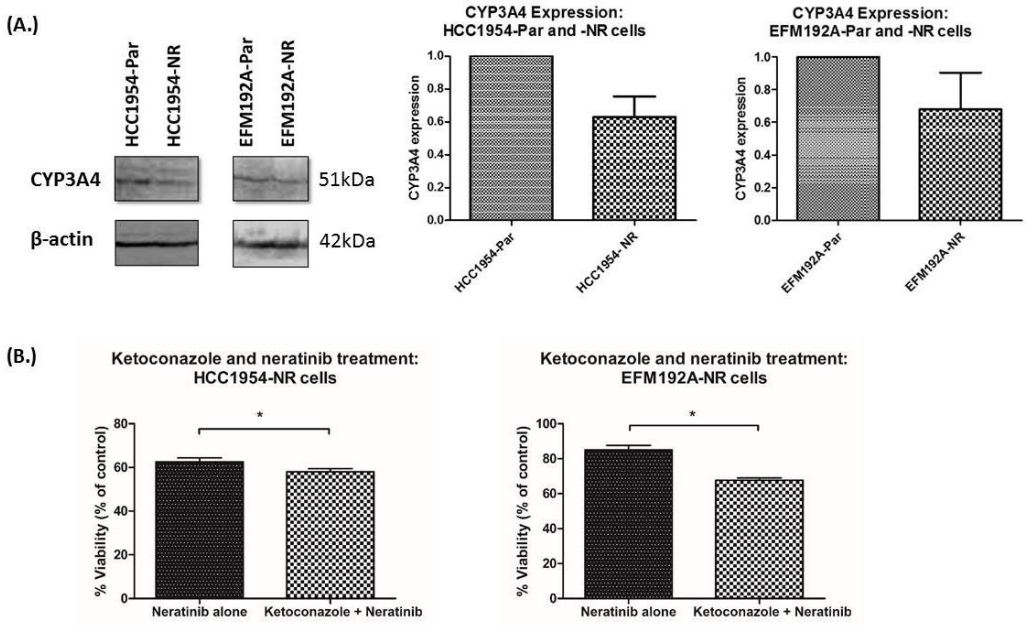

Figure 3.3 Investigation of CYP3A4 in HCC1954 and EFM19.2A cell lines
Representative immunoblots showing CYP3A4 protein expression in HCC1954-Par and HCC1954-NR cells and EFM19.2A-Par and EFM19.2A-NR cells (A.). Densitometry from HCC1954-Par and HCC1954-NR immunoblots and EFM19.2A-Par and EFM19.2A-NR immunoblots. For patental cell line variants, CYP3A4 expression was set to 1, CYP3A4 expression in NR-variants was normalized to 1 (A). Co-administration of ketoconazole and neratinib significantly decreased cell viability in both HCC1954-NR and EFM19.2A-NR cells when compared to neratinib alone (B). n=3±SEM, *p<0.05 (Student's t-test).

3.2.3. Establishment of SKBR3 neratinib-resistant variants

As described in Section 2.2, the SKBR3-NR cell line was developed over a period of 6 months by stepwise increased concentrations (0-80nM) of neratinib. Aged-matched SKBR3-Par (neratinib-sensitive) cells were maintained in culture during the duration of NR establishment.

3.2.4. Characterisation of SKBR3 neratinib-sensitive and neratinib-resistant cell lines

Toxicity assays were performed to determine the IC_{50} of neratinib for both SKBR3-Par and SKBR3-NR. The IC_{50} value for neratinib in SKBR3-Par was found to be approximately 9nM (R^2=0.98). The IC_{50} value for SKBR3-NR was approximately 74nM (R^2=0.98). This

indicated that the SKBR3-NR cell line has an 8.2 fold increase in resistance when compared to SKBR3-Par (Figure 3.4 and Table 3.1)

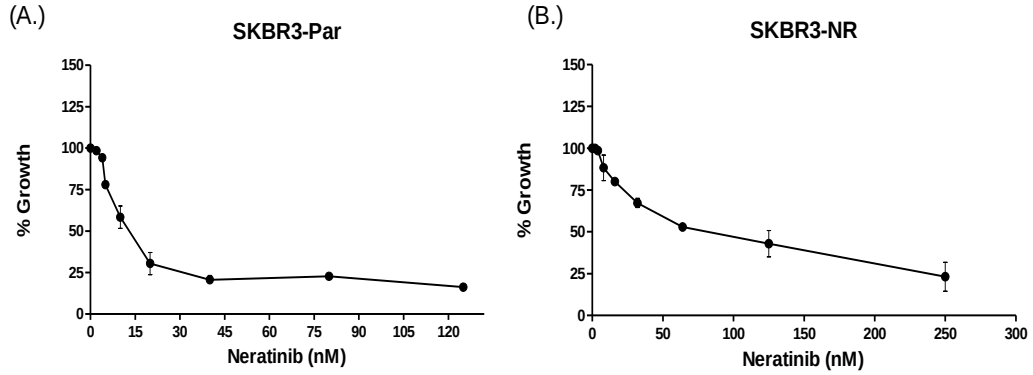

Figure 3.4: In vitro cytotoxicity results for SKBR3 parent and neratinib-resistant cell line variants
IC_{50} values were calculated for both SKBR3-Par (A.) and SKBR3-NR (B.) cell line variants using acid phosphatase assays. (n=3 ± SEM).

Cell line	*SKBR3-Par*	*SKBR3-NR*
IC_{50}	9nM	74nM
Fold difference		8.2±1.08

Table 3.1: SKBR3 cell lines IC_{50} values and fold difference
IC_{50} results for SKBR3 parent and neratinib-resistant cell line variants derived from Figure 3.4. (n=3).

3.2.5. EV characterisation from HER2+ neratinib-sensitive and neratinib-resistant cell line variants

To confirm successful EV isolation as described in Section 2.6, characterisation of EVs from HER2+ EFM19.2A, HCC1954 and SKBR3 cell line variants were performed (Figure 3.5). Immunoblotting for the negative marker (GRP-94) and positive markers (ALIX, TSG101) confirmed the presence of EVs in EFM19.2A-, HCC1954- and SKBR3 cell line variant-derived EVs (Figure 3.5 (A.)). Protein quantification using a BCA assay was performed as a surrogate measurement of the quantity of EVs in all cell line variants (Figure 3.5 (B.)). Nanoparticle tracking analysis was performed using a NanoSight and revealed that the vesicles isolated using this method ranged between 106-144nm in diameter (Figure

3.5 (C.)). TEM was used to determine the size and morphology of EVs (Figure 3.5 (D.)). The EV-track score for this study is 78% (98th percentile of all experiments).

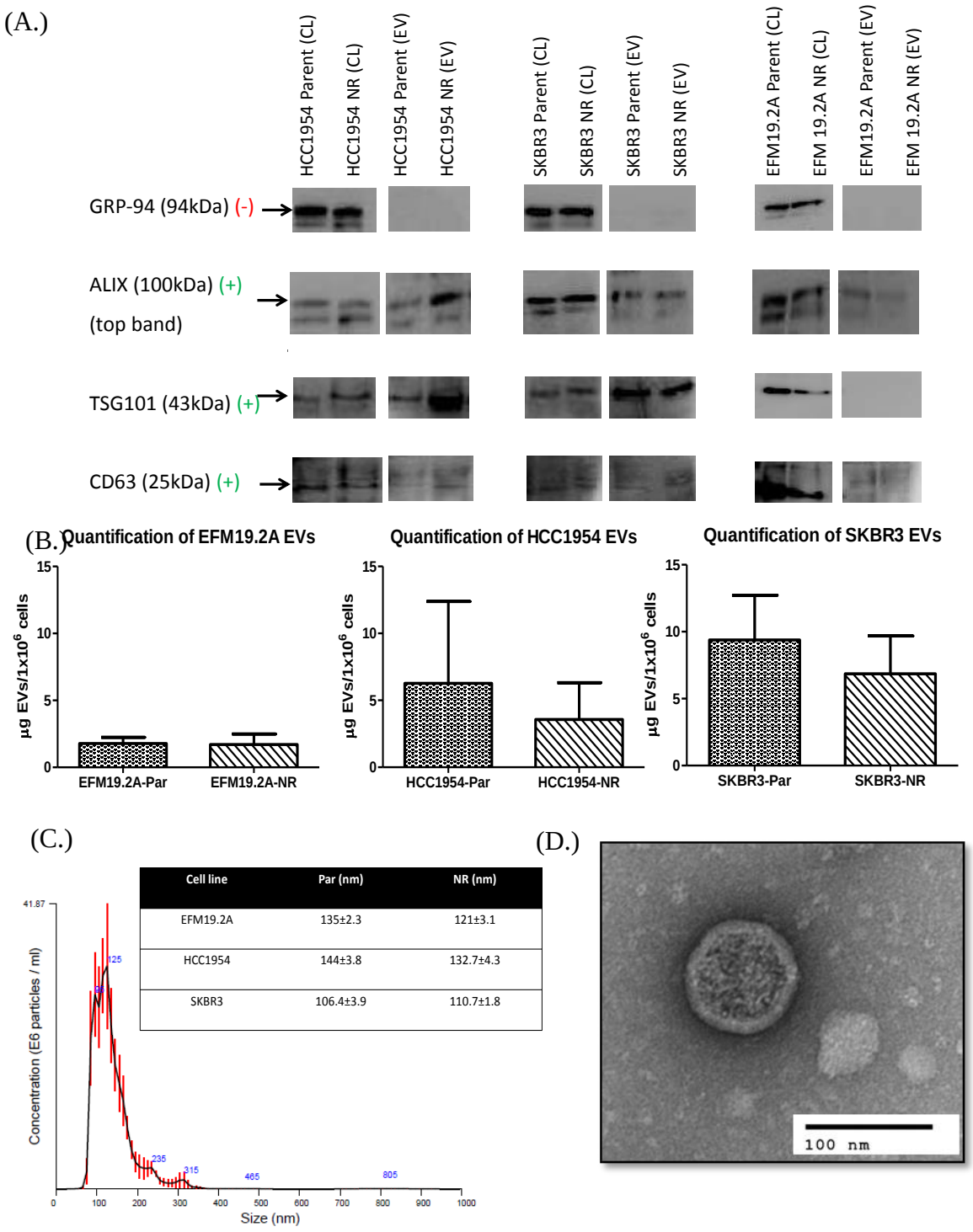

Figure 3.5: EV characterisation

EV characterisation was performed. (A.) Immunoblotting successfully detected the EV negative marker (GRP-94) and EV positive markers (ALIX and TSG101). BCA analysis was performed as a surrogate for determining the number of particles (B.). NTA analysis determined the mean diameter of EVs, image shown is representative of all cell lines (C.). TEM image is representative of EVs (D.). (n=3 ± SEM) (Student's t-test).

3.2.6. Sequenom

3.2.6.1. dsDNA is present in EFM19.2A, HCC1954 and SKBR3 cells and their respective EVs

DNA was isolated from cells and their respective EVs and then quantified using Qubit. The high sensitivity kit quantified dsDNA (see Section 2.8.2) from cell and EV samples. No significant differences in DNA quantities were observed between EFM19.2A-Par and EFM19.2A-NR (*p-value*=0.69), HCC1954-Par and HCC1954-NR (*p-value*=0.89) and SKBR3-Par and SKBR3-NR cells (*p-value*=0.73) (Figure 3.6 (A.)). Interestingly, dsDNA was present in EVs (Figure 3.6. (B.)). There were no significant differences in EV-derived DNA concentrations when comparing sensitive and neratinib EFM19.2A ((*p-value*=0.14), HCC1954 (*p-value*=0.85) and SKBR3 (*p-value*=0.08) cells.

(A.)

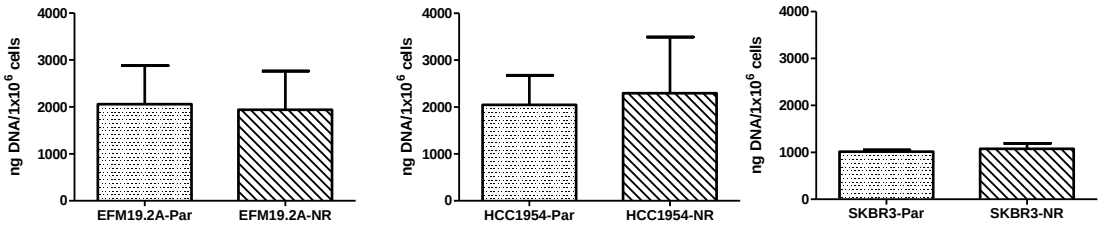

(B.)

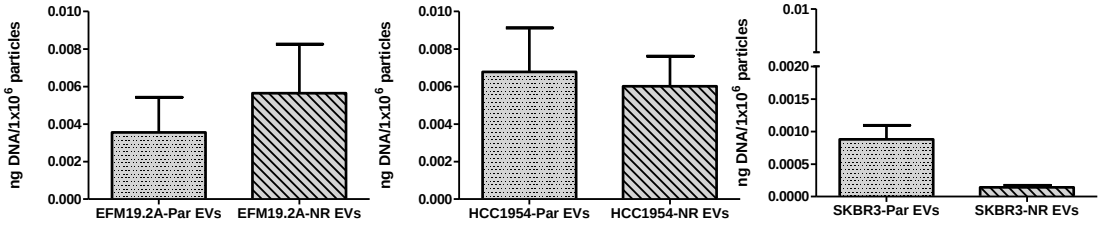

Figure 3.6: Cellular DNA and EV DNA concentrations
A Qubit was used to quantify DNA isolated from cells and EVs. Cellular DNA (A.) is represented per $1x10^6$ cells for EFM19.2A, HCC1954 and SKBR3 variants, respectively. DNA quantities for EFM19.2A-derived EVs, HCC1954-derived EVs and SKBR3-derived EVs (B.) are shown. (n=3 ± SEM) (Student's t-test).

3.2.6.2. dsDNA mutations

[Sequenom was performed on EFM19.2A, HCC1954 and SKBR3 cell line variants and their derived EVs by Dr Sinead Toomey, Sequenom Core Facility, RSCI, Beaumont hospital, Dublin.]

Sequenom analysis was performed for 284 SNPs spanning over 47 genes (APPENDIX I) using DNA from neratinib-sensitive and neratinib-resistant EFM19.2A, HCC1954 and SKBR3 cell line variants and using DNA from their respective EVs. This analysis revealed two mutations in PIK3CA gene in both HCC1954-Par and HCC1954-NR cell lines and their EVs. A further mutation was found in PIK3R1 in these cell lines and their respective EVs. A mutation in the PHLPP2 gene was found in all EFM19.2A cells and EVs. No mutations were found in SKBR3 parent and NR cell lines or EVs. This information is summarised in Figure 3.7.

Figure 3.7: SNP analysis in cell line variants and EVs
Summary diagram of results from sequenom SNP analysis of DNA isolated from all cell line variants and their respective EVs.

3.2.7. Olink proteomics

[Olink protein proteomics was performed on protein isolated from HCC1954-Par, SKBR3-Par, HCC1954-NR and SKBR3-NR as well as protein from the EVs derived from these cell line variants.]

On receiving the data, analysis was performed (as described in Section 2.9) on all 181 proteins evaluated (APPENDIX I).

3.2.7.1. Protein quantification of HCC1954 and SKBR3 cell line variants and their respective EVs

Protein was isolated from cells and their respective EVs and quantified by BCA analysis. No significant differences were observed between HCC1954-Par and HCC1954-NR (*p-value*= 0.11) (Figure 3.8 (A.)) and SKBR3-Par and SKBR3-NR (*p-value*= 0.37) cell line variants (Figure 3.8 (B.)). Similarly, no difference were observed between protein quantities in HCC1954-Par and HCC1954-NR EVs (*p-value*= 0.35) (Figure 3.8 (A.)) and for SKBR3-Par and SKBR3-NR EVs (*p-value*= 0.89) (Figure 3.8 (B.)).

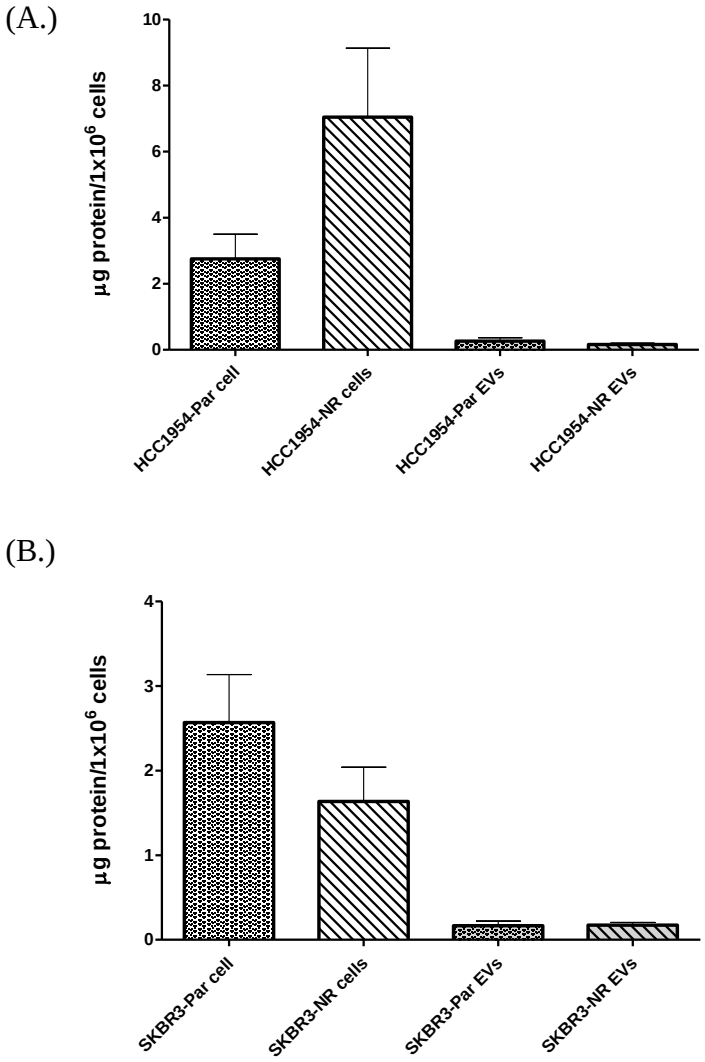

Figure 3.8: Cellular protein and EV protein concentrations
BCA analysis was used to quantify protein from cell line variants and EVs. Cellular and EV-derived protein are represented per $1x10^6$ cells for HCC1954 cell variants and EVs (A.) and SKBR3 cell line variants and EVs (B.). (n=3) ±SEM. (student's t-test).

3.2.7.2. Bioinformatics analysis (Olink data)

Heatmap data representation
Proteomic analysis was performed using the data generated by Olink proteomics to evaluate protein expression differences between parent and neratinib-resistant variants. Heatmaps were generated using R software and sample relationship and variability were assessed using hierarchical clustering. Heatmaps are represented according to the Olink inflammation and oncology panels as HCC1954-Par and HCC1954-NR cell line variants and EVs (inflammation in Figure 3.9; oncology in Figure 3.10) and SKBR3-Par and

SKBR3-NR cell line variants and their EVs (inflammation in Figure 3.11; oncology in Figure 3.12). The green colour represents the maximum expression levels and the pink colour represents the lowest expression levels for each protein of interest.

Hierarchical clustering was performed on all proteins in the panels, thus each heatmap grouped the proteins together according to similarities in expression levels (*y-axis*). As evidenced from this, the expression patterns of proteins were evidently different. Thus, indicating that there was no evidence that a complete pathway was altered when comparing neratinib-sensitive variants with neratinib-resistant variants, as all proteins that are clustered together are indicative of different biological pathways (as seen for all cell line variants and each panel). Similarly, when comparing hierarchical clustering for the protein samples (*i.e.* each group of n=3 for each cell line variant and their derived EVs), all 3 samples were not grouped together, showing that there was slight variability either between the n=3 biological repeats or variability in readings from the proteomic platform itself. Interestingly, when comparing protein expression patterns between cell line variants and their derived EVs, there were visible differences for HCC1954 (Figure 3.9 and Figure 3.10). Similarly, for SKBR3 cell line variants and EVs (Figure 3.11 and Figure 3.12) the protein expression patterns were visibly different when comparing cells to EVs, in particular in the oncology panel of proteins.

Figure 3.9 Heatmap plot for inflammation panel of proteins detected HCC1954 cell line variants and EVs

Heatmap representing the differences in protein levels between HCC1954-Par and HCC1954-NR cells and EVs. Triplicate samples are shown as 1,2 and 3. Cells and EVs are coded as follows; HCC1954-Par cells (HCCP), HCC1954-NR cells (HCCNR), HCC1954-Par EVs (HCCPEV) and HCC1954-NR EVs (HCCNREV).

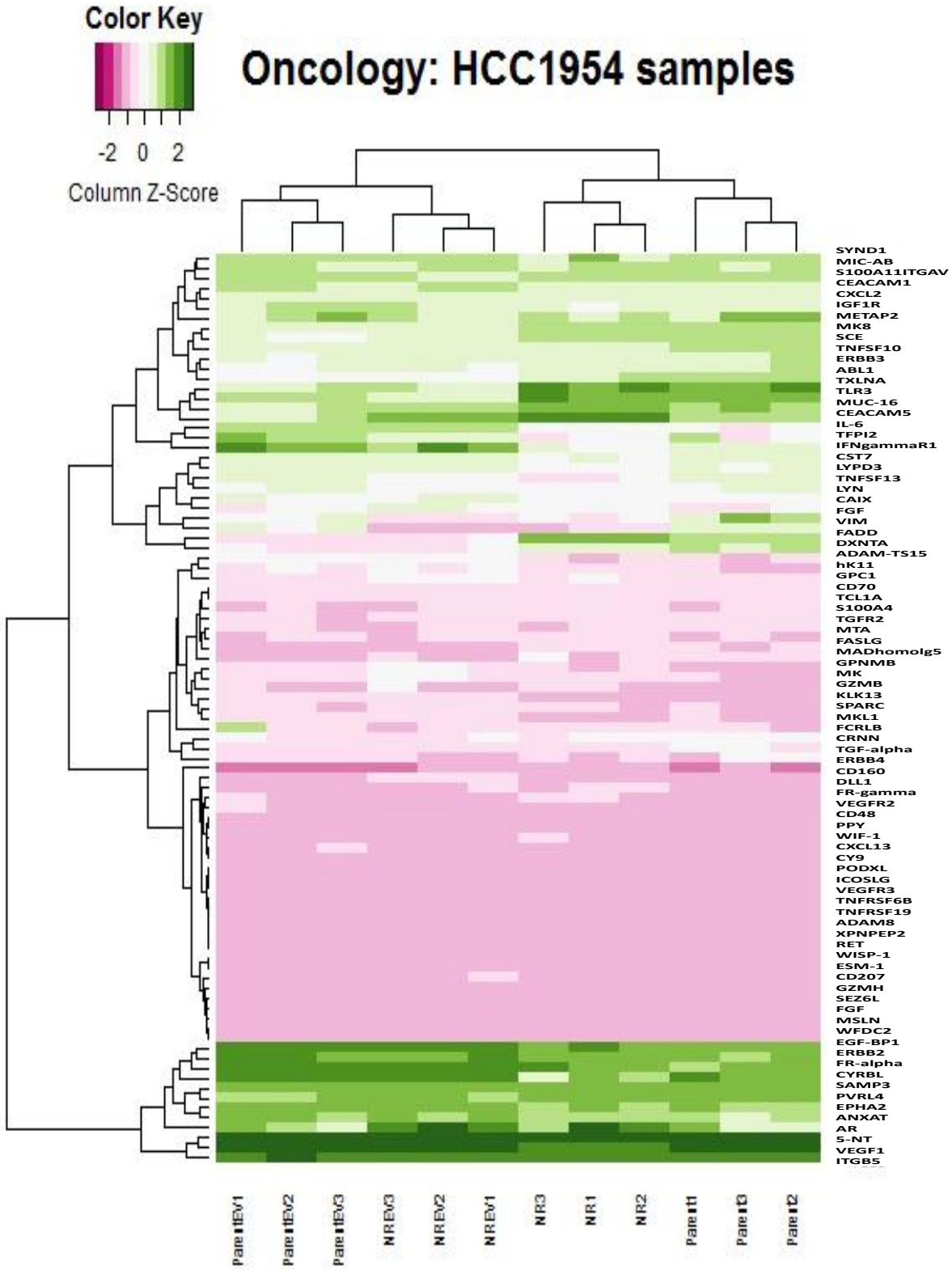

Figure 3.10 Heatmap plot for oncology panel of proteins detected HCC1954 cell line variants and EVs

Heatmap representing the differences in protein levels between HCC1954-Par and HCC1954-NR cells and EVs. Triplicate samples are shown as 1,2 and 3. Cells and EVs are coded as follows; HCC1954-Par cells (HCCP), HCC1954-NR cells (HCCNR), HCC1954-Par EVs (HCCPEV) and HCC1954-NR EVs (HCCNREV).

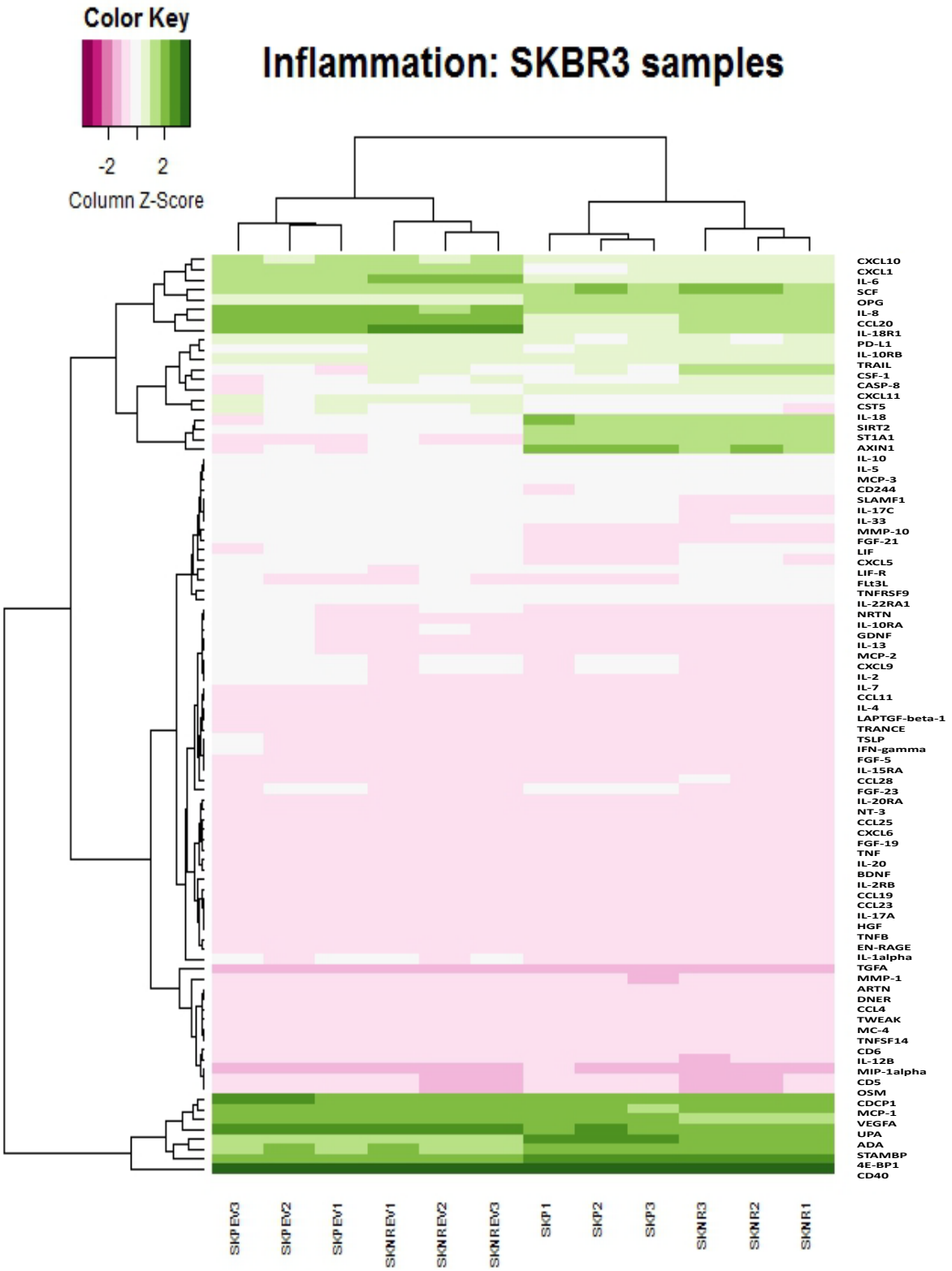

Figure 3.11 Heatmap plot for inflammation panel of proteins detected SKBR3 cell line variants and EVs

Heatmap representing the differences in protein levels between SKBR3-Par and SKBR3-NR cells and EVs. Triplicate samples are shown as 1,2 and 3. Cells and EVs are coded as follows; SKBR3-Par cells (SKP), SKBR3-NR cells (SKNR), SKBR3-Par EVs (SKPEV) and SKBR3-NR EVs (SKNREV).

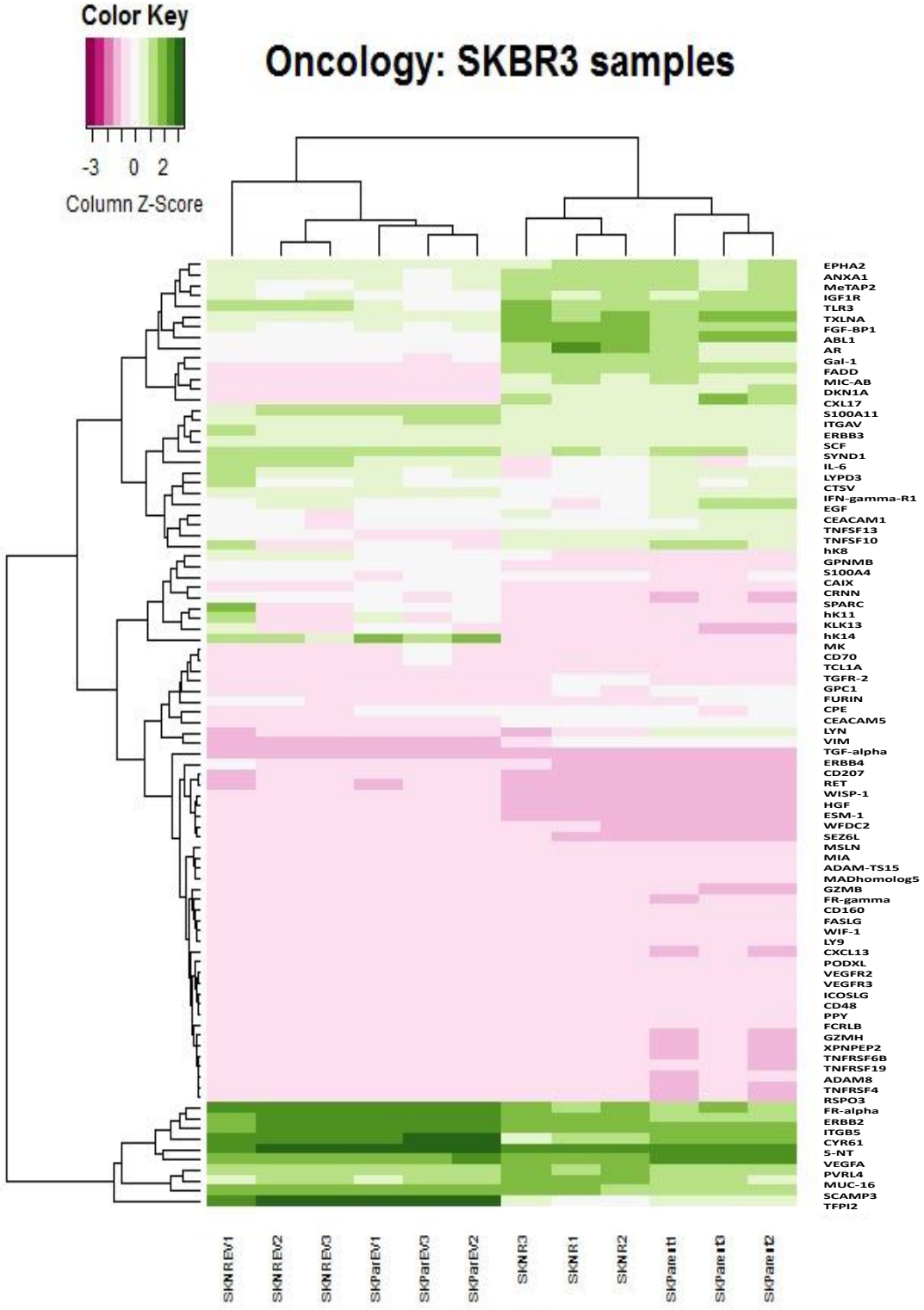

Figure 3.12 Heatmap plot for oncology panel of proteins detected SKBR3 cell line variants and EVs

Heatmap representing the differences in protein levels between SKBR3-Par and SKBR3-NR cells and EVs. Triplicate samples are shown as 1,2 and 3. Cells and EVs are coded as follows; SKBR3-Par cells (SKP), SKBR3-NR cells (SKNR), SKBR3-Par EVs (SKPEV) and SKBR3-NR EVs (SKNREV).

Volcano plot data representation

Volcano plots illustrate the significantly altered proteins in all cell line variants and EVs when comparing neratinib-sensitive to neratinib-resistant. The volcano plots generated in this project represent any proteins that were altered (either increased or decreased) between cell line variants and EVs; this was performed to determine which proteins were significantly altered between cell line variants. The volcano plots were generated based on fold changes greater than 1.2 (labelled proteins in graphs) and adjusted *p-values* (*adjp*) when comparing neratinib-resistant variants to neratinib-sensitive variants. The volcano plots represent the distribution of proteins for HCC1954 cells (Figure 3.13 (A.)), HCC1954-EVs (Figure 3.13(B.)), SKBR3 cells (Figure 3.14 (A.)) and SKBR3-EVs (Figure 3.14 (B.)).

When comparing significantly altered proteins with a greater than 1.2 fold change between HCC1954-Par and HCC1954-NR cell line variants and their respective EVs, the only protein that was significantly altered in HCC1954-NR cell line variants and EVs when compared to HCC1954-Par and EVs was FGF19 (Figure 3.13 (A.) and (B.)). When comparing protein in the SKBR3 cell line variants and their EVs, there were more many proteins significantly altered in SKBR3-NR cell line variants and their respective EVs when compared to SKBR3-Par cell line variant and EVs; FR-alpha, TNFRSF9, IL-6, CD40, LIF, TFPI2, CSF-1, CCL20, TLR3, TRAIL and TNFSF10 (Figure 3.14 (A.) and (B.)).

(A.) (B.)

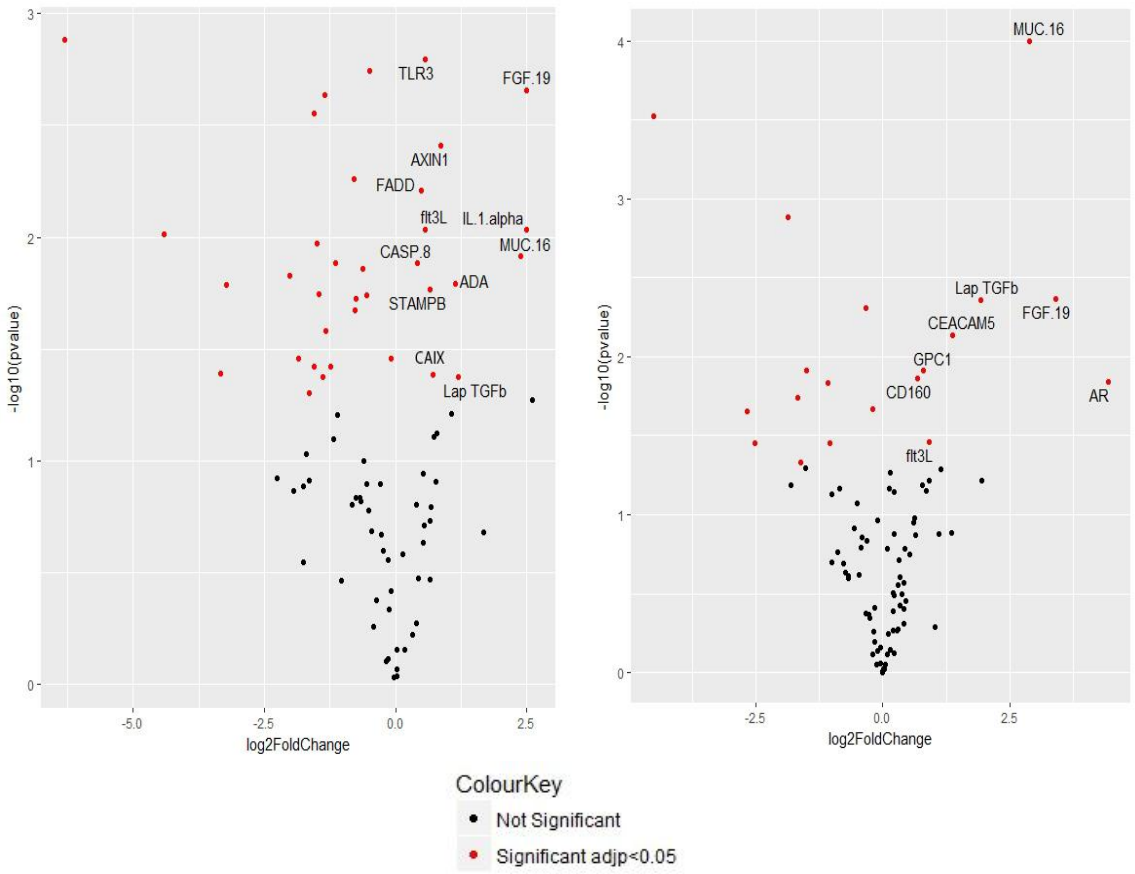

Figure 3.13 Volcano plot HCC1954-Par vs HCC1954-NR cell line variants and EVs
Volcano plot representing the differences in protein levels between HCC1954-Par and HCC1954-NR cell line variants (A.) and EVs (B.). The colour key deciphers between significant and non-significant proteins based on *adjp*<0.05. Entries that are labelled represent proteins that are statistically significantly different and that have a fold-change difference greater than 1.2 when comparing HCC1954-Par to HCC1954-NR cell line variants (A.) and EVs (B.).

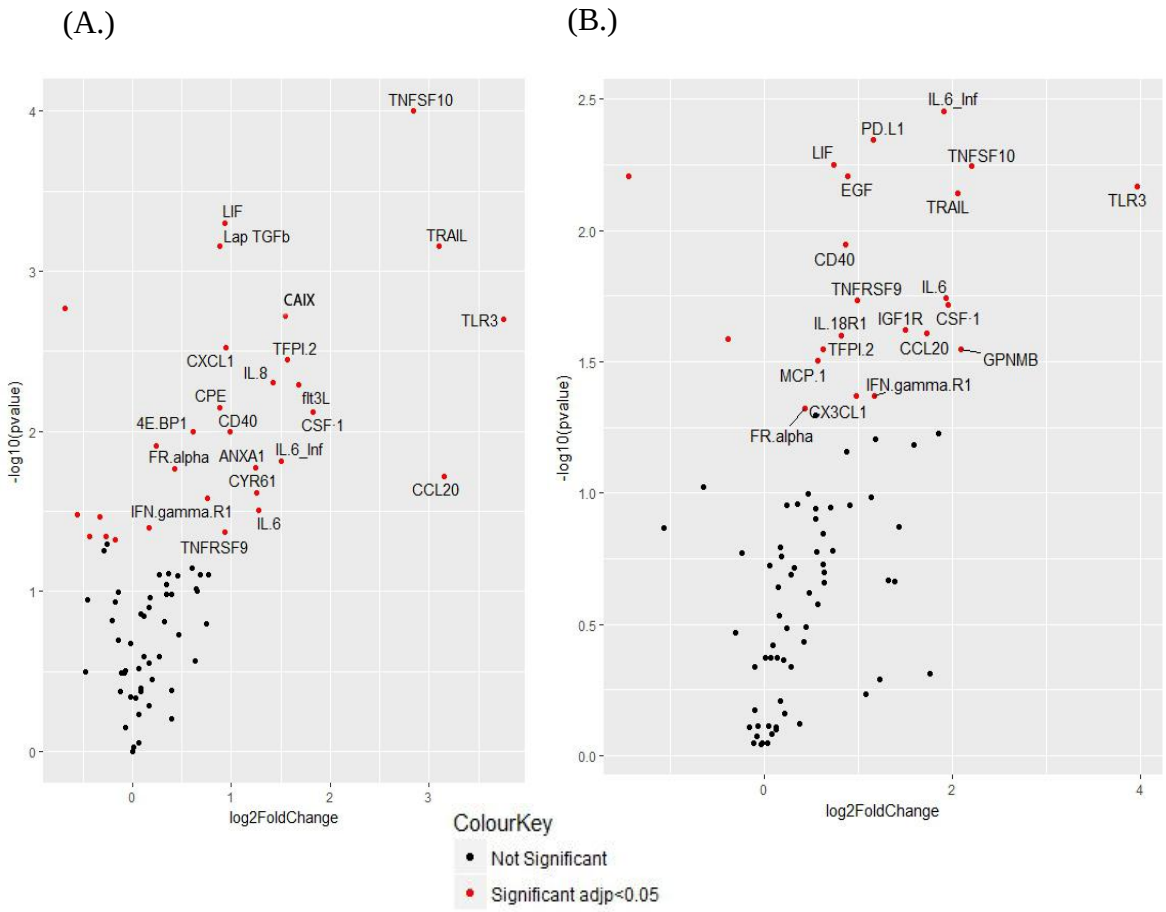

Figure 3.14 Volcano plot SKBR3-Par vs SKBR3-NR cell line variants and EVs
Volcano plot representing the differences in protein levels between SKBR3-Par and SKBR3-NR cells (A.) and EVs (B.). The colour key deciphers between significant and non-significant proteins based on *adjp*<0.05. Entries that are labelled represent proteins that have a fold-change greater than 1.2.

3.2.8. Olink preliminary proteomic analysis

To exclude type I error, a false discovery rate (FDR) was determined using the Benjamini and Hochberg statistics test. Unpaired Student's t-tests were performed on each set of proteins.

Graphical representation of the top 3 proteins increased in HCC1954-NR and SKBR3-NR cells and their respective EVs, compared to HCC1954-Par and SKBR3-Par and their EVs were chosen for follow up studies and are displayed as follows: TLR3 (Figure 3.15), CSF-1 (Figure 3.16) and CAIX (Figure 3.17).

TLR3 was significantly increased in HCC1954-NR and SKBR3-NR cell line variants compared to HCC1954-Par and SKBR3-Par ($p<0.01$ for both) (Figure 3.15 (A.) and (B.)). There was no significant difference in TLR3 quantification in HCC1954-Par and

HCC1954-NR EVs (*p-value*=0.11) (Figure 3.15 (C.)). TLR3 was significantly increased in SKBR3-NR EVs compared to SKBR3-Par EVs ($p<0.01$) (Figure 3.15 (D.)).

CSF-1 was significantly increased in SKBR3-NR cell line variants ($p<0.01$) (Figure 3.16 (B.)) and their EVs ($p<0.05$) (Figure 3.16 (D.)) compared to SKBR-Par and their EVs. There were no significant differences in CSF-1 quantification in HCC1954 cell line variants (Figure 3.16 (A.)) and EVs (Figure 3.16 (C.)).

CAIX was significantly increased in HCC1954-NR ($p<0.05$) and SKBR3-NR ($p<0.01$) cell line variants compared to their sensitive counterparts (Figure 3.17 (A.) and (B.)). There were no significant differences in CAIX in the EVs from either HCC1954 (*p-value*=0.13) cell line variants or SKBR3 (*p*-value=0.07) cell line variants (Figure 3.17 (C.) and (D.)).

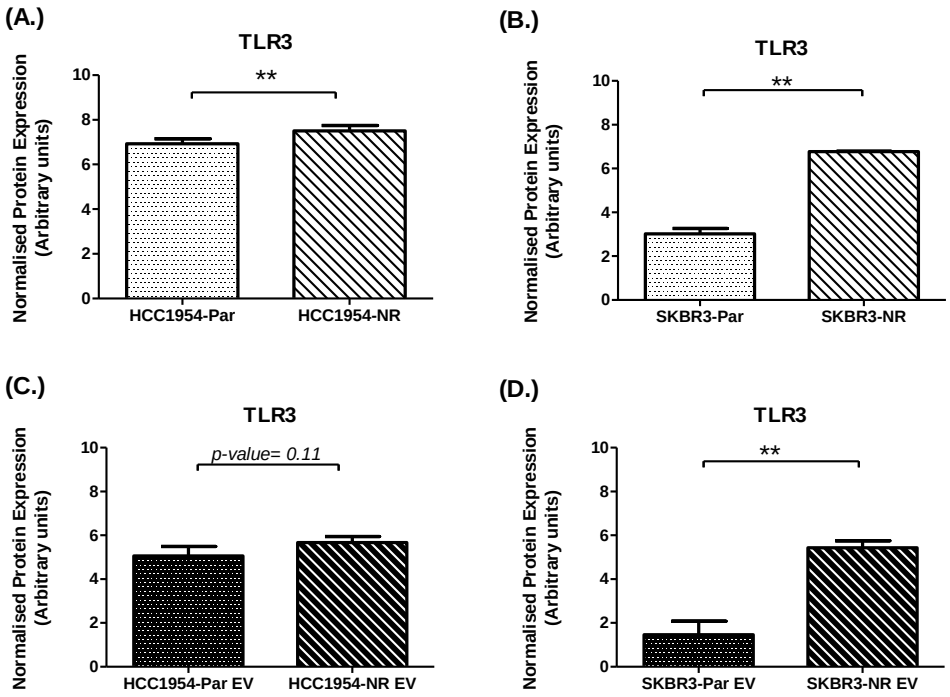

Figure 3.15: TLR3 quantification by Olink Proteomics in cells and EVs
TLR3 quantification in both cell lines (A.) and (B.) and their respective EVs (C.) and (D.) is represented. Normalised protein expression (NPX) was used for analysis. (n=3 ± SEM), **p<0.01, (Student's t-test).

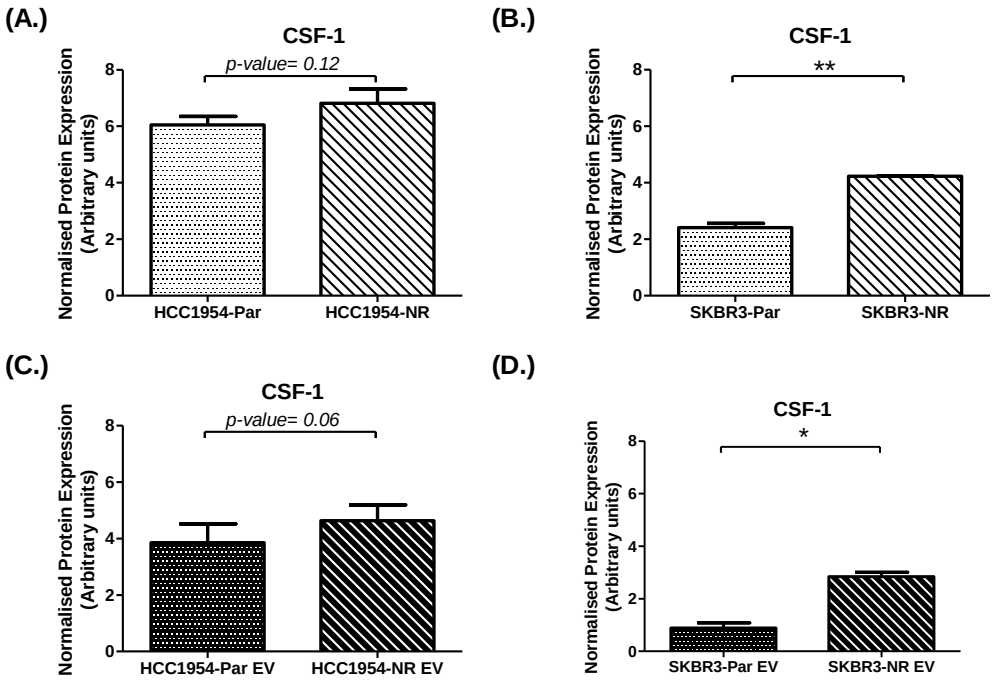

Figure 3.16 CSF-1 quantification by Olink Proteomics in cells and EVs
CSF-1 quantification in both cell lines (A.) and (B.) and their respective EVs (C.) and (D.) is represented. Normalised protein expression (NPX) was used for analysis. (n=3 ± SEM), *p<0.05, **p<0.01 (Student's t-test).

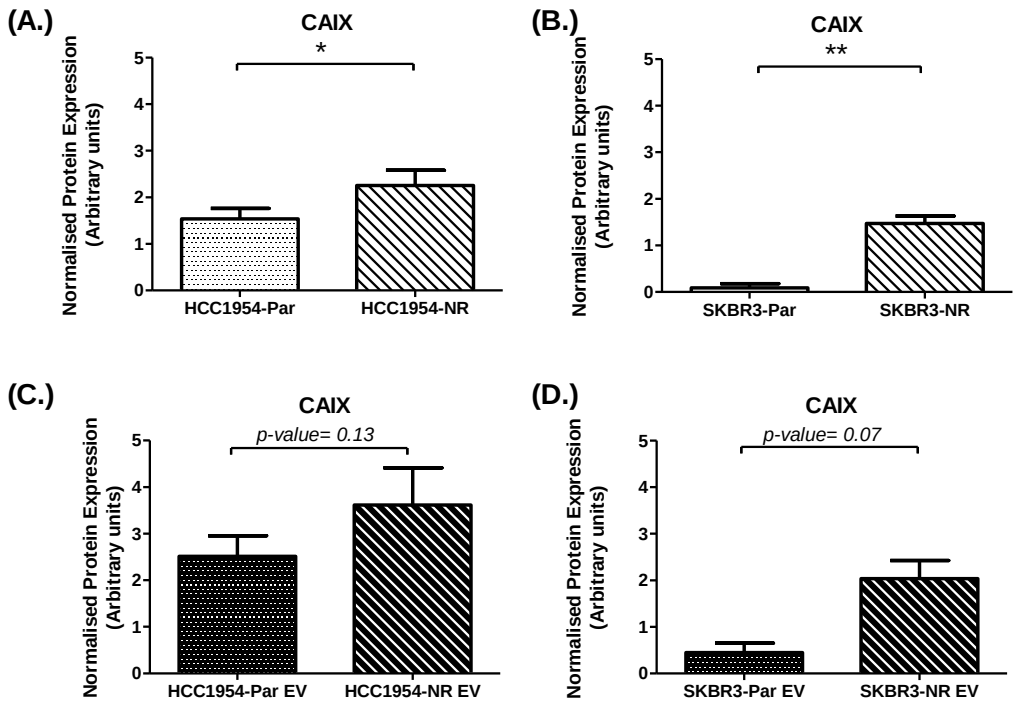

Figure 3.17 CAIX quantification by Olink Proteomics in cells and EVs
CAIX quantification in both cell lines (A.) and (B.) and their respective EVs (C.) and (D.) is represented. Normalised protein expression (NPX) was used for analysis. (n=3 ± SEM), *p<0.05, **p<0.01 (Student's t-test).

3.2.9. Proteomic validation: TLR3

3.2.9.1. TLR3 immunoblots

In an attempt to validate the Olink proteomic results for TLR3, EFM19.2A, HCC1954 and SKBR3 cell line variants were used. The anti-TLR3 polyclonal antibody (Abcam antibody) and the anti-TLR3 monoclonal antibody (Santa Cruz) were tested. The molecular weight of TLR3 is 104kDa. Due to the difficulties observed when detecting TLR3, the full immunoblots are displayed. The polyclonal Abcam antibody gave high levels of non-specific bands (Figure 3.18 (A.)). Very faint bands are present at approximately 100kDa in all samples. The monoclonal antibody from Santa Cruz was tested and although there were fewer non-specific binding bands, TLR3 was not detected in the cell line variants (Figure 3.18 (B.)).

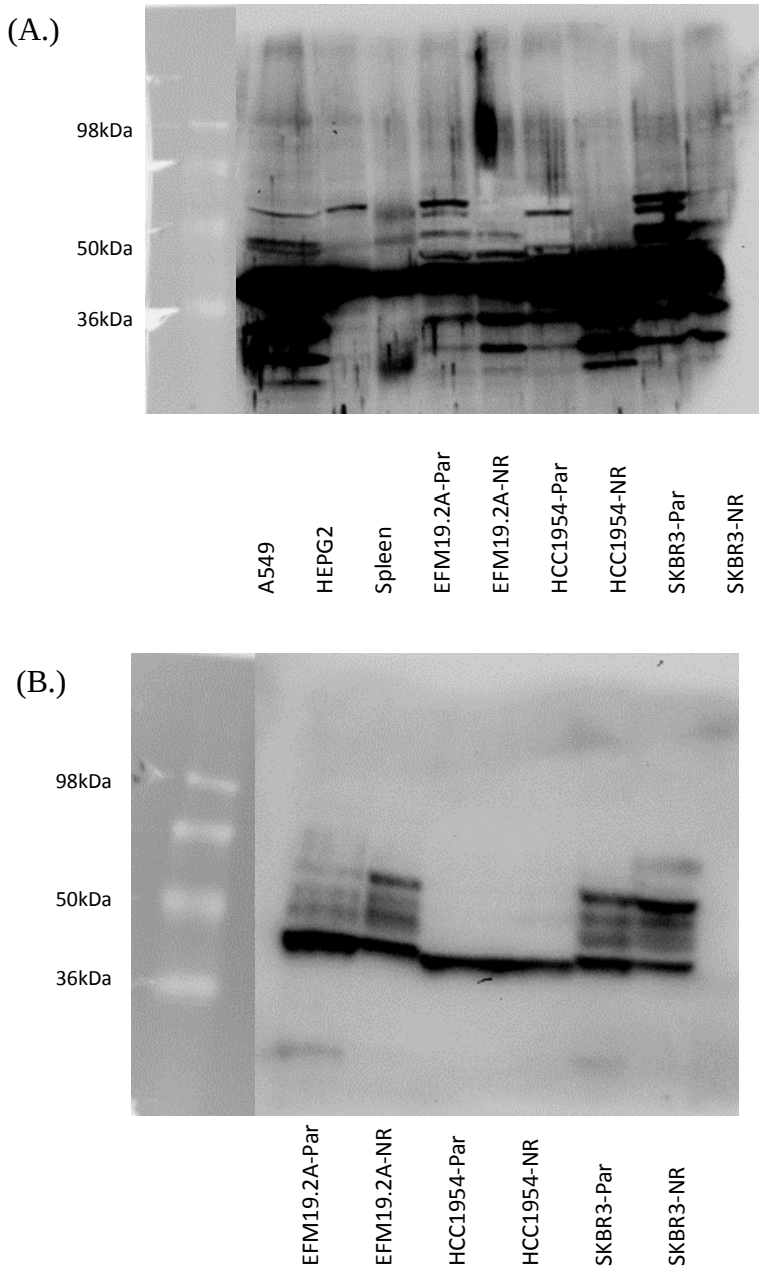

Figure 3.18: TLR3 immunoblots
Representative image for TLR3 immunoblots (30µg protein) performed with the Abcam polyclonal anti-TLR3 antibody for n=3 immunoblots (A.). Positive controls used were HEPG2 and mouse spleen protein lysates. TLR3 immunoblot performed with the Santa Cruz monoclonal anti-TLR3 antibody (B.).

3.2.9.2. TLR3 immunoblots (inducing TLR3 activation with Poly(I:C) treatment)

As shown in the Section 3.2.9.1, the antibodies against TLR3 were unsuccessful in detecting TLR3. It was decided to treat HCC1954-Par and HCC1954-NR with Polyinosinic:polycytidylic acid (Poly (I:C) for 24hr at various concentrations to activate TLR3. Immunoblotting again was very unsuccessful, with a very faint band for TLR3

(104kDa) in the HCC1954-NR cell line variant when treated with 50µg/mL of Poly (I:C) (Figure 3.19).

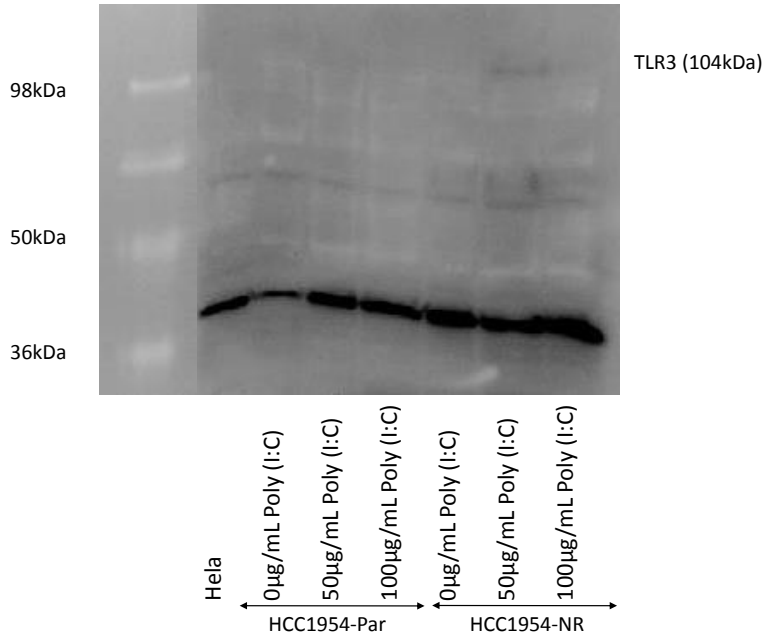

Figure 3.19: TLR3 immunoblots (Poly (I:C) treatment)
HCC1954-Par and HCC1954-NR were treated with Poly (I:C) for 24hr. Non-specific binding was observed at approx. 40kDa. The molecular weight of TLR3 is 104kDa and is slightly observed in the 50µg/mL Poly (I:C) in HCC1954-NR. HeLa lysate was used as a positive control (TLR3 expression in HeLa cells as per the human protein atlas (https://www.proteinatlas.org/ENSG00000164342-TLR3/cell), 30µg loaded for all samples.

3.2.10. Proteomic validation: CSF-1

3.2.10.1. CSF-1 immunoblots

To validate the Olink results for CSF-1, EFM19.2A, HCC1954 and SKBR3 cell line variants were used. We first isolated protein from all cell lines and assessed the cellular expression of CSF-1 with both Abcam (Figure 3.20) and Santa Cruz antibodies (Figure 3.21) (both detect soluble CSF-1 (47kDa)). CSF-1 was detectable at the correct size. For the Abcam antibody, no significant differences in expression were observed for CSF-1 between cell line variants. While CSF-1 was detected in HCC1954 cell line variants with the Abcam antibody, no detection was evident with the Santa Cruz antibody used. Similarly, there were no significant differences in CSF-1 expression between cell line variants. However, there were inconsistencies between the levels of detection for both antibodies.

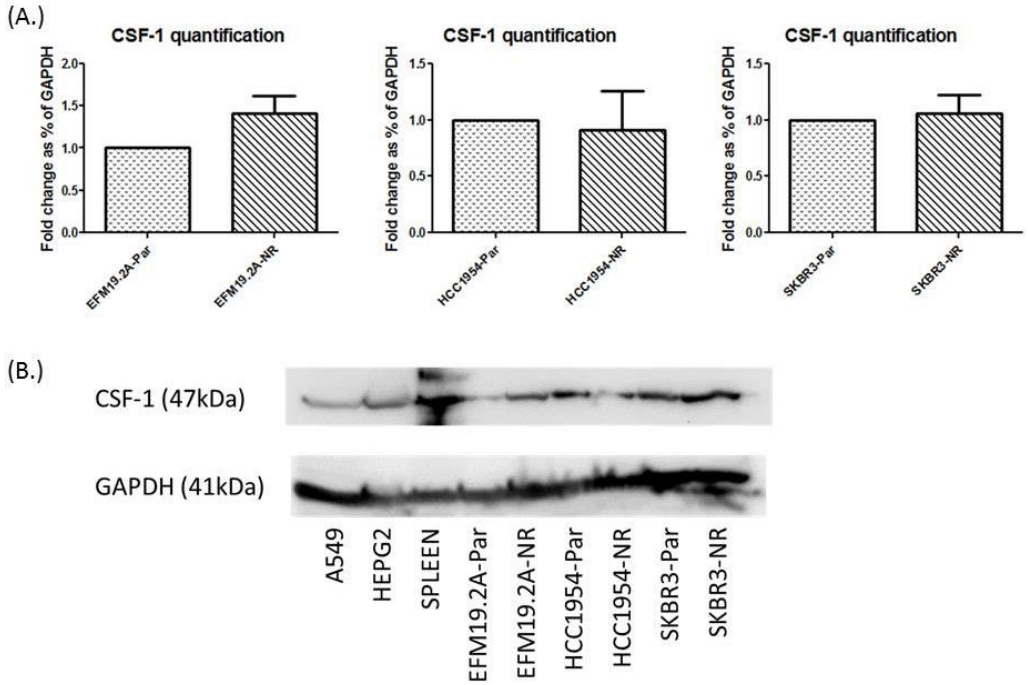

Figure 3.20: CSF-1 immunoblots (Abcam antibody)
CSF-1 densitometry for all cell lines using the Abcam CSF-1 antibody (A.) and representative immunoblot (B.). Results represent (n=3 ± SEM) (Student's t-test).

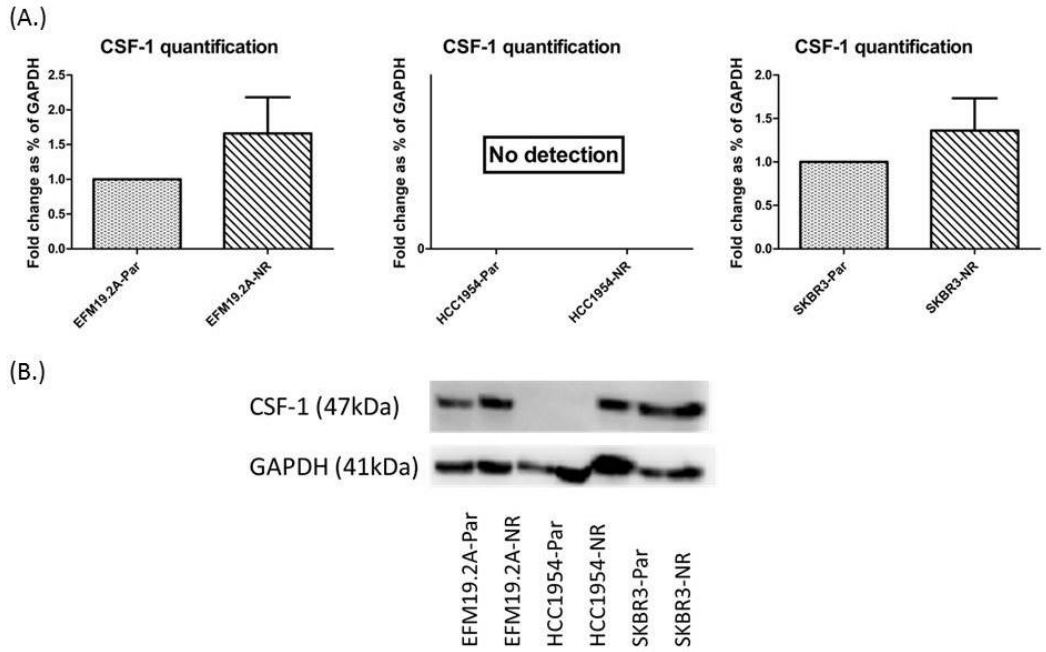

Figure 3.21: CSF-1 immunoblots (Santa Cruz antibody)
CSF-1 densitometry for all cell lines using the Santa Cruz CSF-1 antibody (A.) and representative immunoblot (B.). Results represent (n=3 ± SEM) (Student's t-test).

3.2.10.2. ELISA analysis

Due to the inconsistencies observed using two different antibodies for CSF-1 immunoblotting, CSF-1 ELISAs were tested. CSF-1 quantification in EFM19.2A, HCC1954 and SKBR3 cell line variants and lysed EVs were measured by ELISA. In comparison to the immunoblots only detecting soluble CSF-1 (47kDa), this ELISA detects both the soluble 47kDa and the 60kDa forms. It is also very likely that the ELISA will detect isoform 3 (29kDa), because isoform 3 is identical to isoform 1 and 2 in amino acids 1-182 which includes the epitope recognised by the antibody. CSF-1 in EFM19.2A cell line variants and EVs was below the levels of detection for the ELISA. CSF-1 concentration was significantly increased in HCC1954-NR cells compared to HCC1954-Par cells (Figure 3.22 (A.)) (*p-value*=0.0427). There was no significant difference in CSF-1 expression between SKBR3-Par and SKBR3-NR cell line variants (Figure 3.22 (B.)). There were no significant differences in CSF-1 between HCC1954-Par EVs and HCC1954-NR EVs (Figure 3.22 (C.)). There was no CSF-1 expression in SKBR3-Par EVs, CSF-1 was detected in SKBR3-NR EVs (Figure 3.22 (D.)).

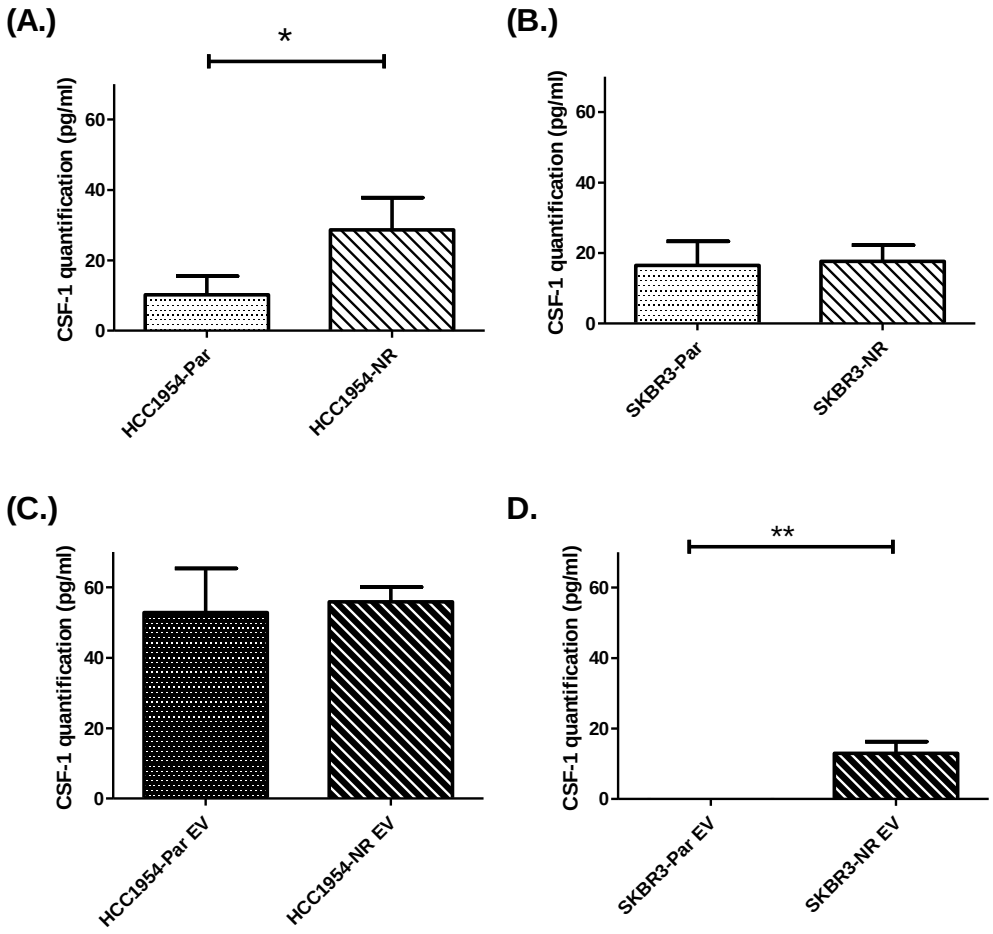

Figure 3.22 CSF-1 ELISA results for HCC1954 and SKBR3 cell line variants and their EVs
Concentration of CSF-1 in HCC1954-Par and HCC1954-NR cells (A.), SKBR3-Par and SKBR3-NR cells (B.), HCC1954-Par and HCC1954-NR EVs (C.) and SKBR3-Par and SKBR3-NR EVs (D.) as determined by ELISA. CSF-1 detection in EFM19.2A cell line variants and EVs was unsuccessful using the ELISA kit. (n=3 ± SEM), **p<0.01, *p<0.05 (Student's t-test).

3.2.11. Proteomic validation: CAIX (normoxia)

3.2.11.1. CAIX immunoblots-Abcam

To establish if the Olink results for CAIX, EFM19.2A, HCC1954 and SKBR3 cell line variants were used. We first isolated protein from all cell lines and initially assessed the cellular expression of CAIX (50/54kDa protein) with the Abcam antibody (Cat. #: ab107257). This antibody did not show any variation in CAIX between cell line variants under the immunoblot conditions using BSA as blocking and PBST (Figure 3.23 (A.)). The immunoblot conditions were altered to using milk and TBST as recommended by Abcam.

The resulting immunoblot (Figure 3.23 (B.)) displayed many non-specific binding and inconsistencies between immunoblots. It is advised on the Abcam website that CAIX is detectable at 50kDa, it was evident from this blot that two bands at 50 and 54kDa were detectable (Figure 3.23 (B.)). From literature searches and from communication with the Abcam technical support, it was evident that this antibody was not tested with lysates from hypoxic conditions and was deemed unreliable as an antibody for CAIX.

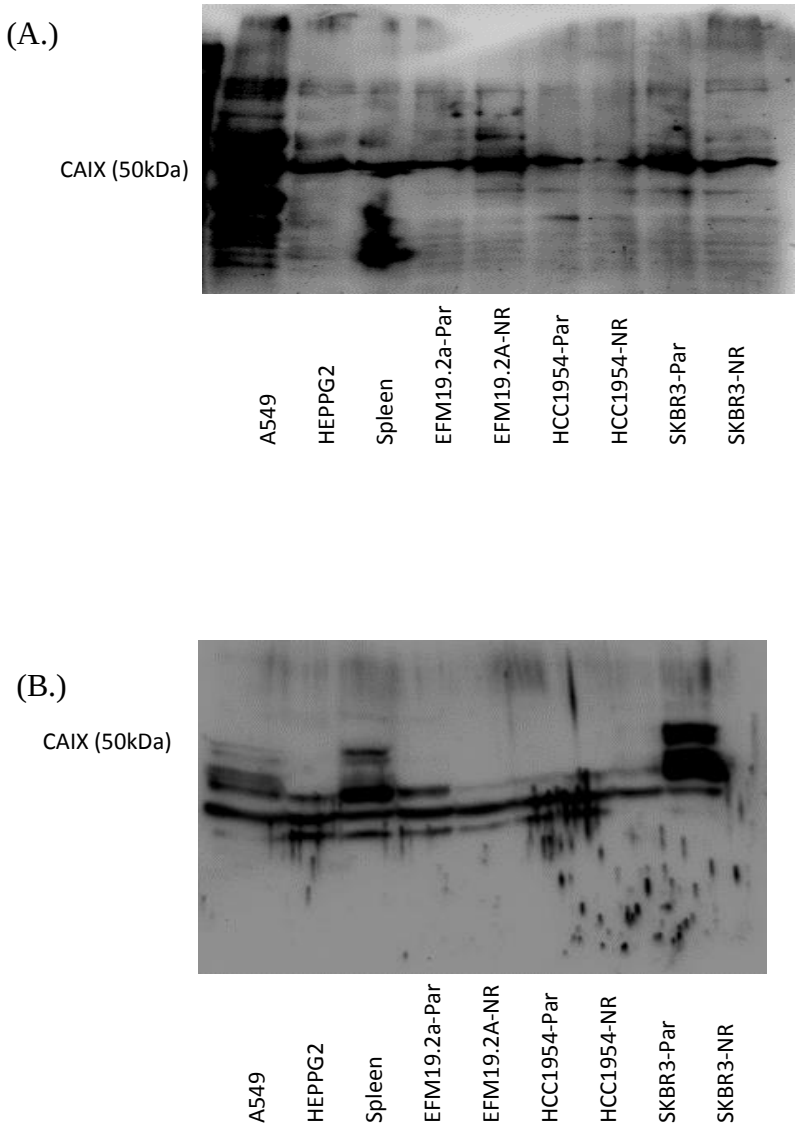

Figure 3.23: CAIX antibody testing (Abcam)
Representative immunoblot image for all cell lines using the Abcam CAIX antibody. Positive controls used were A549 and mouse spleen protein lysates. Immunoblotting conditions of BSA and PBST (A.) and milk and TBST (B.).

3.2.11.2. CAIX immunoblots-Biosciences Slovakia (normoxia)

Preliminary immunoblotting for CAIX using the Abcam antibody produced non-specific binding. From the literature (139), the M75 clone CAIX antibody is specific to CAIX. This antibody detects both constitutively expressed CAIX and CAIX that is responsive to hypoxic conditions as opposed to other commercial CAIX antibodies that interact with non-specific proteins and do not detect CAIX that is responsive to hypoxic conditions. Thus, CAIX expression in HER2+ breast cancer cell lines from normoxic conditions was analysed using the CAIX M75 clone antibody (Bioscience Slovakia). CAIX was detected in the positive control (human epithelial lung carcinoma cells (A549) cell lysate) but not in EFM19.2A-Par, EFM19.2A-NR, HCC1954-Par, HCC1954-NR, SKBR3-Par, SKBR3-NR cell lines from normoxic conditions (Figure 3.24). CAIX double bands at 50 and 54kDa were observed in the positive control, confirming that this antibody is detecting CAIX. Strong non-specific protein binding was observed at 36kDa. Of note, following immunoblotting of CAIX from normoxic conditions, it was noted from the literature (140), that CAIX becomes degraded if samples are not lysed within a 2hr period. Further lysate collection was strictly completed within 2hr for lysates collected following DFO treatment and from lysates collected from hypoxic conditions.

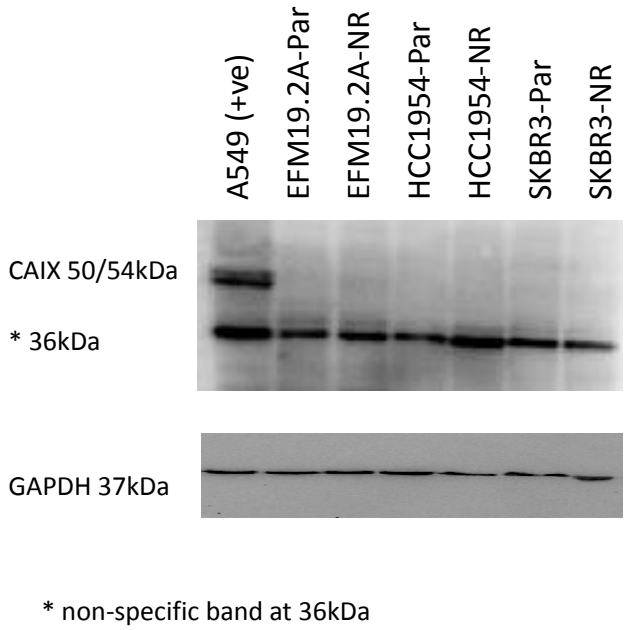

Figure 3.24: CAIX antibody testing (Bioscience Slovakia)
Immunoblotting for CAIX was performed on HER2+ breast cancer cell lines. A549 cell lysate was used as a positive control for CAIX. GAPDH was used as a loading control. Blot shown is a representative blot for n=3 immunoblots.

3.2.12. Proteomic validation: CAIX (hypoxia)

To determine if CAIX is detectable in HER2+ cell lines in response to hypoxic conditions, the hypoxia mimic (DFO) was used. Firstly, to determine suitable DFO treatment concentrations in all cell lines, toxicity assays were performed with DFO (Figure 3.25). DFO-induced toxicity levels were variable between the cell lines; there were no significant differences in toxicity levels in the EFM19.2A cell variants or the HCC1954 cell variants. SKBR3-Par cells were significantly more sensitive to DFO than SKBR3-NR at 200µM and 400µM (*p*-value <0.05 and *p-value*<0.01, respectively). DFO treatment was determined to be less toxic to all cell lines (Figure 3.25, EFM19.2A cells (A.), HCC1954 cells (B.) and SKBR3 cells (C.)) at 50µM.

Immunoblots were performed on lysates from DFO-treated (25µM and 50µM DFO) neratinib-sensitive and –NR variants of EFM19.2A cell, HCC1954 cells and SKBR3 cells. CAIX was undetectable in EFM19.2A-Par and EFM19.2A-NR cell variants following 24hr DFO-treatment (Figure 3.26), thus no densitometry was performed. CAIX was detected in HCC1954 cell line variants (Figure 3.27 (A.)) and SKBR3 cell lines (Figure 3.28 (A.)). Densitometry was performed on HCC1954 (Figure 3.27 (B.) and SKBR3 immunoblots (Figure 3.28 (B.)). No significant differences were observed between the untreated and DFO-treated HCC1954 cell lines at 25µM and 50µM DFO. SKBR3-NR had significantly increased levels of CAIX compared to the SKBR3-Par cells following treatment with 50µM DFO (*p-value*=0.048). As expected, HCC1954-Par, SKBR3-Par and SKBR3-NR cells lines had a trend towards increased CAIX with increasing DFO concentrations. HCC1954-NR cell lines remained unchanged with DFO treatment.

(A.)

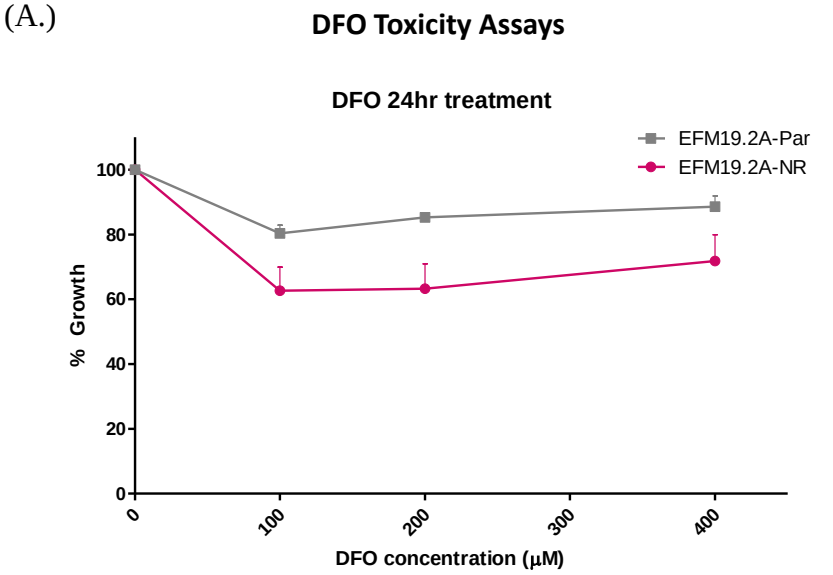

(B.)

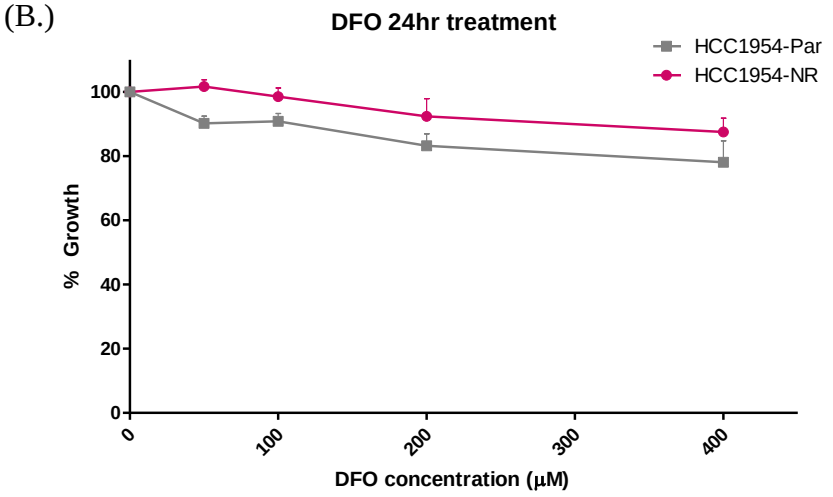

(C.)

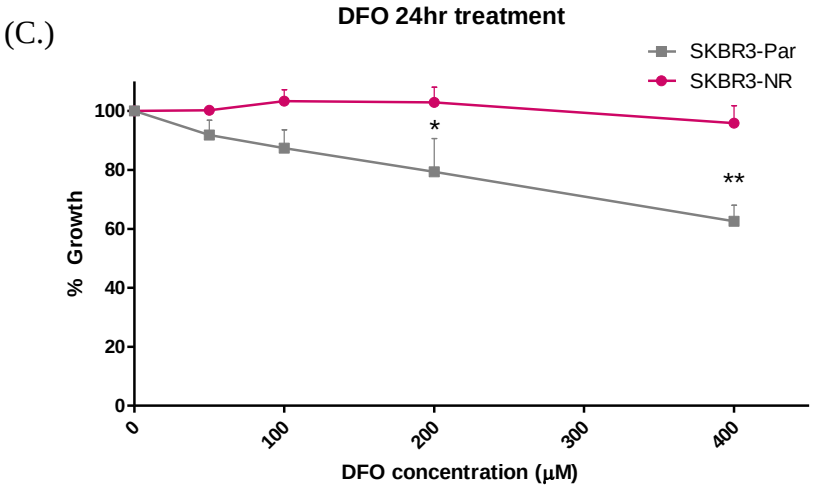

Figure 3.25: DFO-treated cells analysed with acid phosphatase assays
All cell line variants were treated with DFO (0-400µM) for 24hr. Acid phosphatase assays were performed on EFM19.2A-Par and EFM19.2a-NR (A.), HCC1954-Par and HCC1954-NR (B.) and SKBR3-Par and SKBR3-NR (C.). n=3±SEM, *p<0.05. **p<0.01.

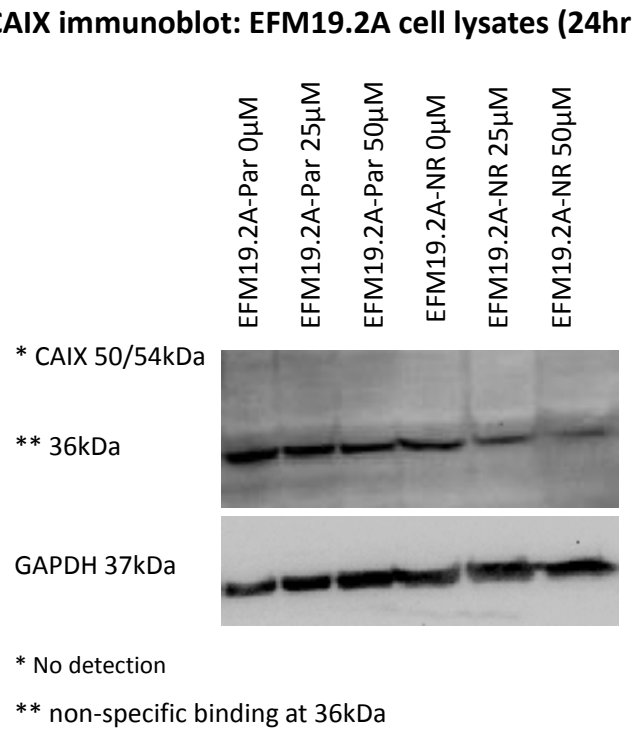

Figure 3.26: CAIX quantification in DFO-treated EFM19.2A cell line variants
EFM19.2A-Par and EFM19.2A-NR cell lines were treated with DFO (0-50µM) for 24hr. Immunoblots were performed to quantify CAIX. Blot image shown is representative of triplicate blots. GAPDH was used as a loading control.

(A.)

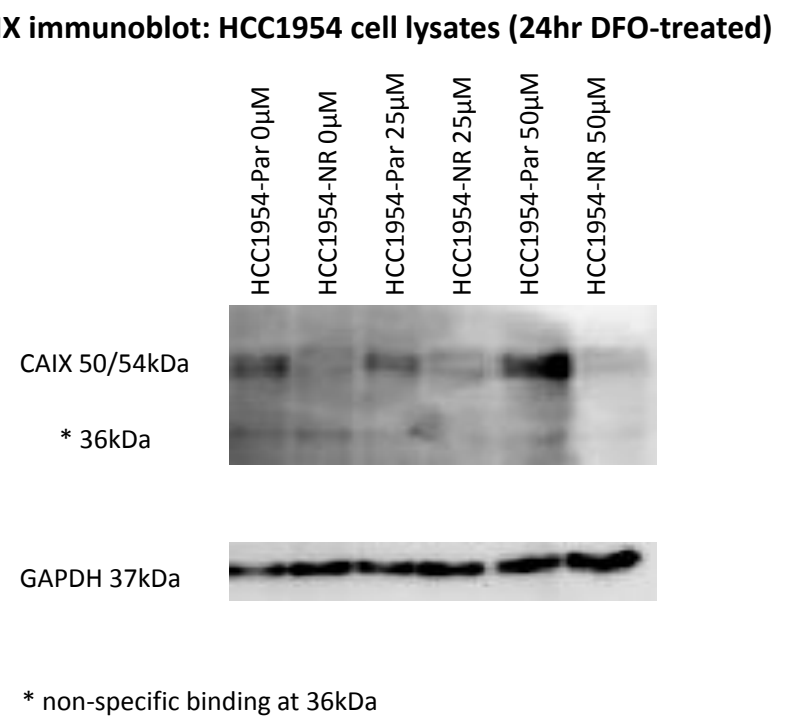

* non-specific binding at 36kDa

(B.)

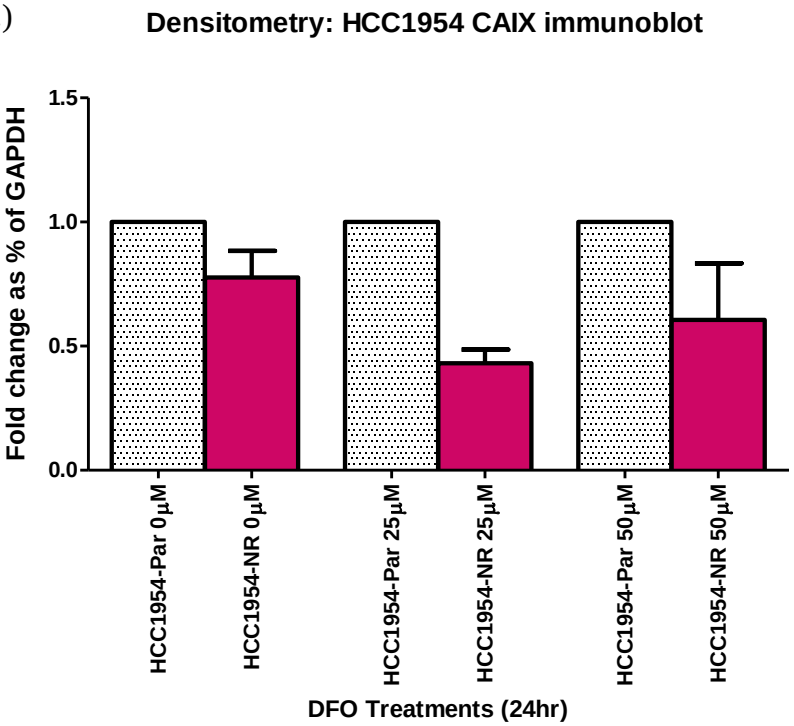

Figure 3.27: CAIX quantification in DFO-treated HCC1954 cell variants
HCC1954-Par and HCC1954-NR cell lines were treated with DFO (0-50µM) for 24hr. Immunoblots were performed to quantify CAIX (A.). GAPDH was used as a loading control. Densitometry was performed (B.). Blot image shown is representative of triplicate blots. n=3±SEM (Student's t-test).

(A.) **CAIX immunoblot: SKBR3 cell lysates (24hr DFO-treated)**

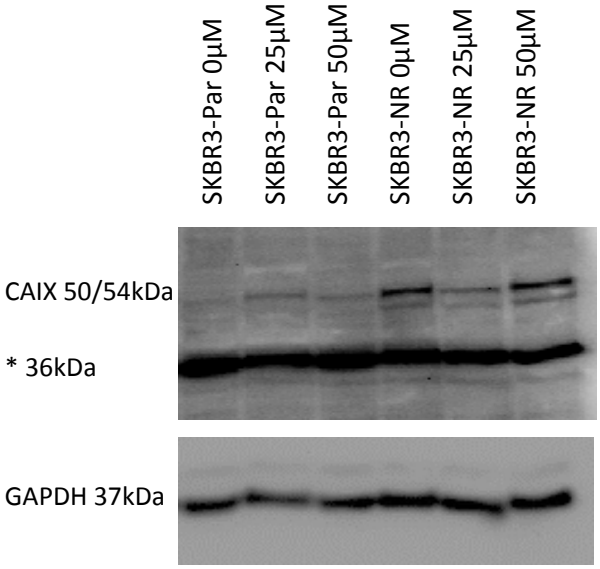

* non-specific binding at 36kDa

(B.)

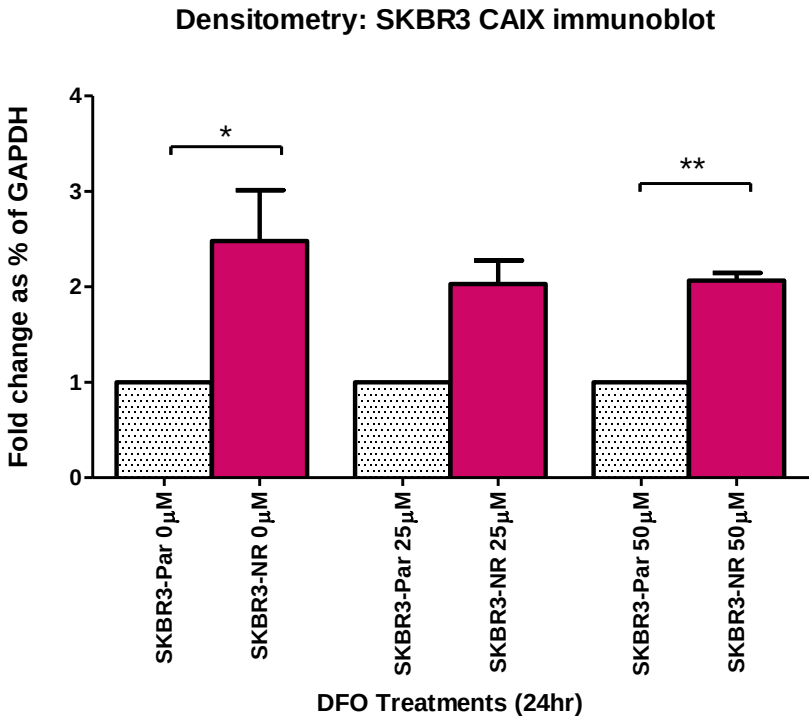

Figure 3.28: CAIX quantification in DFO-treated SKBR3 cell line variants
SKBR3-Par and SKBR3-NR cell lines were treated with DFO (0-50µM) for 24hr. Immunoblots were performed to quantify CAIX (A.). GAPDH was used as a loading control. Densitometry was performed (B.). Blot image shown is representative of triplicate blots. n=3±SEM, * $p<0.05$ (Student's t-test).

3.3. Discussion

In recent years, diagnostic and treatment methods have greatly improved for patients with breast cancer; however, the reality is that more studies are required to give patients more options, to understand tumours better, to develop new treatments and to work towards personalised therapies. Neratinib has clinical activity in HER2+ metastatic breast cancer. A recent clinical trial has shown that following chemotherapy and trastuzumab-based adjuvant therapy, a 12-month treatment regime of neratinib alone significantly improved 2-year invasive disease-free survival when compared with patients receiving placebo after chemotherapy and trastuzumab-based adjuvant therapy (141). The breast cancer patients were previously given chemotherapy and trastuzumab-based adjuvant therapy prior to this clinical trial.

In this study, we sought to investigate *in vitro* neratinib-resistance both at a cellular level and at an EV level. Of note, no single cell line is representative of all tumours and so we selected three HER2+ cell line variants; HCC1954-Par, HCC1954-NR, EFM19.2A-Par and EFM19.2A-NR cell line variants were obtained from Dr. Susan Breslin. The SKBR3 neratinib-resistant cell line was developed over a 6-month period in this project. The SKBR3-NR cell line variant successfully acquired neratinib-resistance with an 8.2 fold increase in IC_{50} compared to age-matched parent cells.

3.3.1. Mechanisms of neratinib-resistance: CYP3A4

While the SKBR3-NR variant was being developed over a 6-month period, it was important to complete previous work performed by Dr Breslin looking at the potential role of CYP3A4 in neratinib-resistance. Firstly, it was confirmed that the HCC1954-NR cell line variant was significantly more migratory (21% increase in migration) than its sensitive counterpart was. Dr Breslin determined that CYP3A4 activity was significantly increased in neratinib-resistant cell line variants. Herein, CYP3A4's role in neratinib-resistance was further investigated. CYP3A4 protein levels were not altered between cell line variants, thus the activity of CYP3A4 was determined to play the main role. When CYP3A4 activity was blocked with ketoconazole, the NR cell line variants had a slight increase in sensitivity to neratinib (4.4% and 17.4% for HCC1954-NR and EFM19.2A-NR, respectively) when compared to treatment with neratinib alone. Although the results of this study are promising, neratinib-resistant cell line variants only displayed a slight increase in

sensitivity to neratinib and thus CYP3A4 could be slightly involved in the mechanisms of resistance but it is not the underlying mechanism of resistance.

3.3.2. Determining alternative mechanisms of neratinib-resistance: Cell lines and EVs

EVs are key components in cellular communication and have been shown to be involved in a plethora of mechanisms and diseases. EVs were successfully isolated from the medium conditioned by EFM19.2A, HCC1954 and SKBR3 parent cells and their respective NR-variants. EV characterisation was performed to ensure successful isolation methods were performed. Using immunoblotting, TEM and NTA, the characteristic markers (negative for GRP-94, positive for TSG101, PD6CI/ALIX and CD63) and the vesicle size and shape were determined and it was confirmed that EVs were present. BCA assay was performed as a surrogate measurement of the quantity of EVs. No significant differences were observed between neratinib-sensitive and neratinib-resistant cell line variants. Following on from this, it was decided to investigate the contents of EVs from each of the cell line variants. Due to the small quantities of EVs obtained from isolations, the EV isolation process for DNA and protein sequencing was completed separately.

Sequenom

DNA isolations were performed on cell pellets and EV pellets. No significant differences between cell line variants or their derived-EVs were determined, however, the standard deviations for each cell line variant and the derived EVs were very high, for the EV samples this may be due to the very low quantities of DNA. Interestingly, although limited amounts, DNA was successfully isolated from the EVs. This was a promising result as EV DNA from NSCLC patient plasma has been shown to more representative of tumour biopsy than DNA in plasma alone (142), thus suggesting that EVs are suitable for biomarker discovery. Using the Sequenom MALDI-TOF mass spectrometry system, two SNPs were found in the HCC1954-Par and HCC1954-NR cell line variants and their EVs: one in the PIK3CA gene and one SNP in PIK3R1. PIK3CA and PIK3R1 are co-expressed and are involved in PI3K/AKT signalling leading to cellular growth and metabolism. These results correlate with findings by Kirouac *et. al* (143), where 18 HER2+ cell lines were studied and where SKBR3 cells were found to signal through the PI3K pathway but the HCC1954 cells are apparently dependent on the MAPK pathway. This is notable due to

the mutations found in PI3K pathway components in this cell line causing a dependency to switch to the MAPK pathway. Similarly, breast cancer patient (n=825) data has shown that 8% and 42% of HER+ breast cancer patient's tumours have mutations in PIK3R1 and PIK3CA, respectively (144). It is not surprising that HCC1954 cells have mutations in the PI3K pathway, as it is one of the most frequently mutated pathways in breast cancer and is involved in resistance to therapy and thus poorer PFS (reviewed by (145). There were no SNPs identified across the 47 genes analysed in SKBR3 cell line variants or EVs. In the EFM19.2A cell line variants and EVs, only one SNP was identified in both, *i.e.* PHLPP2. PHLPP2 functions as a tumour suppressor in cancers (146). PHLPP2 mutations are most commonly found in luminal the breast cancer subtype (147), therefore it is not surprising that this SNP was found in the luminal B cell line, EFM19.2A. It has also been shown that downregulation of this gene in colon cancer contributes to hypoxia-induced chemoresistance (148). Collectively, there were no SNPs common to all cell line variants in this study of 284 SNPs. Thus, no SNPs were assumed to be involved in the mechanisms of neratinib-resistance. It is concluded that the SNPs identified in this study are cell line-specific, therefore strengthening the need for multiple cell lines in all experiments.

Olink proteomics

Our next investigation was to decipher the cellular protein and EV-protein differences between parent and NR groups. This is a very novel study as the contents of neratinib-resistant cell lines and EVs have not yet previously been studied. Di Luca *et. al (149),* used liquid chromatography-mass spectrometry to investigate alterations in HER2+ breast cancer cell lines (SKBR3, BT474 and HCC1954) following 12hr and 24hr treatments with HER2 inhibitors ((lapatinib, neratinib or afatinib). This study revealed what proteins are initially changed following the start of treatment, but does not give a perspective on longitudinal treatment, or importantly drug resistance in cells or associated EVs. In their study, comparing all three cells lines, 3 proteins (Phosphoglycerate kinase 1, Heat shock cognate 71kDa protein and 6-phosphogluconate dehydrogenase) common to both SKBR3 and HCC1954 were significantly altered, however, opposite trends were observed between cell lines. There was no overlap in the proteins analysed in this study to my investigation here. Protein samples from cells and EVs (HCC1954 and SKBR3) were obtained and sent to Olink proteomics for protein profiling. Two protein panels were chosen and a total of 181 proteins were investigated. From this analysis, the 3 top proteins were chosen as

potential biomarkers and therapeutic targets to add value to neratinib, *i.e.* CAIX, CSF-1 and TLR3.

Toll-like receptor 3 (TLR3)

Toll-like receptors (TLRs) recognize pathogen-associated molecule patterns (PAMPs) and promote innate and adaptive immune responses (reviewed by (150)). TLR3 is a 103kDa protein that recognises double stranded RNA and is not expressed on the cell surface. In breast cancer cell lines (inflammatory breast cancer cell line (SUM190), breast ductal carcinoma cell line (BT-483), adenocarcinoma cell line (Cama-1) and the TNBC cell line (SUM149)), stem-cell phenotypes were promoted (2- to 17-fold in all cell lines) following TLR3 stimulation which induced β-Catenin and NF-κB co-activation (151). Following the inhibition of β-Catenin and NF-κB with the small molecule cardamonin (one of the main ingredients from the seeds of Alpinia katsumadai Hayata, which has antibacterial and anti-inflammatory effects), growth of breast cancer xenografts (established in nude mice with SUM190 or SUM149 cells) was controlled. Cardomonin suppressed poly(I:C)-induced mammosphere formation and inhibited translocation of both NF-κB and β-catenin. This is an important study for understanding the roles of cancer stem cells (CSCs) during breast cancer therapies. TLR3 was investigated in IHC analysis of breast tumours (n=74) (invasive ductal carcinoma patients divided by recurrence and no recurrence). This study did not include HER2+ tumours but found higher TLR3 expression to be associated with higher probability of metastasis (152).

Macrophage colony stimulating factor-1 (CSF-1)

M-CSF, (also termed CSF-1) was first found to generate macrophages from bone-marrow precursor cells. It circulates in peripheral blood at detectable levels and can exist as different isoforms *i.e.* a soluble molecule (90kDa), a membranous forms (45 and 60kDa) and a proteoglycan anchored in stromas (200kDa) (153). Breast cancer mortality was predicted using tumour tissue from breast cancer patients (tumour tissue taken at time of primary surgery for breast cancer (n=68), with axillary lymph node metastases (n=38) and without metastases (n=30)) by studying CSF-1 expression (154). High CSF-1 expression with a high density of infiltrating tumour-associated macrophages (TAMs) and CD3+ T-lymphocytes was associated with breast cancer progression. Metastasized primary cancer had higher CSF-1 and CSF-1R when compared to non-metastatic cancer. Similarly, in

postmenopausal women with breast cancer, serum CSF-1 levels were elevated and with nodal involvement when compared to women with benign breast tumours. Elevated CSF-1 in early breast cancer with nodal involvement and in postmenopausal women was found to be associated with poorer overall survival (155).

Carbonic anhydrase IX (CAIX)

Carbonic anhydrases are a family (18 carbonic anhydrases in total) of zinc metalloproteins that play many roles in the body but primarily convert carbon dioxide and water to carbonic acid. CAIX (also termed CA9) is a 50/54kDa transmembrane glycoprotein that is either constitutively expressed or is induced under hypoxic conditions (139). As stated in Section 1.5.4.1, hypoxia is associated with poor prognosis in many cancers. CAIX is expressed in breast cancer tumours. CAIX was found to be a marker of poor prognosis and an independent predictor of survival in premenopausal breast cancer patients (n=400). This marker was only valid in patients with one to three positive lymph nodes, CAIX was also found to be a marker of radioresistance. In this study however, there was no significant association between CAIX and HER2+ breast cancer (156). CAIX is present in normal tissues but its overexpression in breast cancer tissue makes it an ideal target for developing CAIX inhibitors. However, in one study, CAIX was shown not to be an independent prognostic marker of loco-regional recurrence (LRR), distant metastases (DM), disease-specific survival (DSS) or overall survival (OS) when analysed in TMAs from high-risk premenopausal and postmenopausal women (n=945) (157). CAIX-positive basal-like tumours were chemoresistant compared to CAIX-negative basal-like tumours (158). In other recent studies, CAIX inhibition was found to have a more favourable outcome in basal-like, luminal B and TNBC than in luminal A and HER2+ subtypes (159). However, in a cohort of breast cancer patients (n=209) treated with doxorubicin, CAIX expression correlated with worse progression-free survival (PFS) and OS, these results were shown to be independent of HER2 gene amplification (160). CAIX may be beneficial in predicting therapy responses and should be investigated in more detail.

TLR3, CSF-1 and CAIX proteins showed the greatest trends towards increased protein expression in neratinib-resistant cell lines and EVs. To investigate if these proteins were strong targets for determining neratinib-resistant mechanisms, bioinformatics tools were used. Heatmap analysis showed that expression patterns from one sample in each group

being significantly different from the other two. Therefore n=3 was determined as too low a sample size for Olink proteomic screening. Volcano plots were created for all Olink data to provide a summarised representation of all significantly altered proteins. It is clear from the volcano plots that many proteins identified by Olink are cell-line specific. However, like with the heatmap expression patterns, the 3 proteins identified proteins were displayed again here, further confirming that CAIX, CSF-1 and TLR3 warrant further investigation.

Using the cancer proteome atlas (MD Andersen Center) (https://tcpaportal.org/) datasets, the proteins of interest were investigated. There was no overlap of the proteins from this study with the datasets, indicating that the proteins selected are novel proteins being investigated in breast cancer, and more specifically, HER2+ breast cancer. In a study of 825 breast cancer patients, reverse phase protein array (RPPA) analysis was performed to determine protein expression. This study revealed that HER2+ patient's tumours highly expressed HER1 and HER2 protein and their phosphorylated forms (144). A similar RPPA study was performed and analysed 82 proteins in 52 breast cancer cell lines, 10 snap frozen primary breast tumour tissues and 95 frozen primary breast tumours from M.D Anderson Cancer Center, all tumour tissues were representative of luminal A, luminal B, normal-like, HER2+ and basal-like breast tumours. Of these 82 proteins, the 3 proteins chosen from my study were not investigated (161). Follow-up studies are necessary to confirm the presence of these proteins using immunoblotting and to perform functional experiments based on the studies presented here.

The results for TLR3 in this study are very promising; *i.e.* the levels of protein in both cell lines and EVs are similar. The results indicate a significant increase in TLR3 levels in HCC1954-NR cells, SKBR3-NR cells and SKBR3-NR derived EVs (*p-values:* 0.001, 0.002 and 0.007, respectively). The Benjamini-Hochberg test (used to discover type I errors) results correlated with these results. Although there were no significant changes in TLR3 levels in HCC1954-NR-derived EVs compared to HCC1954-Par EVs (*p-value:* 0.11) (Figure 3.15 C), the graphical representation is very similar to that of the HCC1954 cell line variant graph. With this in mind it was very interesting to try to validate the expression results using immunoblotting, however TLR3 was not found to be expressed in the cell lines, even with activation of TLR3 with Poly(I:C).

No published studies were found investigating CSF-1 in EVs or in drug resistance in breast cancer, highlighted that this study is a very novel study. The expression levels of CSF-1 in neratinib-sensitive and neratinib-resistant cell line variants (HCC1954-NR and SKBR3-NR) were determined in this study. Although no significant differences were found when

comparing CSF-1 levels in HCC1954-Par and HCC1954-NR (*p-value:* 0.123), CSF-1 was significantly increased in SKBR3-NR cells when compared to SKBR3-Par cells (*p-value:* 0.007). This strong trend in SKBR3 cell line pair highlighted the importance of investigating this protein further using immunoblotting to determine the accuracy of the protein expression technique. Similarly, no significant change in CSF-1 levels was observed in HCC1954-Par and HCC1954-NR cells derived-EVs. However, a trend towards increased levels in HCC1954-NR derived EVs was observed (Figure 3.16 C) (*p-value:* 0.065). In the SKBR3 derived EVs, CSF-1 levels were significantly increased in SKBR3-NR EVs compared to SKBR3-Par EVs (Figure 3.16 D) (*p-value:* 0.019*)*. The Benjamini-Hochberg test confirmed the results obtained from the Student's t-test. CSF-1 was thus, considered a good target for further investigation into deciphering the neratinib-resistant mechanisms.

Protein analysis was performed and using the Student's t-test, CAIX expression levels were significantly increased in the neratinib-resistant cell lines (HCC1954-NR and SKBR3-NR) (*p-values:* 0.041 and 0.002, respectively). The Benjamini–Hochberg test was used to discover type I errors and the results correlated with the Student's t-test results. This signifies that CAIX is a strong candidate to bring forward for investigating neratinib-resistance mechanisms. The quantity of CAIX in the cell line-derived EVs was also determined and *albeit* no statistically significant results were found, a similar trend towards increased CAIX in EVs derived from neratinib-resistant cell line variants (HCC1954-NR and SKBR3-NR was observed) (*p-values:* 0.13 and 0.06, respectively). The differences in CAIX levels in cells and EVs was validated using immunoblotting/ELISA; this allowed us to attempt to validate the results obtained from Olink and to determine that the correct protein is being detected. CAIX levels in cells and EVs in this study and the results from previous studies suggests that CAIX is a good candidate for further investigating the mechanisms of neratinib-resistance.

Efforts at proteomic validation

The anti-TLR3 antibodies used in this study were very poor at detecting TLR3 or the levels of TLR3 in the cell line variants are too low for detection by immunoblot. To overcome the issue with low TLR3 levels in all cell line variants, Poly (I:C) was used to test if TLR3 could be activated and thus detected more efficiently. Poly(I:C) is a synthetic dsRNA that mimics the effects of naturally occurring dsRNA (a PAMP) when it binds to TLR3.

HCC1954-Par and HCC1954-NR were used to test for TLR3 activation by Poly (I:C) treatment as it was determined from the Olink proteomics, that the cell line variants expressed the most TLR3. Following treatment with Poly (I:C), a very faint band was detected in the HCC1954-NR cell line variant. From this analysis, it was evident that TLR3 was not a suitable protein for carrying out further validation and functional work.

Two antibodies were used to detect CSF-1 in the cell line variants. It was observed that large variability in the antibodies ability to recognise and bind CSF-1 was observed. For example, the Abcam antibody apparently detected CSF-1 in all cell line variants, however there were no significant differences between variants. Using the Santa Cruz antibody, no detection of CSF-1 was observed in the HCC1954 cell line variants, thus displaying inconsistencies when trying to validate this protein. Similarly, when using the CSF-1 ELISA (detects both soluble and membrane-bound CSF-1), CSF-1 was undetectable in EFM19.2A cell line variants. Although CSF-1 was significantly increased in HCC1954-NR cells and SKBR3-NR EVs, this protein was determined to be unsuitable for further studies as all three methods of its analysis gave different results.

Two different antibodies were utilised for CAIX detection in all cell line variants. The first antibody (Abcam) gave very stark differences between immunoblot conditions. CAIX was observed in the positive control A549 lysates. However, this antibody was deemed as unsuitable as it was not tested with lysates collected from hypoxic conditions. The A549 constitutively expresses CAIX regardless of O_2 levels. Thus immunoblots with the M75 clone antibody were performed. Again, the positive control (A549) displayed CAIX levels with two bands at 50 and 54kDa. CAIX protein was undetectable in the HER2+ cell line variants during normoxic conditions. This is due to the fact that CAIX protein increases during hypoxic conditions and it seems that immunoblots were not sensitive enough to detect the low levels of CAIX in normoxic conditions.

It was also noted that CAIX is degraded if lysates are not processed within 2hr, thus this was evidence that CAIX is not constitutively expressed in the HER2+ cell line variants as it is in A549 cells as protein lysis in A549 cells was not completed within 2hr. Hence, the cell line variants were treated with the hypoxia-mimic (DFO) to induce CAIX expression. DFO has been shown to be anti-proliferative and cytotoxic to tumour cells. In this study, in comparison to the SKBR3-NR cell line variant, SKBR3-Par cells were found to be more sensitive to DFO treatment. The reasoning for this is unknown, however, this could be due to high levels of V-ATPase in cell lines or decreased ROS-dependent HIF-1α (162, 163). DFO treatment successfully induced CAIX expression in HCC1954 and SKBR3 cell line

variants, but not in the EFM19.2A cell line variants. DFO was determined to be a suitable hypoxia mimic in the cell line variants. CAIX was significantly increased in the SKBR3-NR cells compared to SKBR3-Par cells at 50µM DFO treatment. This result validated the results obtained from the Olink proteomics. However, HCC1954-NR cell line variant showed the opposite trend to the Olink proteomics results. With trends towards increased CAIX in HCC1954-Par cells compared to HCC1954-NR cells when treated with DFO. Further investigations into CAIX using true hypoxic conditions (using a hypoxia chamber) were deemed warranted. The reasoning behind the selection of bringing CAIX forward into further validation investigations is summarised in Figure 3.29.

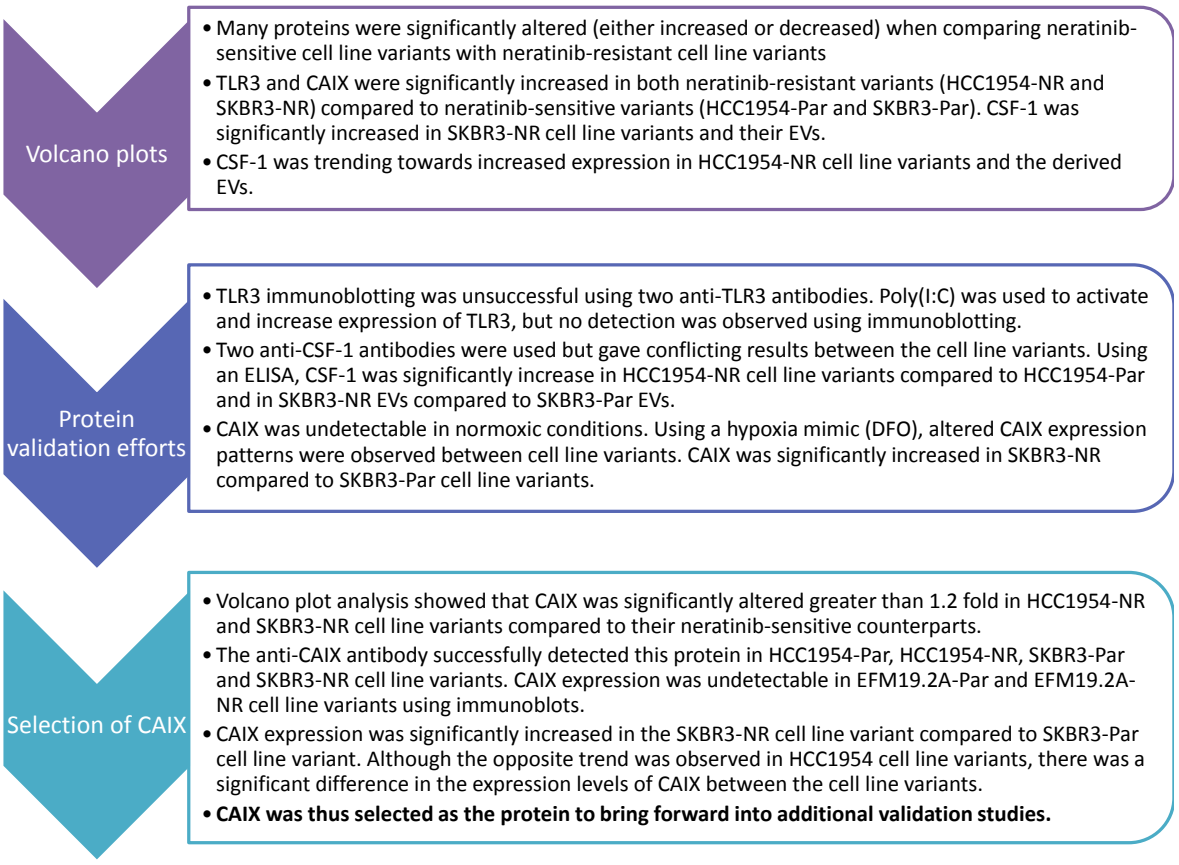

Figure 3.29: Summary of the selection process for CAIX

3.1. Conclusions

In conclusion, neratinib-resistant cell line (SKBR3-NR) was successfully generated in this project, which was validated using toxicity assays. DNA was present in EVs. 2 SNPs were identified in HCC1954-Par and HCC1954-NR and one SNP was identified in EFM19.2A-Par and EFM19.2A-NR cell line variants but were determined to be cell line specific and not related to mechanisms of neratinib-resistance. Of the 181 proteins investigated in neratinib-sensitive and neratinib-resistance cells and their respective EVs, we identified 3 proteins as candidates potentially associated with neratinib-resistance. Following bioinformatics analysis and protein validation experiments, CAIX was determined as the best target to bring forward into further validation and functional studies.

CHAPTER FOUR: The roles of CAIX in the mechanisms of acquired HER2-targeted drug resistance in HER2+ breast cancer cell lines and the added benefit of its inhibition by S4

Parts of this chapter are published in the following review article:

- Can hi-jacking hypoxia inhibit extracellular vesicles in cancer. Lowry MC, O'Driscoll L. Drug Discovery Today. 2018 Jun;23(6):1267-1273.

4. Abstract

Hypoxia contributes to significant micro-environmental changes and stresses, but, tumour cell have the ability to adapt and survive these acute conditions. Hypoxia alters metabolism, pH regulation, EMT, angiogenesis and resistance to chemotherapy. Tumour cells regulate the fluctuations in pH through modulation of CAIX. High expression of CAIX has been found to be associated with poor survival in many breast cancer subtypes. High expression of CAIX has also been associated with radiation therapy resistance and chemotherapy resistance. We aimed to (a.) investigate the overexpression of CAIX in HER2-targeted therapy resistant cell lines in both normoxic and hypoxic conditions and (b.) to inhibit CAIX expression in drug-resistant cell lines to re-sensitise the cell line variants to neratinib.

Following their culture in both hypoxic and normoxic conditions, by ELISA, CAIX levels were found to be increased in drug-resistant variants (BT474-TR, EFM19.2A-NR, HCC1954-LR, SKBR3-NR, SKBR3-TR and SKBR3-TLR) when compared to their sensitive counterparts. Immunoblots and ELISAs were performed to investigate the ability of S4 to inhibit CAIX levels in drug-resistant and drug-sensitive cell line variants. The CAIX inhibitory effects of S4 were overcome by the drug-resistant cell lines and this correlated with increasing neratinib-resistance (determined by Spearman correlation). Using acid phosphatase assays, cytotoxicity levels were performed to investigate the efficacy of the combination of S4 with anti-HER2 therapies compared to HER2-therapies alone. The combination of S4 with neratinib was synergistic in all neratinib-resistant cell lines. The level of synergy for the combination therapy directly correlated with increased neratinib-resistance. This trend was not evident for the combination of S4 with either lapatinib or TDM-1 in HER2-targeted drug-resistant cell line variants (lapatinib-resistant, trastuzumab-resistant and lapatinib plus trastuzumab-resistant).

To conclude, our results suggest that CAIX plays a role in the mechanism of neratinib-resistance. We have evidence to suggest that the combination of S4 with neratinib may overcome this resistance in HER2+ breast cancer cell lines. This synergism is specific to neratinib and does not occur with other HER2-targeting drugs (lapatinib and TDM-1, tested as examples). These findings may be investigated further in *in vivo* studies and clinical trials in the future.

4.1. Introduction

As tumour growth progresses, oxygen and nutrient deprivation ensue, resulting in a hypoxic microenvironment and the initiation of the 'angiogenic switch' to alleviate this imbalance. The induction of tumour angiogenesis *via* the hypoxic pathway initially increases nutrient and oxygen levels but ultimately causes vascular leakiness or an inadequate blood vessel system (164). This vessel instability may account for the fluctuations in normoxic and hypoxic conditions in the tumour (165). The blood vessels mature through multiple cellular steps including the recruitment of platelets, perivascular cells, fibroblast cells and the remodelling of the extracellular matrix (ECM).

4.1.1. Hypoxia and cancer

Hypoxia (as discussed in Section 1.5.4.1) is a pathophysiological property that is defined as a state of depressed oxygen tension. The presence of hypoxia in solid tumours, first described by Thomlinson and Gray (166), is strongly associated with tumour growth, angiogenesis, malignant progression, metastasis and resistance to therapy, thereby affecting the curability of solid tumours regardless of treatment modality (167). A key mechanism by which cancer cells and stromal cells of the microenvironment adapt their metabolism to hypoxia is through the transcriptional activity of hypoxia-inducible factors (HIFs). HIFs function as heterodimers that consist of an oxygen-related HIF1α (or HIF2α) subunit and a constitutively expressed HIF1β subunit. Overexpression of HIFα in cancer cells has been associated with an unfavourable prognosis in several cancer types (168). Similarly, the membrane-tethered enzyme carbonic anhydrase isoform IX (CAIX), which is inducible by hypoxia, is quite selectively associated with cancer. As CAIX is not expressed at substantial level in normal tissue -with the exception of stomach staining for CAIX expression is now an established marker of tumour hypoxia and a clinical indicator of aggressive cancers with poor prognosis (169).

4.1.2. The role of CAIX in cancer

During hypoxic conditions, tumour cells can adapt to the altered environment. In tissues, O_2 concentrations range from 2-9%, <2% for hypoxic conditions and <0.02% for severe hypoxic conditions (129). HIF-1α gets degraded by the ubiquitin-proteasome pathway under normoxic conditions. However, during hypoxic conditions, HIF-1α translocates to the nucleus and up-regulates the hypoxic response elements (HREs) (CAIX, VEGF, PDGF-β and GLUT1).

CAIX is a transmembrane glycoprotein that is involved in regulating cellular pH balance. CAIX is a member of the carbonic anhydrase family of zinc-metalloenzymes. CAIX catalyses the reversible hydration of carbon dioxide to carbonic acid. In doing so, CAIX controls the intracellular and extracellular pH balance (reviewed by (169)). Intracellular pH in tumour cells ranges from 7-7.4 (170). Vascular instability and poor perfusion inhibits nutrients and waste removal, the latter resulting in acidosis. CAIX maintains pH balance, specifically by maintaining an alkaline intracellular pH and extracellular acidic pH. The pH changes both intracellularly (intracellular pH in most tumours is 7.0-7.4) and extracellularly (extracellular pH in most tumours is 6.0-7.0, reviewed by (171)) promote drug resistance (172) and radiotherapy resistance (156). Tumour cells induce an extracellular acidic pH to promote ECM degradation and thus increased migration and invasion (173). In maintaining and alkaline intracellar pH, tumour cells can promote cell survival and prevent the activation of apoptotic stimuli by preventing the activation of caspases (require intracellular acidic pH) (174).

CAIX expression in normal tissues is restricted to gut epithelial tissue (175). Similarly to HIF-1α, in a meta-analysis study, CAIX expression is associated with hypoxic regions and high expression has been found to be associated with poor prognosis in many cancers including bladder, brain, breast, oesophageal, gall bladder, head and neck, lung, pancreatic and stomach (176). Contrastingly, high expression of CAIX is associated with better overall survival in renal cell carcinoma (177).

4.1.3. CAIX in breast cancer

CAIX expression was found in cell membranes of breast cancer tissue and some in the adjacent stroma of tissue (178). CAIX-positive specimens had HER2 overexpression

(n=26) (*p-value*=0.05). In this study, CAIX was not found in benign lesions. Upregulation of CAIX was also observed in basal-like breast tumour samples (n=62) (158). High CAIX expression was associated with shorter RFS/DFS (HR 0.21) and OS (HR=0.19) in breast cancer patients (179). Elevated CAIX was also associated shorter RFS in patients with grade I and II tumours (HR 0.028) and poorer OS (HR=0.2). Lymph node negative patients had poorer RFS (HR=0.14) and OS (HR=0.05) (179). Similarly, Pinheiro *et. al* found CAIX to be associated with large tumour size and high histological grade in basal-like tumours (180).

Similarly, a meta-analysis study on CAIX expression in breast cancer and many solid tumours was performed (176). The analysis revealed that high expression of CAIX was associated with worse prognosis in breast cancer patients. Results indicated high CAIX expression was associated with poorer overall survival (HR 1.9), disease-free survival (HR 1.74), disease-specific survival (HR 1.75), metastasis-free survival (HR 1.76) and progression-free survival (HR 1.88). Further investigation in CAIX in the different subtypes of breast cancer were investigated, it was found that CAIX overexpression was observed in ER-, PR- and HER2+ breast cancer patients and associated with poor survival (n=111) (181). Serum levels of CAIX did not correlate with tissue CAIX mRNA in breast cancer patients (n=140). However this group found that CAIX mRNA from tumour tissue was associated with prognostic factors and poor patient outcome (182).

CAIX was detectable in breast tumour tissues and found to be associated with adjuvant chemotherapy resistance and resistance to endocrine therapy (183). Here, it was hypothesised that CAIX expression reversely correlated with ER status and positively correlated with HER2. CAIX was found to be a marker of poor prognosis in premenopausal breast cancer patients (156). This study found that CAIX in patients with one to three positive lymph nodes was an independent predictor of survival and may be associated with radiotherapy resistance. In a Danish breast cancer patient trial investigating CAIX in response to postmastectomy radiation therapy, CAIX was not found to be an independent prognostic marker for survival (184). In basal-like tumours, upregulation of CAIX was associated with chemotherapy resistance (158). In doxorubicin-treated breast cancer patients (n=209), CAIX expression correlated with worse PFS and OS, the correlation was found to be independent of HER2 amplification (160). CAIX in resectable early-stage breast cancer patients following neoadjuvant chemotherapy was found to correlate with pathological response to paclitaxel, lymph node metastasis and lymph-

vascular invasion (185). Following lapatinib or trastuzumab treatment, CAIX was not found to be associated with response to therapy (186).

Although there has been many studies investigating CAIX as a potential prognostic and predictive biomarker, to the best of our knowledge, there are no publications investigating the roles of CAIX in neratinib-resistance in breast cancer. In this study, we aimed to investigate the relevance of CAIX in HER2-targeted therapy resistance in HER2+ breast cancer cell subtypes. We aimed to compare protein levels of CAIX between neratinib-sensitive cell lines and neratinib-resistant cell lines. If relevant, we aimed to inhibit CAIX expression to determine if this would re-sensitise the cells to neratinib. If validated, we aimed to investigate the clinical relevance of CAIX using patient plasma specimens.

4.2. Results

4.2.1. CAIX quantification in HER2+ cell lines using immunoblotting (normoxia *vs* hypoxia)

Following the successful detection of CAIX using DFO (Section 3.2.12), a hypoxia chamber (ProOx hypoxia chamber (model C21)) was used to validate the findings. All cell lines were placed in the hypoxia chamber at 1% O_2 for 24hr, similarly lysates were collected from cell line variants cultured at 21% O_2 for 24hr. Immunoblots were performed on EFM19.2A, HCC1954 and SKBR3 cell line variants. CAIX levels in EFM19.2A cell line variants were determined to be too low for reliable detection *via* immunoblotting. (Figure 4.1). CAIX was detectable in HCC1954 cell line variants following 1% O_2 incubation for 24hr (Figure 4.2 (A.)). Densitometry was performed on the HCC1954 blots (Figure 4.2(B.). At 1% O_2, HCC1954-NR had significantly decreased levels of CAIX when compared to the HCC1954-Par cell line variant (*p-value*=0.0498). CAIX was detectable in SKBR3 cell line variants following incubation at 1% O_2 for 24hr (Figure 4.3 (A.)). Densitometry was performed on the immunoblots (Figure 4.3 (B.)) SKBR3-NR cell line variant had significantly more CAIX at 1% O_2 compared to SKBR3-Par at 1% O_2 (*p-value*= 0.0472).

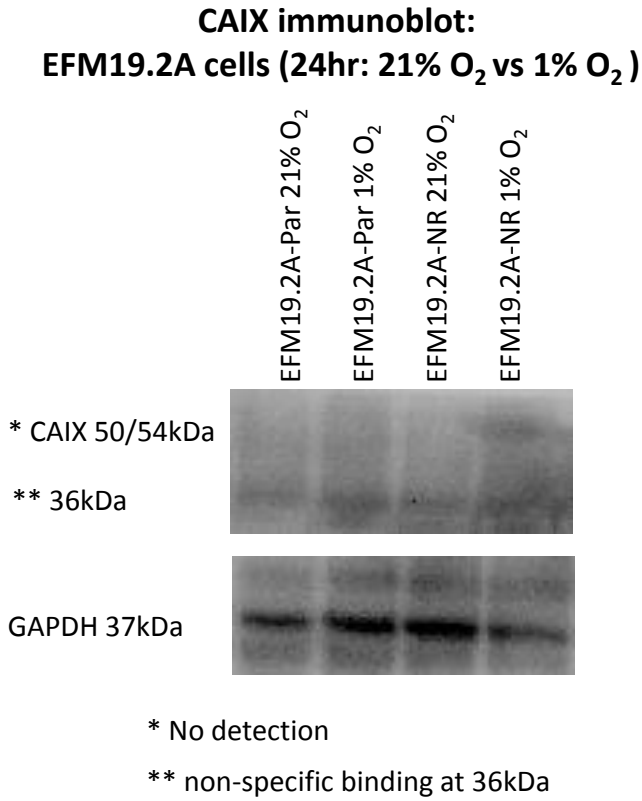

Figure 4.1: CAIX expression in EFM19.2A cell line variants (21% O_2 vs 1% O_2)
Lysates from EFM19.2A-Par and EFM19.2A-NR cell lines were collected following incubation at 21% O_2 and 1% O_2 for 24hr. Immunoblots were performed to check the expression levels of CAIX. Blot image shown is representative of n=3 blots. GAPDH was used as a loading control.

(A.)

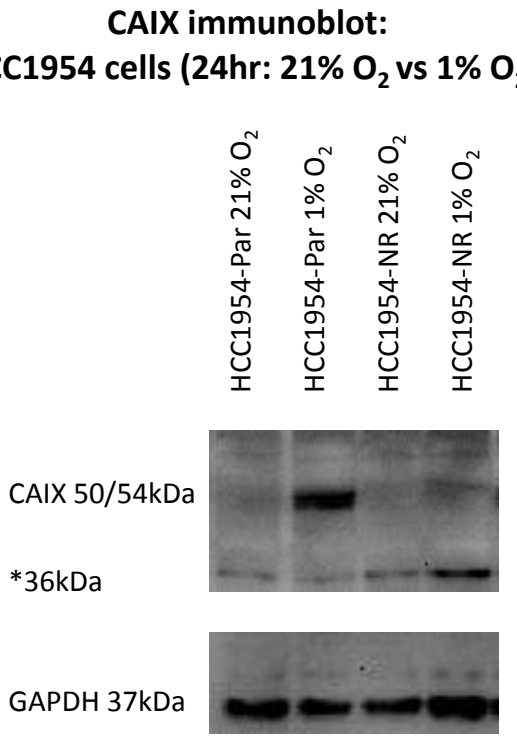

(B.)

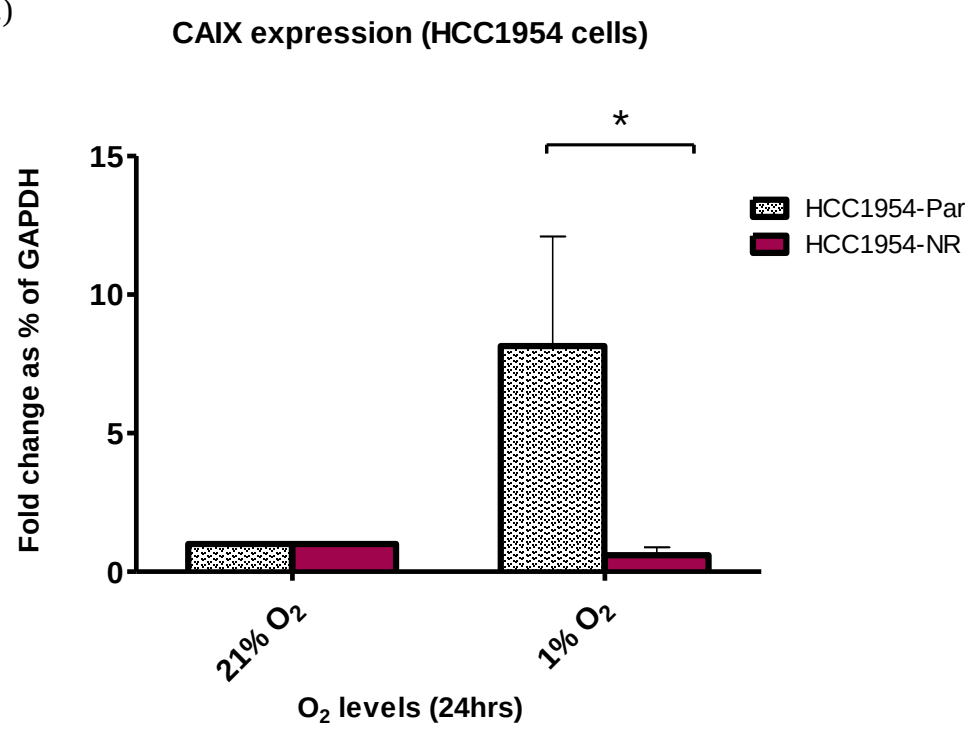

Figure 4.2: CAIX quantification in HCC1954 cell line variants (21% O_2 vs 1% O_2)
Lysates from HCC1954-Par and HCC1954-NR cell lines were collected following incubation at 21% O_2 and 1% O_2 for 24hr. Immunoblots were performed to quantify CAIX (A.). Densitometry was performed (B.). Blot image shown is representative of triplicate blots. GAPDH was used as a loading control. n=3±SEM, *p<0.05 (Student's t-test).

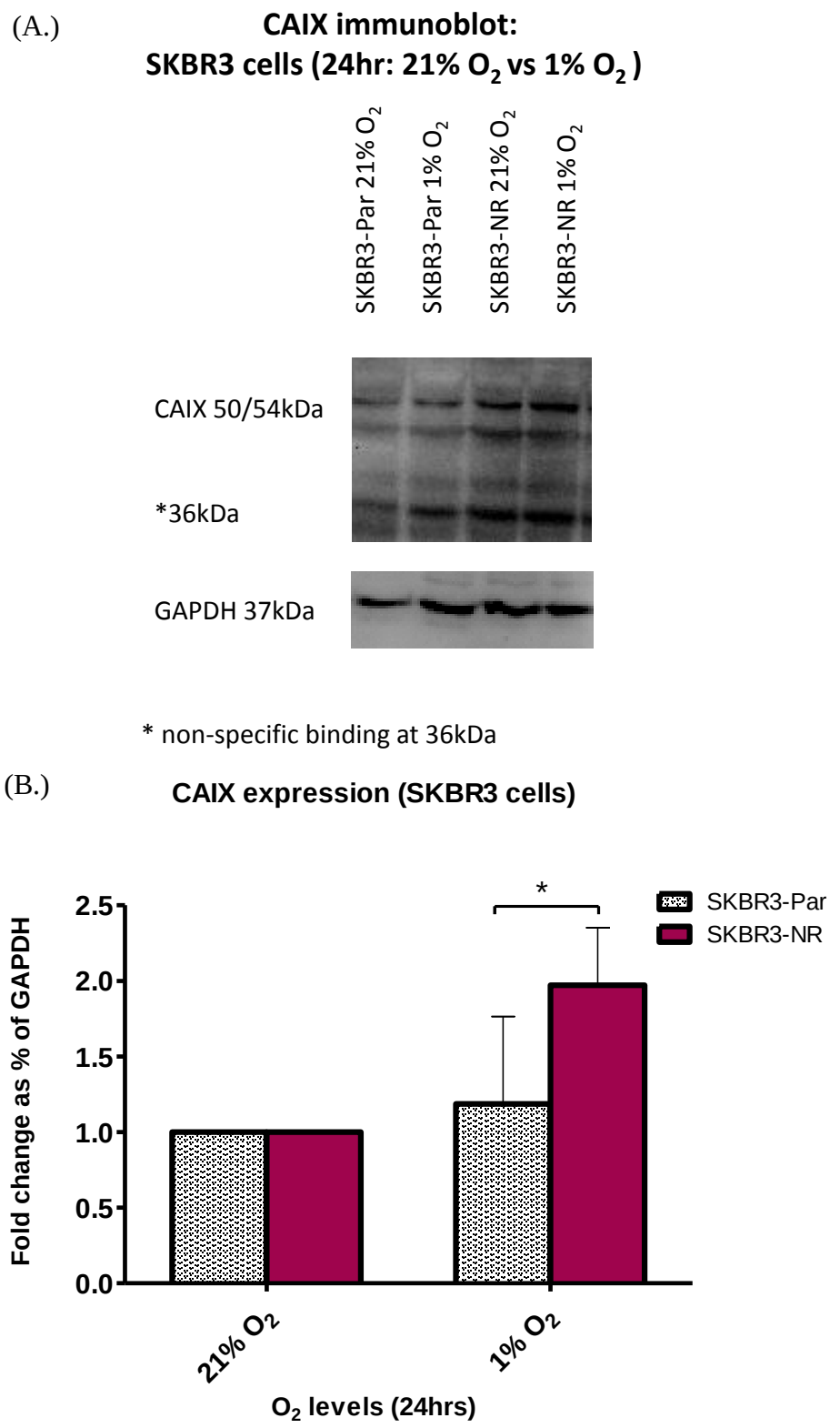

Figure 4.3: CAIX quantification in SKBR3 cell line variants (21% O_2 vs 1% O_2)
Lysates from SKBR3-Par and SKBR3-NR cell lines were collected following incubation at 21% O_2 and 1% O_2 for 24hr. Immunoblots were performed to quantify CAIX (A.). GAPDH was used as a loading control. Densitometry was performed (B.). Blot image shown is representative of triplicate blots. GAPDH was used as a loading control. n=3±SEM (Student's t-test).

4.2.2. CAIX quantification in HER2+ cell lines using ELISA (normoxia *vs* hypoxia)

[Work performed utilising the H35 hypoxystation (Whitley) in the Department of Surgery, Trinity Translational Medicine Institute, Trinity College Dublin, St James's Hospital, Dublin 8]

Immunoblotting is semi-quantitative but provides a method for assessing if the protein of interest is present. Immunoblots detected CAIX with the 50 and 54kDa bands but immunoblots are not highly sensitive, as seen when CAIX was not detected in the EFM19.2A cell line variants (Figure 4.1). ELISAs were used as a more sensitive and quantitative method for quantifying the levels of CAIX in all cell line variants. The error bars for the CAIX immunoblots were very variable between cell lines. It was noted that the hypoxia chamber used was not efficient at reducing O_2 levels immediately and thus a different hypoxia chamber was used. To ensure the mechanism of CAIX in neratinib-resistance was not cell line-specific, additional cell line variants (as described in 2.1.1) (BT474-Par, BT474-TR (trastuzumab-resistant), HCC1954-LR (lapatinib-resistant), SKBR3-TR and SKBR3-TLR (trastuzumab- and lapatinib-resistant) were obtained from Dr Neil Conlon. These cell lines were also selected to test if the mechanism of resistance was also applicable to other HER2-targeted therapy resistance. A fixed number of cells were seeded (Section 2.1) and incubated at 21% O_2 or 1% O_2 for 24, 48 and 72hr. CAIX levels varied for each cell line variant when comparing 24, 48 and 72hr treatments (summarised in Table 4.4 24hr, Table 4.5 48hr and Table 4.6 72hr).

4.2.2.1. CAIX levels in BT474 cell line variants

There were no significant differences in CAIX levels in the BT474 variants at 24hr (Figure 4.4 (A.)). After 48hr (Figure 4.4 (B.)), CAIX levels were significantly increased in BT474-TR cell line variants at 21% O_2 compared to BT474-Par at 21% O_2 (*p-value*=0.0014), CAIX was significantly increased in BT474-TR cell line variants at 21% O_2 compared to 1% O_2 (*p-value*=0.0019). At 72hr (Figure 4.4 (C.)), CAIX was significantly increased in BT-474-TR cell line variants compared to BT474-Par cell line variants at 21% O_2 (*p-value*=0.0376) and 1% O_2 (*p-value*=0.0016). When comparing BT474-TR variants at varying O_2 concentrations, CAIX levels increased at 1% O_2 compared to 21% O_2 (*p-value*=0.0040).

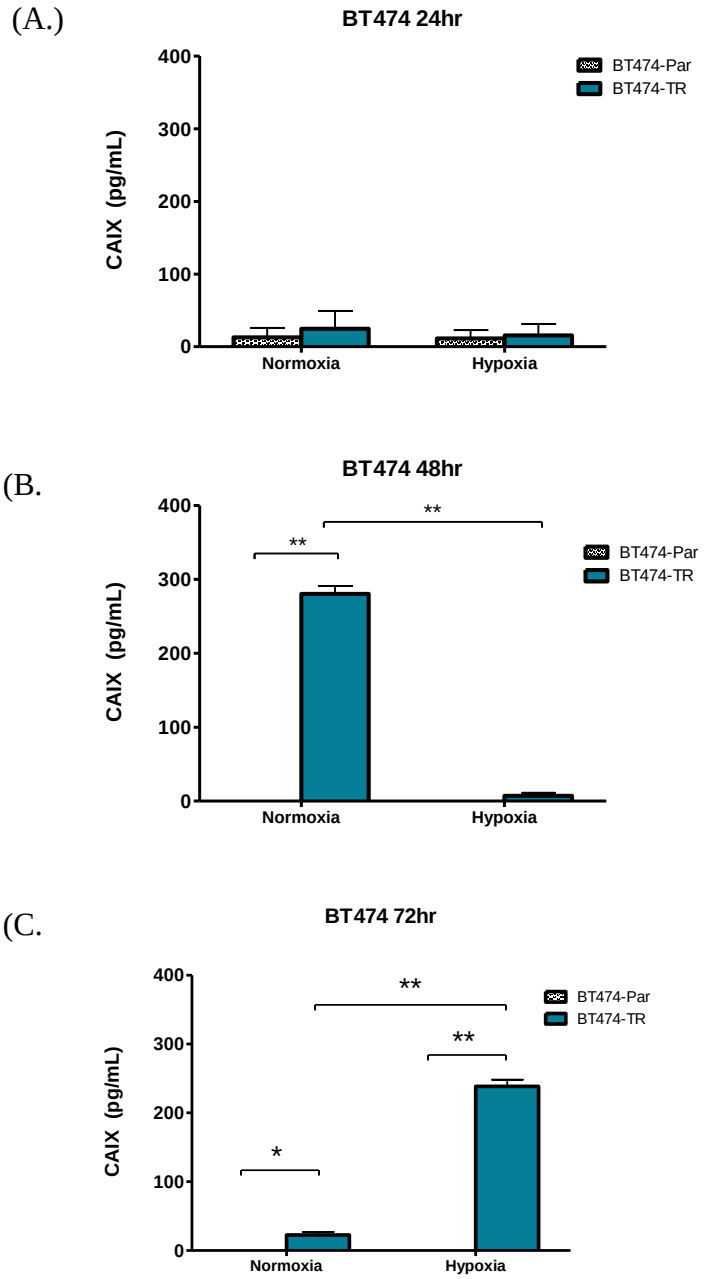

Figure 4.4: CAIX ELISAs from normoxic and hypoxic BT474 cell line variants
ELISAs were performed to compare CAIX levels in BT474-Par and BT474-TR cell line variants under normoxic (21% O_2) and hypoxic (1% O_2) conditions for 24hr (A.), 48hr (B.) and 72hr (C.). n=3±SEM, where *p<0.05 and **p<0.01. (*ANOVA*, Tukey's post hoc test).

4.2.2.2. CAIX levels in EFM19.2A cell line variants

There were no significant differences in CAIX levels in the EFM19.2A cell variants at 24hr (Figure 4.5 (A.)) or at 48hr (Figure 1.9 (B.)). At 72hr (Figure 4.5 (C.)), CAIX levels

were significantly increased in EFM19.2A-NR cell line variants at 1% O_2 compared to BT474-Par at 1% O_2 (p-value=0.0064). CAIX was significantly increased in EFM19.2A-NR cell line variants at 1% O_2 compared to 21% O_2 (p-value= 0.0064).

(A.)

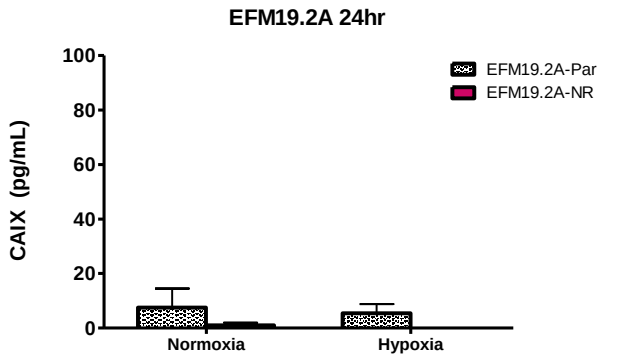

(B.

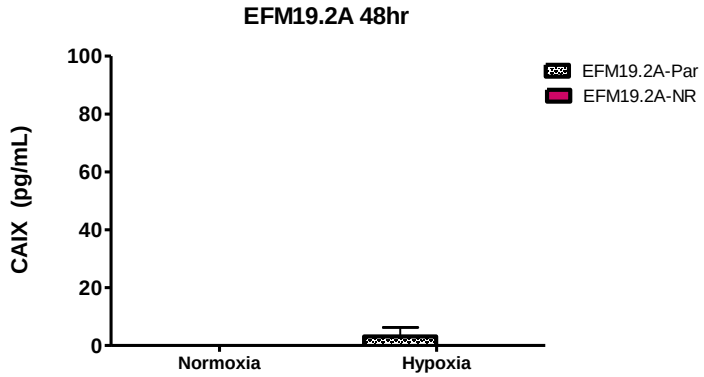

(C.

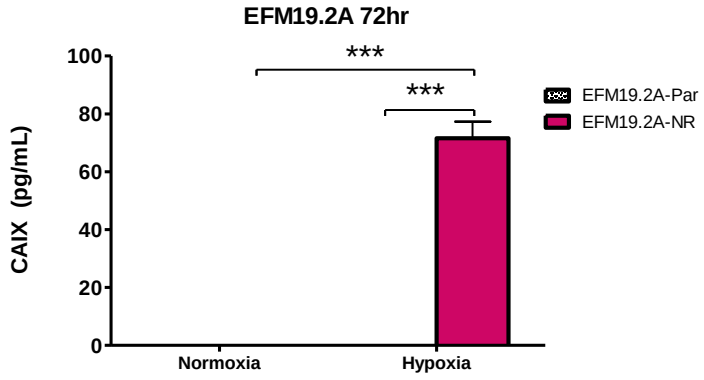

Figure 4.5: CAIX ELISAs from normoxic and hypoxic EFM19.2A cell line variants
ELISAs were performed to compare CAIX levels in EFM19.2A-Par and EFM19.2A-NR cell line variants under normoxic (21% O_2) and hypoxic (1% O_2) conditions for 24hr (A.), 48hr (B.) and 72hr (C.). n=3±SEM, where ***p<0.001. (*ANOVA*, Tukey's post hoc test).

4.2.2.3. CAIX levels in HCC1954 cell line variants

At 24hr (Figure 4.6 (A.)), when comparing 21% O_2 with 1% O_2, CAIX was increased in HCC1954-Par at 1% O_2 (*p-value*= 0.0012), increased in HCC1954-NR at 1% O_2 (*p-value*= 0.0031) and no significant difference was observed in HCC1954-LR cell line variants. When comparing CAIX levels in all cell variants at 1% O_2, a HCC1954-Par cell line variants had significantly more CAIX than HCC1954-NR (*p-value*= 0.0004) and HCC1954-LR (0.0092).

At 48hr (Figure 4.6 (B.)), CAIX levels were significantly increased in HCC1954-Par cell line variants at 1% O_2 compared to 21% O_2 (*p-value*= 0.0062), increased in HCC1954-NR cell line variants at 1% O_2 compared to 21% O_2 (*p*-value=0.0067) and no significant difference was observed for HCC1954-LR cell line variants. At 1% O_2, CAIX levels in HCC1954-Par were significantly increased when compared to HCC1954-NR (*p-value*= 0.0104) and HCC1954-LR (*p-value*= 0.0049).

At 72hr (Figure 4.6 (C.)), when looking at CAIX levels in 21% O_2 compared to 1% O_2, HCC1954-Par has significantly more CAIX at 1% O_2 (*p-value*= 0.0069), as did HCC1954-NR cell line variants (*p-value*= 0.0235) and HCC1954-LR (*p-value*=0.0432). At 1% O_2, CAIX was significantly decreased in HCC1954-NR compared to HCC1954-Par (*p-value*= 0.0004) and significantly increased in HCC1954-LR compared to HCC1954-Par (*p-value*= 0.0249).

CM was collected to determine if soluble CAIX was detectable in HCC1954-Par and HCC1954-NR cell-derived CM following 72hr incubation at 21% O_2 and 1% O_2. Soluble CAIX (or potentially EV-associated CAIX) was significantly increased in HCC1954-Par CM compared to HCC1954-NR CM (*p-value*=0.0036) (Figure 4.7).

(A.)

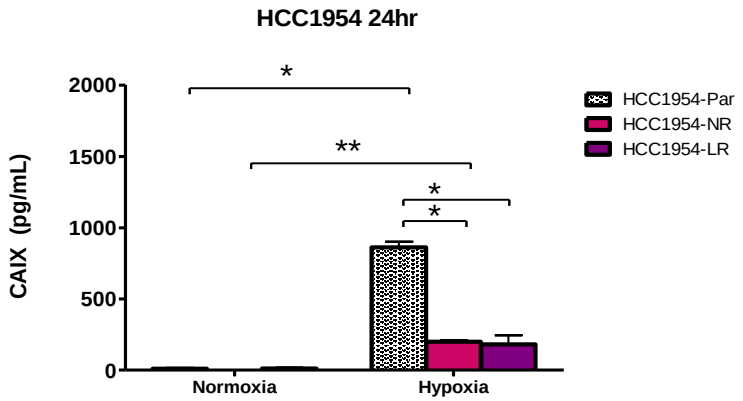

(B.)

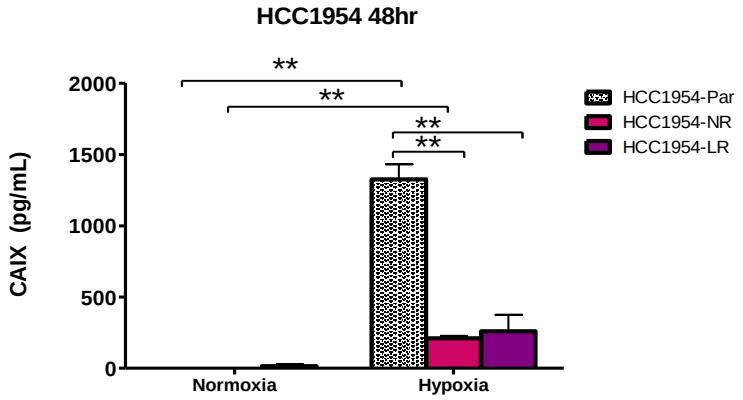

(C.)

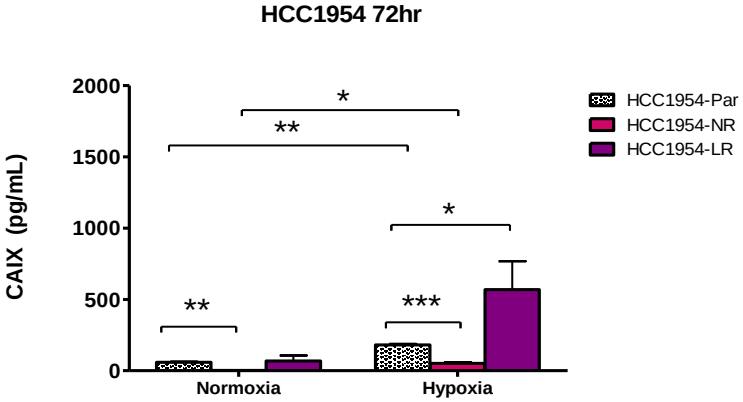

Figure 4.6: CAIX ELISAs from normoxic and hypoxic HCC1954 cell line variants
ELISAs were performed to compare CAIX levels in HCC1954-Par, HCC1954-NR and HCC1954-LR cell line variants under normoxic (21% O_2) and hypoxic (1% O_2) conditions for 24hr (A.), 48hr (B.) and 72hr (C.). n=3±SEM, where *p<0.0, **p<0.01 and ***p<0.001. (*ANOVA*, Tukey's post hoc test).

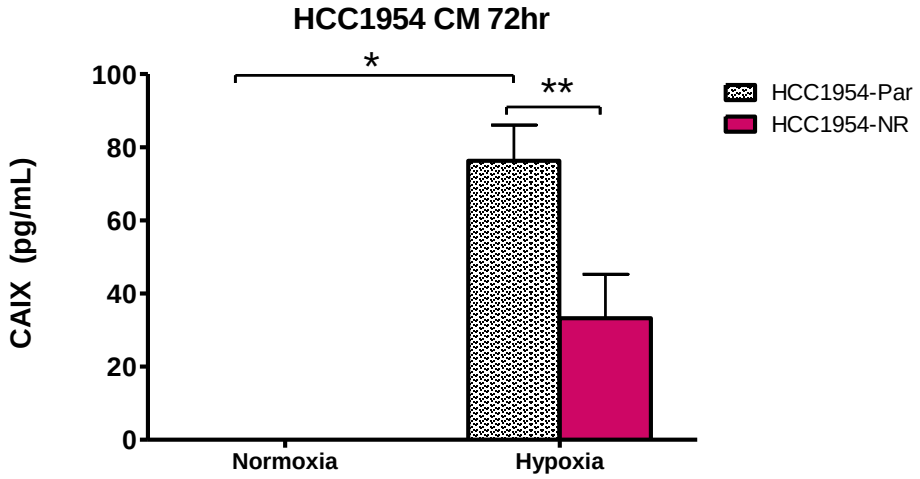

Figure 4.7: CAIX ELISAs from normoxic and hypoxic from HCC1954 cell line variants conditioned media
ELISAs were performed to compare CAIX levels in the CM from HCC1954-Par and HCC1954-NR cell line variants under normoxic (21% O_2) and hypoxic (1% O_2) conditions for 72hr. n=3±SEM, where **p<0.01 (*ANOVA, Tukey's post hoc test)*.

4.2.2.4. CAIX levels in SKBR3 cell line variants

At 24hr (Figure 4.8 (A.)), when comparing CAIX levels between variants at 21% O_2, CAIX was significantly increased in SKBR3-TR compared to SKBR3-Par (*p=value*= 0.0202). When comparing CAIX levels between variants at 1% O_2, SKBR3-TLR has significantly increased CAIX compared SKBR3-Par (*p-value*= 0.0123). At 1% O_2, SKBR3-TLR has significantly increased CAIX compared to 21% O_2 (*p-value*= 0.0170).

At 48hr (Figure 4.8 (B.)) and at 21% O_2, SKBR3-TR has significantly increased CAIX levels compared to SKBR-Par (*p-value*= 0.0003). At 1% O_2, SKBR3-NR has significantly increased CAIX compared to SKBR3-Par (*p-value*= 0.0018). When comparing 21% O_2 to 1% O_2, SKBR3-NR (*p-value*= 0.0107) and SKBR3-TLR (*p-value*=0.0240) had significantly increased CAIX at 1% and SKBR3-TR had significantly increased levels of CAIX at 21% O_2 (*p-value*= 0.0004)

After 21% O_2 incubation for 72hr (Figure 4.8 (C.), CAIX is significantly increased in SKBR3-TR compared to SKBR3-Par (*p-value*=0.0009). At 1% O_2, when compared to SKBR3-Par cell line variants, CAIX is significantly increased in SKBR3-NR (*p-value*= 0.0044) and SKBR3-TLR (*p-value*= 0.0006). When comparing CAIX levels in a variant at

21% O_2 to 1% O_2, SKBR3-NR and SKBR3-TLR have significantly increased levels of CAIX at 1% O_2 (*p-value*= 0.0040 and 0.0014, respectively) and SKBR3-TR has significantly increased CAIX at 21% O_2 (*p-value*= 0.0009).

(A.)

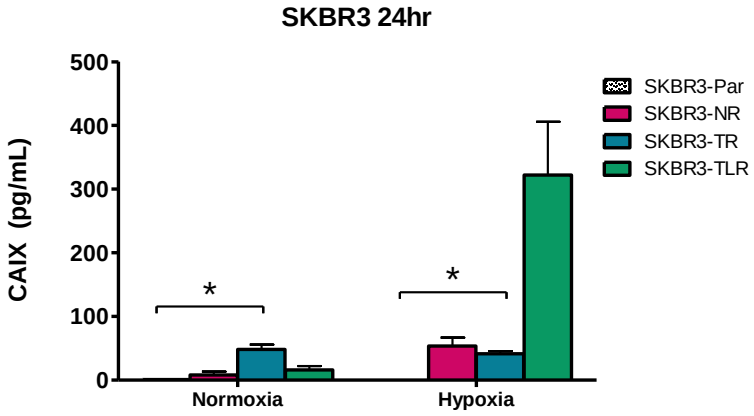

(B.

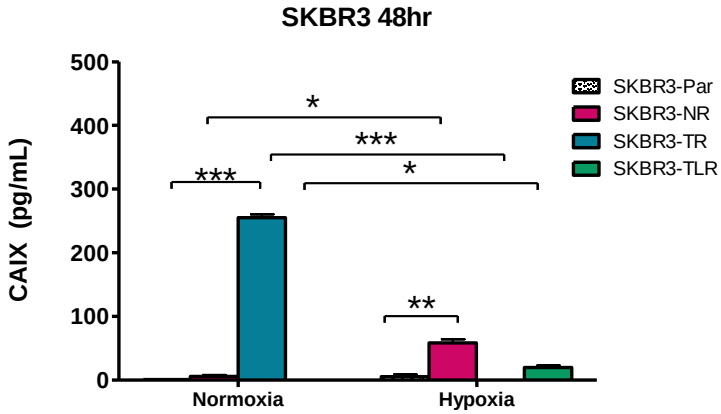

(C.

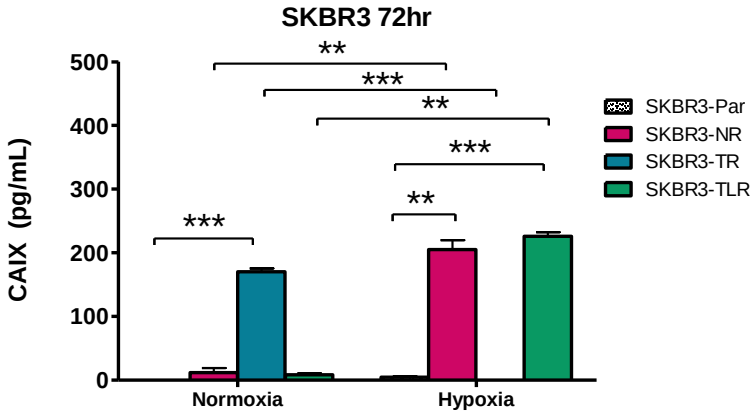

Figure 4.8: CAIX ELISAs from normoxic and hypoxic SKBR3 cell line variants
ELISAs were performed to compare CAIX levels in SKBR3-Par, SKBR3-NR, SKBR3-TR and SKBR3-TLR cell line variants under normoxic (21% O_2) and hypoxic (1% O_2) conditions for 24hr (A.), 48hr (B.) and 72hr (C.). n=3±SEM, where *p<0.05, **p<0.01 and ***p<0.001. (*ANOVA*, Tukey's post hoc test).

4.2.2.5. CAIX levels in EVs derived from cell line variants

EVs were successfully characterised as evidenced in Section 3.2.5. CAIX was detectable on the surface of cell line-derived EVs. However, there were no significant differences in the quantity of CAIX between EFM19.2a cell line variants (*p-value*=0.29), HCC1954 cell line variants (*p-value*=0.68) or SKBR3 cell line variants (*p-value*=0.51) (Figure 4.9).

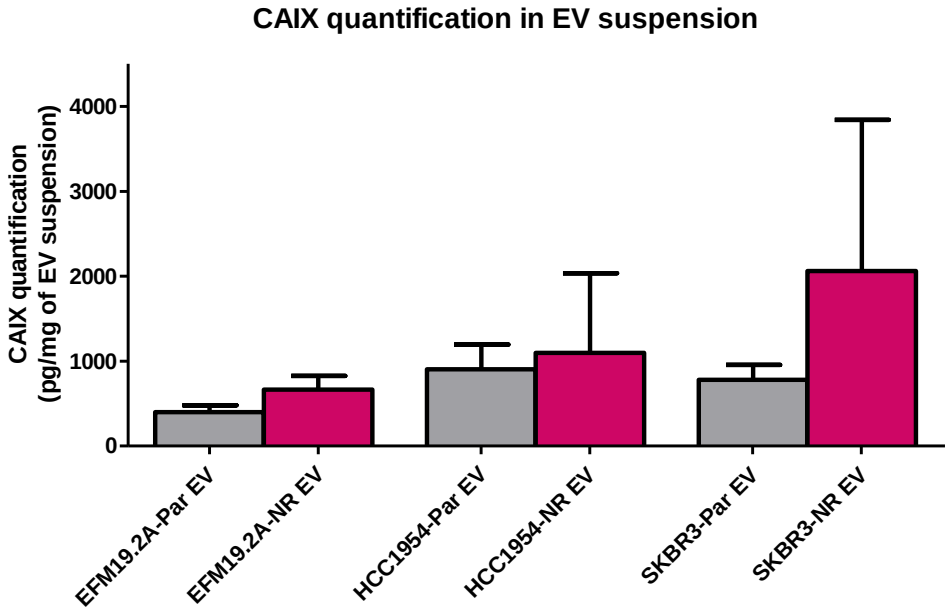

Figure 4.9: CAIX ELISAs of EVs derived from cell line variants
ELISAs were performed to compare CAIX levels on the surface of EVs isolated from EFM19.2A, HCC1954 and SKBR3 cell line variants under normoxic (21% O_2) conditions. There were no significant differences in CAIX between all neratinib-sensitive and neratinib-resistant EVs. n=3±SEM. (Student's t-test).

4.2.2.6. Summary Tables for CAIX ELISA

Summary Tables display the ability of all cell line variants to produce CAIX at either 21% O_2 or 1% O_2 at 24hr, 48hr and 72hr. At 24hr it is evident that there are few differences between CAIX expression between drug-sensitive and drug-resistant cell line variants (Table 4.1). At 48hr, when comparing O_2 conditions, an increase in CAIX expression becomes evident in many of the drug-resistant cell line variants and the HCC1954-Par cell line variant (Table 4.2). At 72hr, when comparing O_2 conditions, the greatest increases in CAIX expression are observed for drug-resistant variants (BT474-TR, EFM19.2A-NR,

HCC1954-NR, SKBR3-NR, SKBR3-TR and SKBR3-TLR) (Table 4.3). CAIX expression in the HCC1954-Par cell was significantly increased at 72hr (Table 4.3).

Cell line variant	**O_2 conditions in which CAIX differences (if any) were observed**	**Significance level**
24hr		
BT-474-Par	No differences	No significant difference
BT474-TR	No differences	No significant difference
EFM19.2A-Par	No differences	No significant difference
EFM19.2A-NR	No differences	No significant difference
HCC1954-Par	At 1% O_2 conditions	↑*
HCC1954-LR	No differences	No significant difference
HCC1954-NR	At 1% O_2 conditions	↑**
SKBR3-Par	No differences	No significant difference
SKBR3-NR	No differences	No significant difference
SKBR3-TR	No differences	No significant difference
SKBR3-TLR	No differences	No significant difference

Table 4.1: Summary Table comparing CAIX levels between 21% O_2 and 1% O_2 in cell line variants at 24hr.

Cell line variant	**O_2 conditions in which CAIX differences (if any) were observed**	**Significance level**
24hr		
BT-474-Par	No difference	No significant difference
BT474-TR	At 21% O_2 conditions	↑**
EFM19.2A-Par	No difference	No significant difference
EFM19.2A-NR	No difference	No significant difference
HCC1954-Par	At 1% O_2 conditions	↑**
HCC1954-LR	No difference	No significant difference
HCC1954-NR	At 1% O_2 conditions	↑**
SKBR3-Par	No difference	No significant difference
SKBR3-NR	At 1% O_2 conditions	↑*
SKBR3-TR	At 21% O_2 conditions	↑***
SKBR3-TLR	At 1% O_2 conditions	↑*

Table 4.2: Summary Table comparing CAIX levels between 21% O_2 and 1% O_2 in cell line variants at 48hr.

Cell line variant	**O_2 conditions in which CAIX differences (if any) were observed**	**Significance level**
48hr		
BT-474-Par	No difference	No significant difference
BT474-TR	At 1% O_2 conditions	↑***
EFM19.2A-Par	No difference	No significant difference
EFM19.2A-NR	At 1% O_2 conditions	↑***
HCC1954-Par	At 1% O_2 conditions	↑**
HCC1954-LR	No difference	No significant difference
HCC1954-NR	At 1% O_2 conditions	↑*
SKBR3-Par	No difference	No significant difference
SKBR3-NR	At 1% O_2 conditions	↑**
SKBR3-TR	At 21% O_2 conditions	↑***
SKBR3-TLR	At 1% O_2 conditions	↑**

Table 4.3: Summary Table comparing CAIX levels between 21% O_2 and 1% O_2 in cell line variants at 72hr.

Similarly, Summary Tables representing CAIX levels in all resistant cell line variants compared to their parent counterparts at 24hr (Table 4.4), 48hr (Table 4.5) and 72hr (Table 4.6) in both normoxic and hypoxic conditions are displayed. At 24hr, the SKBR3-TR cell line variant was the only cell line to have a significant increase in CAIX at 21% O_2 and 1% O_2 ($p<0.05$ for both). There was a significant decrease in CAIX levels in HCC1954-LR and HCC1954-NR cell line variants at 1% O_2 when compared to the HCC1954-Par cell line variant (Table 4.4). At 48hr, both trastuzumab-resistant cell line variants (BT474-TR and SKBR3-TR) had increased CAIX levels at 21% O_2 compared to their parent counterparts (BT474-Par and SKBR3-Par) (Table 4.5). At 48hr, there was a significant decrease in CAIX levels in HCC1954-LR and HCC1954-NR cell line variants at 1% O_2 when compared to the HCC1954-Par cell line variant ($p<0.01$) (Table 4.5). At 72hr, trastuzumab-resistant cell line variants (BT474-TR and SKBR-TR) has increased CAIX at 21% O_2 when compared to BT474-Par and SKBR3-Par cell line variants (Table 4.6).

HCC1954-NR has a significant decrease in CAIX at 1% O_2 when compared to HCC1954-Par. All other drug-resistant cell line variants (EFM19.2A-NR, HCC1954-LR, SKBR3-NR and SKBR3-TLR) has increased CAIX expression at 1% O_2 when compared to their drug-sensitive counterparts (Table 4.6).

Cell line variant (compared to respective parent cell line variant)	**CAIX trends in normoxia**	**CAIX trends in hypoxia**
24hr		
BT-474-TR	No significant difference	No significant difference
EFM19.2A-NR	No significant difference	No significant difference
HCC1954-LR	No significant difference	↓*
HCC1954-NR	No significant difference	↓*
SKBR3-NR	No significant difference	No significant difference
SKBR3-TR	↑*	↑*
SKBR3-TLR	No significant difference	No significant difference

Table 4.4: Summary Table comparing CAIX levels in resistant cell line variants to parent cell line variants at 24hr.

Cell line variant (compared to respective parent cell line variant)	**CAIX trends in normoxia**	**CAIX trends in hypoxia**
48hr		
BT-474-TR	↑**	No significant difference
EFM19.2A-NR	No significant difference	No significant difference
HCC1954-LR	No significant difference	↓**
HCC1954-NR	No significant difference	↓**
SKBR3-NR	No significant difference	↑**
SKBR3-TR	↑***	No significant difference
SKBR3-TLR	No significant difference	No significant difference

Table 4.5: Summary Table comparing CAIX levels in resistant cell line variants to parent cell line variants at 48hr.

Cell line variant (compared to respective parent cell line variant)	**CAIX trends in normoxia**	**CAIX trends in hypoxia**
72hr		
BT-474-TR	↑*	↑**
EFM19.2A-NR	No significant difference	↑***
HCC1954-LR	No significant difference	↑*
HCC1954-NR	↓**	↓***
SKBR3-NR	No significant difference	↑**
SKBR3-TR	↑***	No significant difference
SKBR3-TLR	No significant difference	↑***

Table 4.6: Summary Table comparing CAIX levels in resistant cell line variants to parent cell line variants at 72hr.

4.2.3. Preliminary analysis of S4 as a suitable CAIX inhibitor

Due to the increased levels of CAIX in resistance cell line variants compared to sensitive cell line variants, the CAIX inhibitor, S4 was used to test if this protein is functional in the mechanism of resistance. Firstly, the efficacy of S4 as a CAIX inhibitor in cell line variants was investigated. Acid phosphatase assays were performed on EFM19.2A, HCC1954 and SKBR3 cell lines following treatment with the CAIX inhibitor (S4) for 72hr (Figure 4.10). No significant changes were evident between cell line variants. The maximum concentration chosen for the treatment of all cell lines was 25µM. To test the efficacy of S4 as a CAIX inhibitor, HCC1954-Par cell line variants were treated at varying concentrations (6, 12 and 25µM) for 24, 48 and 72hr (Figure 4.11 (A.)). Densitometry was performed on n=3 blots and statistical analysis was performed using *ANOVA* (Figure 4.11 (B.)).CAIX was shown to be significantly decreased following 12 and 25µM treatment for 24hr (*p*-value=0.0468 and 0.0034, respectively) and at 25µM treatment for 48hr (*p*-value=0.0464). At 72hr, S4 no longer decreases CAIX production at 25µM. To ensure the ELISA was correlating with the trends evident in the immunoblot results, the experiments were repeated and CAIX levels were analysed using the ELISA kit with fixed amount of protein (Figure 4.12). Similar trends were observed for both the ELISA and immunoblots. At 48hr, S4 significantly reduced CAIX at 25µM (*p-value*= 0.029).

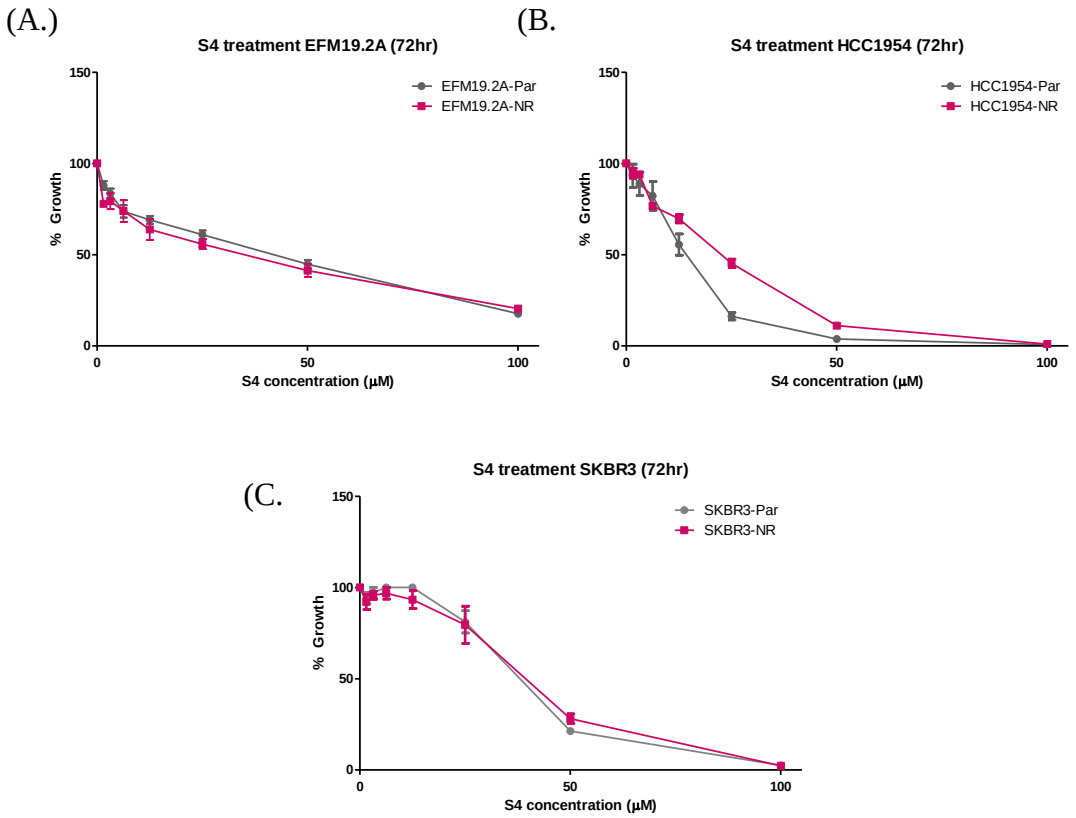

Figure 4.10: Toxicity assays for S4 treatment (72hr) in EFM19.2A, HCC1954 and SKBR3 cell line variants

Acid phosphatase assays were performed on EFM19.2A (A.), HCC1954 (B.) and SKBR3 (C.) cell line variants following treatment with S4 (0-100µM) for 72hr. n=3±SEM.

(A.)

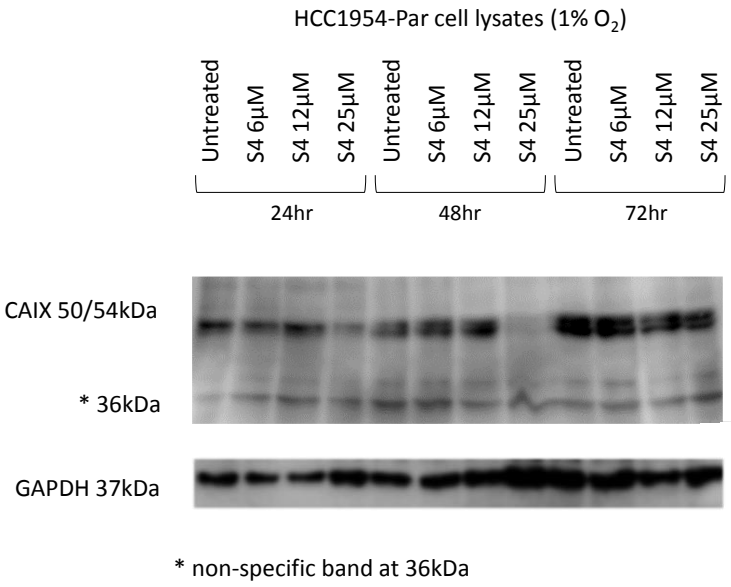

(B.)

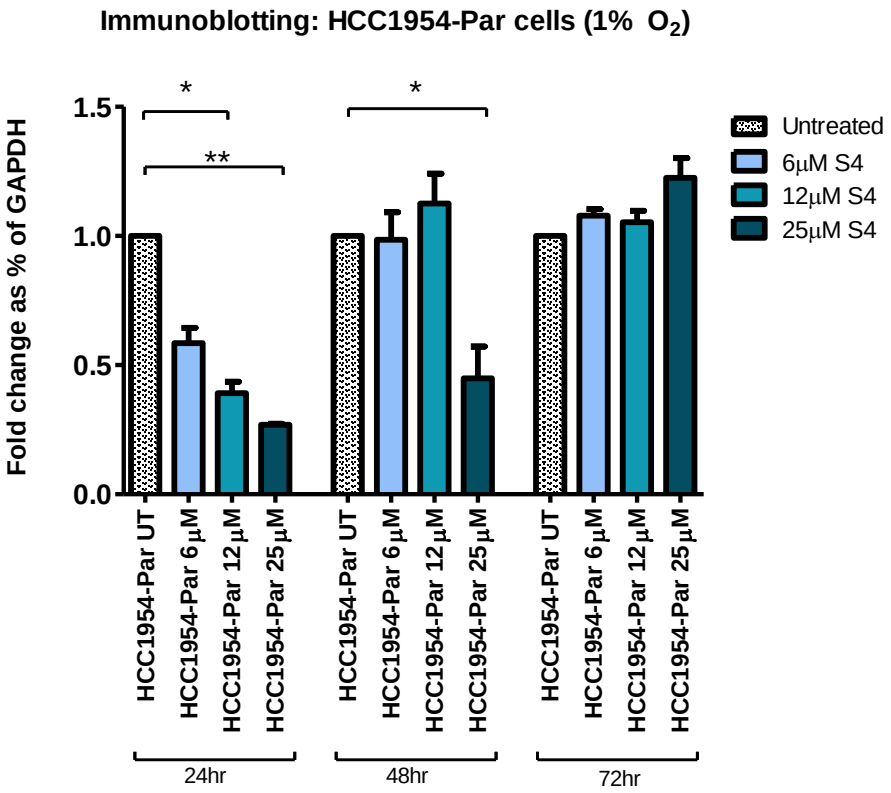

Figure 4.11: Immunoblot of CAIX in S4-treated HCC1954-Par cell line variants at 24, 48 and 72hrs

Immunoblots were performed to quantify CAIX following S4 treatment (6µM, 12µM and 25µM) at 24, 48 and 72hr (A.). GAPDH was used as a loading control. Densitometry was performed (B.). Blot image shown is representative of triplicate blots. GAPDH was used as a loading control. n=3±SEM, *p<0.05. **p<0.01. (*ANOVA*).

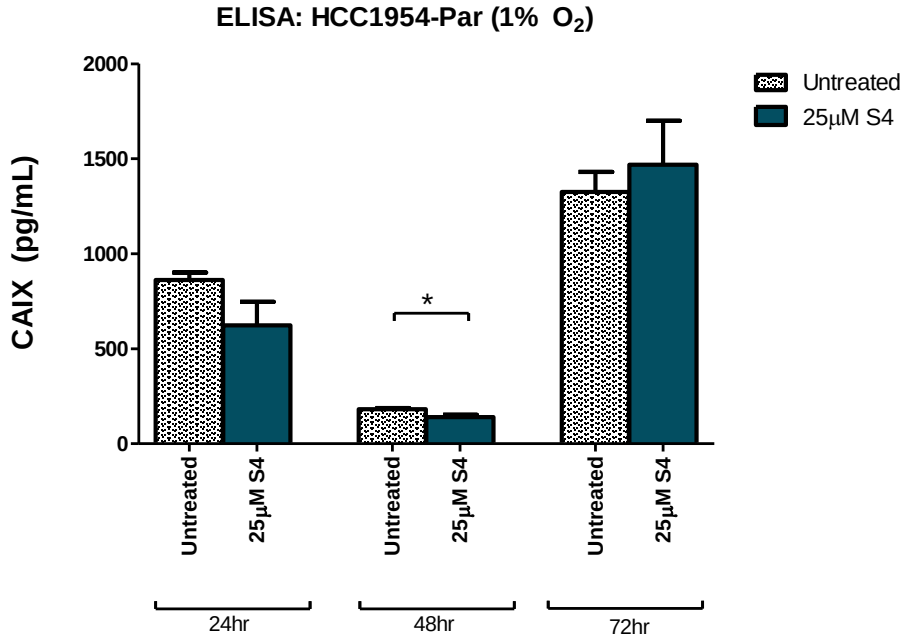

Figure 4.12: CAIX levels in S4-treated HCC1954-Par cell line variants using ELISA
ELISAs were performed to quantify CAIX levels in the S4-treated HCC1954-Par (1% O_2) for 24, 48 and 72hr. n=3±SEM, *p<0.05. (Student's t-test).

4.2.4. CAIX quantities following S4 treatment for 24, 48 and 72hr (ELISA)

Cell line variants were treated with S4 at 25μM for 24, 48 and 72hr at 1% O_2. ELISAs were used to quantify CAIX levels in all cell lines and compare to their untreated counterparts (no treatment, 1% O_2) (Summary of all results Table 4.7). As evidenced in Figure 4.10, S4 induces variable toxic effects in cell line variants, thus CAIX levels were normalised to protein quantity for all cell line variants. As BT474-TR and SKBR3-TR cell line variants displayed increased CAIX levels in normoxic condition (Figure 4.4) additional tests were performed using S4 during normoxic conditions.

At 24hr, (no CAIX expression at 48 or 72hr), there were no significant differences in CAIX levels between untreated and S4-treated BT474-Par cell line variants (Figure 4.13 (A.)). For BT474-TR cell line variants (Figure 4.13 (B.)), there were no significant changes in CAIX at 24 or 48hr S4 treatment but at 72hr, S4 significantly reduced CAIX levels (*p-value*= 0.0106). Similarly, for BT474-TR cell line variant treated with S4 under normoxic conditions for 72hr (Figure 4.13 (C.)), CAIX was significantly inhibited by S4 (*p*-value=0.0021), however there was large variability (standard deviations) for the 24 and 48hr conditions. There were no significant differences in CAIX levels for untreated and S4-treated EFM19.2A-Par or EFM19.2A-NR for all time points (Figure 4.14 (A.) and

(B.)), large errors were observed in EFM19.2A-Par cell line variants at 48hr. However, EFM19.2A-NR was trending towards increased CAIX following 72hr S4 treatment (*p-value*=0.051). There were no significant changes in CAIX levels between treated and untreated HCC1954-Par cell line variants (Figure 4.15 (A.)). There were no significant changes for HCC1954-LR cell lines (Figure 4.15 (B.)). At 24hr, S4 inhibition of CAIX was disrupted, CAIX was increased in HCC1954-NR cell line variants compared to HCC1954-Par cell line variants (*p-value*=0.0049) (Figure 4.15 (C.)). S4 did not significantly inhibit CAIX levels in SKBR3-Par, SKBR3-TR or SKBR3-TLR at all time points when cultured at 1% O_2 (Figure 4.16 (A.), (C.) and (D.)). S4 significantly decreased CAIX levels in SKBR3-NR cell line variants at 24hr (*p-value*=0.0362) (Figure 4.16 (B.)). SKBR3-TR cell line variants had significantly increased CAIX following 48hr S4 treatment during normoxic conditions (*p-value*=0.035) (Figure 4.16 (E.)). Correlation between CAIX expression post-S4 treatments (*i.e.* ability of cell line variant to overcome S4 inhibitory effects) and neratinib sensitivity (IC_{50} value) was evaluated by Spearman rank correlation analysis for non-parametric measurements. Neratinib-resistance positively correlated with increased CAIX expression/ability of cell line variants to overcome S4 treatment at 72hr (*p-value*=0.002) (Spearman r = 0.82) (Figure 4.17).

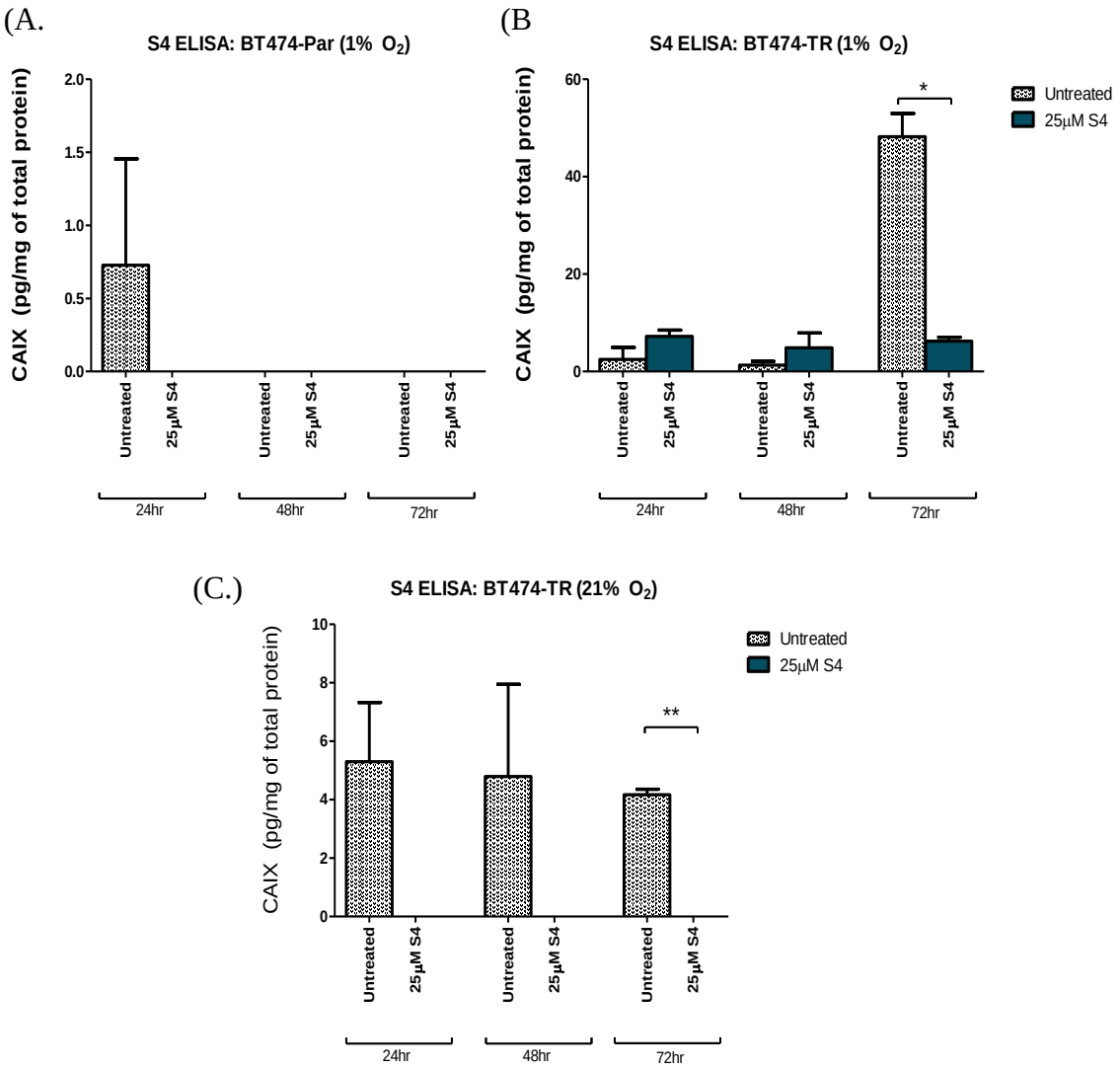

Figure 4.13:CAIX levels in S4-treated BT474 cell line variants

CAIX levels were quantified in BT474 cell line variants with ELISA. BT474-Par treated with S4 for 24, 48 and 72hr at 1% O_2 (A.), BT474-TR treated with S4 for 24, 48 and 72hr at 1% O_2 (B.) and BT474-TR treated with S4 for 24, 48 and 72hr at 21% O_2 (C.). n=3±SEM, *p<0.05, **p<0.01. (Student's t-test).

(A.)

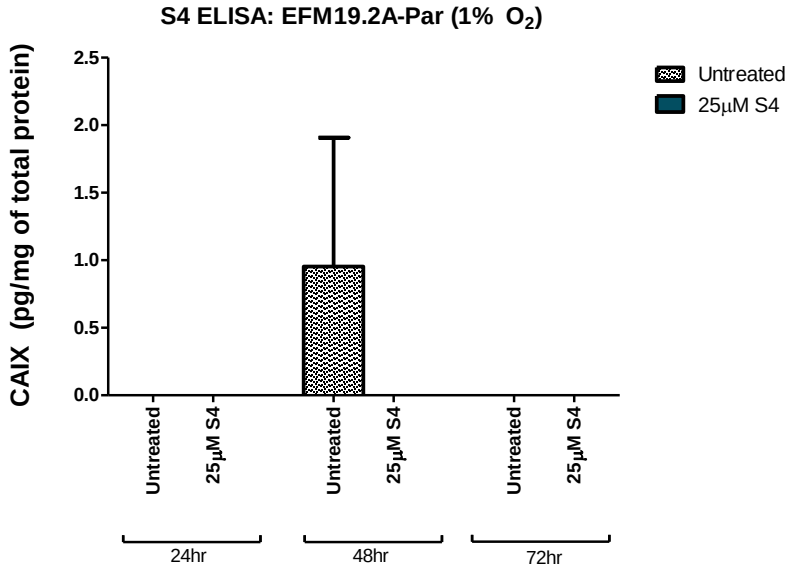

(B.)

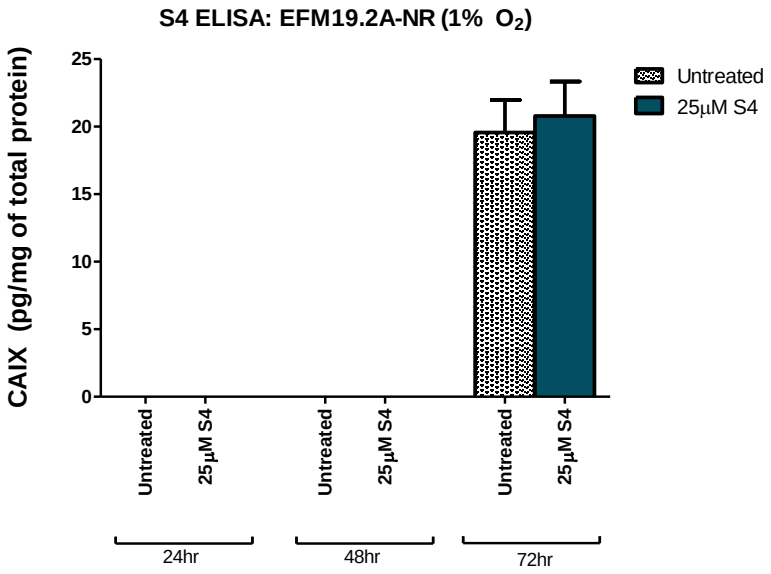

Figure 4.14: CAIX levels in S4-treated EFM19.2A cell line variants
CAIX levels were quantified in EFM19.2A cell line variants with ELISA. EFM19.2A-Par (A.) and EFM19.2A-NR (B.) treated with S4 (25µM) for 24, 48 and 72hr at 1% O_2. (Student's t-test).

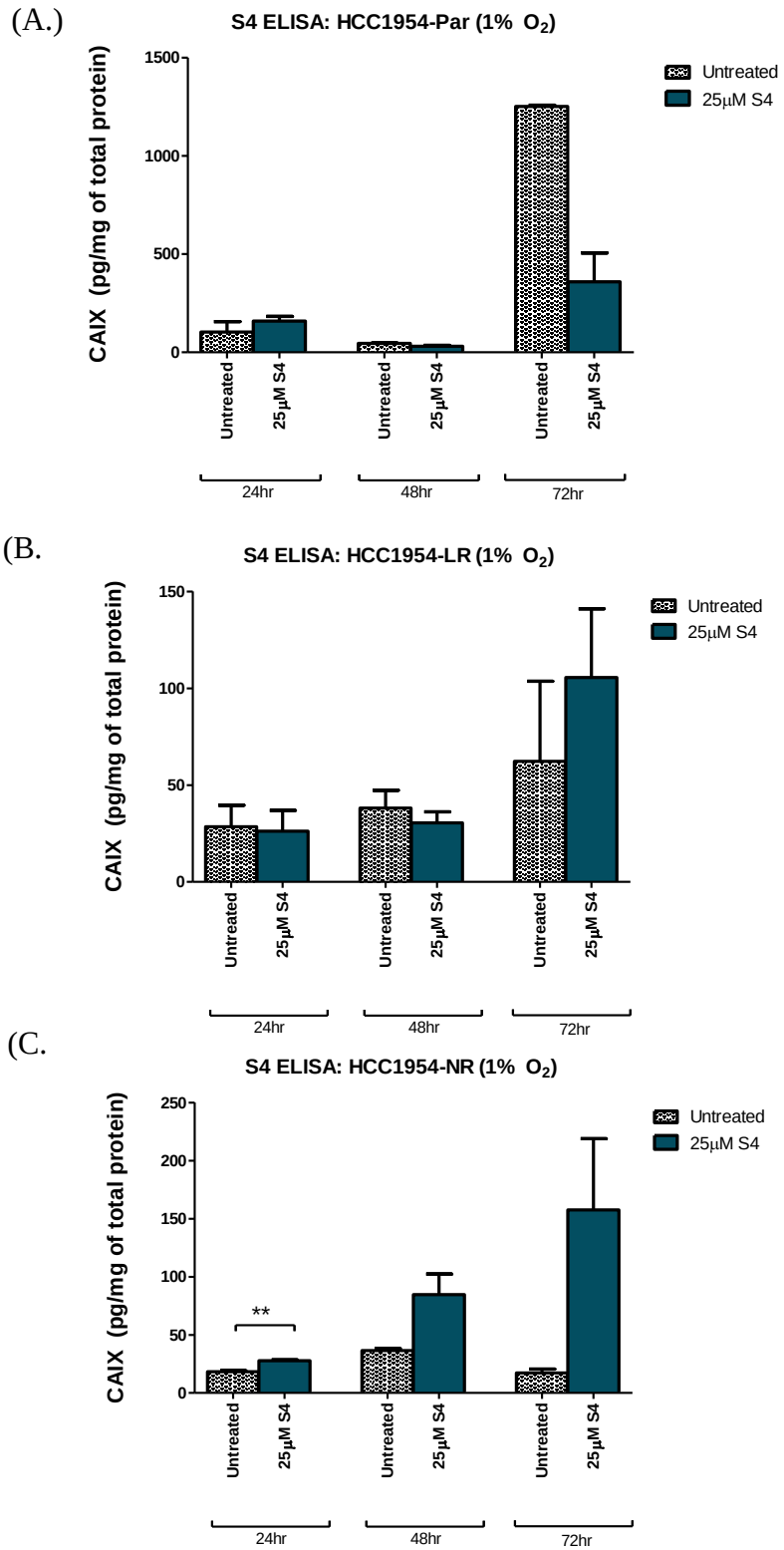

Figure 4.15: CAIX levels in S4-treated HCC1954 cell line variants
CAIX levels were quantified in HCC1954 cell line variants with ELISA. HCC1954-Par (A.), HCC1954-LR (B.) and HCC1954-NR (C.) were with S4 (25µM) for 24, 48 and 72hr at 1% O_2. n=3±SEM, **p-value<0.01. (Student's t-test).

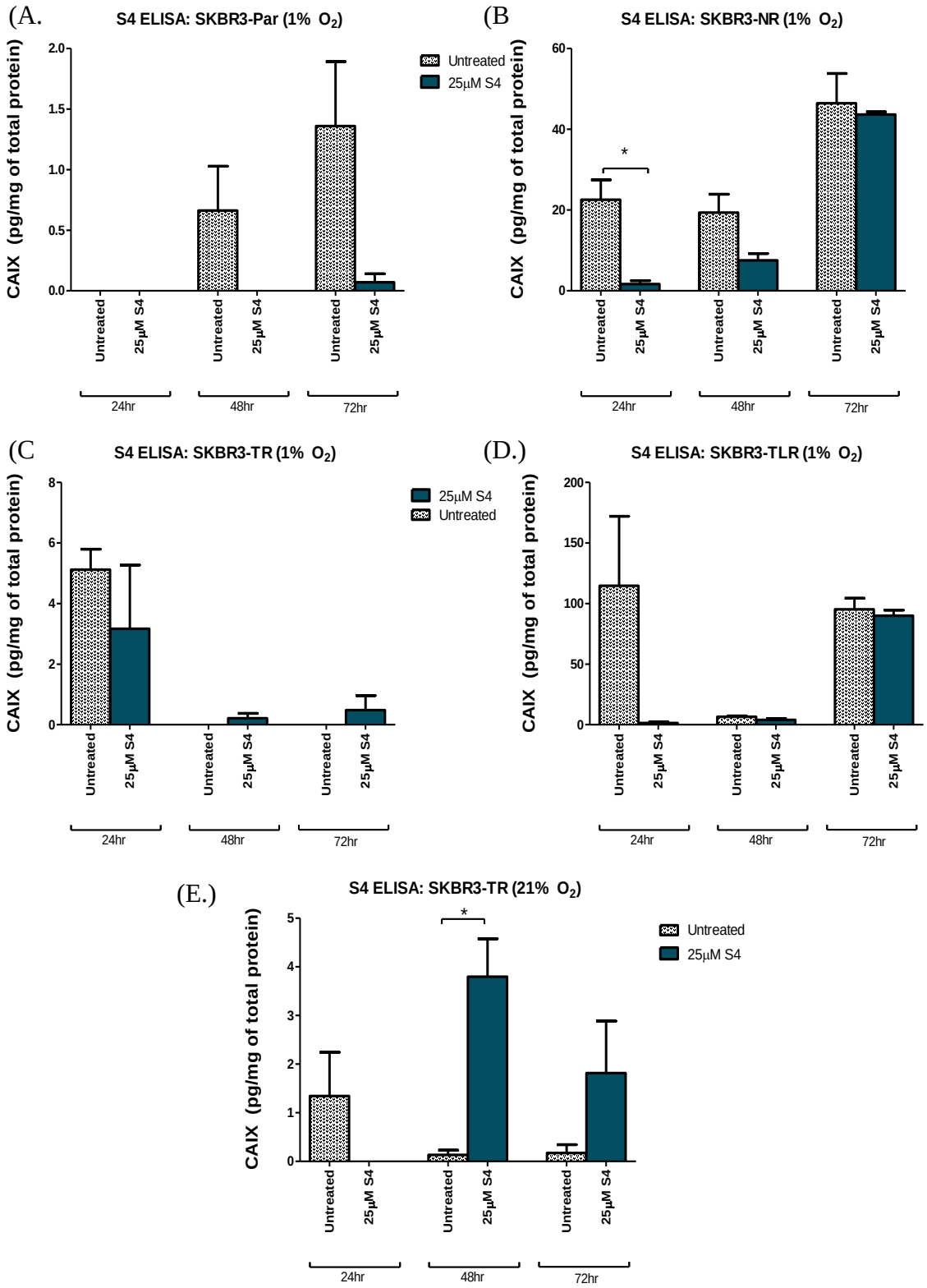

Figure 4.16: CAIX levels in S4-treated SKBR3 cell line variants
CAIX levels were quantified in SKBR3 cell line variants with ELISA. SKBR3-Par (A.), SKBR3-NR (B.), SKBR3-TR (C.) and SKBR3-TLR (D.) treated with S4 for 24, 48 and 72hr at 1% O_2. SKBR3-TR treated with S4 for 24, 48 and 72hr at 21% O_2. n=3±SEM, *p<0.05. (Student's t-test)

Cell line, O_2 conditions	**CAIX trends following S4 treatment**
S4 continually reduces CAIX at 24, 48 and 72hr	
BT474-Par, 1% O_2	CAIX expression low, trend towards partial inhibition at 24hr
BT474-TR, 1% O_2	S4 reduces CAIX expression at 72hr (*p-value*= 0.0106)
BT474-TR, 21% O_2	S4 continually inhibits CAIX production, S4 inhibits CAIX expression at 72hr (*p-value*= 0.002)
EFM19.2A-Par, 1% O_2	CAIX expression low, trend towards partial inhibition at 48hr
SKBR3-Par, 1% O_2	Trend towards partial inhibition at 48 and 72hr
Loss of S4 efficacy over time	
EFM19.2A-NR, 1% O_2	Trend towards no inhibition at 72hr
HCC1954-Par, 1% O_2	Trend towards partial inhibition at 72hr
HCC1954-LR, 1% O_2	No inhibition at 72hr
HCC1954-NR, 1% O_2	No inhibition at 24hr (*p-value*= 0.0049), 48hr or 72hr
SKBR3-NR, 1% O_2	Reduced CAIX expression at 24hr (*p-value*= 0.0362) and 48hr. No inhibition at 72hr.
SKBR3-TR, 1% O_2	Partial inhibition at 24hr. No inhibition at 48 and 72hr
SKBR3-TR, 21% O_2	Partial inhibition at 24hr. No inhibition at 48 (*p-value*=0.035) and 72hr
SKBR3-TLR, 1% O_2	Partial inhibitory effects at 24hr. No inhibition at 48 and 72hr

Table 4.7 Summary of CAIX levels following S4-treatments at 24, 48 and 72hr

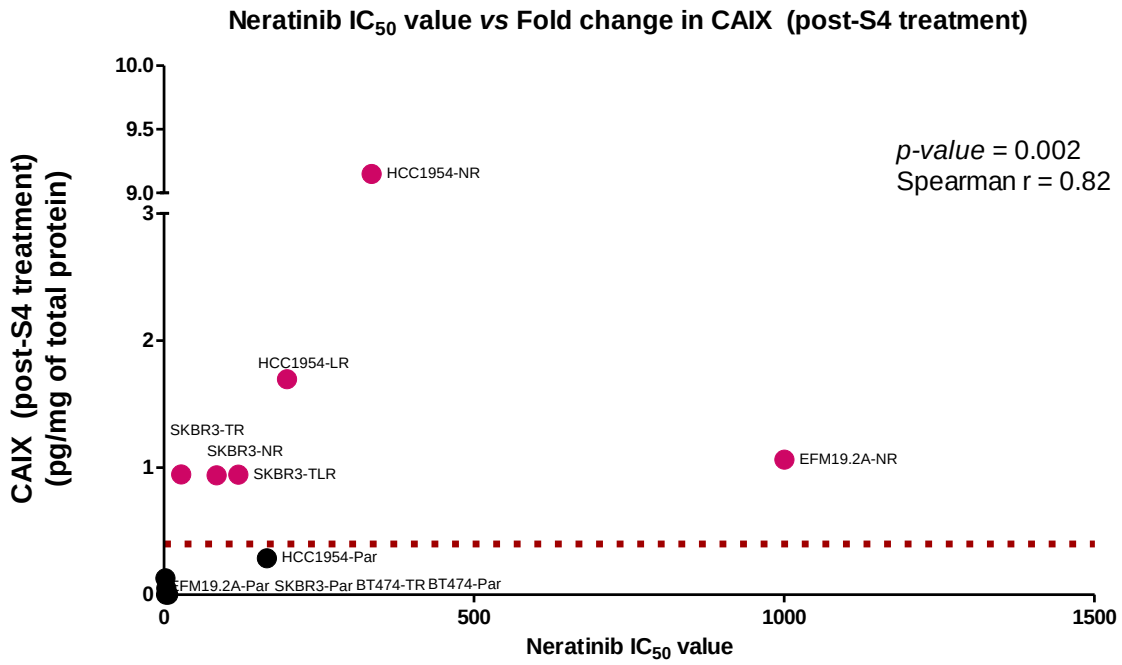

Figure 4.17: Spearman correlation analysis for neratinib sensitivity vs CAIX expression post-S4 treatment

Spearman correlation analysis was performed on CAIX expression levels for all cell line variants post-S4 treatment vs neratinib sensitivity. Pink dots indicate the neratinib-resistant variants, black dots represent the neratinib-sensitive variants. (*p-value*=0.002). (Spearman r =0.82). (Spearman correlation test).

4.2.5. S4 toxicity assays (normoxia *vs* hypoxia)

Cell line variants were treated with S4 for 5 days at 21% O_2 or 1% O_2. Acid phosphatase assays were used to determine any variation in toxicity between the two conditions.

BT474-Par and BT474-TR cell lines were significantly more sensitive to S4 in normoxic conditions compared to hypoxic conditions (*p-value*=0.001 and 0.013, respectively) (Figure 4.18, Table 4.8). Normoxic EFM19.2A-Par cell line variants were significantly more sensitive to S4 than hypoxic cell line variants (*p-value*=0.001) (Figure 4.19, Table 4.8). There was no significant difference for EFM19.2A-NR cell line variants. HCC1954-NR cell line variants were more resistant to S4-related toxicity in hypoxic conditions compared to normoxic conditions (*p-value*= 0.028) (Figure 4.20, Table 4.8). There were no significant differences for HCC1954-Par or HCC1954-LR. SKBR3-Par and SKBR3-NR cell line variants were more sensitive to S4 during normoxic conditions compared to hypoxic conditions (*p-value*=0.006 and 0.007, respectively) (Figure 4.21, Table 4.8). There were no significant differences in SKBR3-TR or SKBR3-TLR.

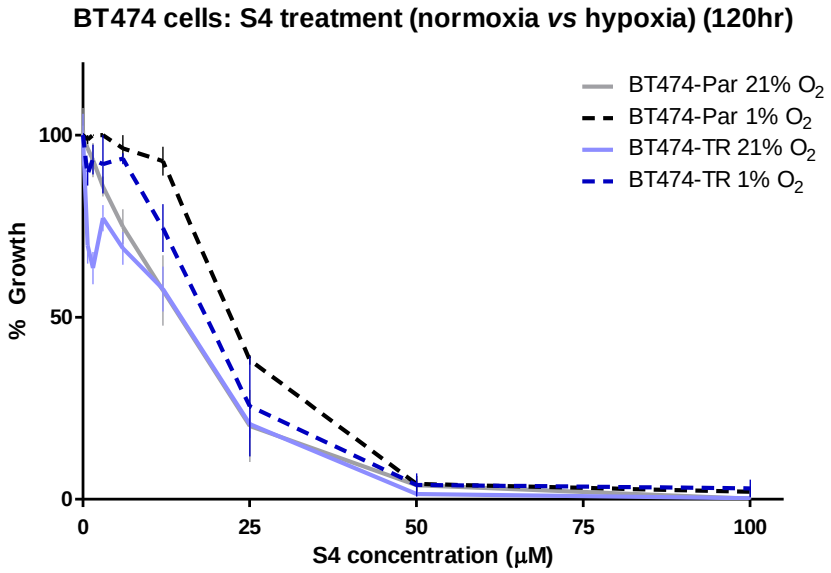

Figure 4.18: Toxicity assays for S4-treated BT474 cell line variants (normoxia vs hypoxia)
Toxicity assays for BT474-Par and BT474-TR cell line variants treated for 5 days with S4 at normoxia (full line) and hypoxia (broken line). n=3±SEM.

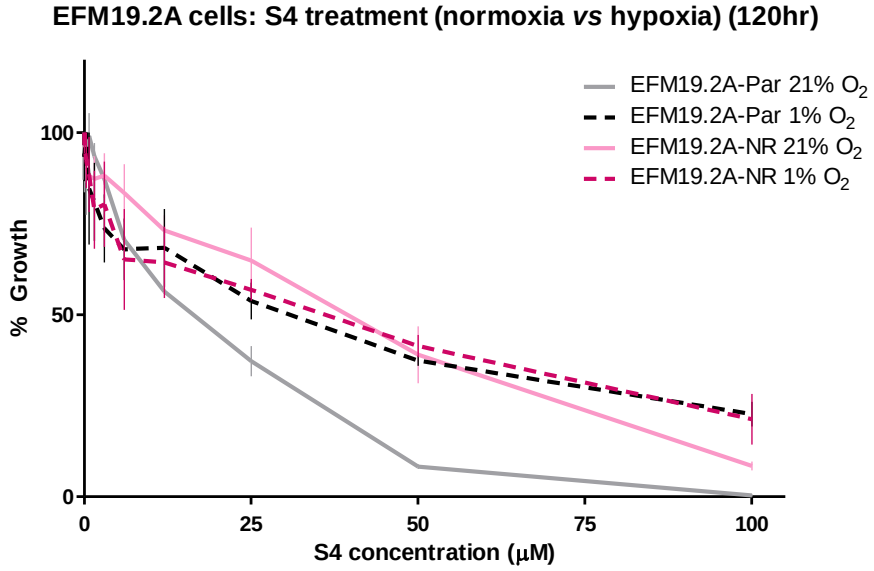

Figure 4.19: Toxicity assays for S4-treated EFM19.2A cell line variants (normoxia vs hypoxia)
Toxicity assays for EFM9.2A-Par and EFM9.2A-NR cell line variants treated for 5 days with S4 at normoxia (full line) and hypoxia (broken line). n=3±SEM.

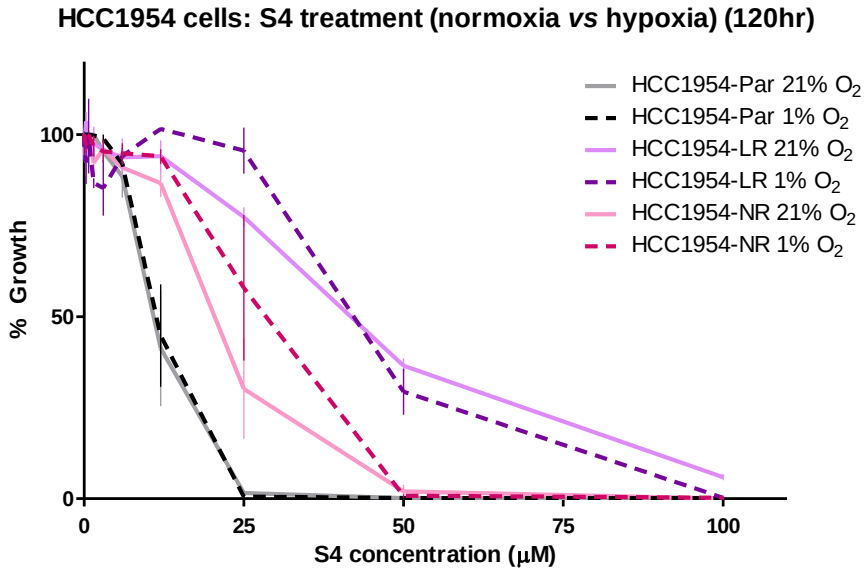

Figure 4.20: Toxicity assays for S4-treated HCC1954 cell line variants (normoxia vs hypoxia)
Toxicity assays for HCC1954-Par, HCC1954-LR and HCC1954-NR cell line variants treated for 5 days with S4 at normoxia (full line) and hypoxia (broken line). n=3±SEM.

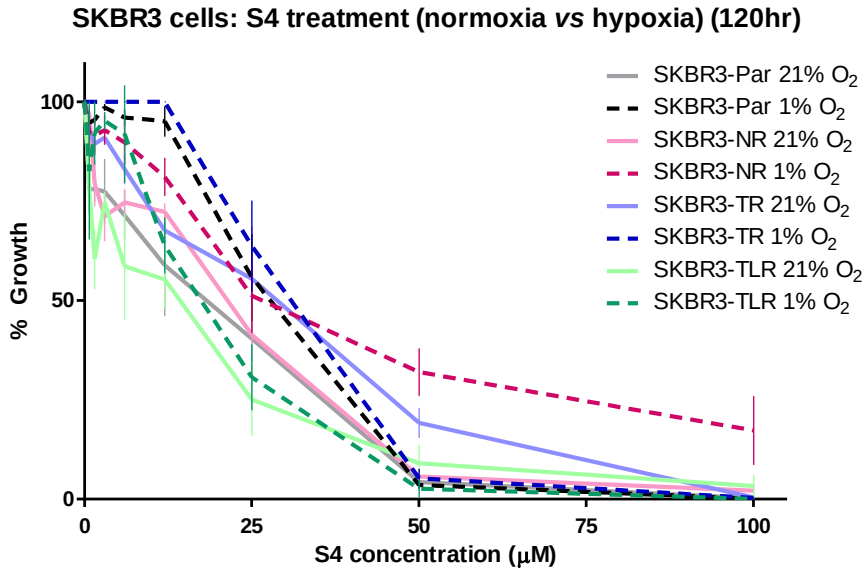

Figure 4.21: Toxicity assays for S4-treated SKBR3 cell line variants (normoxia vs hypoxia)
Toxicity assays for SKBR3-Par, SKBR3-NR, SKBR3-TR and SKBR3-TLR cell line variants treated for 5 days with S4 at normoxia (full line) and hypoxia (broken line). n=3±SEM.

Cell line	***IC_{50} value (normoxia)***	***IC_{50} value (hypoxia)***	***p-value***
BT474-Par	14.83	21.43	0.001
BT474-TR	14.93	18.40	0.013
EFM19.2A-Par	17.93	31.53	0.001
EFM19.2A-NR	38.62	36.00	0.051
HCC1954-Par	10.87	11.25	0.695
HCC1954-LR	41.47	41.03	0.594
HCC1954-NR	21.22	28.37	0.028
SKBR3-Par	17.83	28.33	0.006
SKBR3-NR	21.47	26.97	0.007
SKBR3-TR	29.13	30.23	0.332
SKBR3-TLR	14.23	17.60	0.088

Table 4.8: S4 IC_{50} values for cell line variants cultured in normoxic and hypoxic conditions

Cell line	***IC_{50} value (normoxia)***	***Fold difference***	***p-value***
BT474-Par	14.83	-	-
BT474-TR	14.93	1.01	0.89
EFM19.2A-Par	17.93	-	-
EFM19.2A-NR	38.62	2.15	0.17
HCC1954-Par	10.87	-	-
HCC1954-LR	41.47	3.82	0.046
HCC1954-NR	21.22	1.95	0.08
SKBR3-Par	17.83	-	-
SKBR3-NR	21.47	1.20	0.0059
SKBR3-TR	29.13	1.63	0.0003
SKBR3-TLR	14.23	0.80	0.5707

Table 4.9: S4 IC_{50} values and fold differences between cell line variants (normoxia)

Cell line	*IC_{50} value (hypoxia)*	*Fold difference*	*p-value*
BT474-Par	21.43	-	-
BT474-TR	18.40	0.86	0.51
EFM19.2A-Par	31.53	-	-
EFM19.2A-NR	36.00	1.14	0.39
HCC1954-Par	11.25	-	-
HCC1954-LR	41.03	3.65	0.057
HCC1954-NR	28.37	2.52	0.004
SKBR3-Par	28.33	-	-
SKBR3-NR	26.97	0.95	0.54
SKBR3-TR	30.23	1.07	0.017
SKBR3-TLR	14.23	0.50	0.13

Table 4.10: S4 IC_{50} values and fold differences between cell line variants (hypoxia)

4.2.6. Combination toxicity assays (S4 and neratinib)

All cell line variants were tested for sensitivity to neratinib and S4 (previously represented in Section 4.2.5, but displayed again for clarity) during normoxic conditions. Following analysis of toxicity levels, combination assays with S4 and neratinib were performed. All combination assay CI values per cell line variant are displayed in Summary Table 4.13. The levels of synergism were identified from the literature (187).

4.2.6.1. BT474 cell line variants

BT474-Par and BT474-TR cell line variants displayed similar toxicity levels to both neratinib (*p-value*=0.38) (Figure 4.22 (A.)) and S4 (*p-value*=0.23) (Figure 4.22 (B.)) (Summarised in Table 4.11 and Table 4.12). Thus, indicating that neither cell line was more resistant or more sensitive to the drugs used.

Combination assays of neratinib plus S4 were not synergistic in BT474-Par (Figure 4.23 (A.)) or BT474-TR cell line variants (Figure 4.23 (B.)) (CI value at ED_{50}=1.17 and 1.10, respectively), summarised in Table 4.13.

(A.)

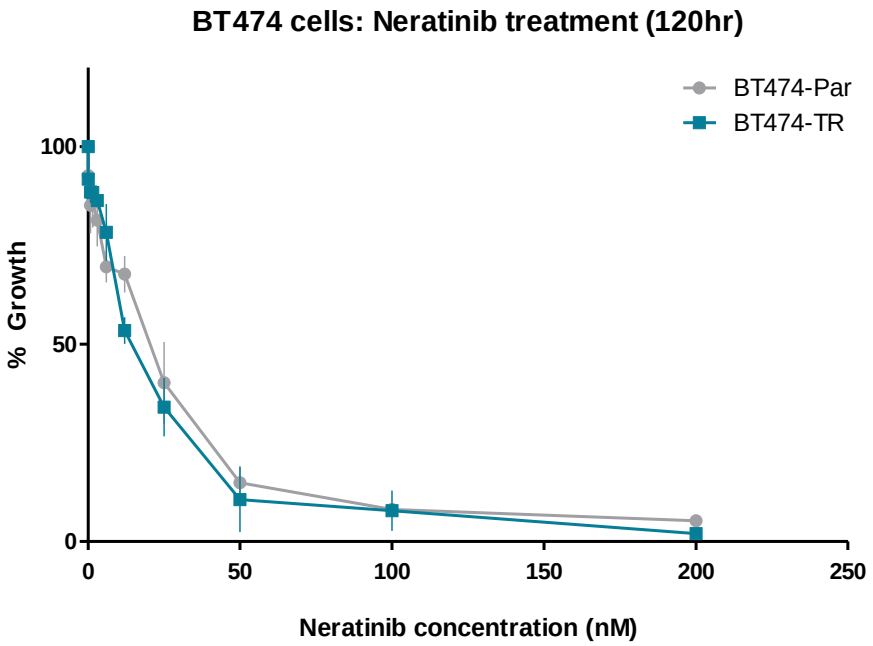

(B.

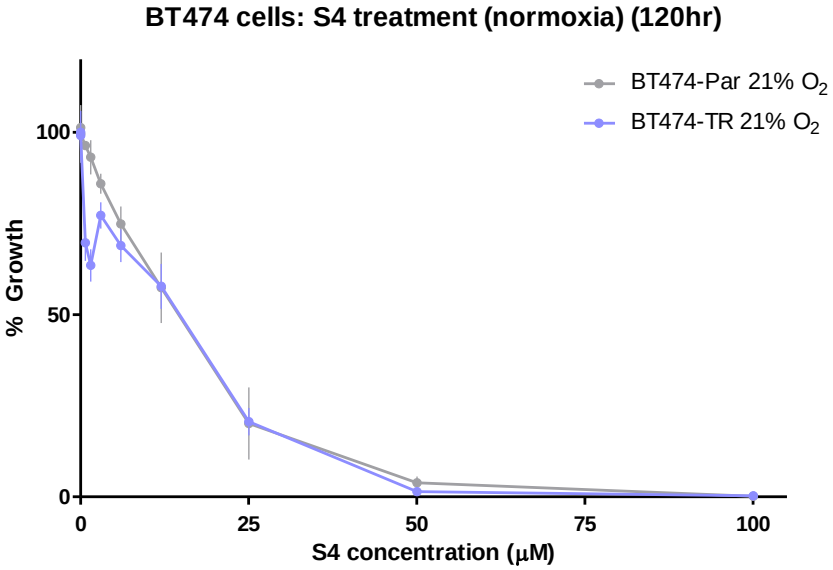

Figure 4.22: S4 and neratinib toxicity assays for BT474 cell line variants
Acid phosphatase assays were performed on BT474-Par and BT474-TR cell line variants treated with neratinib (A.) and S4 (B.) at 21% O_2 for 5 days. n=3±SEM.

(A.)

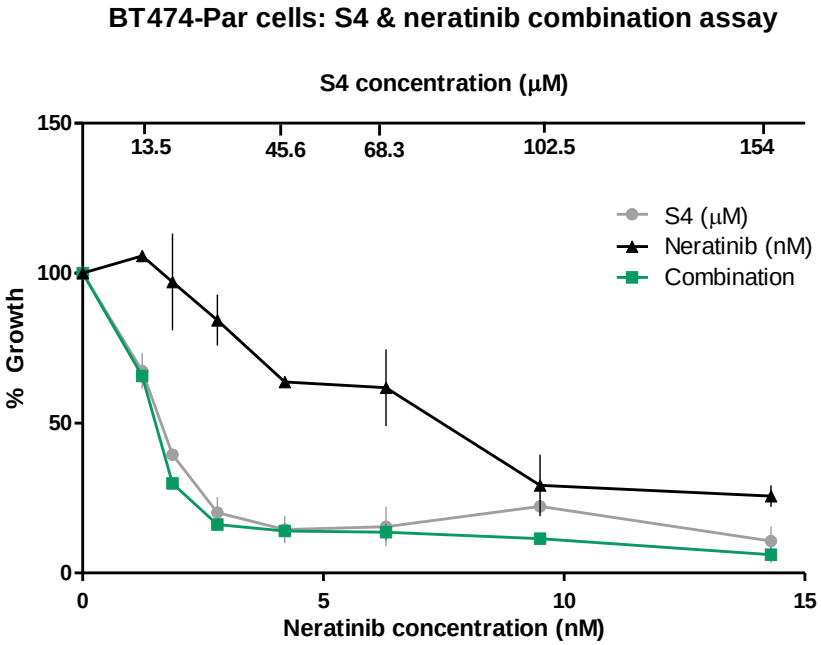

(B.

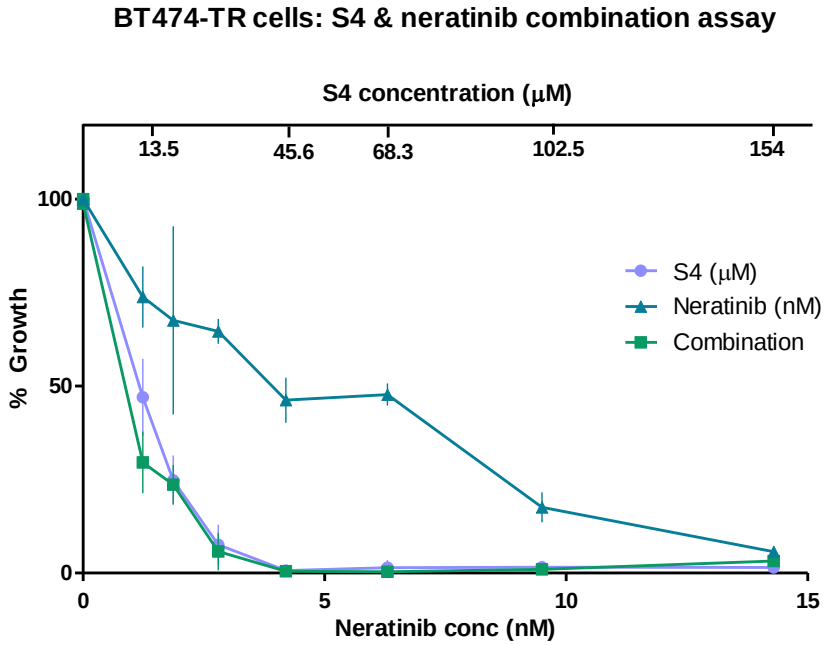

Figure 4.23: Combination (neratinib plus S4) assays for BT474 cell line variants
Acid phosphatase assays were performed on BT474-Par (A.) and BT474-TR cell line variants (B.) treated with neratinib, S4 and neratinib plus S4 at 21% O_2 for 5 days. n=3±SEM.

4.2.6.2. EFM19.2A cell line variants

EFM19.2A-NR cell line variants have increased resistance to neratinib compared to EFM19.2A-Par (*p-value*=0.034) (Figure 4.24 (A.)). EFM19.2A-NR cell line variants are more resistant to S4 treatment than EFM19.2A-Par (*p-value*=0.0009) (Figure 4.24 (B.)). Results are summarised in Table 4.11 and Table 4.12.

Combination assay of neratinib plus S4 was not synergistic in EFM19.2A-Par at ED_{50} (CI value=1.31) (Figure 4.25 (A.)). The combination of S4 plus neratinib was slightly synergistic at ED_{50} in EFM19.2A-NR (CI-value=0.77), CI results are summarised in Table 4.13.

(A.)

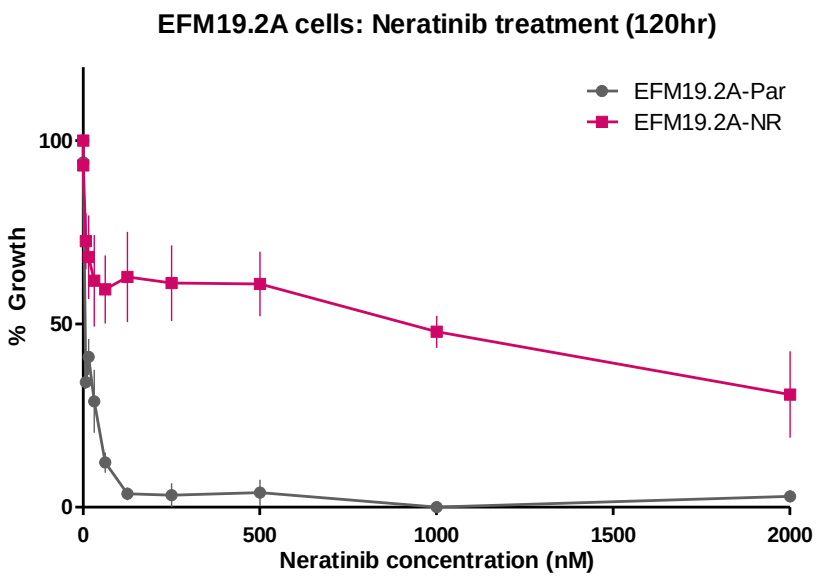

(B.)

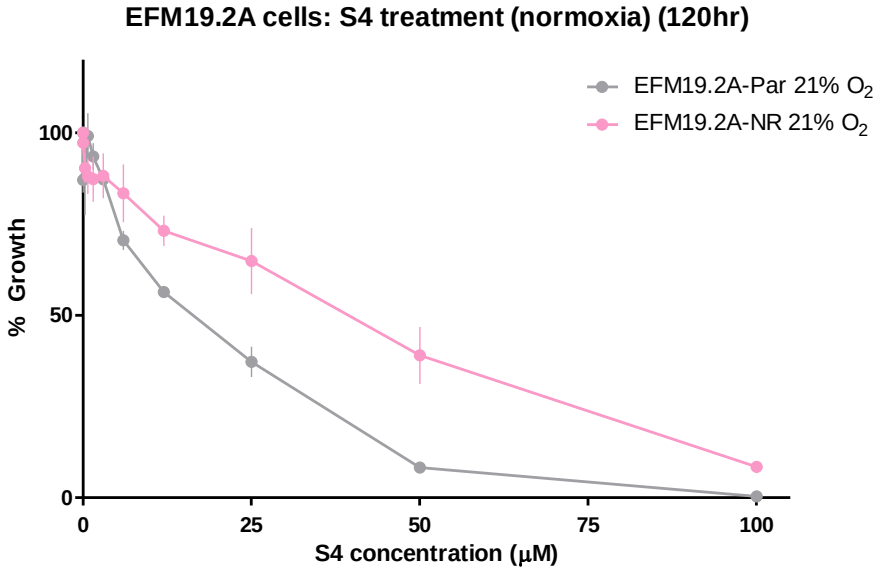

Figure 4.24: S4 and neratinib toxicity assays for EFM19.2A cell line variants
Acid phosphatase assays were performed on EFM19.2A-Par and EFM19.2A-NR cell line variants treated with neratinib (A.) and S4 (B.) at 21% O_2 for 5 days. n=3±SEM.

(A.)

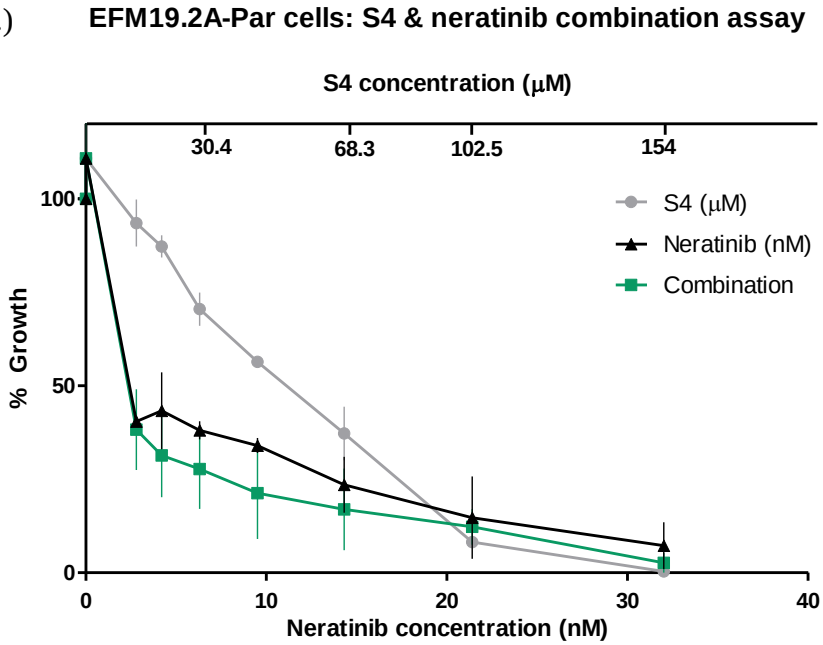

(B.)

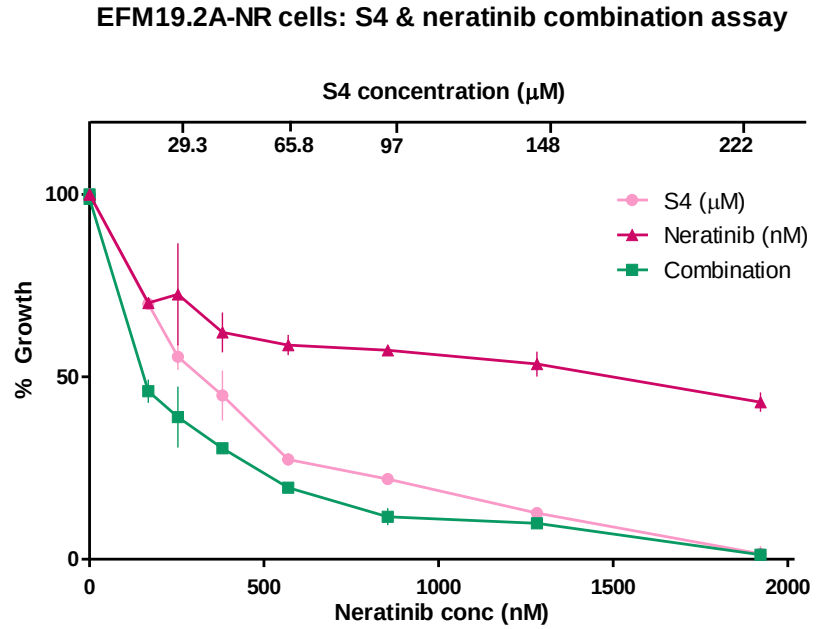

Figure 4.25: Combination (neratinib plus S4) assays for EFM19.2A cell line variants
Acid phosphatase assays were performed on EFM19.2A-Par (A.) and EFM19.2A-NR cell line variants (B.) treated with neratinib, S4 and neratinib plus S4 at 21% O_2 for 5 days. n=3±SEM.

4.2.6.3. HCC1954 cell line variants

HCC1954-LR and HCC1954-NR are more resistant to neratinib than HCC1954-Par (*p-value*=0.044 and 0.44, respectively) (Figure 4.26 (A.) and summarised in Table 4.11). HCC1954-LR and HCC1954-NR are significantly more resistant to S4 treatment than

HCC1954-Par (*p-value*=0.001 and 0.004), respectively) (Figure 4.26 (B.) and summarised in Table 4.12).

At ED_{50}, the combination assays of neratinib and S4 showed strong synergy in HCC1954-Par (CI value=0.21), moderate synergy in HCC1954-LR (CI-value=0.54) and very strong synergy in HCC1954-NR cell line variant (CI value=0.03) (Figure 4.27). CI summary results are summarised in Table 4.13.

(A.)

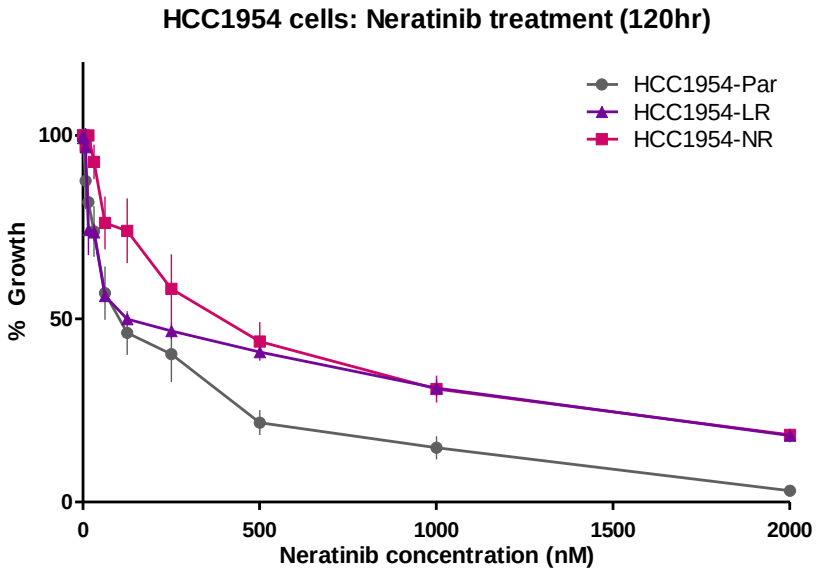

(B.

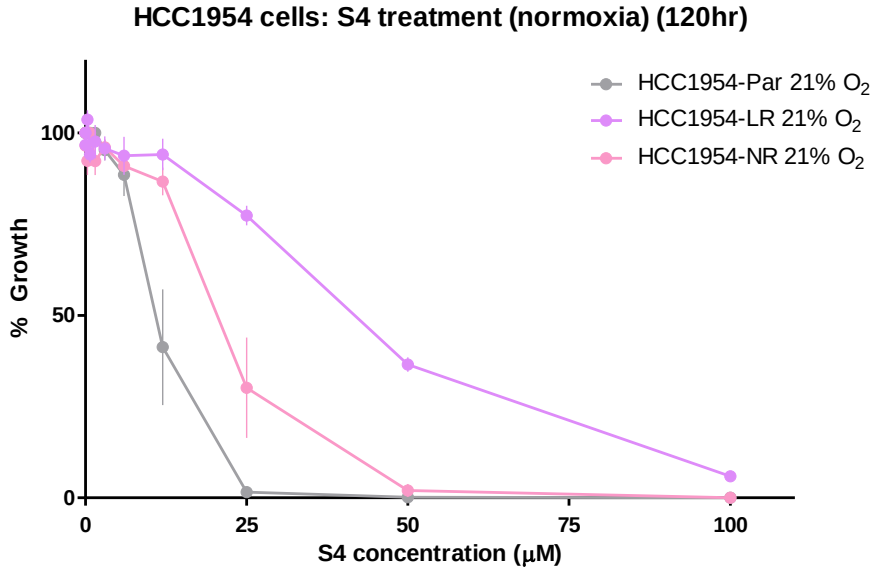

Figure 4.26 S4 and neratinib toxicity assays for HCC1954 cell line variants
Acid phosphatase assays were performed on HCC1954-Par, HCC1954-LR and HCC1954-NR cell line variants treated with neratinib (A.) and S4 (B.) at 21% O_2 for 5 days. n=3±SEM.

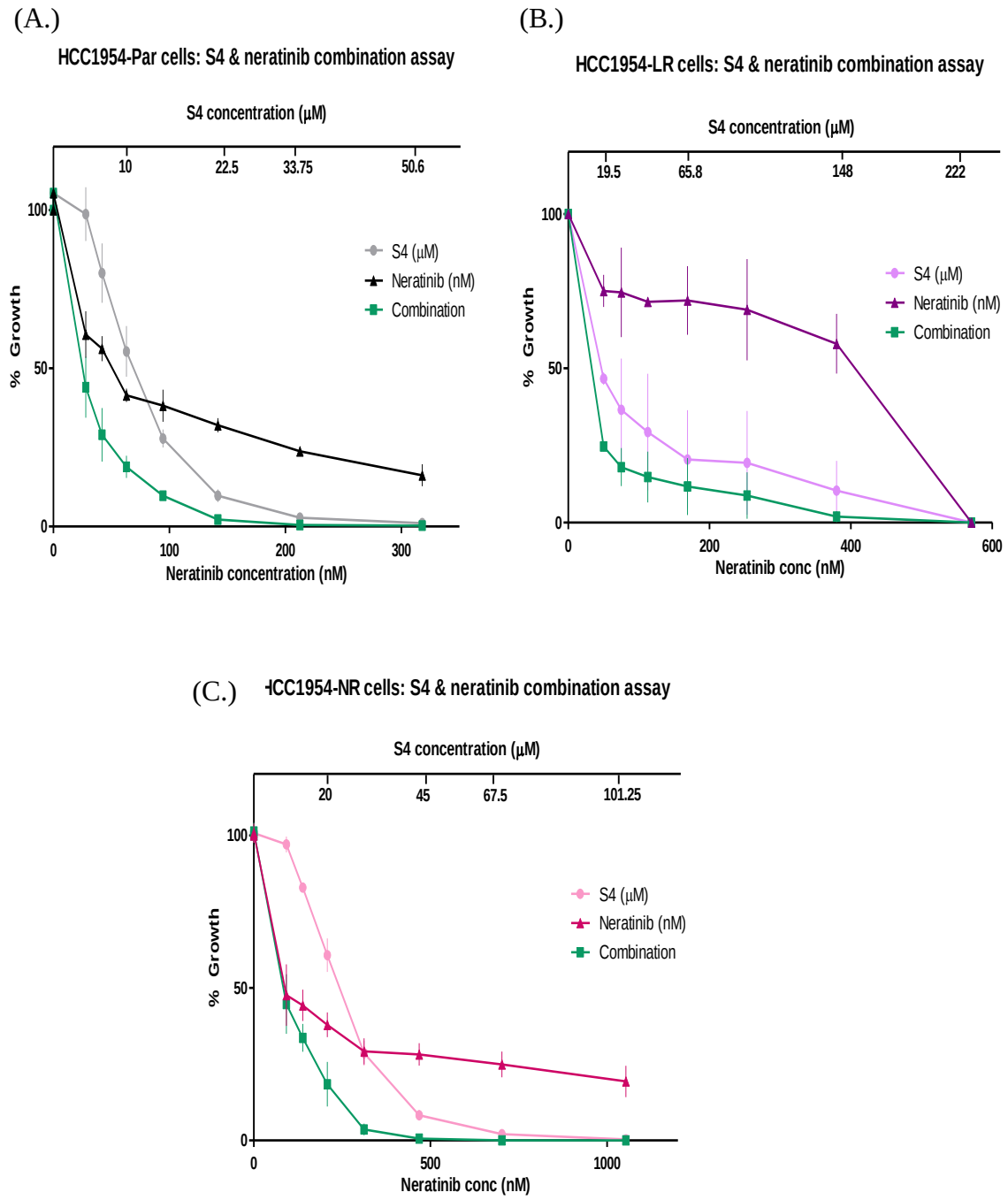

Figure 4.27: Combination (neratinib plus S4) assays for HCC1954 cell line variants
Acid phosphatase assays were performed on HCC1954-Par (A.), HCC1954-LR (B.) and HCC1954-NR cell line variants (C.) treated with neratinib, S4 and neratinib plus S4 at 21% O_2 for 5 days. n=3±SEM.

4.2.6.4. SKBR3 cell line variants

SKBR3-NR and SKBR3-TLR are significantly more resistant to neratinib than SKBR3-Par (*p-value*=0.043 and 0.0008, respectively) (Figure 4.28 (A.) and Table 4.11). Although not a significant increase in neratinib-resistance, SKBR3-TR displayed a 8-fold increase in resistance to neratinib compared to SKBR3-Par (*p-value*=0.16) (Figure 4.28 (A.) and Table 4.11). SKBR3-NR and SKBR3-TR were significantly more resistant to S4 treatment than SKBR3-Par, there was no significant difference between SKBR3-TLR and SKBR3-Par (Figure 4.28 (B.) and Table 4.12).

At ED_{50}, the combination assays of neratinib and S4 were not synergistic in the SKBR3-Par cell line variant (CI value=2.09). The combination showed moderate synergy in SKBR3-NR (CI value=0.61), moderate synergy in SKBR3-TR (CI-value=0.65) and moderate synergy in SKBR3-TLR cell line variant (CI value=0.36) (). Combination assays are displayed in Figure 4.29 and Figure 4.30. CI results are summarised in Table 4.13.

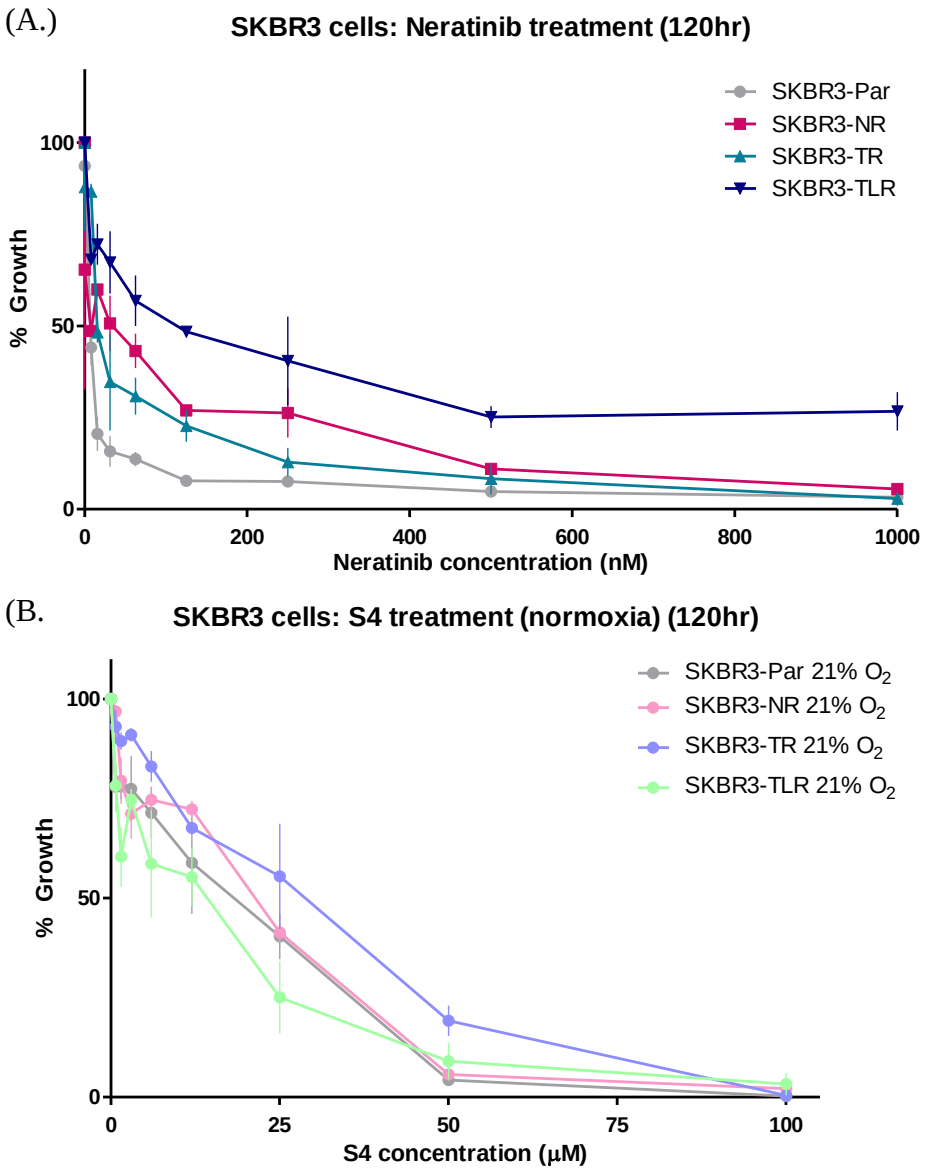

Figure 4.28: S4 and neratinib toxicity assays for SKBR3 cell line variants
Acid phosphatase assays were performed on SKBR3-Par, SKBR3-NR, SKBR3-TR and SKBR3-TLR cell line variants treated with neratinib (A.) and S4 (B.) at 21% O_2 for 5 days. n=3±SEM.

(A.)

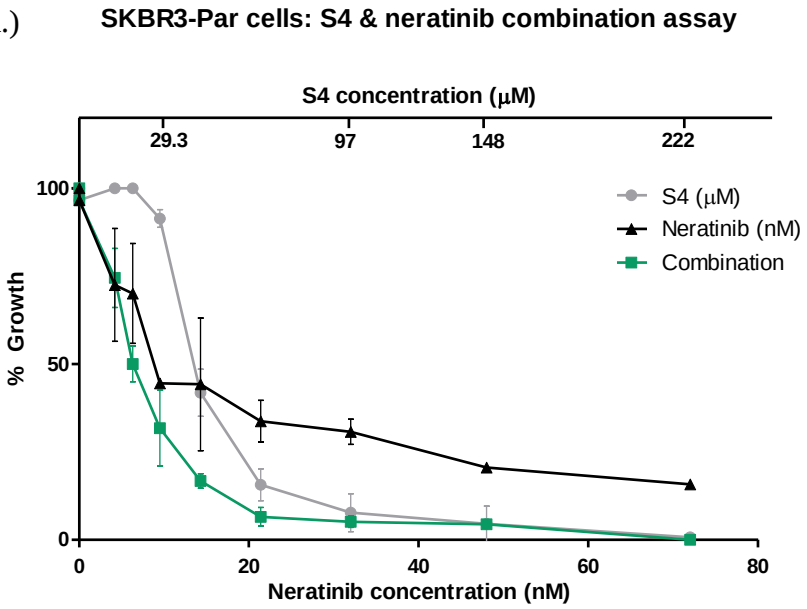

(B.)

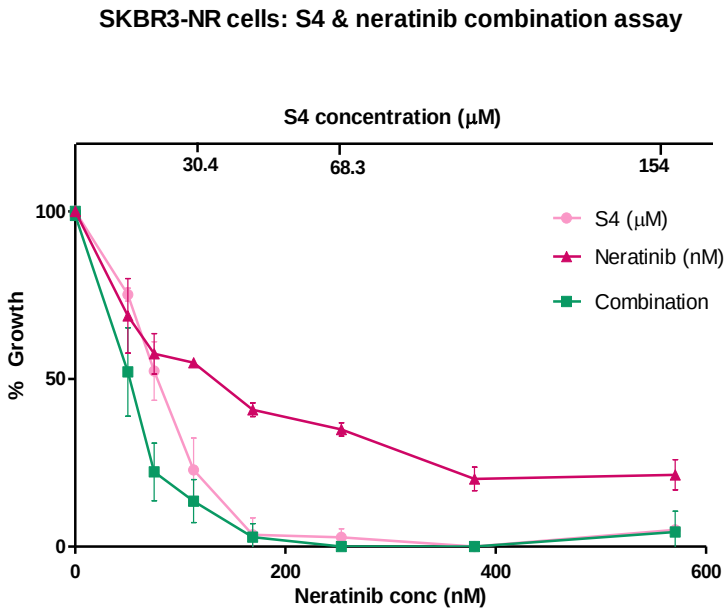

Figure 4.29: Combination (neratinib plus S4) assays for SKBR3-Par and SKBR3-NR cell line variants

Acid phosphatase assays were performed on SKBR3-Par (A.) and SKBR3-NR (B.) treated with neratinib, S4 and neratinib plus S4 at 21% O_2 for 5 days. n=3±SEM.

(A.) **SKBR3-TR cells: S4 & neratinib combination assay**

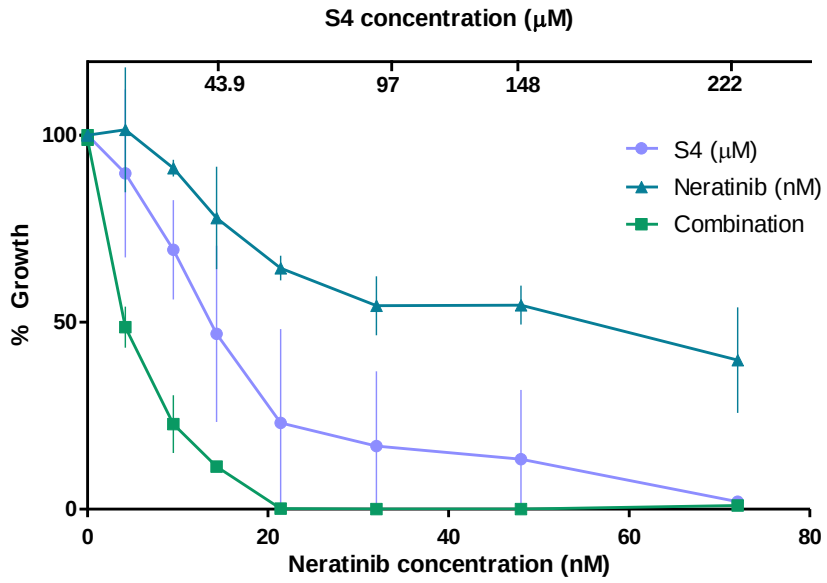

(B. **SKBR3-TLR cells: S4 & neratinib combination assay**

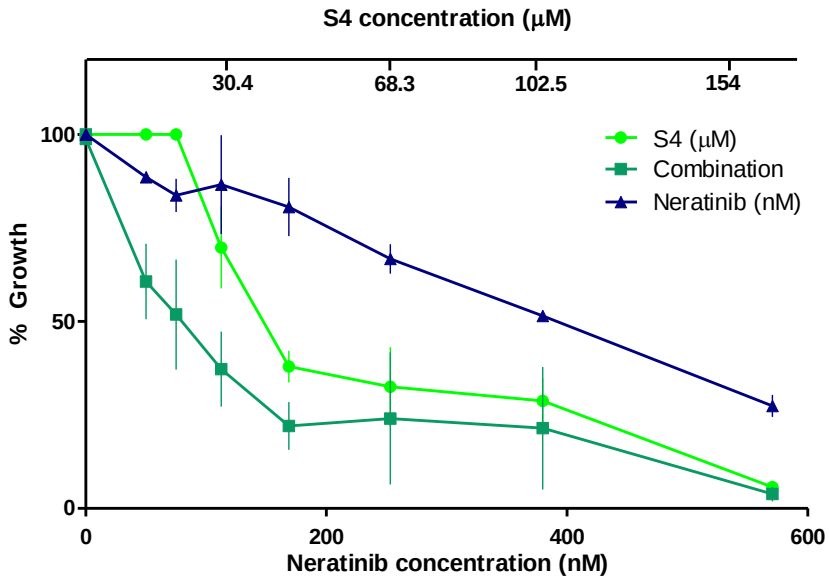

Figure 4.30: Combination (neratinib plus S4) assays for SKBR3-TR and SKBR3-TLR cell line variants

Acid phosphatase assays were performed on SKBR3-TR (A.) and SKBR3-TLR (B.) treated with neratinib, S4 and neratinib plus S4 at 21% O_2 for 5 days. n=3±SEM.

Cell line variant	**Neratinib IC_{50} (nM)**	**Fold difference (compared to Par cell line variant)**	***p-value***
BT474-Par	3.5	1	-
BT474-TR	2.3	0.66	0.38
EFM19.2A-Par	6.8	1	-
EFM19.2-NR	1000	147.06	* *p-value*=0.034
HCC1954-Par	166	1	-
HCC1954-LR	198.5	1.2	* *p-value*=0.044
HCC1954-NR	334.8	2.02	* *p-value*=0.044
SKBR3-Par	3.7	1	-
SKBR3-NR	85	22.97	* *p-value*=0.043
SKBR3-TR	27.8	7.51	0.16
SKBR3-TLR	120	32.43	*** *p-value*=0.0008

Table 4.11: Neratinib IC_{50} values for all cell line variants

Cell line variant	**S4 IC_{50} (µM)**	**Fold difference (compared to Par cell line variant)**	***p-value***
BT474-Par	14.4	1	-
BT474-TR	14.93	1.03	0.23
EFM19.2A-Par	17.93	1	-
EFM19.2-NR	31.53	1.75	*** *p-value*=0.0009
HCC1954-Par	10.87	1	-
HCC1954-LR	41.47	3.82	*** *p-value*=0.001
HCC1954-NR	21.2	1.95	** *p-value*=0.004
SKBR3-Par	17.83	1	-
SKBR3-NR	21.47	1.20	* *p-value*=0.05
SKBR3-TR	29.13	1.63	** *p-value*=0.01
SKBR3-TLR	14.23	0.80	0.067

Table 4.12: S4 IC_{50} values for all cell line variants

Cell line variant	**CI-value at ED_{50}**	**Compusyn index definition**
Non-synergistic		
BT474-Par	1.17	Slight antagonism
BT474-TR	1.10	Nearly additive
EFM19.2A-Par	1.31	Moderate antagonism
SKBR3-Par	2.09	Antagonism
Synergistic		
EFM19.2A-NR	0.77	Moderate synergism
HCC1954-Par	0.21	Strong synergism
HCC1954-LR	0.54	Synergism
HCC1954-NR	0.03	Very strong synergism
SKBR3-NR	0.61	Synergism
SKBR3-TR	0.65	Synergism
SKBR3-TLR	0.36	Synergism

Table 4.13: CI values per cell line variant following combination assays of neratinib and S4

4.2.7. Combination assays (S4 and lapatinib)

All lapatinib-resistant cell line variants and their lapatinib-sensitive cell variant were tested for sensitivity to lapatinib and S4 during normoxic conditions. Following analysis of toxicity levels, combination assays with S4 and lapatinib were performed. All combination assay CI values per cell line variant are displayed in Summary Table 4.15.

HCC1954-LR and SKBR3-TLR have a fold-increase in lapatinib resistance (3.62 and 3.9, respectively) when compared to HCC1954-Par and SBR3-Par cell line variants (Figure 4.31 (A.) and Figure 4.33 (A.), summarised in Table 4.14). As previously described in Table 4.12, HCC11954-LR cell line variant is significantly more resistant to S4 than HCC1954-Par (*p-value*=0.001).

At ED_{50}, the combination assays of lapatinib and S4 was very strongly synergistic in HCC1954-LR (CI value=0.054) (Figure 4.32 (B.), moderately synergistic in HCC1954-Par

(CI value=0.134) (Figure 4.32 (A.) and moderately synergistic in both SKBR-Par and SKBR3-LR cell line variants (CI value=0.476 and 0.221, respectively) (Figure 4.34). All results are summarised in Table 4.15.

(A.)

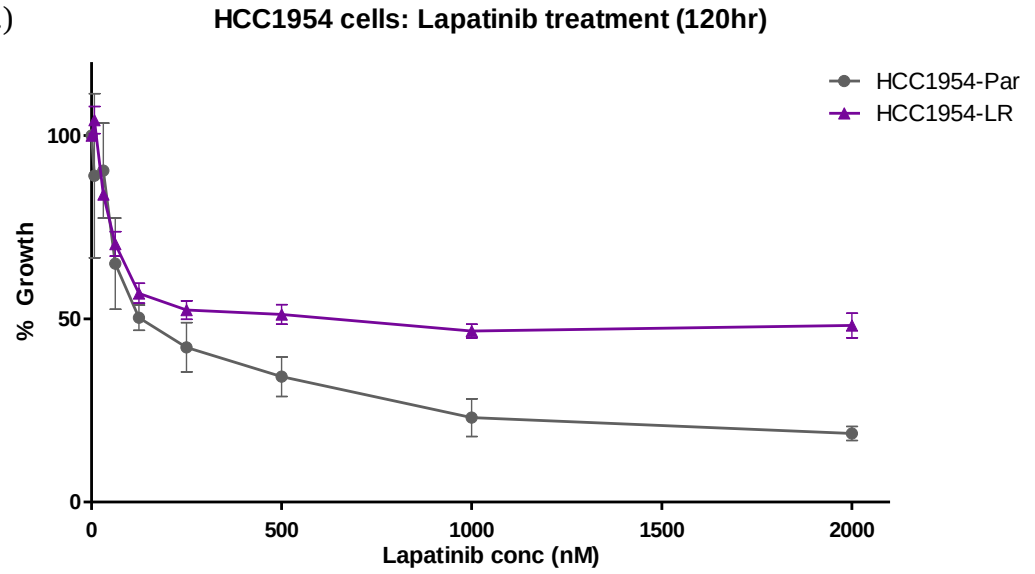

(B.)

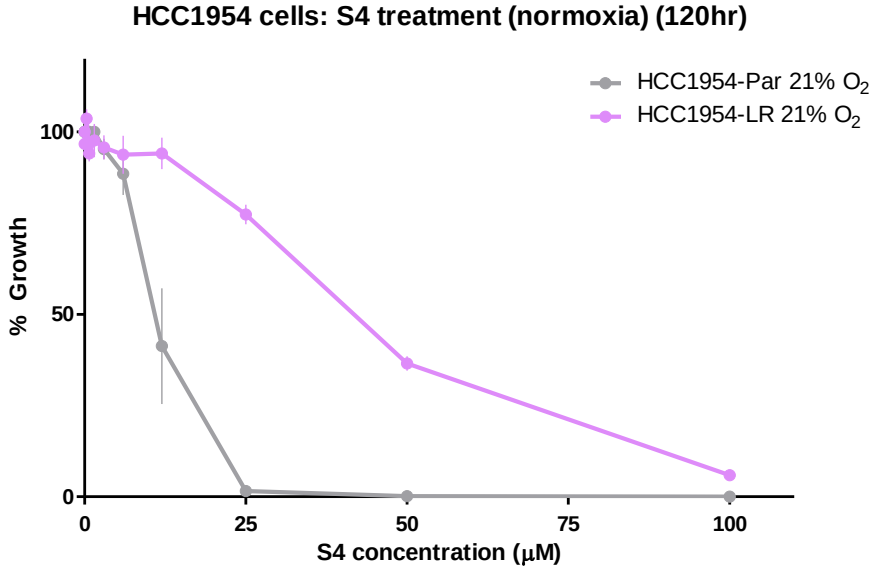

Figure 4.31: S4 and lapatinib toxicity assays for HCC1954 cell line variants
Acid phosphatase assays were performed on HCC1954-Par and HCC1954-LR cell line variants treated with lapatinib (A.) and S4 (B.) at 21% O_2 for 5 days. n=3±SEM.

(A.)

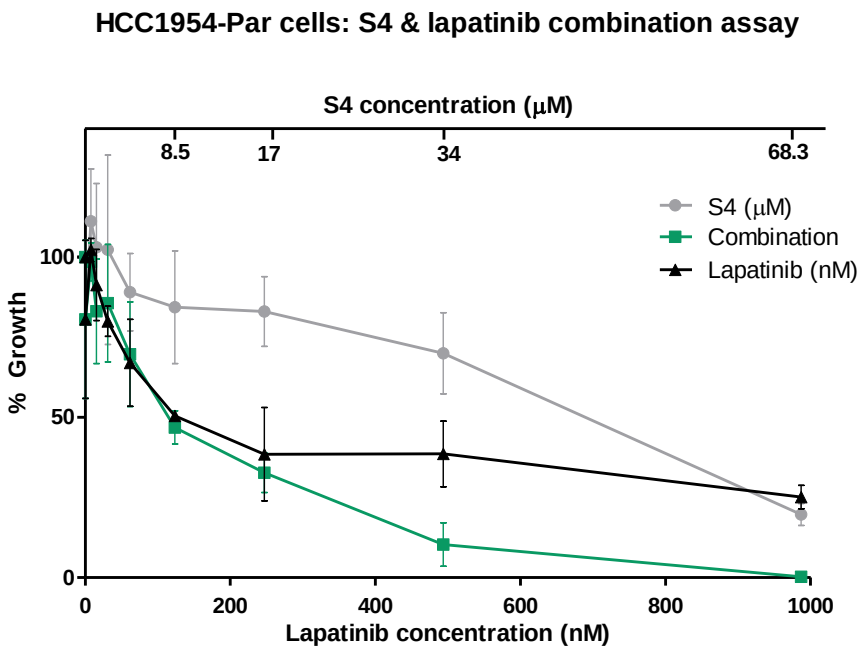

(B.)

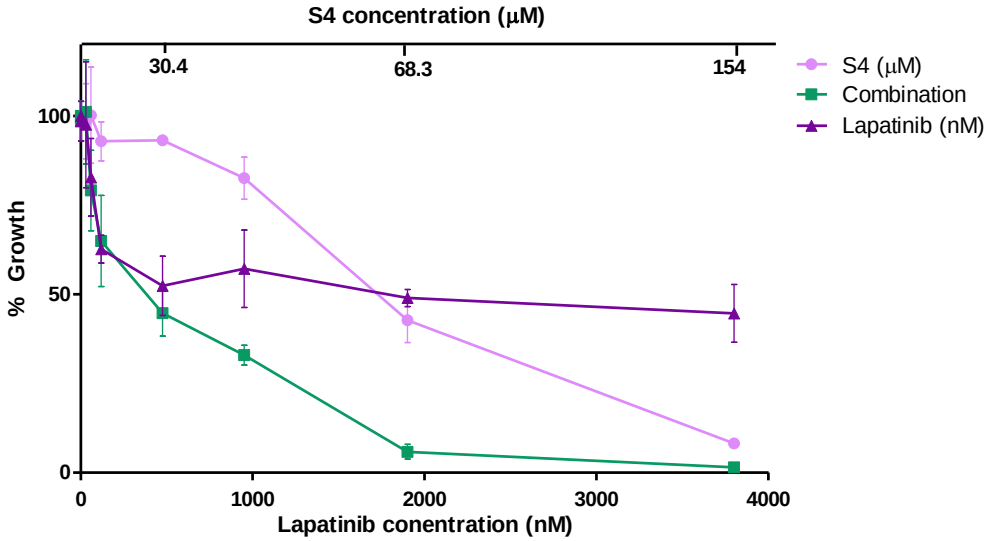

Figure 4.32: Combination (lapatinib plus S4) assays for HCC1954-Par and HCC1954-LR cell line variants

Acid phosphatase assays were performed on HCC1954-Par (A.) and HCC1954-LR (B.) treated with lapatinib, S4 and lapatinib plus S4 at 21% O_2 for 5 days. n=3±SEM.

(A.)

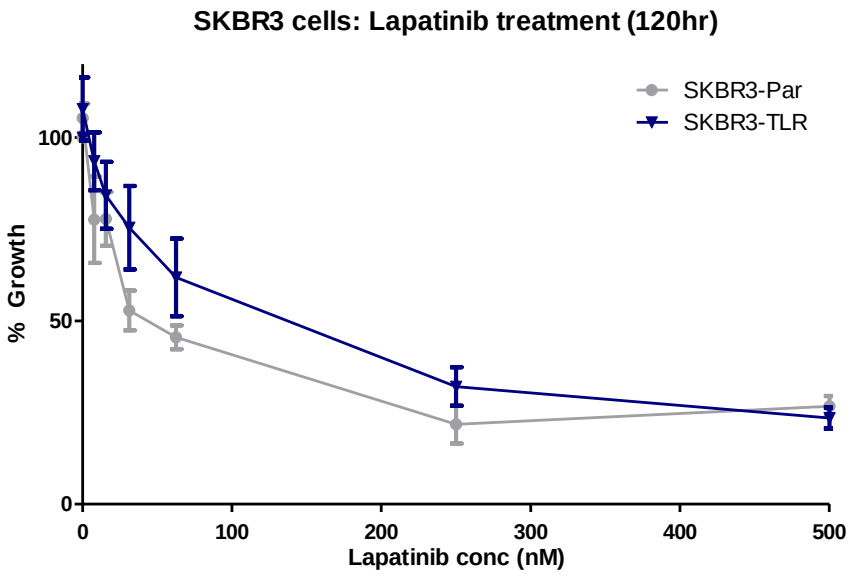

(B.)

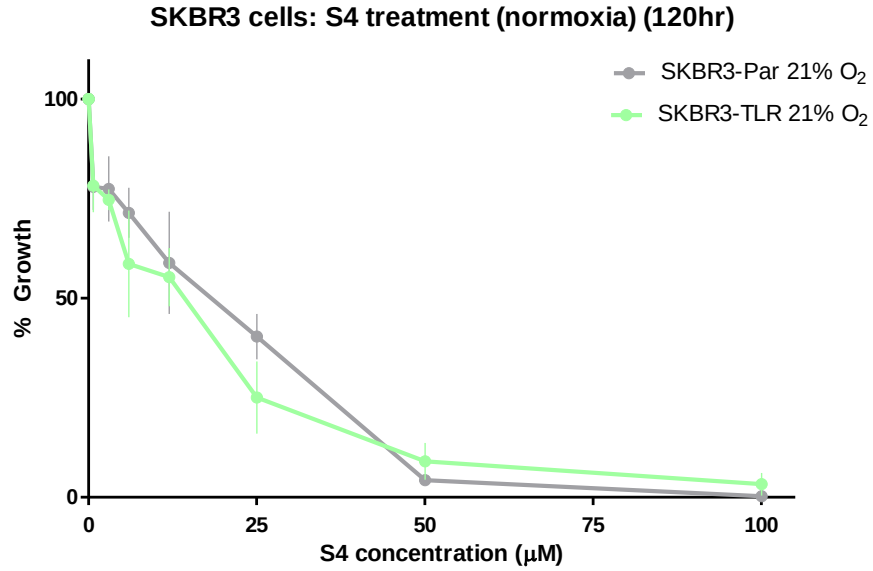

Figure 4.33: S4 and lapatinib toxicity assays for SKBR3 cell line variants
Acid phosphatase assays were performed on SKBR3-Par and SKBR3-TLR cell line variants treated with lapatinib (A.) and S4 (B.) at 21% O_2 for 5 days. n=3±SEM.

(A.) **SKBR3-Par cells: S4 & lapatinib combination assay**

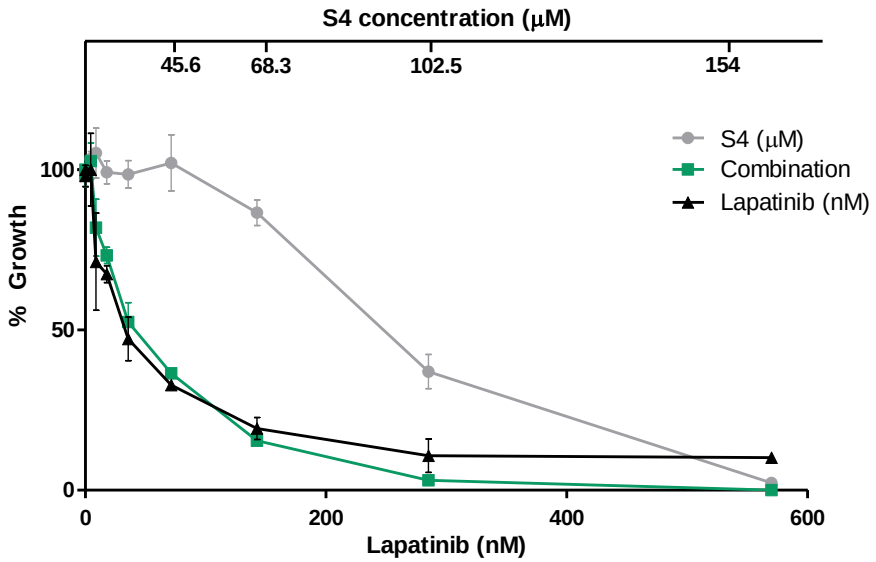

(B.) **SKBR3-TLR cells: S4 & lapatinib combination assay**

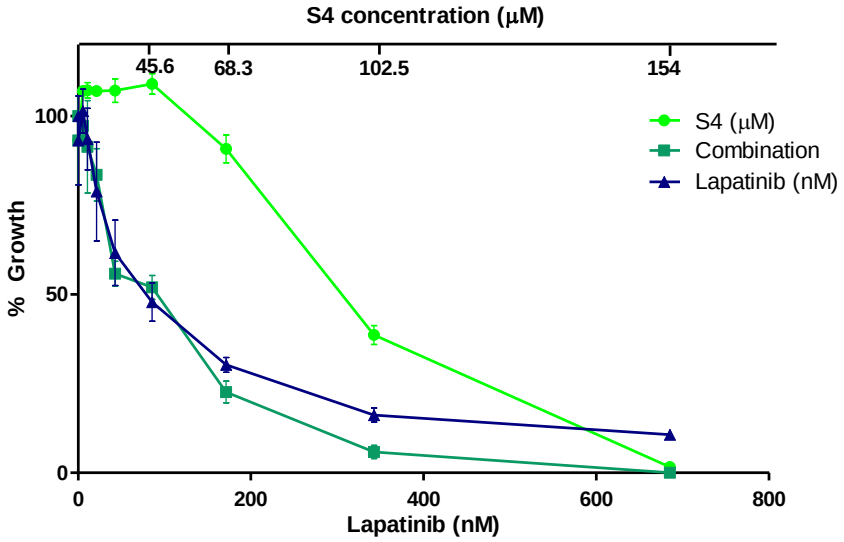

Figure 4.34: Combination (lapatinib plus S4) assays for SKBR3-Par and SKBR3-TLR cell line variants

Acid phosphatase assays were performed on SKBR3-Par (A.) and SKBR3-TLR (B.) treated with lapatinib, S4 and lapatinib plus S4 at 21% O_2 for 5 days. n=3±SEM.

Cell line variant	**Lapatinib IC_{50} (nM)**	**Fold difference (compared to Par cell line variant)**	***p-value***
HCC1954-Par	154.7	-	-
HCC1954-LR	560.7	3.62	0.14
SKBR3-Par	38.2	-	-
SKBR3-TLR	148.2	3.9	0.057

Table 4.14: Lapatinib IC_{50} values for all cell line variants

Cell line variant	**CI-value at ED_{50}**	**Compusyn index definition**
Synergistic		
HCC1954-Par	0.134	Strong synergism
HCC1954-LR	0.054	Very strong synergism
SKBR3-Par	0.476	Synergism
SKBR3-TLR	0.221	Strong synergism

Table 4.15: CI values per cell line variant following combination assays of lapatinib and S4

4.2.8. Combination assays (S4 and TDM-1)

BT474-TR cell line variants displayed increased resistance to TDM-1 compared to BT474-Par cell line variants (fold difference=121.2) (Figure 4.35 (A.)). As previously described in Table 4.12, there was no significant difference in sensitivity to S4 treatment. At ED_{50}, the combination assays of TDM-1 and S4 was not synergistic in BT474-Par (CI value=1.32) (Figure 4.36(A.)). The combination of TDM-1 and S4 had moderate synergism in BT-474-TR (CI value=0.49) (Figure 4.36 (B.)). All results are summarised in Table 4.16.

There are no significant differences in sensitivity to TDM-1 in SKBR3-Par, SKBR3-TR or SKBR3-TLR cell line variants (Figure 4.37 (A.) (Table 4.16). As previously described previously in Table 4.12, SKBR3-TR and SKBR3-TLR are more sensitive to S4 treatment. At ED_{50}, the combination assays of TDM-1 and S4 was moderately synergistic in SKBR3-Par (CI value=0.586), slightly synergistic in SKBR3-TR (CI value=0.813) and moderately synergistic in SKBR3-TLR (CI value=0.514) Figure 4.38. All results are summarised in Table 4.17.

(A.)

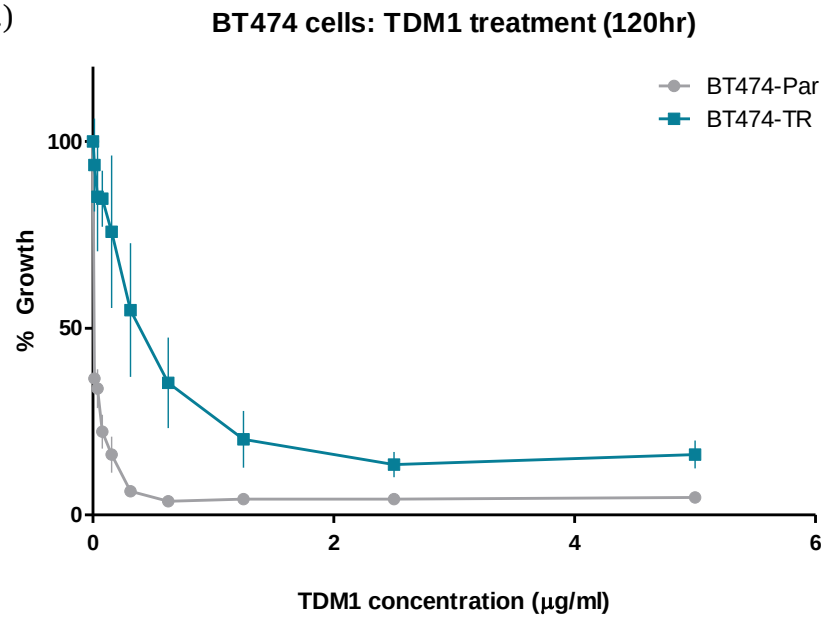

(B.)

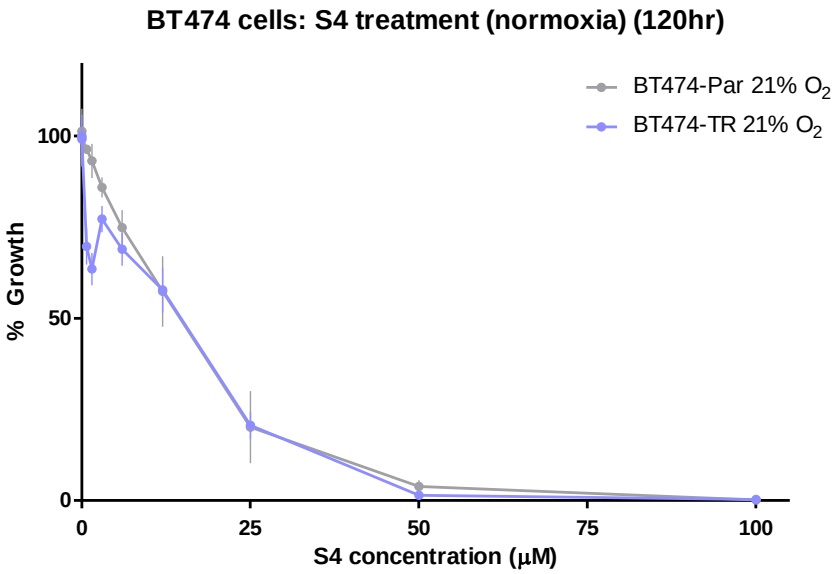

Figure 4.35: S4 and TDM-1 toxicity assays for BT474 cell line variants
Acid phosphatase assays were performed on BT474-Par and BT474-TR cell line variants treated with TDM-1 (A.) and S4 (B.) at 21% O_2 for 5 days. n=3±SEM.

(A.)

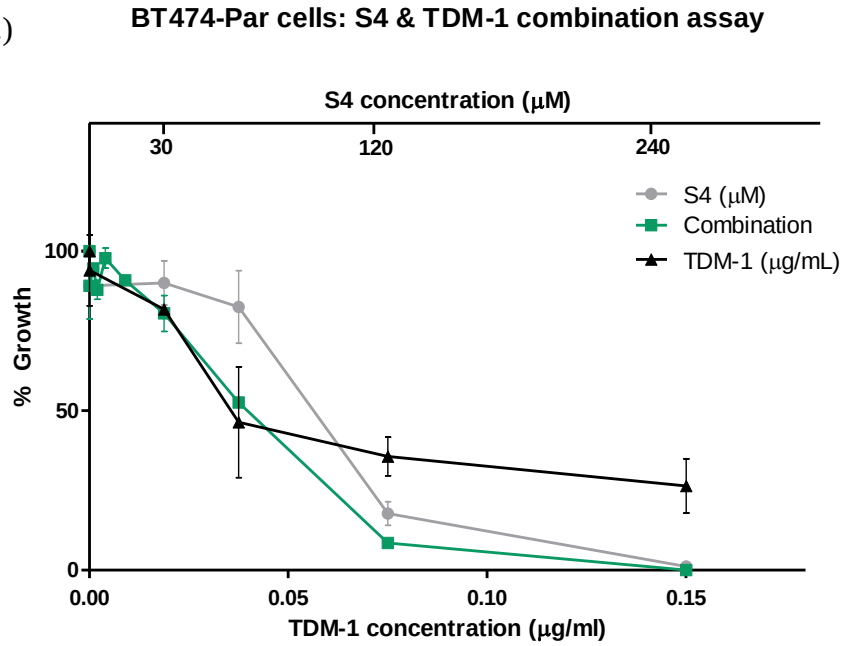

(B.)

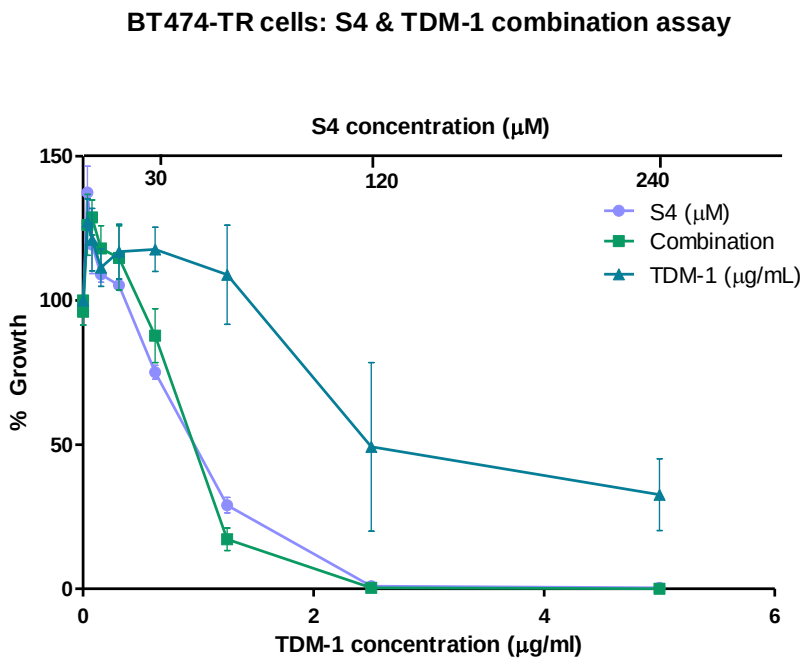

Figure 4.36: Combination (TDM-1 plus S4) assays for BT474-Par and BT474-TR cell line variants

Acid phosphatase assays were performed on BT474-Par (A.) and BT474-TR (B.) treated with TDM-1, S4 and TDM-1 plus S4 at 21% O_2 for 5 days. n=3±SEM.

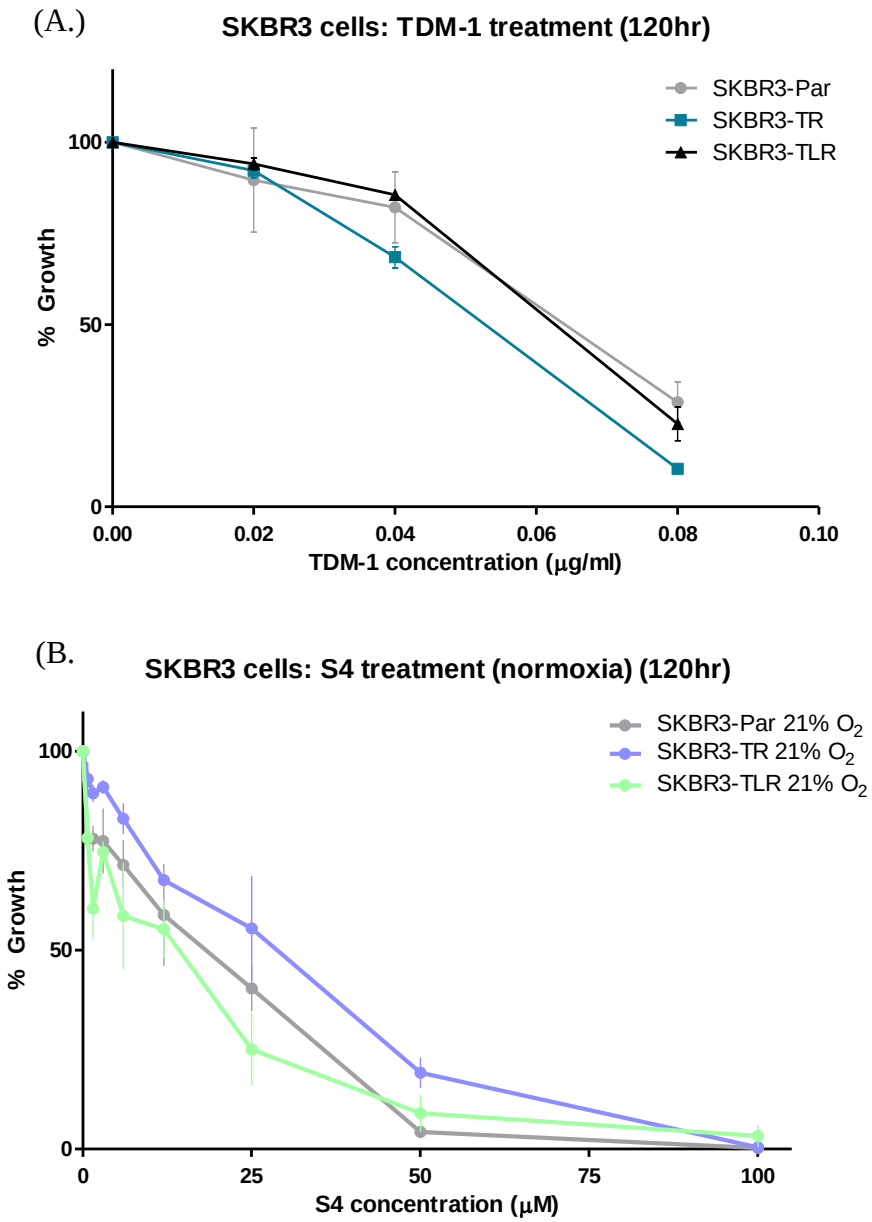

Figure 4.37: S4 and TDM-1 toxicity assays for SKBR3 cell line variants
Acid phosphatase assays were performed on SKBR3-Par and SKBR3-TLR cell line variants treated with TDM-1 (A.) and S4 (B.) at 21% O_2 for 5 days. n=3±SEM.

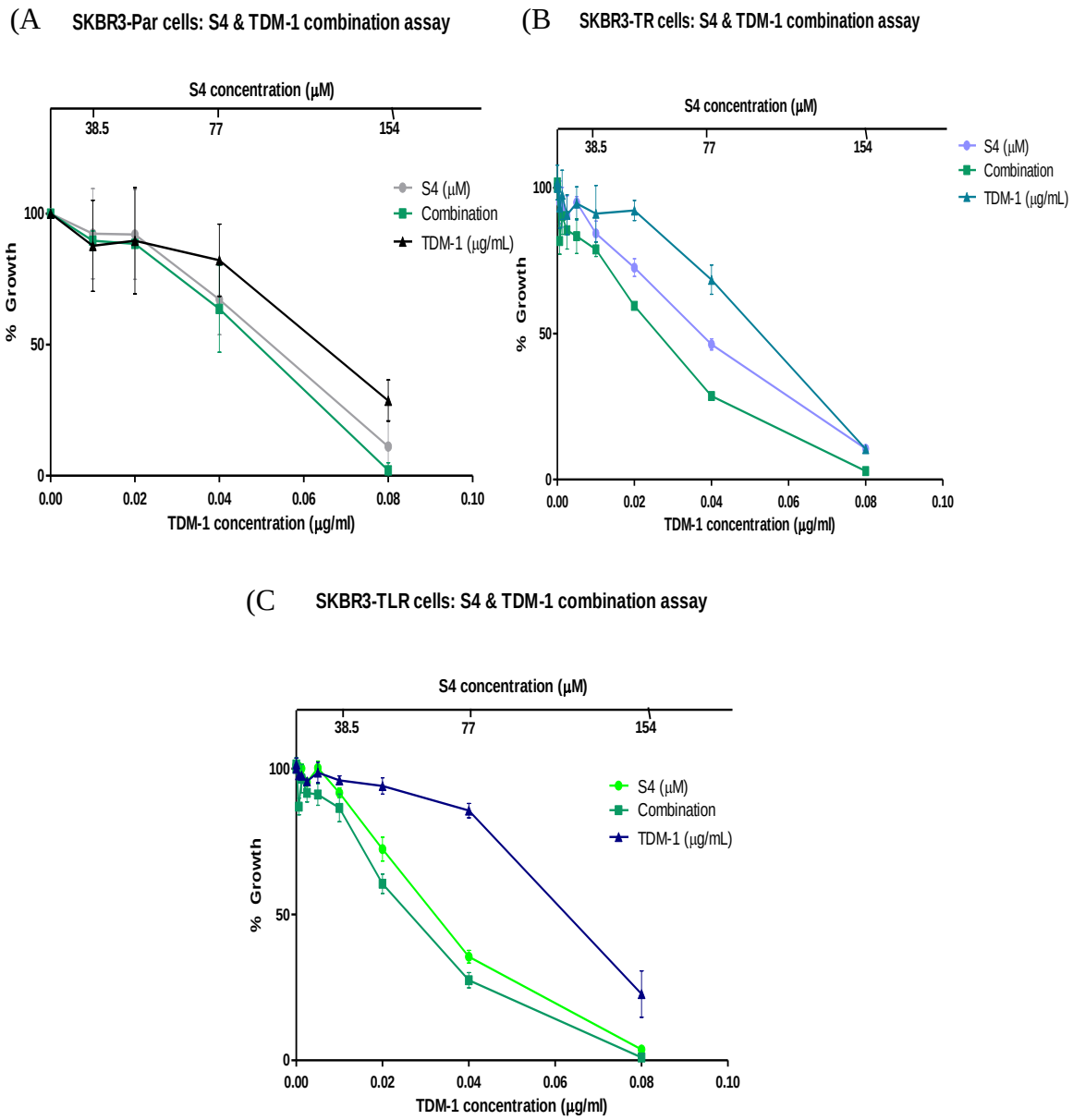

Figure 4.38: Combination (TDM-1 plus S4) assays for SKBR3-Par, SKBR3-TR and SKBR3-TLR cell line variants

Acid phosphatase assays were performed on SKBR3-Par (A.), SKBR3-TR (B.) and SKBR3-TLR (C.) treated with TDM-1, S4 and TDM-1 plus S4 at 21% O_2 for 5 days. n=3±SEM.

Cell line variant	**TDM-1 IC_{50} (µg/mL)**	**Fold difference (compared to Par cell line variant)**	***p-value***
BT474-Par	0.011	-	-
BT474-TR	1.33	121.2	0.12
SKBR3-Par	0.07	-	-
SKBR3-TR	0.053	0.78	0.12
SKBR3-TLR	0.063	0.93	0.58

Table 4.16: TDM-1 IC_{50} values for all cell line variants

Cell line variant	**CI-value at ED_{50}**	**Compusyn index definition**
Non-synergistic		
BT474-Par	1.324	Moderate antagonism
Synergistic		
BT474-TR	0.486	Synergism
SKBR3-Par	0.586	Synergism
SKBR3-TR	0.813	Moderate synergism
SKBR3-TLR	0.514	Synergism

Table 4.17: CI values per cell line variant following combination assays of TDM-1 and S4

4.2.9. Association of combination therapies with drug resistance

Correlation between the synergy (CI value) of the neratinib plus S4 combination with neratinib sensitivity (IC_{50} value) was investigated using Spearman rank correlation analysis. Increasing neratinib-resistance correlated (Spearman r= -0.7) with decreasing CI value (increasing synergy) for the combination of neratinib with S4) (*p-value*=0.017) (Figure 4.39).

There was no correlation between the synergy (CI value) of the lapatinib plus S4 combination with lapatinib sensitivity (IC_{50} value) (Spearman r = -0.95) (*p-value*=0.08) (Figure 4.40 (A.)). There was no correlation between neratinib sensitivity with the combination of lapatinib plus S4 (*p-value*=0.08) (Spearman r= -0.95) (Figure 4.40 (B.)).

Similarly for TDM-1, there was no correlation between the synergy (CI value) of the TDM-1 plus S4 combination with TDM-1 sensitivity (Spearman r = -0.9) (*p-value*=0.08) (Figure 4.41 (A.)). There was no correlation between neratinib sensitivity with the combination of TDM-1 plus S4 (*p-value*=0.95) (Spearman r= 0.1) (Figure 4.41 (B.)).

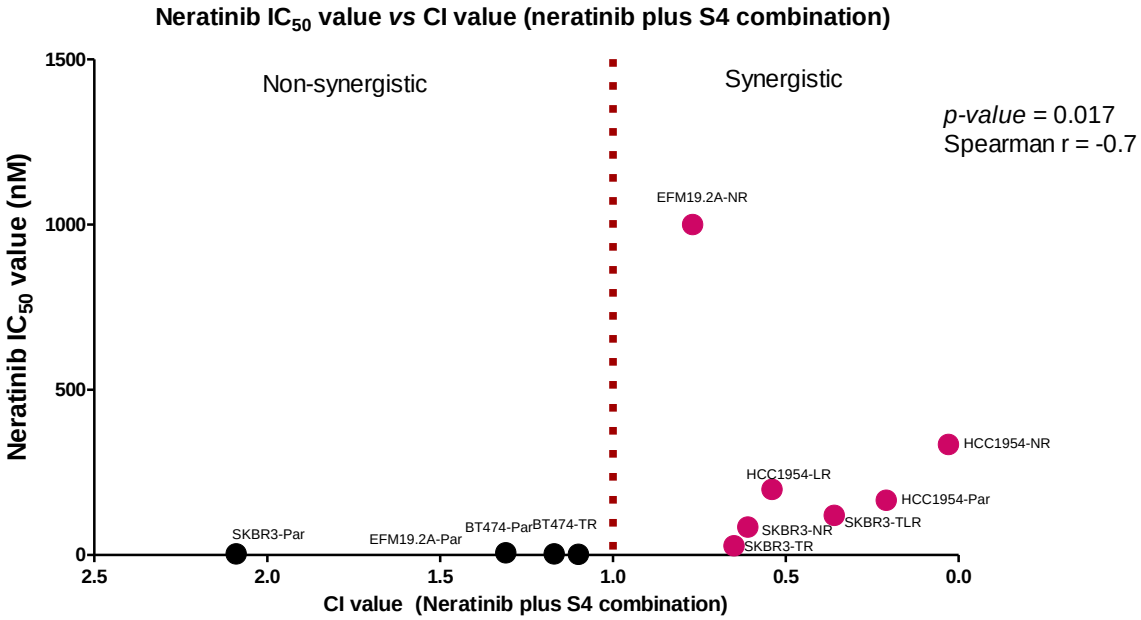

Figure 4.39: Spearman correlation analysis for neratinib sensitivity vs CI value (neratinib plus S4 combination)

Spearman correlation analysis was performed on neratinib sensitivity (IC_{50} value) for all cell line variants *vs* CI value for neratinib plus S4 combination. Pink dots indicate the neratinib-resistant variants, black dots represent the neratinib-sensitive variants. CI value < 1 = synergistic. *p-value*=0.017. (Spearman r = -0.7). (Spearman correlation test).

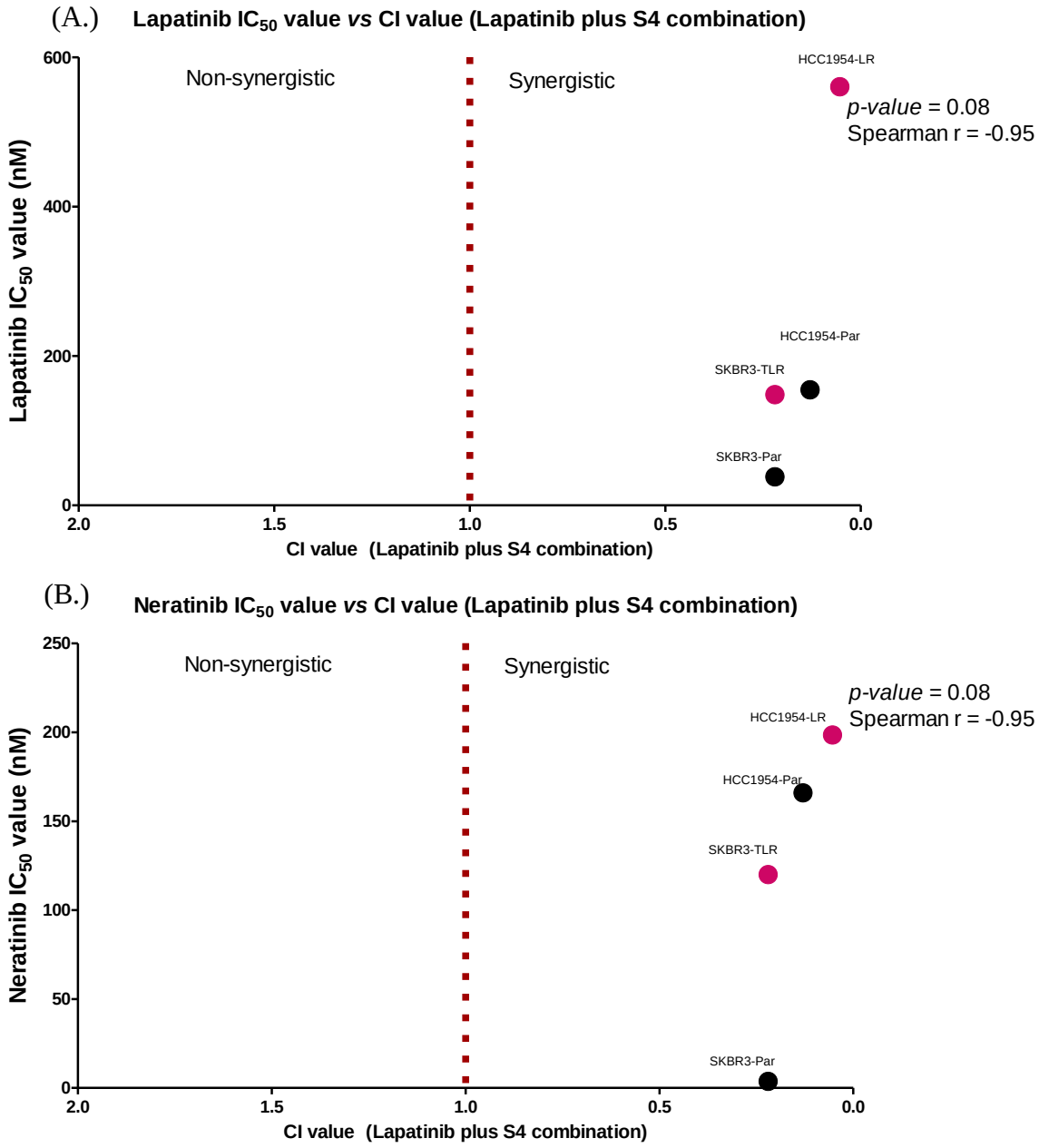

Figure 4.40: Spearman correlation analysis for lapatinib sensitivity vs CI value (lapatinib plus S4 combination)

Spearman correlation analysis on lapatinib sensitivity (IC_{50} value) for all cell line variants vs CI value for lapatinib plus S4 combination. Pink dots indicate the lapatinib-resistant variants, black dots represent the lapatinib-sensitive variants. CI value <1 = synergistic. *p-value*=0.08. (Spearman r = -0.95). (Spearman correlation test).

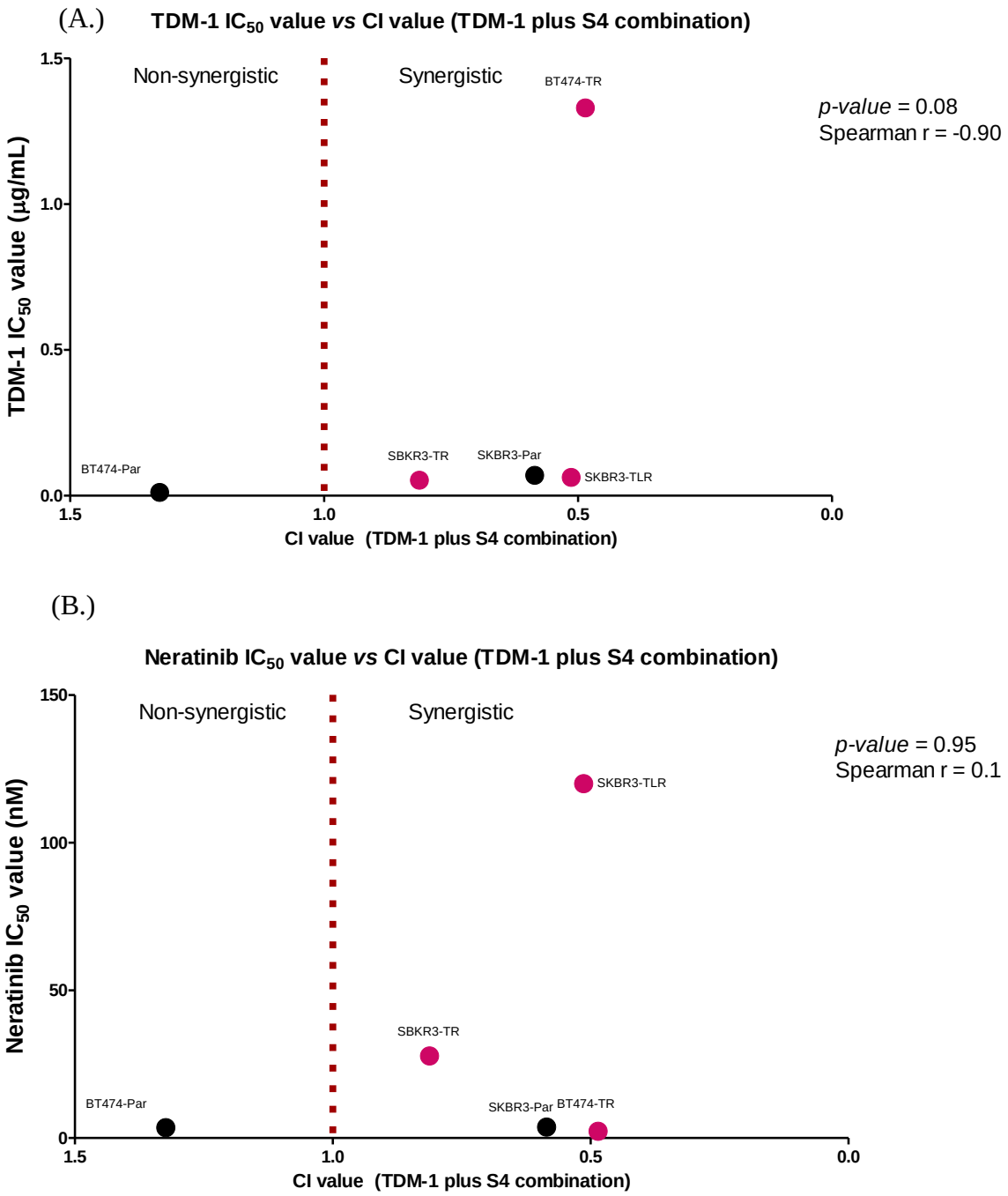

Figure 4.41: Spearman correlation analysis for TDM-1 sensitivity vs CI value (TDM-1 plus S4 combination)

Spearman correlation analysis on TDM-1 sensitivity (IC_{50} value) for all cell line variants vs CI value for TDM-1 plus S4 combination. Pink dots indicate the TDM-1-resistant variants, black dots represent the TDM-1-sensitive variants. CI value < 1 = synergistic. *p-value*= 0.08. (Spearman r = -0.9). (Spearman correlation test).

4.3. Discussion

Neratinib, an irreversible tyrosine kinase inhibitor against EGFR, HER2 and HER4, was approved by the FDA for extended adjuvant treatment of early stage HER2-positive breast cancer in July 2017. Similarly, in July 2018, the EMA recommended granting market authorisation for neratinib for extended adjuvant treatment in HER2+ and hormone receptor positive breast cancer patients. In the clinic, neratinib is having the desired effects in some patients, although, like many HER2-targeted therapies, some patients will not respond to this drug due to innate or acquired resistance. As evidenced in Chapter 3, CAIX was identified as an interesting protein to investigate further in drug-resistant cell line variants. Herein, this study sought to investigate CAIX as a potential mechanism of neratinib-resistance in HER2+ breast cancer cell lines, which may potentially serve as a model for *in vivo* work and potentially benefit patients in the future. For decades, hypoxia has been associated with poor overall survival and drug resistance, this study aimed to determine the mechanism by which cells become resistant to therapies and to determine the role of the hypoxic microenvironment in this process.

4.3.1. CAIX expression in HER2+ breast cancer cell line variants

When cultured under hypoxic conditions, the SKBR3-NR cell line variant displayed increased CAIX expression and decreased CAIX in HC1954-NR. However, the hypoxia chamber used was inefficient and an alternative chamber was used for further studies. To ensure the increased expression of CAIX was not cell-line specific, multiple cell lines were used for this study and many drug-resistant variants also

It was evident that the expression of CAIX fluctuates when the cell line variants are initially exposed to hypoxic conditions, it was hypothesised that this is due to cellular stress and switching on of various mechanisms to return to a homeostatic balance. However, irrespective of the HCC1954-NR cell line variant (which displayed decreased CAIX, compared to HCC1954-Par), all drug-resistant cell line variants produced increased quantities of CAIX after 72hr hypoxic/normoxic conditions when compared to drug-sensitive cell line variants. During normoxic conditions, after 48hr and 72hr, it was observed that the trastuzumab-resistant cell line variants (BT474-TR and SKBR3-TR, respectively) expressed significantly higher levels of CAIX than expressed by their sensitive counterparts. This observation was only evident in the trastuzumab-resistant cell lines, indicating that, irrespective of a hypoxic microenvironment, these cell line variants

produced significantly increased quantities of CAIX. For all other cell line variants, CAIX was significantly increased during hypoxic conditions, thus confirming that, after 72hr culture conditions, CAIX is significantly increased in all the drug-resistant cell line variants used in this study. Interestingly, for the luminal B subtype of cell lines (BT-474 and EFM19.2A), CAIX expression was extremely low/no expression for the drug-sensitive variants. Thus, indicating that CAIX expression may be extremely low in drug-sensitive luminal B tumours. CAIX was detected on the surface of EVs derived from cell line variants. However, there were no significant differences in CAIX quantity between drug-sensitive and drug-resistant cell line-derived EVs. This is not surprising, as CAIX is a transmembrane protein and it functions to catalyse the reversible hydration of carbon dioxide to bicarbonate and protons, thus ensuring the secretion of acid from the cells into the microenvironment to ensure pH homeostasis for tumour survival (169, 188). This mechanism of homeostasis would not be required for EVs.

4.3.2. CAIX inhibition

As CAIX was established as being increased in all drug-resistant cell line variants compared to drug-sensitive cell line variants, we aimed to inhibit CAIX using S4 and determine if this drug was toxic to drug-resistant cell line variants an ultimately if inhibiting CAIX could re-sensitise these drug-resistant cell line variants to the HER2-targeted therapy that they were resistant to. Firstly, by immunoblotting, in a pilot test of HCC1954-Par cells, S4 significantly reduced CAIX expression, thus, confirming that S4 was a suitable CAIX inhibitor for this study. As BT474-TR cells have the ability to increase CAIX in both normoxic and hypoxic conditions, S4 was tested in both hypoxic and normoxic conditions, similarly for the SKBR3-TR cell line variant. CAIX expression in BT474-Par and EFM19.2A-Par cell lines was too low to determine the efficacy of S4 as an inhibitor. Following 72hr treatment of cell line variants with S4 ,S4 significantly inhibited the expression of CAIX in BT474-TR cell line variants (both 21% O_2 and 1% O_2). Similarly, although not significantly decreased for HCC1954-Par and SKBR3-Par, S4 did prevent increased CAIX in these cell lines during hypoxic conditions. In all other cell line variants, all of which are drug-resistant variants, S4 was unable to significantly decrease/prevent CAIX expression after 72hr treatment. This was evident in all neratinib-resistant variants (EFM19.2A-NR, HCC1954-NR and SKBR3-NR), in lapatinib-resistant variant (HCC1954-LR), in trastuzumab-resistant variant (SKBR3-TR) and trastuzumab-lapatinib-resistant variant (SKBR3-TLR). Correlation analysis revealed that increased

neratinib-resistance is directly correlated with inability of S4 to inhibit CAIX expression. Therefore, it is evident that the drug-resistant cell line variants have the ability to overcome the effects of S4, which in turn indicates that the drug-resistant cell line variants require elevated CAIX.

To determine if S4 was cytotoxic to all cell line variants, toxicity assays were performed at both normoxic and hypoxic conditions. Toxicity assays were used to determine the toxicity levels of S4 for both normoxic and hypoxic conditions, thus, determining the toxicity level for both environments (which would be similar to the tumour microenvironment, which contains hypoxic and normoxic pockets). When comparing toxicity levels of cell line variants between normoxic and hypoxic conditions, an significantly increased resistance to S4 was observed in hypoxic conditions for BT474-Par, BT474-TR, EFM19.2A-Par, EFM19.2A-NR, HCC1954-NR, SKBR3-Par, SKBR3-NR and SKBR3-TLR. When comparing drug-resistant variants to drug-sensitive variants in normoxic conditions, HCC1954-LR, HCC1954-NR, SKBR3-NR and SKBR3-TR had significantly increased resistance to S4. Similarly, for hypoxic conditions, HCC1954-NR and SKBR3-TR cell line variants had increased S4 resistance. Thus, indicating that the toxicity of S4 on cell line variants is not predominantly dependent on either normoxic or hypoxic environments. However, the cell line variants with increased CAIX are predominantly more resistant to the cytotoxic effects of S4.

4.3.3. Combination therapy: HER2-targeted therapies with S4

To determine the efficacy of the dual combination of neratinib with S4, combination assays were performed for all cell lines. As expected, the combination of neratinib with S4 was not synergistic in BT474-Par, BT474-TR, EFM19.2A-Par and SKBR3-Par cell line variants. This is partly due to the poor or no expression of CAIX in these cell lines. Secondly, the combination is not synergistic as these cell lines are not resistant to neratinib; therefore, the combination is not required for neratinib to work efficiently. For all neratinib-resistant cell lines, the combination of neratinib with S4 is synergistic; similarly, for all lapatinib resistant, trastuzumab resistant and trastuzumab-lapatinib resistant cell line variants. Interestingly, the combination is synergistic in HCC1954-Par and HCC1954-NR cell lines, HCC1954-Par had increased CAIX levels but HCC1954-NR cell line variants did not. There may be an alternative pathway being used for these cell line variants, for instance, the HCC1954 cell line is innately resistant to trastuzumab *i.e.*

they already have an innate mechanism of resistance. Similarly, this cell line has a slight innate resistance to neratinib, much greater than all other neratinib-sensitive cell lines used in this study, thus it is hypothesised that this innate resistance confers the requirement to produce CAIX. Previous work in our lab by Dr. Vanesa Martinez revealed that the HCC1054-NR cell line variant cannot switch from oxidative phosphorylation to glycolysis (189), thus, we can hypothesise that the HCC1954-NR cell line does not require the same level of CAIX as it will not have an acidic intracellular pH as would cell lines that use glycolysis. Nevertheless, the combination of neratinib and S4 is synergistic in the HCC1954-Par and HCC1954-NR despite these differences. Correlation analysis has revealed that the strong synergy observed for the combination of neratinib with S4 is directly associated with increased neratinib-resistance.

S4 in combination with lapatinib was also completed for lapatinib-resistant cell line variants. The combination of lapatinib and S4 was synergistic in the lapatinib-resistant cell lines and their sensitive counterparts. Thus, indicating that the mechanism of increased CAIX may be an important mechanism for all tyrosine kinase inhibitors not just neratinib. We were unable to test trastuzumab in combination with S4 but the antibody-drug conjugate trastuzumab emtansine (TDM-1) was used instead as this is showing improved PFS and OS in HER2+ metastatic breast cancer patients (190). The combination of S4 with T-DM1 was not synergistic in BT474-Par cell line variants but was in BT-474-TR, SKBR3-Par, SKBR3-TR and SKBR3-TLR, therefore indicating that the mechanism of CAIX in drug resistance is not only with tyrosine kinase inhibitors but also in antibody-drug conjugates. The synergy observed for lapatinib with S4 and TDM-1 with S4 did not directly correlate with increased resistance to neratinib.

4.4. Conclusions

Breast cancer tumours are highly heterogeneous. As described previously, the induction of tumour angiogenesis *via* the hypoxic pathway initially increases nutrient and oxygen levels but ultimately causes vascular leakiness or an inadequate blood vessel system. This vascular leakiness leads to vessel instability, which in turn, causes fluctuations in normoxic and hypoxic conditions in the tumour. Herein, we have determined that CAIX seems to play a role in HER2-targeted drug resistance. The mechanism of resistance is irrespective of hypoxic or normoxic conditions. During hypoxic conditions, CAIX is significantly increased in drug-resistant cell line variants, similarly for some cell line variants during

normoxic conditions. Drug-resistant cell line variants had increased resistance to S4 in both normoxic and hypoxic conditions, thus they may have developed alternative mechanisms to overcome the effects of S4. We have determined that the combination of HER2-targeted therapies with the CAIX inhibitor (S4) is synergistic in all drug-resistant cell lines and in some drug-sensitive cell lines also.

To conclude, the combination of S4 with HER2-targets drugs is not beneficial for drug-sensitive cell line variants or cells with low expression of CAIX. The combination of S4 with HER2-targeted drugs only adds value to neratinib in drug-resistant cell lines that have the ability to increase the expression of CAIX. Notably, the combination of S4 with neratinib is synergistic in all drug-resistant cell line variants and may provide a potential method to clinically overcome neratinib-resistance in HER2+ and luminal B breast cancer patients.

CHAPTER FIVE: The relevance of CAIX as a predictive biomarker in HER2+ breast cancer patients

5. Abstract

The discovery of predictive biomarkers is essential to improving personalised medicine for all cancer patients. We aimed to investigate the potential of CAIX as a predictive biomarker for resistance to HER2-targeted therapy. We used ELISAs to test plasma specimens from the TCHL neo-adjuvant clinical trial, to investigate if the levels of CAIX in pre-treatment plasma specimens correlated with response to therapies. The release of EVs from cells is increased in some cancer types. These EVs are described as mini-maps of their cell-of-origin. EV-cargo can contain DNA, RNA, miRNAs and proteins associated with cancer. They may provide a minimally invasive liquid biopsy analytical tool. Thus, we aimed to isolate EVs from plasma specimens to determine the potential of EVs to carry CAIX and their potential use as predictive biomarkers for HER2-targeted therapies.

In this study, EVs were successfully isolated from plasma specimens using an ultracentrifugation method. Using ELISAs, we have investigated the presence of CAIX in plasma, in EV cargo and on the surface of EVs from HER2+ breast cancer patients' plasma specimens (n=24). The patients' plasma specimens were obtained from patients who subsequently underwent treatment as part of a neoadjuvant trial. CAIX was significantly higher in plasma specimens from HER2+ breast cancer patients that had no response to therapy (TCH, TCL, TCHL), compared to those who experienced a complete or partial response to therapy. CAIX was detectable on EVs from plasma specimens, but the EV isolation technique was deemed unsuitable for detecting CAIX in EVs samples.

We have established that measuring CAIX in raw plasma is a more reliable and cost-effective method for predicting response to therapy than EV-carried CAIX. We have identified CAIX as a potential predictive biomarker of response to the TCHL treatment arms in HER2+ breast cancer, *i.e.* CAIX in plasma was found to be associated with treatment resistance in breast cancer patients.

5.1. Introduction

5.1.1. Biomarkers and personalised medicine

Like all cancer types, breast cancer is a highly heterogeneous disease, thus owing to the discovery of multiple drug targets and the emergence of many targeted therapies following decades of research. The FDA defines precision medicine/personalised medicine "an innovative approach to tailoring disease prevention and treatment that takes into account differences in people's genes, environments, and lifestyles. The goal of precision medicine is to target the right treatments to the right patients at the right time" (https://www.fda.gov/medicaldevices/productsandmedicalprocedures/invitrodiagnostics/precisionmedicine-medicaldevices/default.htm). Although targeted therapies have proven to be highly successful in breast cancer patients (*e.g.* trastuzumab), however, many patients develop or acquire resistance to these therapies. As such, it is imperative to research therapy resistance and make new discoveries in this area for the cohort of patients that do not respond to therapy. Molecular classification (diagnostic biomarkers) of breast cancer subtypes (*e.g.* HER2+, TNBC, luminal A, :luminal B) is essential for selecting the correct targeted therapy for patients. Similarly, predictive and prognostic biomarkers are essential for precision medicine. Prognostic biomarkers provide oncologists with information relating to the overall outcome of the patient, for example, PAM50 and Mammaprint array kits look at 50 and 70 genes associated with outcome and these arrays have been approved as prognostic kits by the FDA. Due to the highly heterogeneous nature of breast cancer tumours, it is difficult to identify biomarkers that are predictive of response to therapy, for example ESR1 has been identified as a potential ctDNA biomarker for resistance to aromatase inhibitors (191). It is important to note that a third of all mechanism of resistance are not yet translational in the clinic, that is, many potential targets of drug resistance are cell-line specific. It is clear that challenges persist in the area of precision medicine and further identification of new therapeutic targets and biomarkers are essential to improving breast cancer patient outcomes.

5.1.2. EVs and their potential as liquid biopsies (hypoxia)

EVs have been described as a means of communication between tumour cells and other cell types including those of the microenvironment and beyond; in breast, as well as other cancer types (64). Dysregulation in this cell-to-cell communication and thus undesirable cellular cross-talk is understood to contribute to cancer development and progression (65).

Tissue biopsies are once-off snapshots of tumours, liquid biopsies have become highly desirable as they can be used to assess real-time observations of tumours, are cheaper and less invasive than tissue biopsies. EVs have been detected in a large range of bodily fluids and are thus highly accessible as liquid biopsies. Cancer cells secrete large amounts of microvesicles and the quantity of MVs can be indicative of tumour stage (192). EVs from cancer patient specimens can contain high levels of proteins associated with disease aggression (193-195).

In addition to promoting tumour progression, hypoxia influences EV secretion and their downstream effects. Many studies investigating exosomes in hypoxic conditions have been completed in different cancer types (previously discussed in Section 1.5.4.1) and may be important for the future of liquid biopsies.

5.1.3. Cancer Trials Ireland 10-15 trial

The Cancer Trials Ireland 10-15 trial (NCT01485926) commenced in December 2011. This clinical trial is a Phase II neo-adjuvant trial assessing the efficacy of TCH (docetaxel, carboplatin and trastuzumab), TCL (docetaxel, carboplatin and lapatinib) and TCHL (docetaxel, carboplatin, trastuzumab and lapatinib) in HER2+ breast cancer patients. 88 patients with HER2+ breast cancer were enrolled in this trial, the median age was 49 years. Of the 88 patients enrolled, 60.2% of patients had ER-positive tumours and 38.6% of patients had PR+ tumours. This trial used pathological CR as the primary endpoint. CR was defined as the absence of invasive carcinoma in breast tissue and lymph nodes. Partial response (PR) was defined as the presence of carcinoma in either or both the tumour and lymph nodes. No response (NoR) was defined as no change in the tumour or lymph nodes when compared to pre-treatment analysis. The rate of pathological complete remission for patients enrolled on this trial was 43.2%. Of which, 43.2% of patients were enrolled on the TCH arm, 45.4% were enrolled on the TCHL treatment arm and 11.4% of patients were enrolled on the TCL arm. The numbers of patients enrolled on the TCL trial were limited; this is due to this treatment arm closing early due to preliminary clinical data that was obtained from the ALTTO (Adjuvant Lapatinib and/or Trastuzumab Treatment Optimisation) study, which indicated that the TCH and TCHL arms were superior to TCL in terms of patient survival outcomes.

As neratinib has recently been approved by the FDA (July 2017), there were no patient specimens available from neratinib-based clinical trials. As such, the TCHL trial

investigated trastuzumab (monoclonal antibody) and lapatinib, a tyrosine kinase inhibitor like neratinib, and it was determined that this trial was an important pilot study for investigating CAIX in HER2-targeted drug resistance. In this study, 52 plasma specimens (24 pre- and post-treatment specimens, with 4 unmatched pre- and post-treatment samples) were obtained from the 10-15 trial. Of which, approximately 57% of patients had a CR, 21% had a PR and 21% had NoR. To investigate the potential of CAIX as a predictive biomarker for HER2-targeted treatment, the samples obtained were blindly analysed. Following CAIX investigation in these samples, during the analysis stage, a limitation to this study was documented. Due to severe toxicities, the TCL arm of the trial was closed early, thus, there were limited numbers of patient specimens available for analysis. Similarly, as this trial has been completed, many of the specimens have been utilised for alternative studies. Therefore, plasma analysis of CAIX was performed for all available samples *i.e.* 24 matched (pre- and post-treatment) samples and an additional two samples (unmatched) for both pre-treatment and post-treatment were obtained. For EV analysis, the plasma volume obtained only allowed for use of the 24 matched samples and the volume was limited for the four unmatched samples. Therefore, statistical analysis could not be performed for all EV samples as only two non-responder samples were analysed. Similarly, as the TCHL trial has a large percentage of patients obtaining CR to therapy, the number of non-responders was limited.

Specimens from 24 patients were available for testing in this study (matched pre-treatment and post-treatment). Additional unmatched patient specimens were available, two for pre-treatment and two for post-treatment. Treatment outcome was assessed following 6 cycles of anti-cancer treatments (as described in Section 2.18), patients were determined to have a CR, partial response (PR) or no response (NoR). A breakdown of overall patient outcome and treatment arms are summarised in Figure 5.1. Post-treatment analysis of the specimens obtained revealed that 57.14% of patients on this trial had a CR, 21.43% had a PR and 21.43% had NoR.

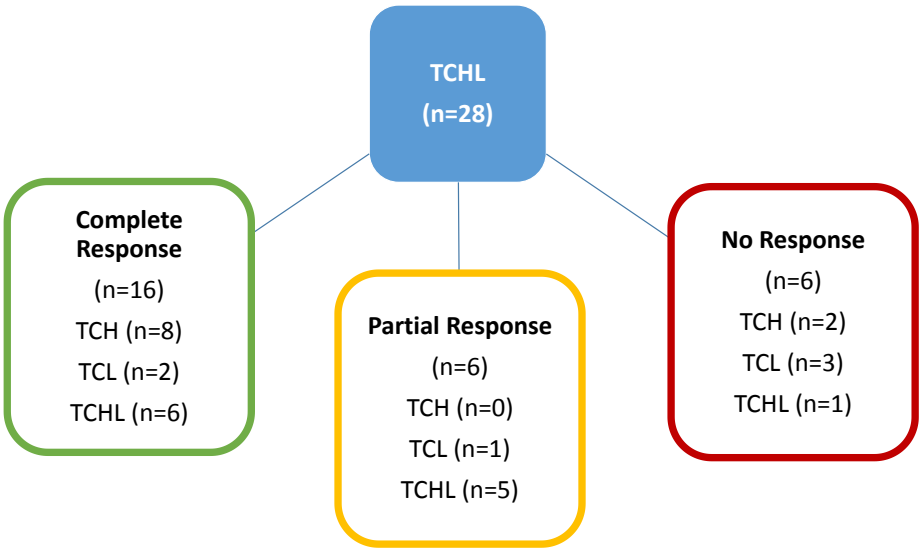

Figure 5.1: Clinical Trial details and treatment outcome
Patient outcome was assessed following treatment with TCH, TCL or TCHL. 57.14% of patients on this trial had a CR, 21.43% had a PR and 21.43% had NoR.

5.1.4. Aims

In this project, CAIX was investigated to elucidate if it is likely to be causally involved in the mechanisms of neratinib-resistance in HER2+ breast cancer. We determined that CAIX plays a role in the mechanism of neratinib-resistance. We have evidence to suggest that the combination of S4 with neratinib may overcome this resistance in HER2+ breast cancer cell lines.

Following on from this work, in this Chapter, we aimed to investigate the potential of CAIX as a predictive biomarker in HER2-targeted therapies using specimens from the Cancer Trials Ireland 10-15 Trial. Using plasma specimens from this trial, we aimed to investigate the levels of CAIX between pre- and post-treatment samples. We also aimed to investigate if CAIX is relevant in predicting response to HER2-target therapies, and finally, we aimed to investigate if CAIX levels were associated with response in a specific treatment arm of this trial. As EVs have been shown to be important in liquid biopsies, we also aimed to investigate the levels of CAIX in EVs and determine if they are suitable as liquid biopsies for testing CAIX in patient samples.

5.2. Results

5.2.1. CAIX Kaplan-Meier plots

The association of CAIX expression and patient survival was assessed in breast cancer patients. This analysis was performed using BreastMark (a publically available database that uses algorithms to identify genes and miRNAs associated with disease progression in breast cancer patients). For this study, overall survival was selected. CAIX expression was investigated in all breast cancer subtypes (Figure 5.2). High expression of CAIX was associated with poorer overall survival in all breast cancer patients (Figure 5.2 (A.)) (*p-value*=0.0000008). When stratified for each subtype, high expression of CAIX was associated with poorer overall survival in HER2+ breast cancer patients (*p-value*=0.002) and luminal B breast cancer patients (*p-value*=0.003) (Figure 5.2 (A.) and (B.)). For breast cancer subtypes basal-like and luminal A, there was no association between CAIX and patient survival. Clinical parameters of patients were assessed, high CAIX expression in lymph node negative (LN-) in all breast cancer patient subtypes was associated with poorer overall survival (*p*-value=0.00007) and this association was observed for HER2+ breast cancer patients only (*p-value*=0.01) (Figure 5.2 (F.)).

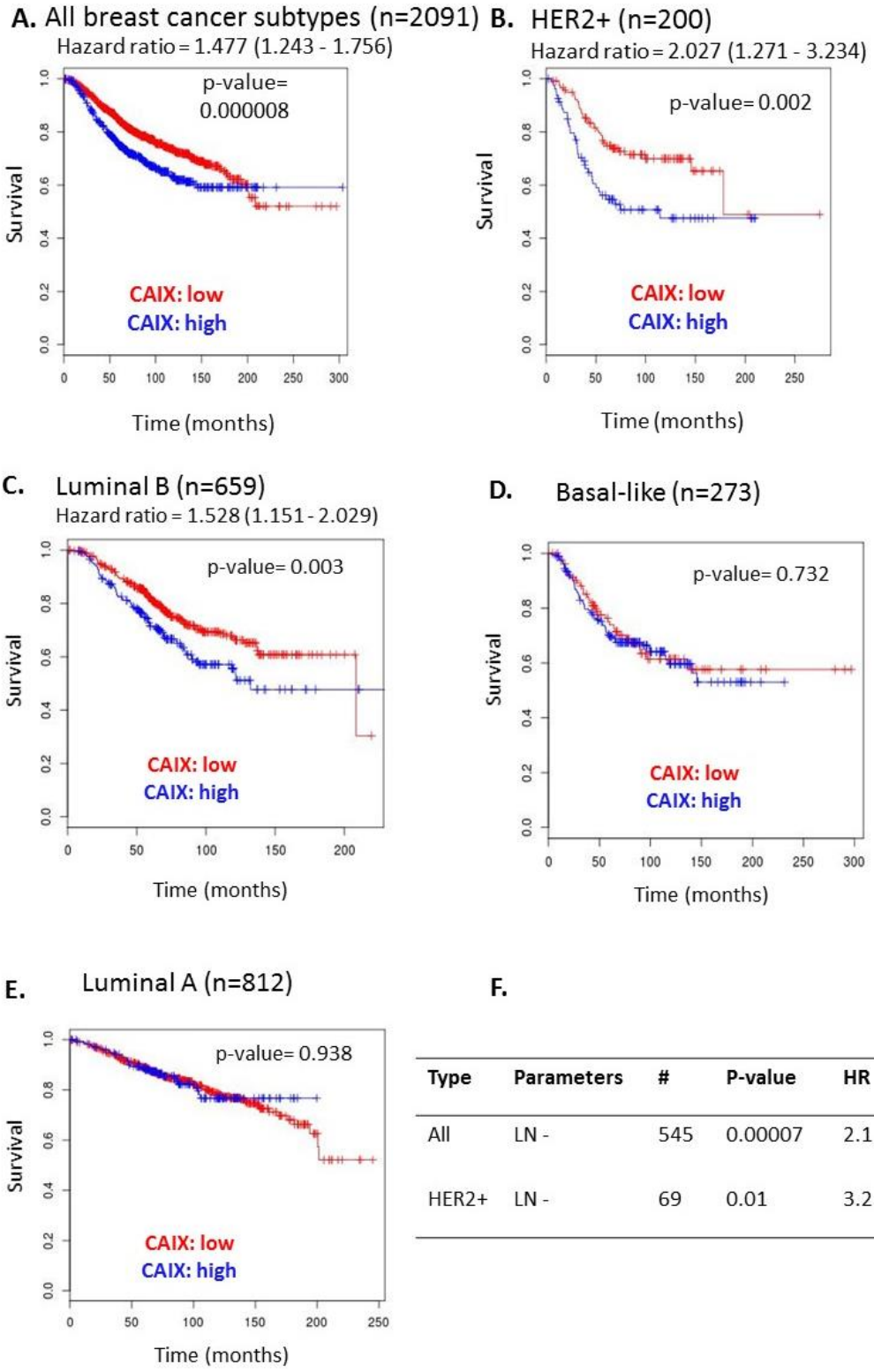

Type	Parameters	#	P-value	HR
All	LN -	545	0.00007	2.1
HER2+	LN -	69	0.01	3.2

Figure 5.2: Overall survival plots for CAIX
Kaplan Meier plots determining the association between early-stage expression of CAIX and overall survival in all breast cancer patients (A.) and subsequently all breast cancer subtypes (B., C., D., E.). Multivariate analysis for clinicopathological parameters was performed (F.).

5.2.2. Quantification of CAIX in patient plasma specimens: Response to treatment

Levels of CAIX in patient plasma specimens were measured by ELISA. CAIX was detected in all pre-treatment and all post-treatment specimens. There was a significant increase in CAIX levels in post-treatment specimens (4.51±0.4pg/mg) compared to pre-treatment specimens (3.06±0.4pg/mg) (Figure 5.3) (*p-value*=0.0325). The levels of CAIX were evidently different when stratified by CR, PR and NoR (Figure 5.4). CAIX levels for CR were significantly increased in post-treatment specimens (3.724±0.5pg/mg) compared to pre-treatment (3.25±0.3pg/mg) (*p-value*= 0.019) (Figure 5.4 A). Similarly, for PR, CAIX levels were significantly increased in post-treatment specimens (4.85±0.7pg/mg) compared to pre-treatment specimens (2.69±0.2pg/mg) (*p-value*= 0.019) (Figure 5.4 B). For NoR specimens, CAIX showed an opposite trend to that of CR and PR. CAIX was trending towards decreased levels in post-treatment specimens (5.97±0.1.3pg/mg) compared to pre-treatment specimens (7.93 ± 1.43pg/mg) (Figure 5.4 C). CAIX levels were compared across all responses for both pre-treatment and post-treatment plasma specimens (Figure 5.5). Pre-treatment CAIX levels in NoR plasma specimens (8.39 ± 1.4pg/mg) was significantly increased when compared to both CR (3.05 ± 0.3pg/mg) ($p<0.001$) and PR (2.69 ± 0.5pg/mg) ($p<0.001$) (Figure 5.5 (A.)). For post-treatment CAIX levels, there were no significant differences in CAIX levels across CR (3.72 ± 0.5pg/mg), PR (4.85 ± 0.7pg/mg) or NoR (5.97± 1.3pg/mg) (Figure 5.5 (B.)).

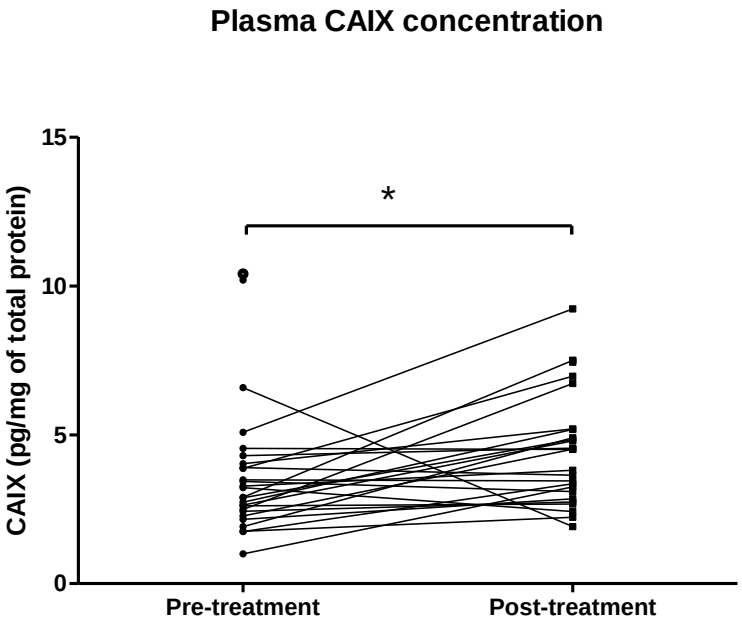

Figure 5.3: CAIX plasma concentration pre- and post-treatment
Plasma levels of CAIX were measured in pre- and post-treatment patient specimens. No significant differences were observed. Outlier value (white data point) as determined by Grubbs test was included in the figure but excluded from statistical analysis. (Student's t-test*).*

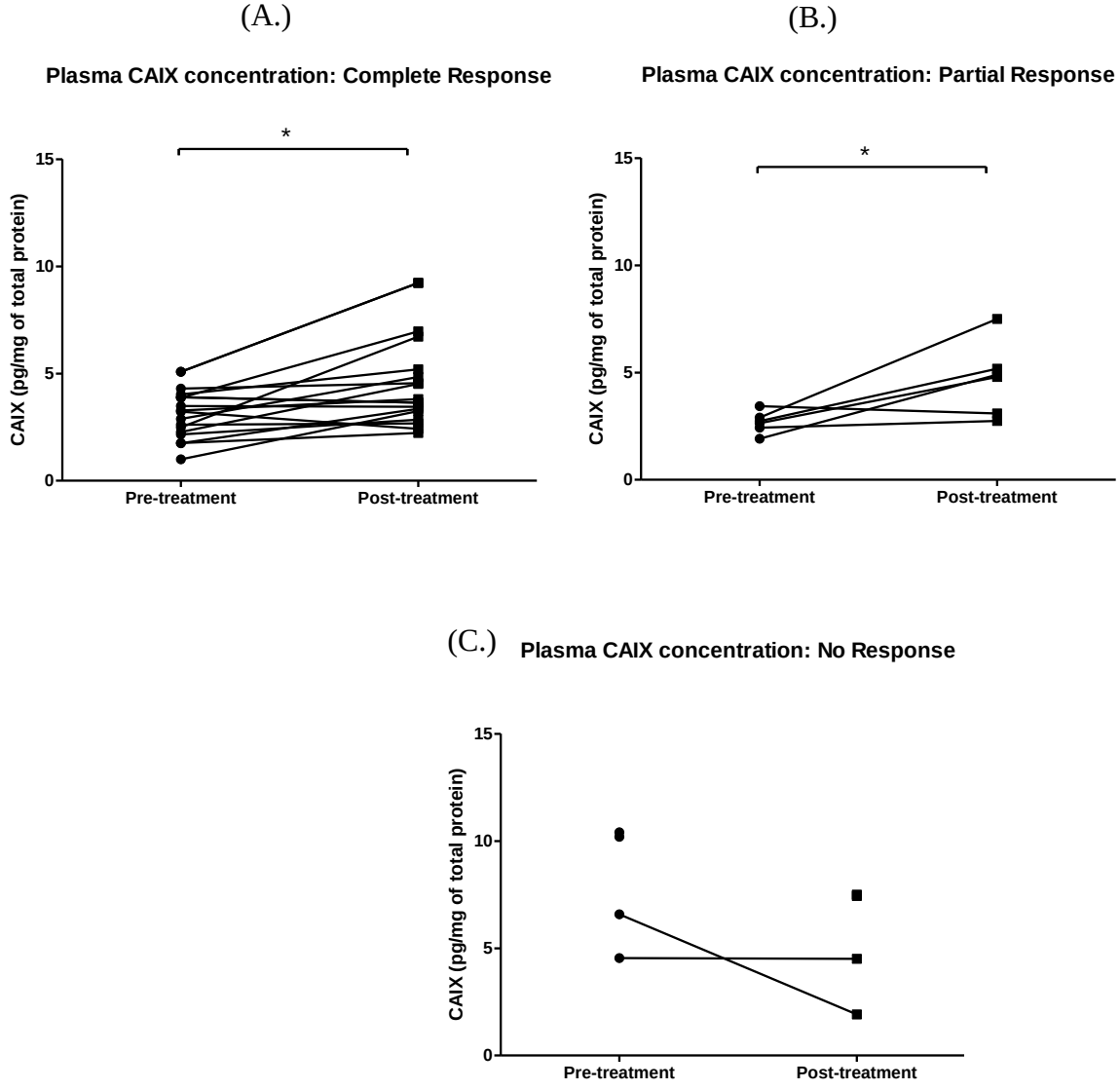

Figure 5.4: CAIX plasma concentration for CR, PR and NoR: pre- and post-treatment
Treatment response CAIX levels were compared between pre- and post-treatment specimens. CAIX was significantly increased in post-treatment CR specimens (*p-value*=0.019) and PR specimens (*p-value=0.019).* There were no significant differences in NoR specimens. *p<0.05 (*Student's t-test)*.

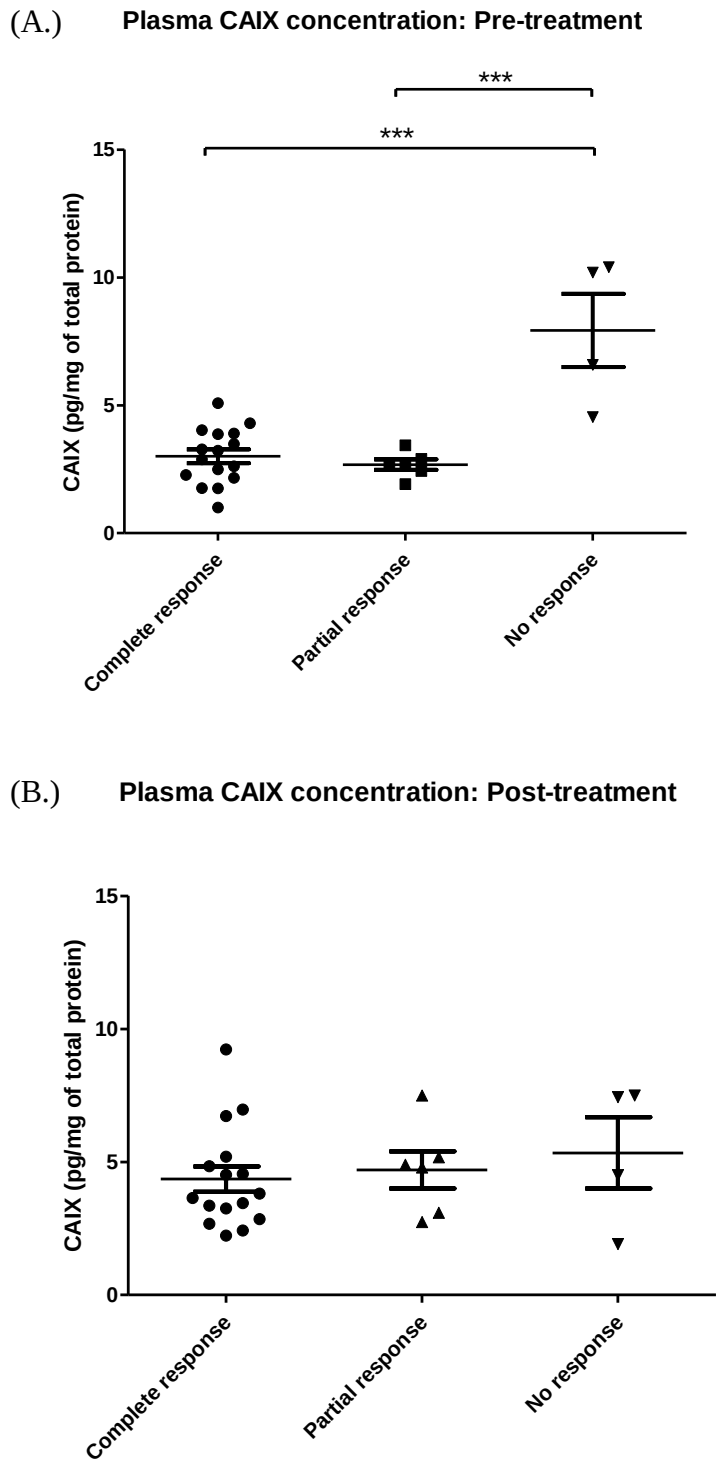

Figure 5.5: CAIX plasma concentration in pre- and post-treatment specimens (all responses)
CAIX levels in pre-treatment specimens were determined in CR, PR and NoR plasma specimens. NoR CAIX levels were significantly increased compared to both CR ($p<0.001$) and PR ($p<0.001$) specimens (A.). There were no significant differences between CR, PR or NoR specimens in post-treatment specimens (B.). ***$p<0.001$ (*ANOVA).*

5.2.3. Quantification of CAIX in patient plasma specimens: Treatment arms

Plasma CAIX levels were measured by ELISA and stratified by treatment arm. For the TCL and TCHL treatment arms, there were no significant differences in CAIX levels between pre-and post-treatment specimens (TCL pre-treatment 2.35±1.3pg/mg and post-treatment 3.209±0.9pg/mg, TCHL pre-treatment 3.06±0.6pg/mg and post-treatment 3.64±0.5pg/mg). CAIX levels were significantly increased in TCH post-treatment specimens (4.54±0.7pg/mg) compared to pre-treatment (2.44±0.5pg/mg) (*p-value*=0.0326) (Figure 5.6). For both the pre-treatment specimens (TCH 2.44±0.5pg/mg, TCL 4.20±1.3pg/mg and TCHL 3.06±0.6) (Figure 5.7 (A.)) and post-treatment specimens (TCH 3.15±0.7pg/mg, TCL 4.9±0.9pg/mg and TCHL 3.64±0.5) (Figure 5.7 (B.)), there were no significant changes in CAIX levels between the treatment arms. However, CAIX levels in pre-treatment TCL samples were trending towards increased CAIX compared to TCHL samples (*p-value*=0.051). The sample sizes per treatment arms are too low to perform statistical analysis. Therefore, the results are presented as pilot data. The TCH graphs are represented for pre-treatment and post-treatment responses (Figure 5.8 (A.) and (B.)), for this treatment arm, most patients had CR and we only obtained two post-treatment specimens available for analysis. The average mean of CAIX in NoR pre-treatment TCL specimens is 7.10 ±2.9pg/mg, compared to 3.18 ±1.0pg/mg for CR. (Figure 5.9 (A.)). For post-treatment TCL specimens, the average mean for CR was 6.84±0.2pg/mg and 3.21± 1.83pg/mg for NoR (Figure 5.9 (B.)). The TCHL specimens were also limited. Data is represented in Figure 5.10 (A.) for pre-treatment responses and Figure 5.10 (B.) for post-treatment responses. The average means for CAIX for pre-treatment CR is 3.09±0.73pg/mg and 2.83± 0.17pg/mg for PR. There is only one specimen available for NoR. The average means for CAIX levels in post-treatment TCHL specimens were 3.4±0.1pg/m for CR and 4.66±1.93pg/mg for PR.

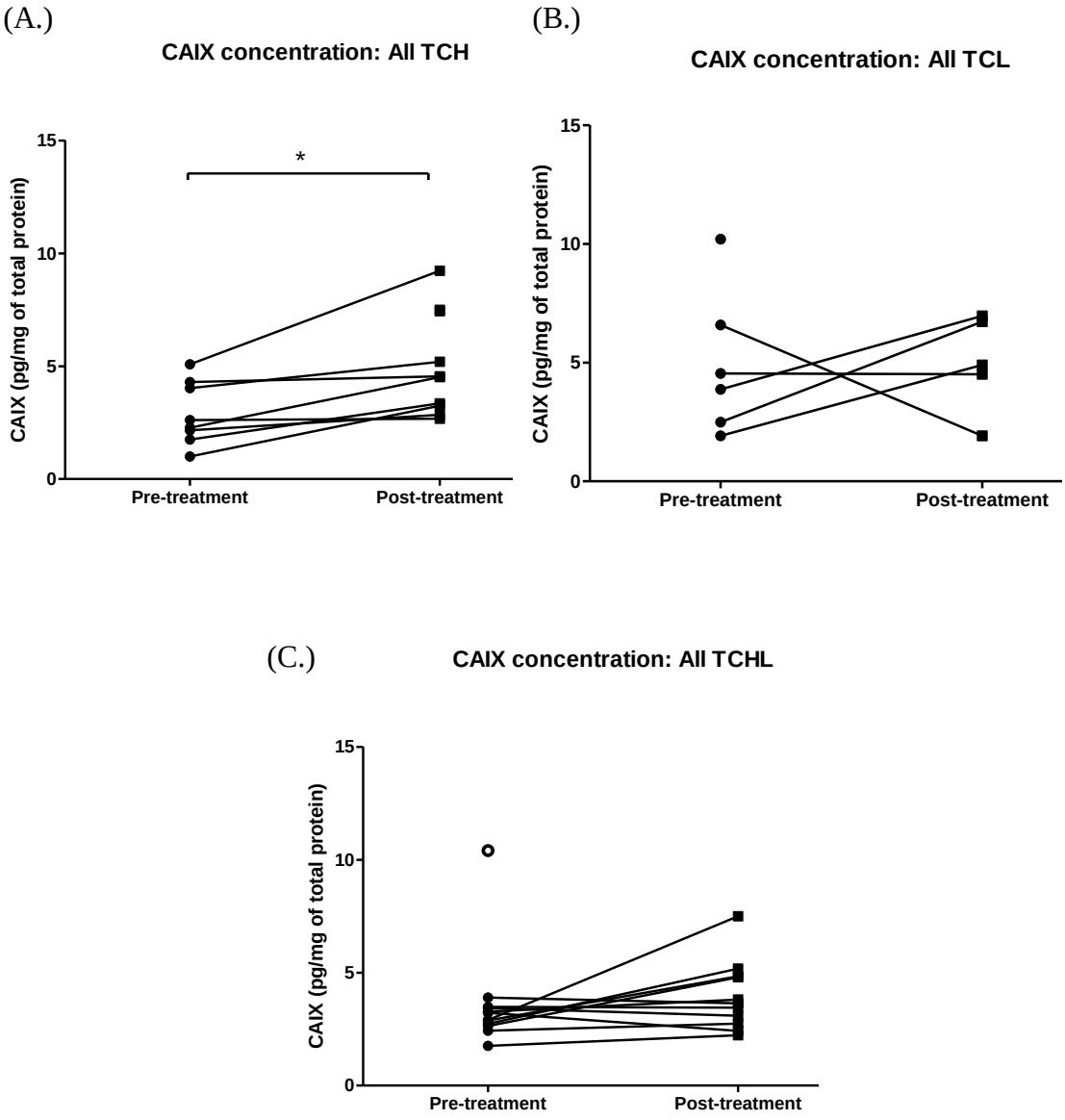

Figure 5.6: CAIX quantification in pre- and post-treatment specimens (treatment arms)
CAIX quantification in all pre- and post-treatment specimens stratified by treatment arm TCH (A.), TCL (B.) and TCHL (C.). Outlier value (white data point) as determined by Grubbs test was included in the figure but excluded from statistical analysis. *$p<0.05$ (Student's t-test).

(A.)

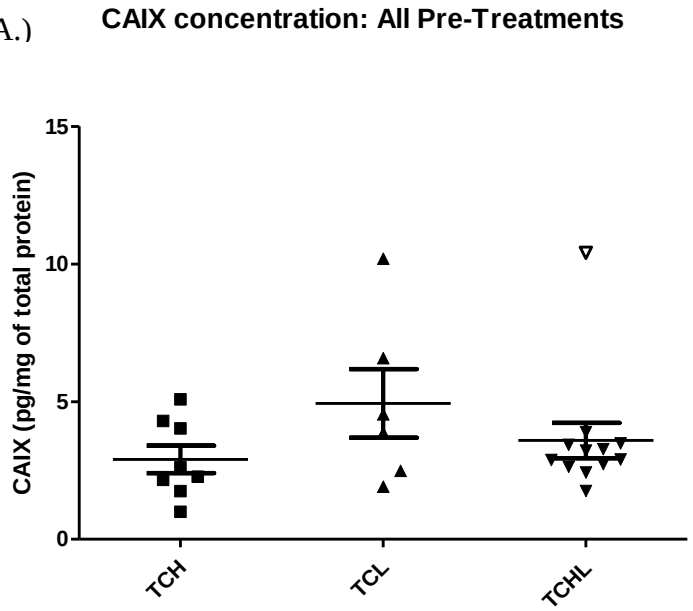

(B.)

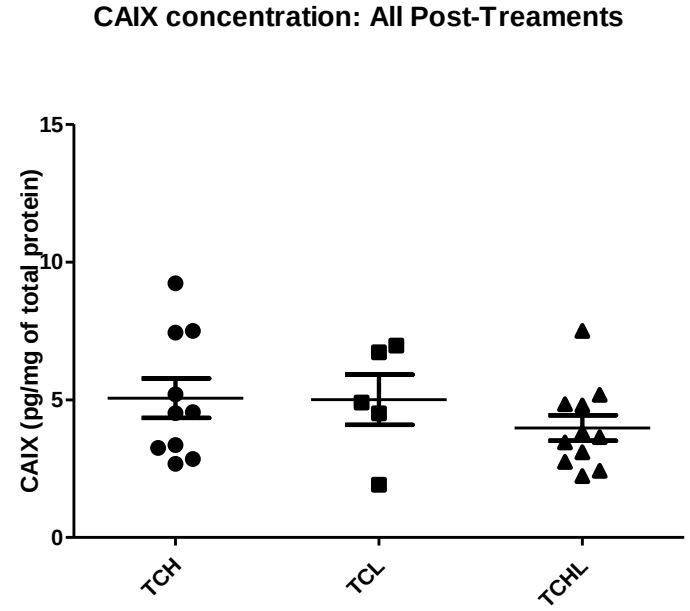

Figure 5.7: CAIX quantification in all treatment arms (pre- and post-treatment)
CAIX quantification in all treatment arm specimens stratified by pre-treatment (A.) and post-treatment (B). Outlier value (white data point) as determined by Grubbs test was included in the figure but excluded from statistical analysis. There were no significant differences between samples, pre-treatment TCL samples were trending towards increased CAIX compared to TCHL (*p-value*=0.051). (*ANOVA*).

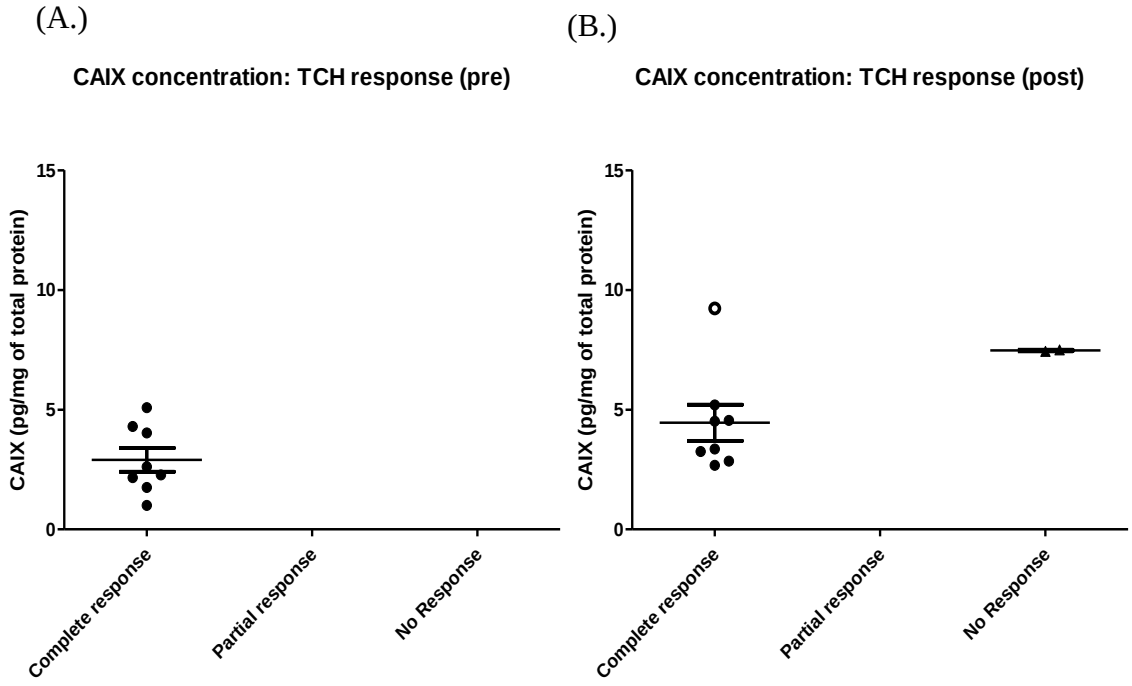

Figure 5.8: CAIX quantification in the TCH treatment arm (pre- and post-treatment)
CAIX quantification in the TCH treatment arm, specimens are stratified by pre-treatment (A.) and post-treatment (B).

(A.)

(B.)

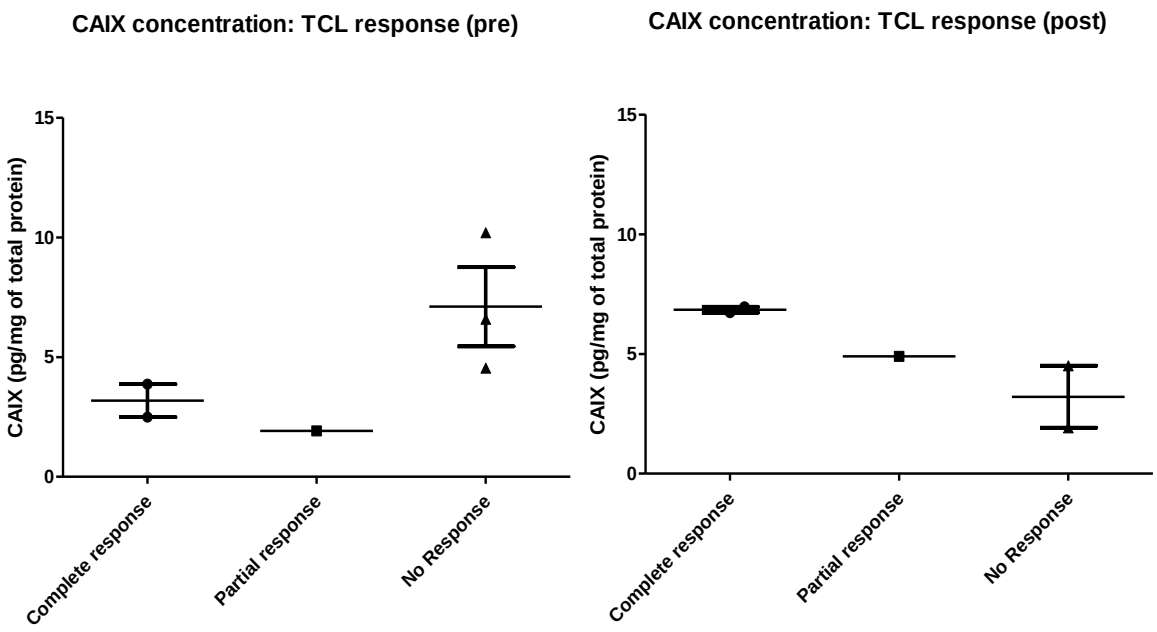

Figure 5.9: CAIX quantification in the TCL treatment arm (pre- and post-treatment)
CAIX quantification in the TCL treatment arm, specimens are stratified by pre-treatment (A.) and post-treatment (B).

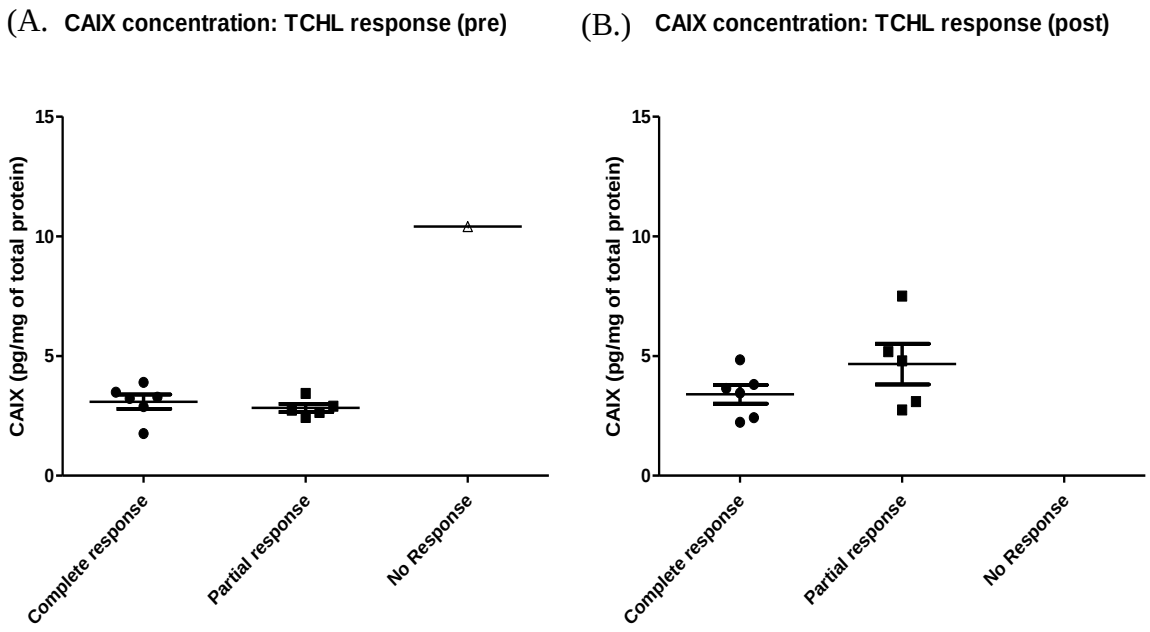

Figure 5.10: CAIX quantification in the TCHL treatment arm (pre- and post-treatment)
CAIX quantification in the TCHL treatment arm, specimens are stratified by pre-treatment (A.) and post-treatment (B). TCHL pre-treatment sample was previously determined to be a significant outlier.

5.2.4. Successful isolation of EVs from plasma specimens

Successful EV isolation from plasma specimens was performed as described in Section 2.6. Only 24 specimens were available for EV isolation, the plasma volume in the four additional unmatched samples was too low (60µL). Due to the limited number of plasma volume available for isolations, immunoblots were performed on one EV sample from pre-treatment plasma isolations and one sample from post-treatment plasma isolations (Figure 5.11 (A.)). SKBR3-Par cell lysate was used as an EV negative control. GRP-94 was detected in cell-derived EV lysates. Plasma specimen EV samples were negative for GRP-94. The presence of EVs was confirmed by the positive markers TSG101 and ALIX. NTA analysis revealed that the EVs isolated were on average 135nm (ranging from 131.8-138.2nm) in diameter (Figure 5.11 (B.)). TEM analysis was performed to determine the size and morphology of EVs (Figure 5.11 (C.)). The EV-track score for this study is 78% (98^{th} percentile of all experiments).

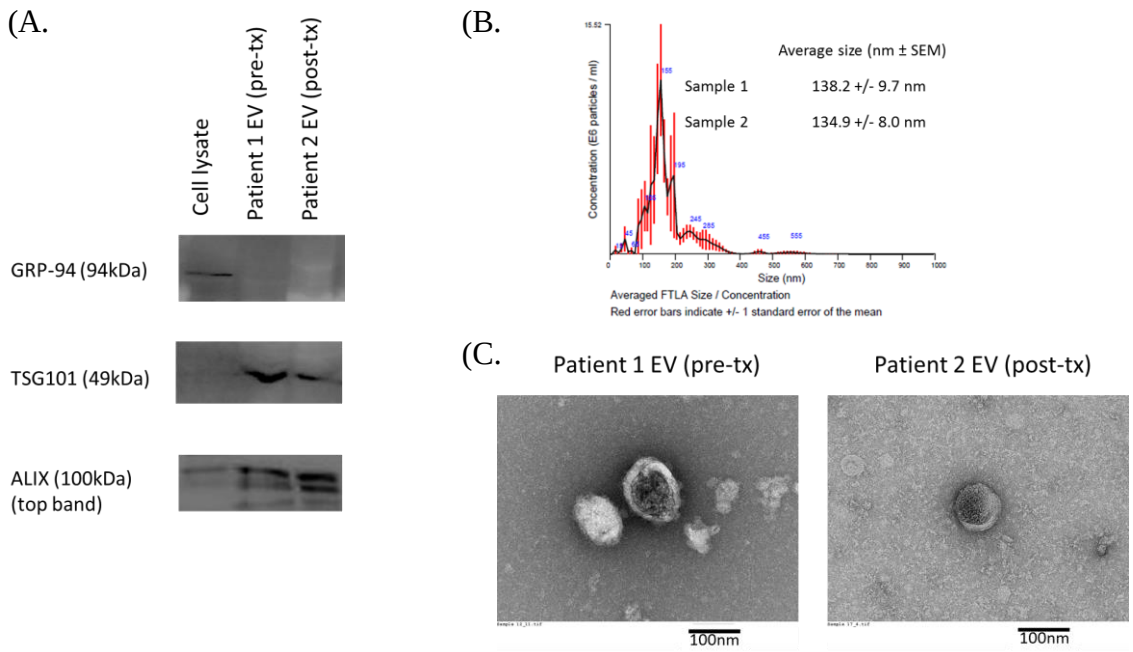

Figure 5.11: Characterisation of EVs isolated from plasma specimens
EV characterisation was performed on EVs from plasma specimens (pre-treatment (sample 1) and post-treatment (sample 2). 30µg of EV protein was separated by immunoblotting. EV samples were positive for EV markers; TSG101 and ALIX. Patient EV samples were negative for GRP-94. (A.). The average diameter of EVs was determined by Nanosight (B.) and found to be 135nm. TEM analysis revealed the morphology and size of EVs for both samples (C.).

5.2.5. EV quantification (plasma specimens)

Protein quantification was performed as a surrogate measurement for EV quantity. The quantity of EVs in post-treatment specimens (21.9±4.3µg/mL) was significantly reduced compared to pre-treatment specimens (28.66±5.7µg/mL) (Figure 5.12) (*p-value*=0.0139). When stratified by CR, there were significantly less EVs in post-treatment specimens (23.42±5µg/mL) compared to pre-treatment specimens (31.53±7.8µg/mL) (Figure 5.13 (A.)) (*p-value*=0.0197). There were no significant differences from EV quantity in partial responder specimens (pre-treatment 19.39±7.7µg/mL and post-treatment 15.96±8.6µg/mL) (Figure 5.13 (B.)). Statistical analysis could not be performed for non-responder specimens due to the limited samples size (n=2) (Figure 5.13 (C.)).

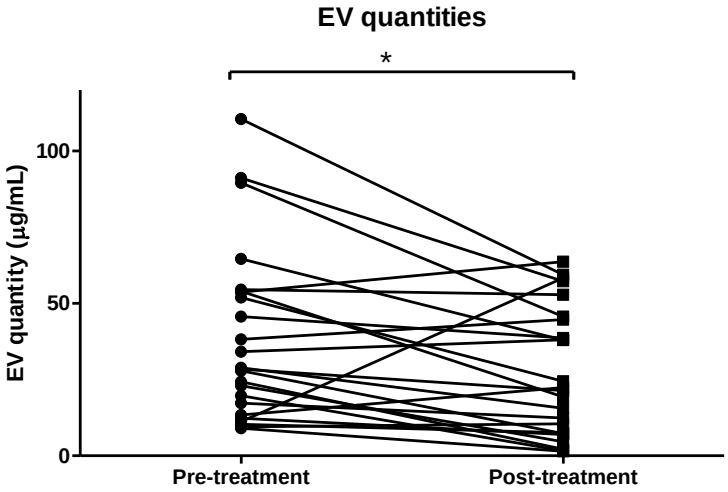

Figure 5.12: EV quantity (pre-treatment and post-treatment)
The quantity of EVs was significantly reduced in post-treatment plasma specimens compared to pre-treatment (*p-value*=0.0139). *p<0.05 (Student's t-test).

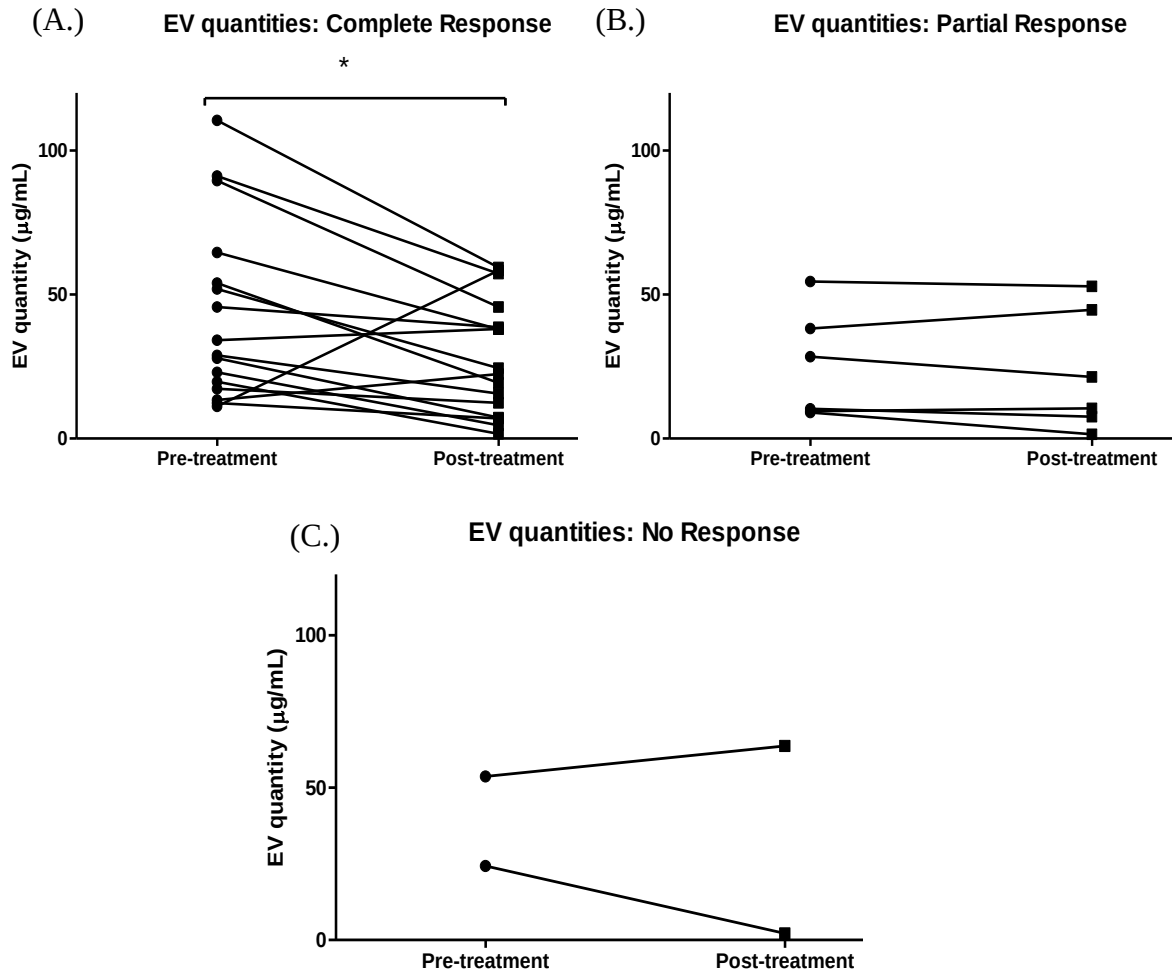

Figure 5.13: EV quantities (treatment response)
The quantity of EVs was significantly reduced in post-treatment complete response plasma specimens compared to pre-treatment (*p-value*=0.0197) (A.). There were no significant differences in EV quantities for partial response specimens (B.). The sample size was limited for EV samples from No response specimens (n=2), therefore no statistical analysis was performed.*$p<0.05$ (Student's t-test).

5.2.6. Quantification of CAIX: Plasma specimen EV surface

CAIX quantification was determined on the surface of EVs derived from plasma specimens. There were no significant differences in the level of CAIX between pre-treatment and post-treatment EV samples (see Appendix I). The quantity of CAIX on the surface of EVs was poor, with the ELISA kit only detecting CAIX in 25% or pre-treatment samples and 42% of post-treatment samples (see Appendix I).

5.2.7. Quantification of CAIX: Plasma specimen EV content

CAIX quantification was performed in EV lysates from patient plasma specimens. There was a trend towards decreased CAIX in post-treatment samples (95.7±33pg/mg) compared to pre-treatment (184.7±28.1pg/mg) (*p-value*= 0.052) (Figure 5.14). CAIX quantities were determined in EV lysates and stratified by treatment response. There were no significant differences in CAIX quantity across treatment responses for both pre-treatment specimens (Figure 5.15 (A.)) and post-treatment (Figure 5.15 (B.)), statistical analysis could not be performed due to the limited sample number (n=2) for NoR samples. EV lysate CAIX quantities was determined for CR, PR and NoR samples (Figure 5.16 (A.), (B.) and (C.)). CAIX levels in EV lysates were significantly decreased in CR post-treatment EV samples (80.8±25.41pg/mg) compared to pre-treatment EV samples (196±29.35pg/mg) (*p-value*=0.01). There were no significant differences in CAIX levels in PR samples (pre-treatment 169.7±30.7pg/mg and post-treatment 166.3±64.3) or NoR samples (limited sample size n=2). When determining the level of CAIX per sample per treatment arm, there were no significant differences in CAIX between pre- (200.6±49pg/mg) and post-treatment TCHL samples (215.5±63.9pg/mg) (Figure 5.17 (C.)). For the TCH treatment arm, post-treatment CAIX levels (90±27.5pg/mg) were significantly decreased compared to pre-treatment (195.5±39.1pg/mg) (*p-value*=0.01). CAIX levels were significantly decreased in TCL post-treatment samples (80.8±38.2pg/mg) compared to pre-treatment EV samples (169.7±63pg/mg) (*p-value*=0.04). CAIX levels in pre-treatment EV samples were unchanged between treatment arms (TCH 195.5±39.1pg/mg, TCL 169.7±63pg/mg, TCHL 200.6±49pg/mg) (Figure 5.18 (A.)). Similarly for post-treatment samples, there were no significant changes in CAIX levels per treatment arms (TCH 89.98±27.5pg/mg, TCL 80.8±pg/mg, TCHL 215.5±63.9pg/mg) (Figure 5.18 (B.)).

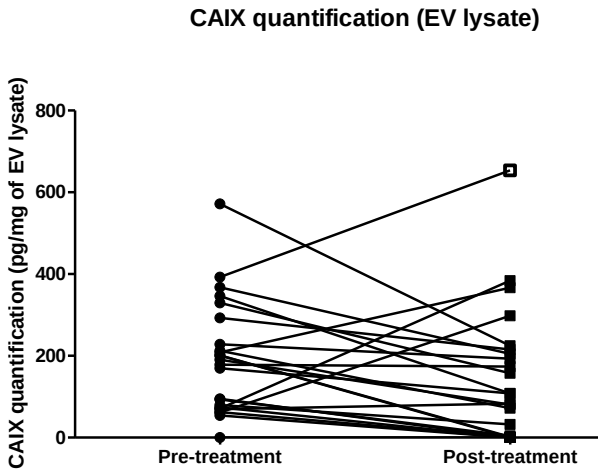

Figure 5.14: CAIX quantification: EV lysate (all samples)
CAIX quantification in EV lysates for all pre-treatment and post-treatment samples. There were no significant differences. Outlier value (white data point) as determined by Grubbs test was included in the figure but excluded from statistical analysis. (Student's t-test).

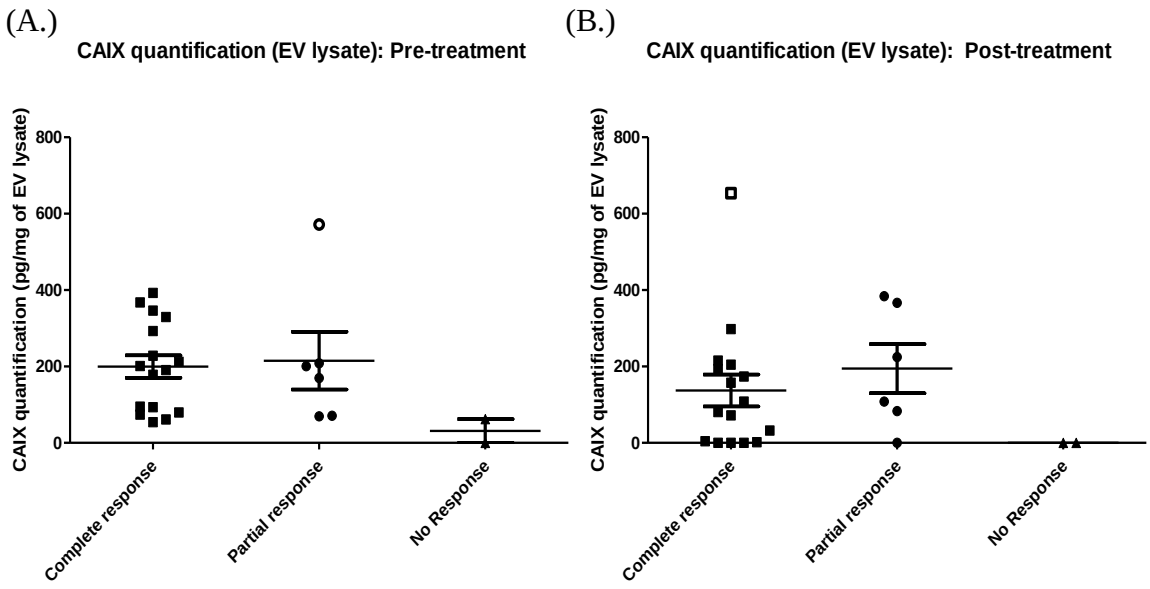

Figure 5.15: CAIX quantification: EV lysate pre-treatment and post-treatment (treatment response)
CAIX quantification in EV lysates for all treatment responses for pre-treatment samples (A.) and post-treatment samples (B.). There were no significant differences. Statistical analysis could not be performed for non-responder samples (n=2).Outlier values (white data points) as determined by Grubbs test were included in the figure but excluded from statistical analysis. (*ANOVA*).

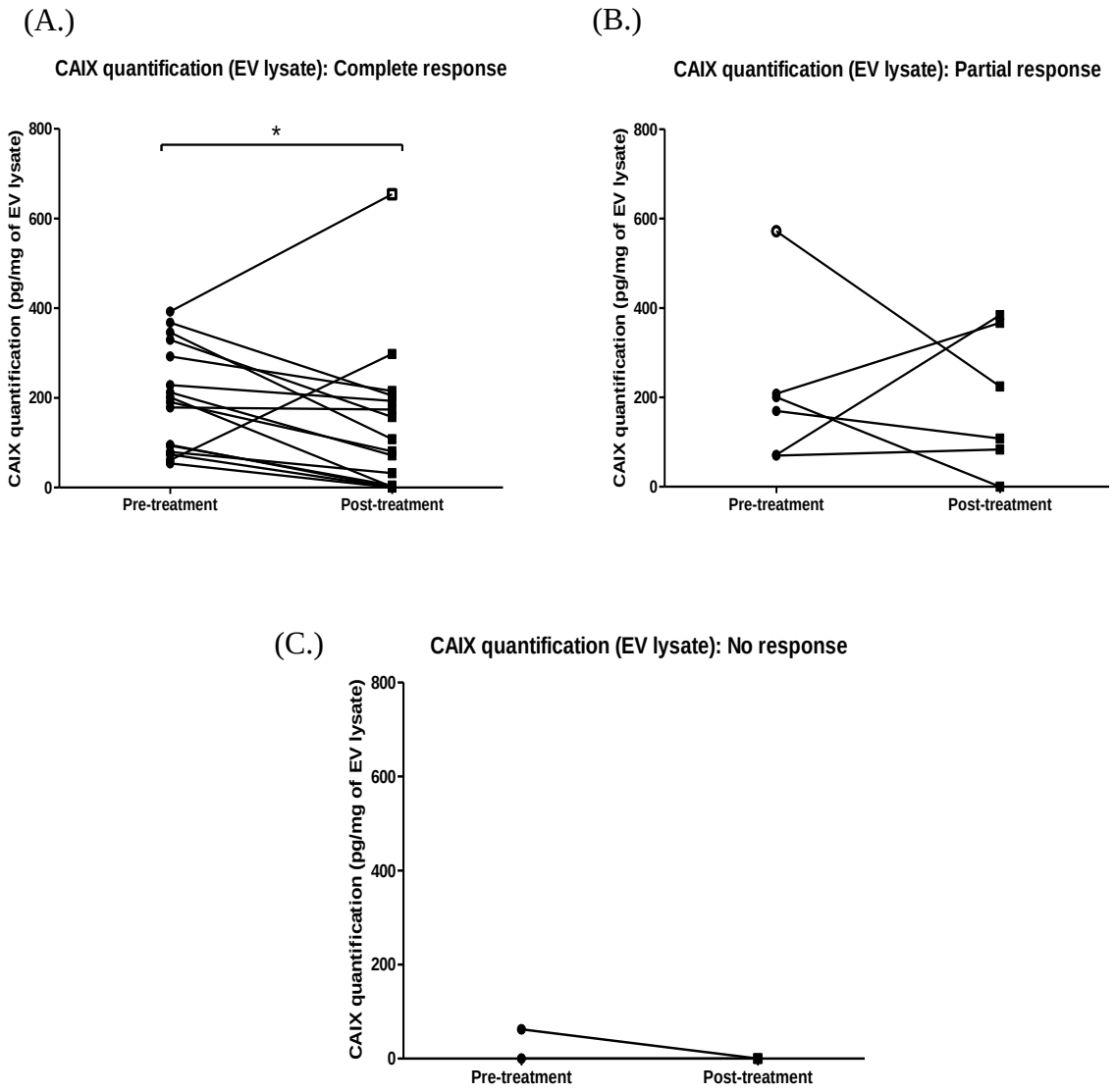

Figure 5.16: CAIX quantification: EV lysate (treatment response)
CAIX quantification in EV lysates for all pre- and post-treatment samples for complete response (A.), partial response (B.) and no response (C.). For complete response samples, CAIX was significantly reduced in post-treatment samples compared to pre-treatment (*p-value*=0.01). There were no significant differences in PR. Statistical analysis could not be performed for non-responder samples (n=2). Outlier values (white data points) as determined by Grubbs test were included in the figure but excluded from statistical analysis. *$p<0.05$ (Student's t-test).

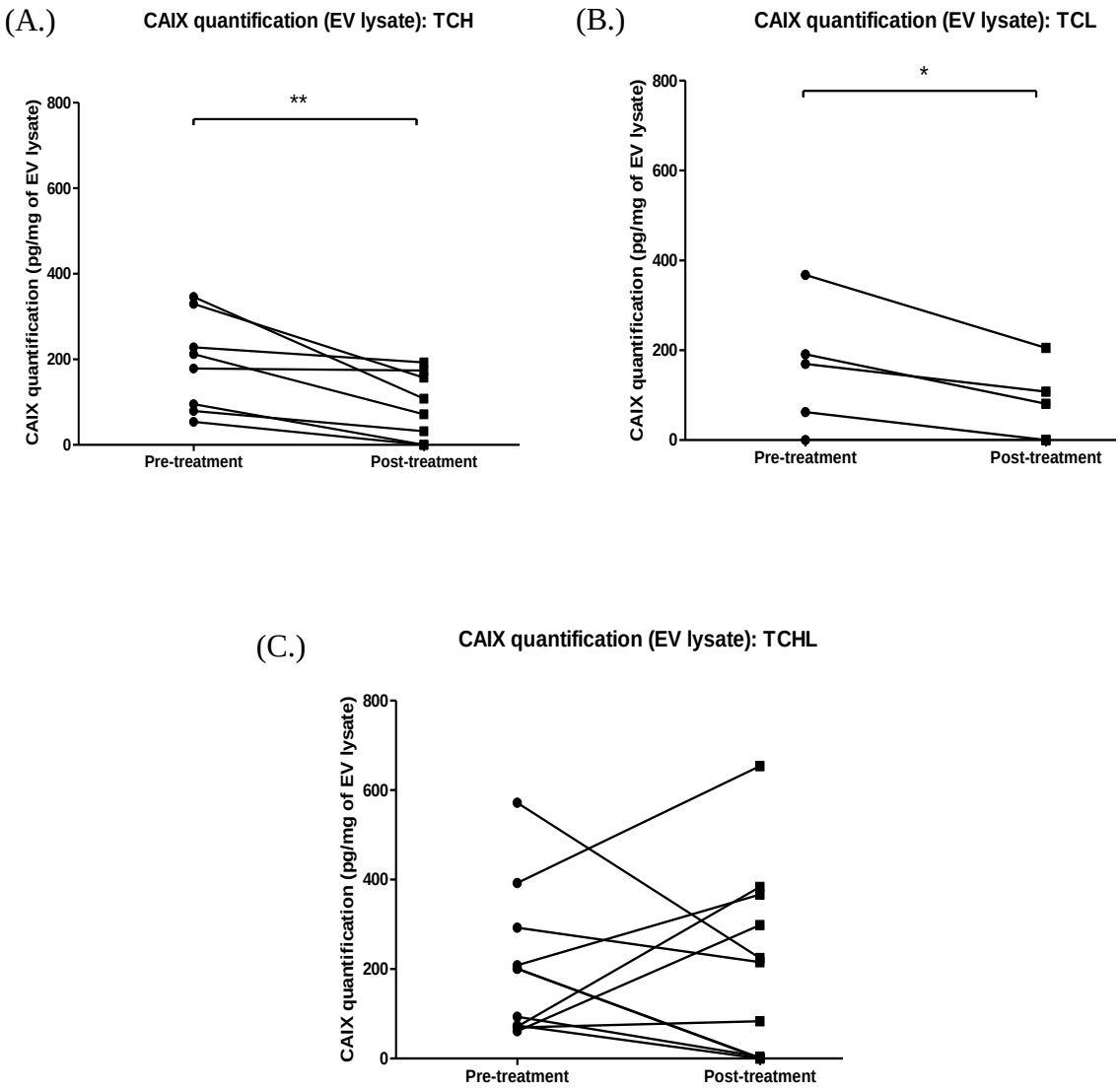

Figure 5.17: CAIX quantification: EV lysate (treatment arms)
CAIX quantification in EV lysates for all pre- and post-treatment samples, stratified by treatment arms; TCH (A.), TCL (B.) and TCHL (C.). CAIX was significantly decreased in TCH and TCL post-treatment samples compared to pre-treatment samples (TCH *p-value*=0.01, TCL *p-value*=0.04). There were no significant differences for non-responder samples TCHL samples. *p<0.05, **p<0.01 (Student's t-test).

(A.)

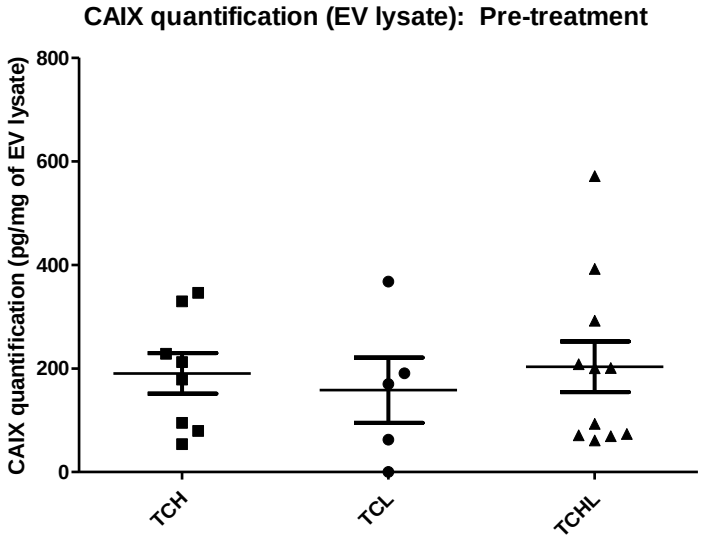

(B.)

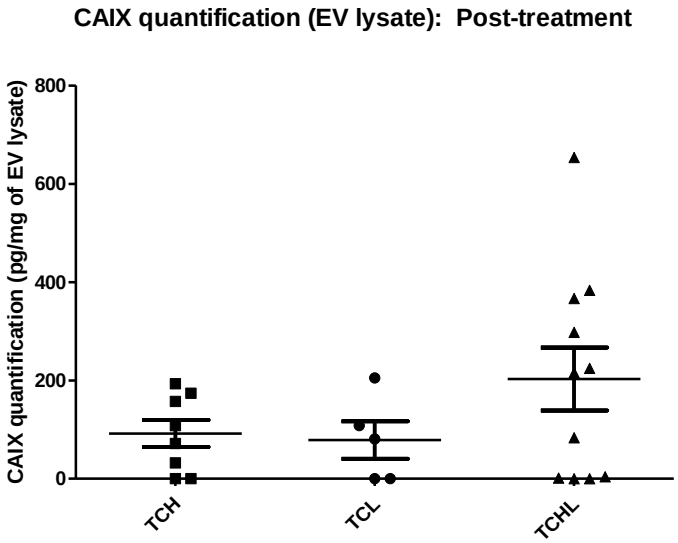

Figure 5.18: CAIX quantification EV lysate treatment arms (pre-treatment and post-treatment)
CAIX quantification in EV lysates for treatment arms in pre-treatment samples (A.) and post-treatment samples (B.). There were no significant differences. (*ANOVA*).

5.3. Discussion

5.3.1. CAIX and patient outcome

BreastMark analysis revealed that early-stage high expression of CAIX mRNA correlated with poorer overall survival in all breast cancer subtypes (Hazard ratio (HR) = 1.477 (1.243-1.756) (*p-value* <0.0001). When investigating the breast cancer subtypes individually, luminal B breast cancer patients had poorer overall survival with early-stage high expression of CAIX (HR = 1.528 (1.15-2.029) (*p-value*=0.003). The strongest association for poorer overall survival with early-stage high expression of CAIX was in the HER2+ breast cancer patients subtype (HR =2.0 (1.271-3.234) (*p-value*=0.002). Clinicopathological parameters were investigated, lymph-node negative breast cancer tumours with high CAIX was associated with poorer overall survival in HER2+ breast cancer patients, therefore determining that high expression of CAIX is associated with poorer overall survival in early-stage/non-metastatic HER2+ breast cancer.

5.3.2. Analysis of CAIX as a suitable predictive biomarker for HER2-targeted treatments

Plasma CAIX was significantly increased in post-treatment plasma specimens compared to pre-treatment samples. Although, a significant increase in CAIX was observed in the post-treatment samples, more information is required to discuss further, therefore, CAIX results were stratified by treatment response and treatment arms. Interestingly, when investigating the levels of CAIX per treatment response, CAIX was significantly increased in post-treatment samples for CR and PR when compared to pre-treatment samples. Thus explaining the increase in CAIX observed when taking all pre- and post-treatments together in this study, this is due to the fact that of the samples obtained, 79% of the patients had either CR or PR. However, when looking at NoR samples, an opposite trend was observed (1.3 fold decrease in post-treatment samples). There was no significant difference but the sample size was very small with n=4 for pre- and post-treatment samples. When all pre-treatment samples were taken together, it is evident that an increase in CAIX levels is highly associated with NoR to therapy compared to CR and PR. CAIX is increased 2.75 and 3.11 times in NoR compared to CR and PR respectively. It is evident that patients respond to therapy or partially respond when CAIX levels are low. It is evident that high expression of CAIX in plasma specimens is predictive of resistance to HER2-targeted therapy.

When investigating CAIX expression in the treatment arms for this study, it is important to note that the treatment responses are as follows; TCH (80% CR, 20% NR), TCL (33% CR, 17% PR, 50% NoR) and TCHL (50% CR, 42% PR, 8% NoR). Thus, when looking at the rate of NoR per treatment arm, the TCL arm had the highest rate (50%), followed by TCH (20%) and TCHL (8%), which is indicative of the overall trial results with TCHL having the highest proportion of CR (45.4%) followed by TCH (43.3%). CAIX levels in the TCH arm are significantly increased in post-treatment samples compared to pre-treatment, this increase in CAIX in post-treatment samples correlates with CAIX levels observed for all CR samples. When taking all pre-treatment samples for all treatment arms, there was a trend towards increased CAIX in TCL specimens compared to TCHL (*p-value*=0.051). This result indicates that CAIX is elevated in pre-treatment samples in the TCL treatment arm, which correlates with the TCL arm having the highest rate of NoR in all treatment arms. The sample size of this study was a limitation with only 6 NoR samples available (TCH (2), TCHL (1) and TCL (3)), thus statistical analysis could not be performed for the individual treatment arms, however, for pre-treatment samples in the TCL arm, there is a trend towards increased CAIX in the NoR samples compared to PR and CR.

5.3.3. Analysis of EV-derived CAIX as a suitable predictive biomarker for HER2-targeted treatments

Extracellular vesicles were successfully isolated from 24 patient specimens (24 pre-treatment and 24 post-treatment) in this study. NTA analysis determined EVs to be between 131-138nm in diameter, EVs were positive for EV markers TSG101 and ALIX and negative for the EV-negative marker GRP-94 (EV specifications as described in the minimal requirements for extracellular vesicle definitions (133, 134)). There were no morphological differences observed when visualising EVs from pre- and post-treatment samples by TEM. The quantity of EVs was investigated to determine if EV quantity is predictive of response, unsurprisingly, EV quantity was reduced in post-treatment samples. This is indicative of decreased tumour size and thus reduced EVs numbers (196). For CR, EV quantity of significantly reduced in post-treatment samples compared to pre-treatment, thus signifying that reduced EV quantity correlates with greater survival. Due to the limited numbers of samples for non-responders, statistical analysis could not be performed.

EV-derived CAIX was investigated as a potential non-invasive biomarker for treatment response. CAIX was investigated on both the surface of EVs and encapsulated inside the

EVs. As previously mentioned, EV-surface CAIX was only detectable in 25% and 42% of pre- and post-treatment samples. It was therefore deemed that EV-surface CAIX was not a reliable test for CAIX. This may in part be due to CAIX being degraded/destroyed during the EV isolation process of ultracentrifugation as CAIX was found to be detected on the surface of NSCLC plasma-derived EVs using an EV array for capturing EVs (197). It was determined that investigating CAIX levels encapsulated inside the EVs was an improved method (CAIX was undetected in 4% of pre-treatment samples and 25% of all post-treatment samples) for detecting EV-derived CAIX. However, CAIX was still undetectable in some samples. CAIX was significantly decreased in post-treatment CR samples as seen with EV-surface CAIX, indicating that CAIX is both on the surface of EVs and encapsulated inside EVs. The results for EV-derived CAIX did not directly correlate with the plasma-derived CAIX results, this may be due to the ELISA not detecting CAIX levels in EVs and also due to the fact that CAIX may be degraded following the EV isolation technique. It is also important to note that the standard deviations for all EV-derived CAIX results are very high, indicating that this method is unsuitable for detecting CAIX. The large error bars observed for EV-derived CAIX could also be associated with the different populations of EVs isolated (198).

5.4. Conclusions

It is apparent from the results presented, that the detection of EV-derived CAIX is not a reliable test for predicting treatment response. The method of ultracentrifugation was deemed unsuitable for EV-derived CAIX analysis, this may be due to the force of the ultracentrifugation steps or degradation of CAIX due to the length of time to complete the isolation steps (greater than 2hr). Using the ELISA to test for CAIX in plasma specimens was a more reliable method. For biomarker analysis, EV isolations are laborious and costly. ELISAs are a cheaper and quicker method for detecting biomarkers in plasma samples. For CAIX, we have determined that using very small quantities (20µL) of plasma samples on ELISAs will suffice in testing CAIX as a predictor of response. It is apparent that high levels of plasma-derived CAIX are predictive of response to HER2-targeted therapies. In the 10-15 trial, the TCL arm observed the poorest survival responses (50% NoR), we have shown that CAIX may be associated with treatment resistance in this arm. This suggests that CAIX is a mechanism of resistance in HER2-targeted treatments and potentially a strong mechanism of resistance to small tyrosine kinase inhibitors (*e.g.* lapatinib or neratinib).

CHAPTER SIX: Investigation of miR-134 in triple negative breast cancer

Parts of this chapter are published in the following research article:

miR-134 in extracellular vesicles reduces triple-negative breast cancer aggression and increases drug sensitivity. O'Brien K*, Lowry MC*, Corcoran C, Martinez VG, Daly M, Rani S, Gallagher WM, Radomski MW, MacLeod RA, O'Driscoll L. Oncotarget. 2015 Oct 20;6(32):32774-89.

6. Abstract

Triple-negative breast cancer (TNBC) is classified by the lack of HER2, ER and PR expression. TNBC is the only subtype of breast cancer that does not have any targeted therapies and is, thus, the subtype with the poorest overall survival rates. Research has involved trying to determine significant targets for TNBC cancer patients.

Previous work in our laboratory showed reduced levels of miR-134 as playing a role in the aggressiveness of HS578Ts(i)$_8$ TNBC cells. Here, using qPCR, transcriptional silencing was observed in the MEG3 gene in the Hs578Ts(i)$_8$. It was previously shown that transfection of miR134 into the more aggressive cell line Hs578Ts(i)$_8$ cells significantly increased cisplatin-induced apoptosis. In this thesis, using apoptosis assays (annexin/PI apoptosis assay), further testing of this combination in a panel of TNBC cell lines, showed that this effect was not observed.

miR-134 was identified as a potential diagnostic biomarker for TNBC. However this was evident in the more invasive cell line Hs578T(i)$_8$ cell line variant compared to the Hs578T cell line. The potential of miR-134 was not confirmed in other TNBC cell lines, this phenomenon may in part be cell line-specific or be specific to more invasive/aggressive TNBC cell lines.

6.1. Introduction

6.1.1. Triple-negative breast cancer overview

Triple-negative breast cancer (TNBC) is responsible for 15-20% of breast cancers and it accounts for a disproportionate number of breast cancer deaths (199). TNBC is characterised by the absence of PR, ER and HER2 expression (reviewed by (200)). However, efforts to categorise TNBC into subtypes have been initiated based on gene expression profiling (2188-gene model (201) and 101 gene model (202)), summarised in Table 6.1. Lehman *et. al.* identified the basal-like 1 (BL1) subtype as being enriched in cell cycle related genes and high levels of Ki-67 and the basal-like 2 (BL2) subtype as having high expression of tyrosine kinase signalling as well as high glycolysis and gluconeogenesis signalling (201). Using the 101-gene expression model, Ring *et. al.* identified that the TNBC subtypes BL2 is significantly associated with poor response in both treatment arms (neoadjuvant doxorubicin/cyclophosphamide followed by randomised to receive either paclitaxel or ixabepilone) in TNBC patients (n=139). Patient with TNBC tumours identified as the subtype BL1 demonstrated an improved response to therapy (203).

Poor outcome corresponds with the innate aggressiveness of TNBC, augmented by the lack of targeted treatments (204-207). Platinum-containing agents are among the drugs showing some benefit in TNBC (208, 209). Anti-Hsp90 drugs also show promising results (210, 211), although some pre-clinical studies indicate TNBC to be less sensitive to Hsp90 inhibitors than HER2-overexpressing tumours (212-214). Interestingly in a meta-analysis of 2826 TNBC patients, androgen receptor tumour positivity was associated with a lower risk of disease recurrence than patients with androgen negative tumours (215). The anti-androgen agent, enzalutamide was tested in a phase II clinical trial with TNBC patients (216). This trial demonstrated that enzalutamide had clinical activity and was well tolerated by androgen receptor positive TNBC. There are many drug intervention clinical trials currently active and recruiting for TNBC patients (summarised in Table 6.3, 10 of 72 clinical trials currently active and recruiting in TNBC).

microRNA (miRNA) profiling has been used in an attempt to discover TNBC sub-classifications (217), as well as to identify biomarkers or therapeutics for TNBC. miRNAs (218) regulate a plethora of cellular processes including apoptosis, proliferation and differentiation (219), are commonly down-regulated in cancers and have relevance as biomarkers and therapeutic potential as tumour suppressing agents in many cancers (220,

221), including breast cancer (222-224). TNBC patients with high levels of miR-155 and low recombinase RAD51 expression in tumours had a better overall survival than low miR-155 expression (225). Exosomes contain miRNAs (226) and it has been established that miRNAs can be transferred from cell-to-cell by exosomes, subsequently mediating epigenetic alterations in recipient cells (227). It has also been shown that exosomes can be manipulated to transfer miRNAs representing therapeutics to recipient cells *e.g.* by acting in combination with VEGF inhibitors in leukaemia treatment (228).

Previously using a TNBC cell line (Hs578T) and its aggressive clonal variant (Hs578Ts(i)$_8$) as models systems, we investigated the potential of exosomes/microvesicles (collectively termed extracellular vesicles/EVs) to influence the phenotype of "recipient"/secondary cells. We also assessed effects of EVs isolated from TNBC patients' sera compared to those from healthy volunteers. These results indicated that the EVs released by the more aggressive cells carried the same traits to all secondary cell lines analysed (*i.e.* increasing their proliferation, migration, and inducing neovascularisation/angiogenesis), in a manner indicative of the innate phenotypes of the cells of origin. Additionally, EVs from TNBC patients' sera, compared to those from healthy controls, increased the invasiveness of recipient breast cancer cells (229).

Here we chose to continue our studies with the same isogenic cell line variants (Hs578T and Hs578Ts(i)$_8$) and their corresponding EVs. Hs578T and Hs578Ts(i)$_8$ have the same genetic background, which make them an interesting comparison model. However, Hs578Ts(i)$_8$, compared to Hs578T cells, have a more aggressive phenotype. Specifically they have 2.5-fold higher migratory capacity, 3-fold higher invasive (through extracellular matrix) capacity, and form 25 times more colonies in soft agar. Furthermore Hs578Ts(i)$_8$, unlike Hs578T, produce tumours *in vivo* in nude mice (230). This cell line pair is, therefore, very useful for investigating the comparative capabilities of EVs to transfer phenotypic traits representative of their cell of origin to secondary recipient cells.

TNBC subtype	**Tumour characteristics**
Basal-like 1 (BL1)	• Enriched in cell cycle-related genes • High ki-67
Basal-like 2 (BL2)	• Enriched in growth factor signalling (*e.g.* EGF, MET) • Enriched glycolysis and gluconeogenesis signalling
Immunomodulatory (IM)	• Enriched B, NK and T cell and cytokine signalling • High levels of tumour-infiltrating lymphocytes (TILs) • Increased chemokine receptors and ligands • Increased complement cascade and antigen presentation
Mesenchymal-like (M)	• High vimentin expression • Activation of EGF, c-MET, mTOR, FGF, TGF-β and Wnt/β catenin pathways • Decreased E-cadherin
Mesenchymal stem-like (MSL)	• Similar to claudin-low breast cancer • High expression of stem cell genes • Enrichment in genes related to angiogenesis and immune signalling
Luminal androgen receptor (LAR)	• Androgen receptor positive • Enrichment in steroid synthesis and metabolism pathways

Table 6.1: TNBC subtypes and the corresponding tumour characteristics (201)

NCT number	**Intervention**	**Drug targets**
NCT03184558	Bemcentinib	AXL receptor tyrosine kinase
NCT03106077	Mirvetuximab soravtansine	Folate receptor 1
NCT03316794	SC-005	Undisclosed
NCT01884285	AZD8186	PI3Kβ
NCT02593175	Panitumumab	EGFR
NCT03361800	Entinostat	HDAC1 and HDAC3
NCT03424005	Atezolizumab	PD-L1
NCT03150576	Olaparib	Poly ADP ribose polymerase
NCT03289819	Pembrolizumab	PD-L1
NCT02393794	Romidepsin	HDAC1

Table 6.2: Example of current TNBC clinical trials

6.1.2. Aims

The aim of this study was to progress the investigation of miR-134 in TNBC. Previous PhD student, Dr. Keith O'Brien, determined that miR-134 acts as a tumour suppressor in $Hs578Ts(i)_8$ cells. The aim of this study was to progress this work further, a panel of TNBC cell lines (MDA-MB-231, HCC1143 and HCC1937) were used to validate the role of miR-134 in other cell lines and to strengthen this observation.

6.2. Results

6.2.1. miR-134 expression

Previous miRNA profiling work completed by Dr. Keith O'Brien revealed that five of the down-regulated miRNAs in Hs578T and Hs578Ts(i)$_8$ cells and EVs were miR-134, miR-655, miR-370, miR-889 and miR-376c. miR-134 was further investigated here. This miRNA was selected as it had the greatest significant fold change of down-regulation in both Hs578Ts(i)$_8$ cells and their EVs compared to Hs578T cells and their EVs, respectively. qPCR was performed to determine miR-134 expression in both cell lines. miR-134 expression was significantly decreased in Hs578Ts(i)$_8$ cells compared to Hs578T cells (*p-value*<0.0001) (Figure 6.1).

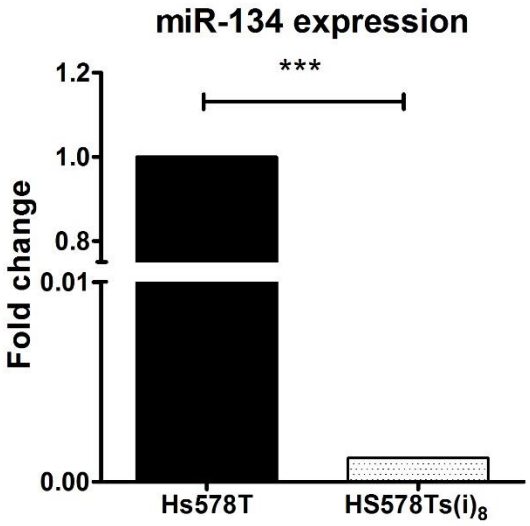

Figure 6.1: qPCR analysis of miR-134 expression in Hs578T and Hs578Ts(i)$_8$ cells
qPCR was performed on Hs578T and Hs578Ts(i)$_8$ cell cDNA to determine the expression levels of miR-134. (n=3 ±SEM), ***p<.0001 (Student's t-test).

6.2.2. MEG3 DLK1 expression

Given the loss of miR-134, transcriptional silencing at this chromosomal region was investigated. Cytogenetic analysis was performed in the lab previously and no structural anomalies at chromosomes 14q32 were observed. However, from literature mining, transcriptional silencing was observed in a cluster of maternally expressed miRNA in the DLK1-MEG3 locus on chromosome 14q32 (203). Thus, miR-134 , qPCR assessment for the neighbouring MEG3 and DLK1 loci were investigated. qPCR for DLK1 and MEG3

expression was performed. While DLK1 was undetected in both cell line variants, MEG3 was detected in Hs578T cells but its expression was significantly decreased in the Hs578Ts(i)$_8$ variant (*p-value*<0.0001) (Figure 6.2). Thus supporting the proposal of transcriptional silencing of this chromosomal region due to uniparental disomy.

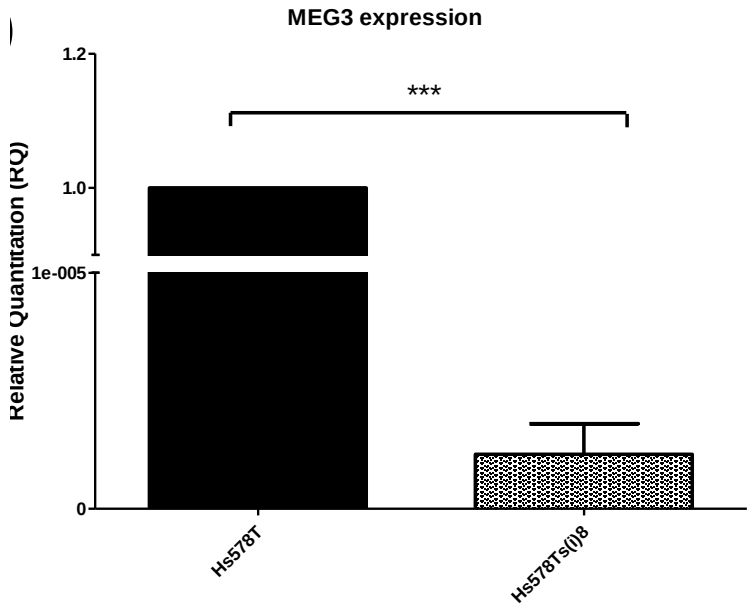

Figure 6.2: Expression of MEG3 in Hs578T and Hs578Ts(i)$_8$ cells.
qPCR assessment for the MEG3 locus showed significantly reduced MEG3 expression levels in Hs578Ts(i)$_8$ compared to Hs578T cells. (n=3 ± SEM), ***p<0.0001. (Student's t-test).

6.2.3. Toxicity assays

From previous data by Dr. Keith O'Brien, apoptosis levels of miR-134 transfected Hs578Ts(i)$_8$ cells were significantly increased after 24hr of 15μM cisplatin treatment when compared to Hs578T cells. To determine the IC_{value} for 15μM cisplatin treatment of Hs578Ts(i)$_8$ cells, mock transfections were set up and IC_{values} were determined using acid phosphatase assays (Figure 6.3 (A.). To progress this study, 15μM cisplatin treatments on TNBC cell lines (Figure 6.3, (B.) HCC1143 and (C.) HCC1937) were performed to determine the correlating IC_{values} for 15μM cisplatin treatment. The MDA-MB-231 cell line was innately resistant to cisplatin treatment and was therefore not brought forward into further studies. Based on the Hs578Ts(i)$_8$ cell IC_{value} at 15μM, the corresponding cisplatin concentrations were determined for HCC1143 and HCC1937 (Table 6.3) to ensure cisplatin-induced toxicity correlated with the Hs578Ts(i)$_8$ cell line 15μM concentration.

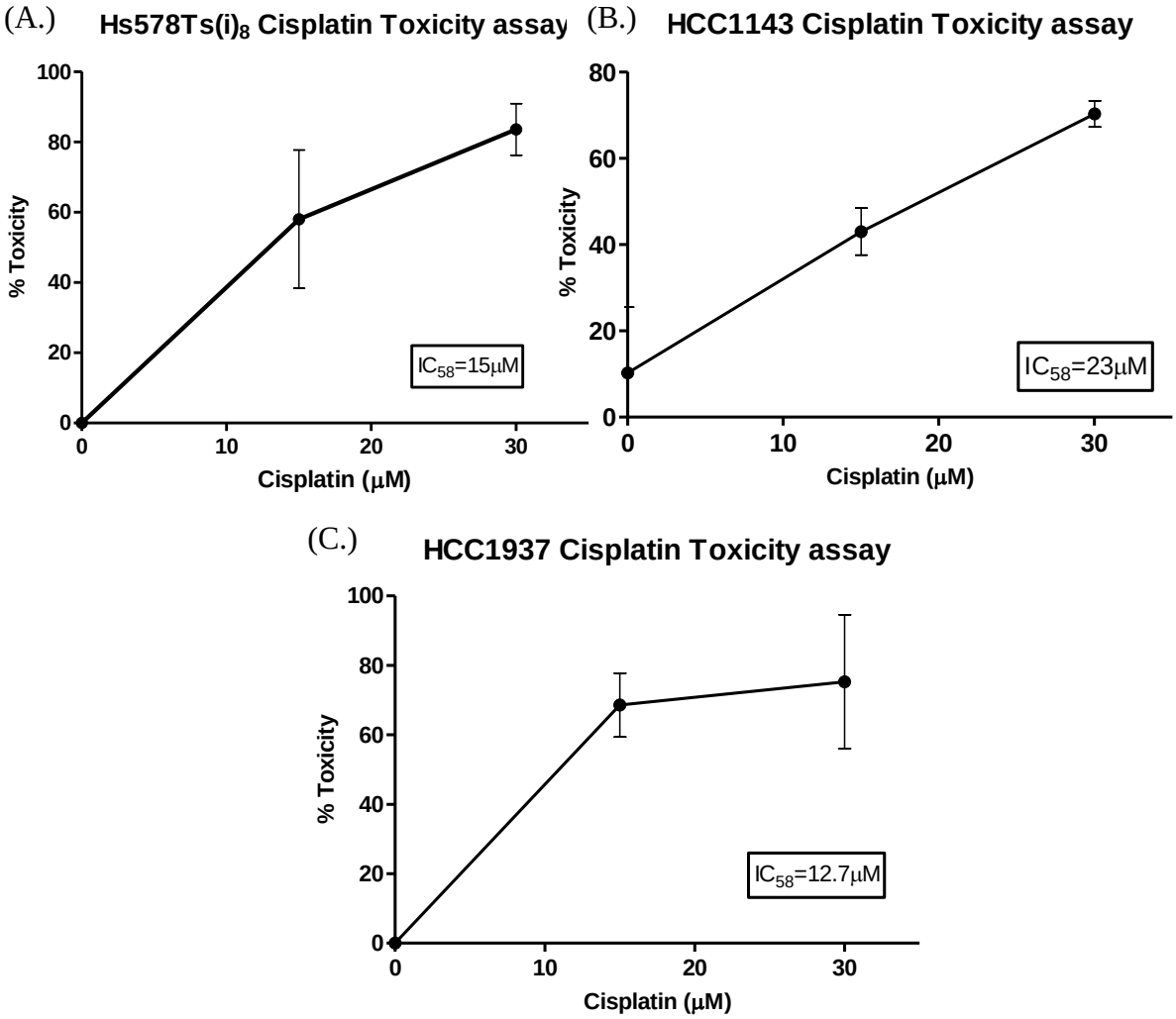

Figure 6.3: Acid phosphatase assays to determine IC_{50} values
Acid phosphatase assays were performed on TNBC cell lines. IC_{50} values were determined at 15μM cisplatin concentrations. IC_{values} for 15μM Cisplatin are represented for (A.) Hs578Ts$(i)_{8,}$ (B.) HCC1143 and (C.) HCC1937 cells. (n=3 ± SEM).

Cell line	**15μM IC_{value}**	**IC_{58} Cisplatin conc.**
Hs578Ts(i)$_8$	58.03	15μM
HCC1143	42.97	23μM
HCC1937	68.57	12.7μM

Table 6.3: TNBC cell line cisplatin concentrations

The representative IC_{values} for TNBC cells are shown. The values are based on 24hr of 15μM cisplatin treatment of Hs578Ts$(i)_8$ cells.

6.2.4. Apoptosis assay of miR-134 transfected cells

Following cisplatin IC_{58} value determination of all TNBC cell lines (Table 6.3), the effects of miR-134 transfection on cisplatin treatments were assessed using apoptosis assays. TNBC cell lines ($Hs578Ts(i)_8$ (Figure 6.4), HCC1143 (Figure 6.5 (B.)) and HCC1937 cells (Figure 6.5 (C.)) were transfected with miR-134 or negative control mimic (NC).

Following transfection, apoptosis assays were performed on $Hs578Ts(i)_8$ after 24hr cisplatin treatment. At 15µM cisplatin treatment, miR-134 transfected $Hs578Ts(i)_8$ had significantly increased apoptosis (*p-value*=0.035) (Figure 6.4 (B.)). There were no significant differences at 7.5µM cisplatin treatment or at 30µM cisplatin treatment (Figure 6.4 (A.) and (C.)).

Similarly, HCC1143 and HCC1937 were transfected with miR-134 and treated with cisplatin (at IC_{58} concentrations for each cell line). However, there were no significant changes in apoptosis between miR-134 transfected and negative control samples for HCC1143 (*p-value*=0.91) or HCC1937 cells (*p-value*=0.31) (Figure 6.5 (B.) and (C.)).

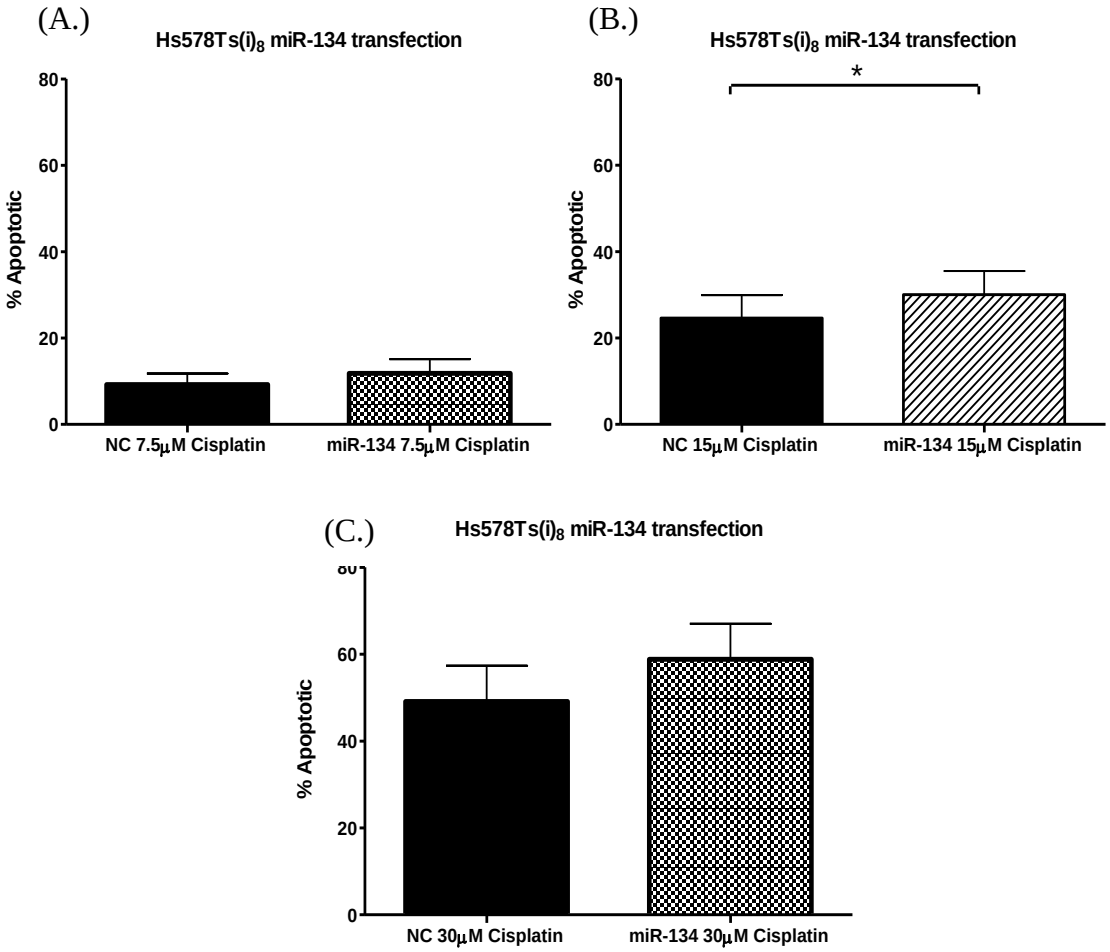

Figure 6.4. Apoptosis assay of cisplatin treatment post-miR-134 transfection of Hs578Ts(i)$_8$ cells
Apoptotic effects after 24hr cisplatin treatment on miR-134 transfected Hs578Ts(i)$_8$ cells was assessed at (A.) 7.5μM, (B.) 15μM and (C.) 30μM cisplatin treatment. (n=3 ± SEM), *p<0.05 (Student's t-test).

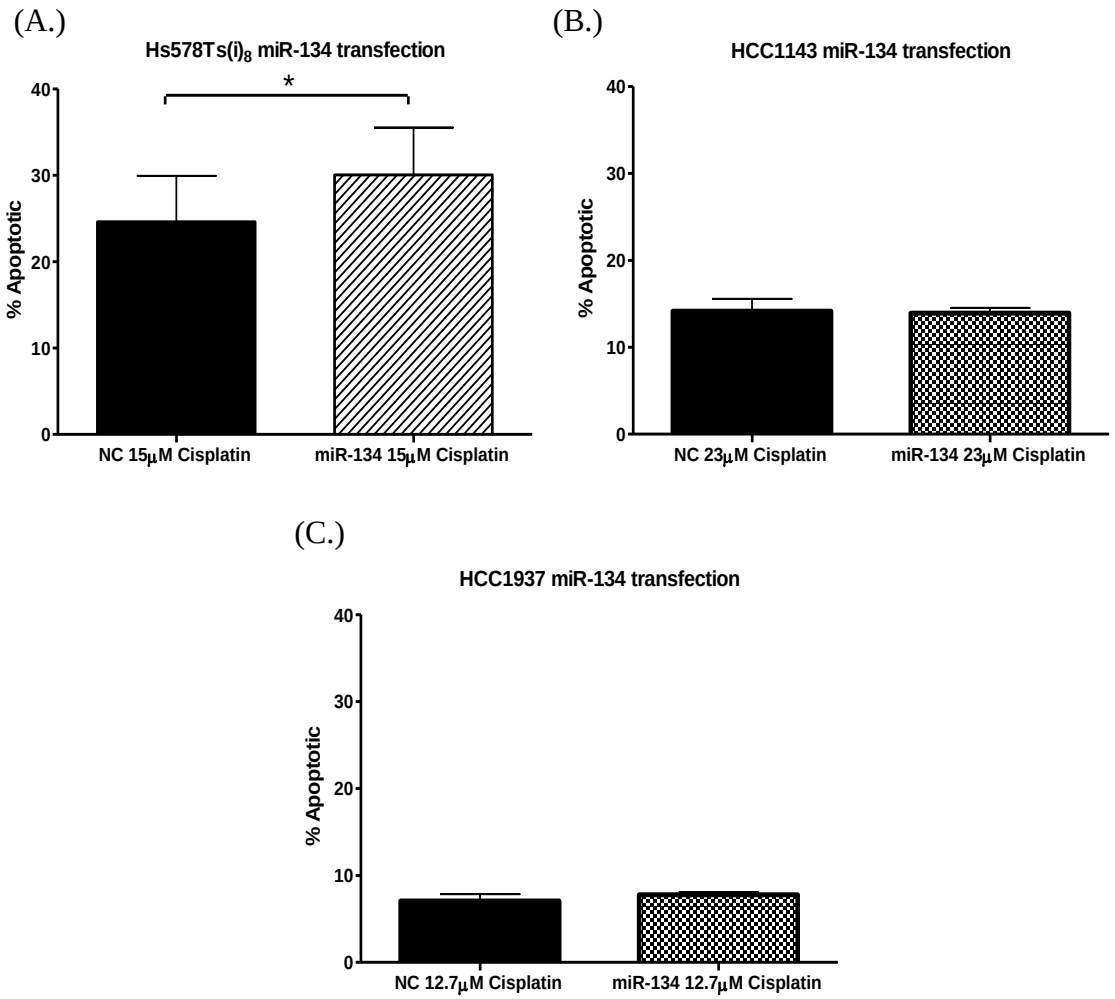

Figure 6.5. Apoptosis assays of cisplatin treatment post-miR-134 transfection of TNBC cells
24hr cisplatin (at Ic_{58} concentrations for each cell line) treatment-related apoptotic effects on miR-134 transfected Hs578Ts(i)$_8$, HCC1143 and HCC1937 cell lines at (A.) 15μM, (B.) 23μM and (C.) 12.7μM, respectively. (n=3 ± SEM) (Student's t-test).

6.3. Discussion

TNBC accounts for 15-20% of all breast cancers. Patients with TNBC have very poor survival rates due to its aggressive nature but also due to the lack of targeted therapies available to patients. Patients lack oestrogen receptors, progesterone receptors and do not overexpress HER2, there is a lack of a target for these patients. New epidemiological studies are required to greater understand this breast cancer, to characterise it and to determine new biomarkers and therapeutic targets. We sought to investigate TNBC, to discover new biomarkers and therapeutic targets in patient samples and EVs.

qPCR analysis determined miR-134 to be significantly decreased ($p<0.001$) in the more aggressive Hs578Ts(i)$_8$ cells compared to Hs578T cells. Transcriptional silencing was investigated, qPCR was performed for the neighbouring loci (DLK1 and MEG3) in this chromosomal region. DLK1 was undetected in both cell lines, MEG3, however was significantly decreased in Hs578Ts(i)$_8$ cells compared to Hs578T cells. This result indicated that uniparental disomy occurred and thus transcriptional silencing is evident at this loci.

Dr Keith O'Brien, previously showed that following miR-134 transfection into Hs578Ts(i)$_8$ cells, apoptosis levels significantly increased following 24hr cisplatin treatment. To further this study, I repeated this experiment under the same conditions and found similar results. To broaden the study, using 15μM cisplatin, I carried out mock transfections to determine the equivalent Hs578Ts(i)$_8$ IC values for a range of TNBC cell lines (HCC1143 and HCC1937). Once the equivalent cisplatin IC value and concentrations were determined, the TNBC cell lines were transfected with miR-134 and apoptosis levels were determined. 15μM cisplatin for 24hr increased apoptosis levels ($p<0.05$) in Hs578Ts(i)$_8$ cells. Following miR-134 transfection, the equivalent concentrations of cisplatin were used but no significant differences were found in HCC1143 and HCC1937.

The transfection conditions were optimised for Hs578Ts(i)$_8$ cells, it may have been beneficial to optimise the appropriate conditions for the other three TNBC cell lines. Upon completion of Dr Keith O'Brien's work and my follow-up work and, this study was published in Oncotarget in 2015 (48).

6.4. Conclusions

In conclusion, we investigated miR-134 as a potential diagnostic biomarker for TNBC and a therapeutic target. Unfortunately, further studies in our lab to determine the levels of miR-134 in serum and in TNBC did not correlate with our findings.

CHAPTER SEVEN: Discussion, conclusions and future directions

7.1. Discussion

7.1.1. Drug resistance study

As discussed in Section 1.2, breast cancer is a highly heterogeneous disease, owing to many differences between patients (inter-tumour heterogeneity) and within an individual tumour (intra-tumour heterogeneity). Cancer cell lines can genetically and transcriptionally evolve and alter when exposed to drugs (231). For this reason and for the highly heterogeneous nature of breast cancer tumours, it is imperative that multiple cell lines are used for all *in vitro* experiments/validation studies. Neratinib, an irreversible tyrosine kinase inhibitor was approved by the FDA in July 2017 and the EMA granted marketing authorisation for Neratinib in July 2018. This new drug has shown promise in the clinic, as previously discussed in Section 1.3. However, like all targeted therapies, patients can either have innate resistance to neratinib or acquire resistance throughout the course of the treatment regime. Using our drug-resistant cell line variants the aim of this project was to investigate the mechanisms of acquired HER2-targeted therapy resistance in HER2-overexpressing breast cancer. Specifically, the objectives of this project were to investigate the mechanisms of neratinib-resistance between drug-sensitive and drug-resistant cell line variants; to determine the differences, if any, in DNA mutations or protein expression between the cell line variants, to validate the potential mechanisms of resistance and to determine the clinical and EV relevance of all findings.

There are a very limited number of publications on neratinib-resistance. Our group were the first group to establish and publish research on neratinib-resistant cell line variants. We sought to determine the mechanisms of resistance in our neratinib-resistant cell lines. Two neratinib-resistant cell line variants were previously developed. As mentioned, due to the heterogeneity of breast cancer tumours, it was imperative to have multiple cell line models. In this project, the SKBR3 neratinib-resistant cell line variant was successfully developed. Preliminary DNA sequencing was performed using the EFM19.2A, HCC1954 and SKBR3 cell line variants and EVs. The sequencing revealed that there were no common SNPs identified between the cell lines, highlighting the heterogeneous nature of breast cancer. While no common breast cancer SNPS were identified in SKBR3 cell lines, 2 SNPS were identified in the HCC1954 variants; PIK3CA and PIK3R1. PIK3CA mutations have been observed to correlate with lower pathological CR compared to wild-type PI3KCA in patients treated with both lapatinib and trastuzumab (232). In this study, our *in vitro* work correlates with this clinical observation, the HCC954 cell line variants have a PIK3CA mutation and are innately resistant to trastuzumab. Interestingly, the EVs derived from all

cell line variants contained the mutations evident in the cell line variants. While the mechanisms of tumour DNA trafficking to EVs has not been established, it has been identified that extracellular DNA from tumour cells is packaged into large EVs (1-5.5µM) rather than small EVs (100-400µM) in prostate cancer cell studies (233). In this study we have found that the DNA packaged into EVs (approx. 100nm in diameter) was indicative of their cells of origin.

Proteomic analysis of HCC1954 and SKBR3 cell line variants and their derived EVs was performed using Olink proteomics. Following data analysis of the protein samples from three biological repeats, it was found that this proteomics platform was not highly reproducible; this was observed following heatmap analysis, where one sample from each cell line variant/EV variant was determined to be different to the other two repeats. For future Olink work, a larger sample size should be used to prevent the establishment of false-positive results. The top three proteins that were elevated in neratinib-resistant variants compared to the neratinib-sensitive variants were TLR3, CSF-1 and CAIX. Following literature mining, bioinformatics analysis and preliminary immunoblotting results, CAIX was determined as the most suitable target for further validation/investigating into its role in neratinib-resistance. Hypoxia has long been associated with poorer overall survival in breast cancer patients, to our knowledge, this is the first study to determine that as part of the hypoxia pathway, CAIX, plays a major role in HER2-targeted drug resistance. Following immunoblot analysis of CAIX in the cell line variants, opposite results were found for the expression patterns observed for the HCC1954 cell line variants when compared to Olink proteomic analysis. Again, indicating problems with the reproducibility of the Olink proteomics platform. When investigating CAIX expression in all cell line variants (BT474, EFM19.2A, HCC1954 and SKBR3), it was observed that CAIX expression was increased in the drug-resistant variants compared to drug-sensitive variants. The HCC1954-Par cell line variant had the ability to increase CAIX; this was hypothesised to be due to innate resistance to trastuzumab and the slight resistance to neratinib when compared to all other parental cell lines. The CAIX expression levels in HCC1954-NR were low in comparison and this was hypothesised to be due to the altered metabolism of this cell line as previously discussed in Chapter 4. All other drug-resistant variants showed increased CAIX in both normoxic and hypoxic conditions when compared to the drug-sensitive variants. CAIX functions to maintain cellular pH and as discussed in Chapter 4, alkaline pH confers resistance to apoptosis. Interstingly, other than our group's previous work on CYP3A4 in neratinib-resistance, Karakas *et. al.* was the only other publication found to investigate neratinib-resistance in cell lines. They found that

decreased BIM and PUMA and increased BCL-2 and BCL-XL were found to be associated with neratinib-resistance in ZR-75-30, SKBR3, and BT474 cell lines, our work may be a continuation of this study in that the reasoning for the altered apoptotic mechanisms in these cells is due to the altered pH which was caused by increased CAIX expression in drug-resistant cell lines.

To determine if elevated CAIX was associated with neratinib-resistance, we sought to block its expression and re-sensitise the drug-resistant cell line variant to neratinib and other HER2-targeted therapies. Using the CAIX inhibitor, we observed a loss of inhibitory efficacy over time in the drug-resistant variants and this directly correlated with increased neratinib-resistance. Thus, indicating that CAIX inhibition caused the drug-resistant variants to find an alternative way either to induce CAIX expression or to become resistant to the inhibitor. The inhibitor was found to inhibit CAIX expression after 24hr exposure in the drug-resistant variants. S4 continually inhibited CAIX production in all drug-sensitive variants. Thus, the combination of the CAIX inhibitor was used to determine its efficacy in re-sensitising the drug-resistant variants to neratinib. The combination was not found to be synergistic in all drug-sensitive cell line variants, including the BT474-TR cell line variant, which was found to be sensitive to neratinib. When investigating the drug-resistant variants, the combination of S4 with neratinib was synergistic in all drug-resistant cell lines and a higher strength of synergy was directly correlated with increased neratinib-resistance. Interestingly, from a therapeutic point of view, PIK3CA mutations have been found to be associated with drug resistance in HER2+ breast cancer patients, here using our HCC1954 cell line variants that harbour a gain-of-function mutation in the PIK3CA, we have shown that the combination of S4 with neratinib can overcome resistance to therapy. We identified that for both subtypes of breast cancer cell lines; luminal B and HER2+ breast cancer, the combination of S4 with neratinib was synergistic, this reiterates the importance of these finding considering the results observed for the Kaplan-Meiier plots, indicating that high expression of CAIX is associated with poorer overall survival in both subtypes of breast cancer. The combination of S4 with lapatinib was found to be synergistic in lapatinib-resistant cell line variants, this was not found to correlate with increased resistance, however only one lapatinib-resistant cell line variant was available for testing.

To investigate the clinical relevance of the findings in this project, plasma clinical specimens were obtained from the TCHL clinical trial. Patients on this trial all received docetaxel and carboplatin with either trastuzumab alone or trastuzumab with lapatinib,

which was relevant to our *in vitro* work, having determined that CAIX expression is increased in the TR, LR and TLR cell line variants. Testing CAIX on the surface of EVs was found to be inefficient when EVs were isolated from the ultracentrifugation method. The excessive force used in this method of EV isolation may cause CAIX degradation. It is noteworthy that Sandfeld-Paulsen *et. al.* used an EV capture array to capture EVs and found CAIX to be present on the surface of EVs derived from lung cancer cells (197). While surface CAIX was undetectable in 25% of samples used, we hypothesised that CAIX may be present and protected inside the EVs. We found CAIX in the lysate of EVs derived from plasma patient samples. CAIX in the lysate of EVs was found to be reduced in post-treatment complete responders compared to pre-treatment samples. When investigating CAIX directly in plasma specimens from patients, CAIX was detectable in all samples. Thus confirming that our EV isolation method or EVs in general were not as consistent as direct plasma. CAIX was significantly increased in pre-treatment non-responder patient specimens compared to both complete responders and partial responders. This result strengthened our *in vitro* findings, in that high-expression of CAIX correlated with resistance to therapy. Unfortunately, as neratinib is newly approved, there have been no translational clinical trials investigating the efficacy of neratinib where plasma specimens are currently available for research. Our results have highlighted that plasma specimens could be used to detect CAIX levels in patient specimens that could be predictive of response to HER2-targeted therapies, this would allow for a cheap, quick and minimally-invasive clinical test without requiring the need for invasive biopsies in breast cancer patients.

7.1.2. miR-134 study

TNBC accounts for 15-20% of all breast cancers. Patients with TNBC have very poor survival rates due to its aggressive nature but also due to the lack of targeted therapies available to patients. Patients lack oestrogen receptors, progesterone receptors and do not overexpress HER2, there is a lack of a target for these patients. New epidemiological studies are required to greater understand this breast cancer, to characterise it and to determine new biomarkers and therapeutic targets. We sought to investigate TNBC, to discover new biomarkers and therapeutic targets in patient samples and EVs.

qPCR analysis determined miR-134 to be significantly decreased ($p<0.001$) in the more aggressive Hs578Ts(i)$_8$ cells compared to Hs578T cells. Transcriptional silencing was

investigated, qPCR was performed for the neighbouring loci (DLK1 and MEG3) in this chromosomal region. DLK1 was undetected in both cell lines, MEG3, however was significantly decreased in Hs578Ts(i)$_8$ cells compared to Hs578T cells. This result indicated that uniparental disomy occurred and thus transcriptional silencing is evident at this loci.

Dr Keith O'Brien, previously showed that following miR-134 transfection into Hs578Ts(i)$_8$ cells, apoptosis levels significantly increased following 24hr cisplatin treatment. To further this study, I repeated this experiment under the same conditions and found the same results. To broaden the study, using 15μM cisplatin, I carried out mock transfections to determine the equivalent Hs578Ts(i)$_8$ IC values for a range of TNBC cell lines (BT549, HCC1143 and HCC1937). Once the equivalent cisplatin IC value and concentrations were determined, the TNBC cell lines were transfected with miR-134 and apoptosis levels were determined. 15μM cisplatin for 24hr increased apoptosis levels ($p<0.05$) in Hs578Ts(i)$_8$ cells. Following miR-134 transfection, the equivalent concentrations of cisplatin were used but no significant differences were found in BT-549, HCC1143 and HCC1937. The transfection conditions were optimised for Hs578Ts(i)$_8$ cells, it may have been beneficial to optimise the appropriate conditions for the other three TNBC cell lines. Upon completion of Dr Keith O'Brien's work and my follow-up work and this study was published in Oncotarget in 2015.

7.2. Conclusions

7.2.1. Drug resistance study

This novel work highlights the importance of drug-resistant cell line models, and highlights the importance of having multiple models for investigations due to the highly heterogeneous nature of tumours. The efficacy of the combination therapy in this project was high in all drug-resistant variants. Thus, even with high intratumoural variation in the clinic, this combination therapy may overcome the differences. We clinically validated our findings in plasma specimens. The results highlighted in this PhD project are promising for overcoming neratinib-resistance in the future. This work sets a premise for future pre-clinical breast cancer models such as *in vivo* models to investigate the efficacy of S4 with neratinib for overcoming neratinib-resistance. Following further trials with neratinib, investigating the expression levels of CAIX in patients is warranted.

7.2.2. miR-134 study

In conclusion, miR-134 may be a potential diagnostic biomarker for TNBC and a therapeutic target. Further studies are warranted in large cohorts of patients, to determine the levels of miR-134 in serum and EVs and to understand the true relevance of this miRNA in TNBC.

7.3. Future directions

A. Neratinib clinical trials

If plasma specimens become available for patients receiving neratinib, CAIX levels should be investigated at pre-treatment and post-treatment to determine if this protein can be validated as a minimally-invasive predictive marker for neratinib. It would be important to also test other EV isolation methods to determine if EV-carried CAIX could be used as a predictive biomarker.

B. CAIX inhibitors in clinical trials

The sulphonamide CAIX inhibitor (SLC-0111) Phase I clinical trial for advanced solid tumours (NCT02215850) was completed in May 2016. Trials are being established to access the safety profile and efficacy of CAIX inhibitors. Similarly, girentuximab, the monoclonal antibody against CAIX is the most clinically advanced monoclonal antibody against CAIX. It has been extensively investigated in renal cell carcinoma, although girentuximab was well-tolerated, but girentuximab was found to have no clinical benefit when used as an adjuvant therapy for clear cell renal cell carcinoma patients in the ARISER clinical trial (234, 235). It had an excellent safety profile in patients on this trial with no reported drug-related serious adverse events. This clinical trial has provided a clinical safety test for the use of girentuximab in other cancer clinical trials. This may be beneficial as a neoadjuvant therapy with neratinib, but further clinical trials are warranted.

C. Alternative S4 inhibitors

The sulfamate inhibitor, S4 was used in this current study, however, new CAIX inhibitors are being developed. Once such CAIX inhibitor is the sulfamate conjugates of betulin and betulinic acid, which have been found to inhibit CAIX and induce cellular death in MCF7 breast cancer cells (236). The development of new CAIX inhibitors could be beneficial for investigating the potential of CAIX inhibition in breast cancer drug resistance. Alternative studies using the cell line variants used in this study with other CAIX inhibitors warrants investigation to further investigate their potential for re-sensitising the resistant cells to neratinib.

D. Antibody-drug conjugate

The HER2-targeted antibody-drug conjugate (ADC), TDM-1 has shown efficacy in clinics. This drug conjugate contains the monoclonal antibody trastuzumab and contains the anticancer drug DM1. Similar to this, a potential future direction (albeit years away), could be a monoclonal antibody similar to girentuximab that targets CAIX conjugated to neratinib. This ADC could potentially overcome drug resistance as evidenced in *in vitro* work in this PhD project.

E. Assessment of CAIX *in vivo* models of breast cancer

Using the cell line variants from this study, the next step would be to implant the cells orthotopically into the mammary fat pad of female nude mice. Using a minimum of 6 mice for each cell line variant used (one age-matched parental cell line and two neratinib-resistant cell line variants). Once the tumours reached a volume of approximately 100-150mm^3, the treatment regimens (5 days on, two days off) would begin. The potential treatment arms plans would be as follows: vehicle control (4% DMSO in saline), neratinib alone (10mg/kg/day) and neratinib with S4 (10mg/kg/day neratinib, 10mg/kg of S4 (as tolerated in a previous study (237)).

F. Assessment of CAIX in PDX models of breast cancer

In recent years, patient-derived xenografts (PDX) models have become important tools in translational cancer research. They provide models more indicative of tumours than *in vitro* cell lines. PDX models of HER2+ breast cancer tumours that are neratinib-resistant would be an increasingly important model of *in vivo* work for this PhD project. We could test the efficacy of neratinib alone and the combination of S4 with neratinib to determine if the latter therapy would provide an improved treatment for this model and thus determine if drug resistance could be overcome with the CAIX inhibitor.

G. Explant tissue analysis

As *in vivo* work, specifically PDX models, can be extremely costly, another validated way to test is to use freshly resected tumour tissue to evaluate response to therapy. *Ex-vivo* neratinib-resistant explant culture could be beneficial to assess sensitivity to neratinib, and to determine if the combination of S4 with neratinib would overcome neratinib-resistance in tissue from HER2+ and luminal B breast cancer tissue.

References

1. Hanahan D, Weinberg RA. The hallmarks of cancer. Cell 2000;100:57-70.
2. Hanahan D, Weinberg RA. Hallmarks of cancer: The next generation. Cell 2011;144:646-74.
3. Howlader N NA, Krapcho M, Miller D, Bishop K, Kosary CL, Yu M, Ruhl J, Tatalovich Z, Mariotto A, Lewis DR, Chen HS, Feuer EJ, Cronin KA (eds). Seer cancer statistics review, 1975-2014, national cancer institute. Bethesda, md, https: //seer.Cancer.Gov/csr/1975_2014/, based on november 2016 seer data submission, posted to the seer web site, april 2017. 2016.
4. Perou CM, Sorlie T, Eisen MB, van de Rijn M, Jeffrey SS, Rees CA, et al. Molecular portraits of human breast tumours. Nature 2000;406:747-52.
5. Carey L, Winer E, Viale G, Cameron D, Gianni L. Triple-negative breast cancer: Disease entity or title of convenience? Nature reviews Clinical oncology 2010;7:683-92.
6. Howlader N, Cronin KA, Kurian AW, Andridge R. Differences in breast cancer survival by molecular subtypes in the united states. Cancer epidemiology, biomarkers & prevention : a publication of the American Association for Cancer Research, cosponsored by the American Society of Preventive Oncology 2018;27:619-26.
7. Xin L, Liu YH, Martin TA, Jiang WG. The era of multigene panels comes? The clinical utility of oncotype dx and mammaprint. World journal of oncology 2017;8:34-40.
8. Sparano JA, Gray RJ, Makower DF, Pritchard KI, Albain KS, Hayes DF, et al. Adjuvant chemotherapy guided by a 21-gene expression assay in breast cancer. The New England journal of medicine 2018;379:111-21.
9. Sorlie T, Perou CM, Tibshirani R, Aas T, Geisler S, Johnsen H, et al. Gene expression patterns of breast carcinomas distinguish tumor subclasses with clinical implications. Proceedings of the National Academy of Sciences of the United States of America 2001;98:10869-74.
10. Sorlie T, Tibshirani R, Parker J, Hastie T, Marron JS, Nobel A, et al. Repeated observation of breast tumor subtypes in independent gene expression data sets. Proceedings of the National Academy of Sciences of the United States of America 2003;100:8418-23.
11. Leyland-Jones B. Trastuzumab: Hopes and realities. Lancet Oncol 2002;3:137-44.
12. Lambertini M, Ponde NF, Solinas C, de Azambuja E. Adjuvant trastuzumab: A 10-year overview of its benefit. Expert Rev Anticancer Ther 2017;17:61-74.
13. Raguz S, Yague E. Resistance to chemotherapy: New treatments and novel insights into an old problem. Br J Cancer 2008;99:387-91.
14. Rabindran SK, Discafani CM, Rosfjord EC, Baxter M, Floyd MB, Golas J, et al. Antitumor activity of hki-272, an orally active, irreversible inhibitor of the her-2 tyrosine kinase. Cancer research 2004;64:3958-65.
15. Singh H, Walker AJ, Amiri-Kordestani L, Cheng J, Tang S, Balcazar P, et al. U.S. Food and drug administration approval: Neratinib for the extended adjuvant treatment of early-stage her2-positive breast cancer. Clinical cancer research : an official journal of the American Association for Cancer Research 2018;24:3486-91.
16. Wong KK, Fracasso PM, Bukowski RM, Lynch TJ, Munster PN, Shapiro GI, et al. A phase i study with neratinib (hki-272), an irreversible pan erbb receptor tyrosine kinase inhibitor, in patients with solid tumors. Clinical cancer research : an official journal of the American Association for Cancer Research 2009;15:2552-8.
17. Burstein HJ, Sun Y, Dirix LY, Jiang Z, Paridaens R, Tan AR, et al. Neratinib, an irreversible erbb receptor tyrosine kinase inhibitor, in patients with advanced

erbb2-positive breast cancer. Journal of clinical oncology : official journal of the American Society of Clinical Oncology 2010;28:1301-7.
18. Martin M, Bonneterre J, Geyer CE, Jr., Ito Y, Ro J, Lang I, et al. A phase two randomised trial of neratinib monotherapy versus lapatinib plus capecitabine combination therapy in patients with her2+ advanced breast cancer. European journal of cancer 2013;49:3763-72.
19. Chan A, Delaloge S, Holmes FA, Moy B, Iwata H, Harvey VJ, et al. Neratinib after trastuzumab-based adjuvant therapy in patients with her2-positive breast cancer (extenet): A multicentre, randomised, double-blind, placebo-controlled, phase 3 trial. Lancet Oncol 2016;Volume 17 Pages 367–77.
20. Martin M, Holmes FA, Ejlertsen B, Delaloge S, Moy B, Iwata H, et al. Neratinib after trastuzumab-based adjuvant therapy in her2-positive breast cancer (extenet): 5-year analysis of a randomised, double-blind, placebo-controlled, phase 3 trial. The Lancet Oncology 2017;18:1688-700.
21. Tao Z, Li SX, Shen K, Zhao Y, Zeng H, Ma X. Safety and efficacy profile of neratinib: A systematic review and meta-analysis of 23 prospective clinical trials. Clinical drug investigation 2018.
22. Seyhan AA, Varadarajan U, Choe S, Liu W, Ryan TE. A genome-wide rnai screen identifies novel targets of neratinib resistance leading to identification of potential drug resistant genetic markers. Mol Biosyst 2012;8:1553-70.
23. Rani S, Corcoran C, Shiels L, Germano S, Breslin S, Madden S, et al. Neuromedin u: A candidate biomarker and therapeutic target to predict and overcome resistance to her-tyrosine kinase inhibitors. Cancer research 2014;74:3821-33.
24. Corcoran C, Rani S, Breslin S, Gogarty M, Ghobrial IM, Crown J, O'Driscoll L. Mir-630 targets igf1r to regulate response to her-targeting drugs and overall cancer cell progression in her2 over-expressing breast cancer. Molecular cancer 2014;13:71.
25. Breslin S, Lowry MC, O'Driscoll L. Neratinib resistance and cross-resistance to other her2-targeted drugs due to increased activity of metabolism enzyme cytochrome p4503a4. British journal of cancer 2017;116:620-5.
26. Canonici A, Ivers L, Conlon NT, Pedersen K, Gaynor N, Browne BC, et al. Her-targeted tyrosine kinase inhibitors enhance response to trastuzumab and pertuzumab in her2-positive breast cancer. Investigational new drugs 2018.
27. Hanker AB, Brewer MR, Sheehan JH, Koch JP, Sliwoski GR, Nagy R, et al. An acquired her2(t798i) gatekeeper mutation induces resistance to neratinib in a patient with her2 mutant-driven breast cancer. Cancer discovery 2017;7:575-85.
28. Sudhan DR, Schwarz LJ, Guerrero-Zotano A, Formisano L, Nixon MJ, Croessmann S, et al. Extended adjuvant therapy with neratinib plus fulvestrant blocks er/her2 crosstalk and maintains complete responses of er+/her2+ breast cancers: Implications to the extenet trial. Clinical cancer research : an official journal of the American Association for Cancer Research 2018.
29. Cocco E, Javier Carmona F, Razavi P, Won HH, Cai Y, Rossi V, et al. Neratinib is effective in breast tumors bearing both amplification and mutation of erbb2 (her2). Science signaling 2018;11.
30. Johnstone RM, Adam M, Hammond JR, Orr L, Turbide C. Vesicle formation during reticulocyte maturation. Association of plasma membrane activities with released vesicles (exosomes). The Journal of biological chemistry 1987;262:9412-20.
31. Thery C, Ostrowski M, Segura E. Membrane vesicles as conveyors of immune responses. Nature reviews Immunology 2009;9:581-93.

32. Xu B, Zhang Y, Du XF, Li J, Zi HX, Bu JW, et al. Neurons secrete mir-132-containing exosomes to regulate brain vascular integrity. Cell research 2017;27:882-97.
33. Bidarimath M, Khalaj K, Kridli RT, Kan FW, Koti M, Tayade C. Extracellular vesicle mediated intercellular communication at the porcine maternal-fetal interface: A new paradigm for conceptus-endometrial cross-talk. Scientific reports 2017;7:40476.
34. Cesi G, Walbrecq G, Margue C, Kreis S. Transferring intercellular signals and traits between cancer cells: Extracellular vesicles as "homing pigeons". Cell communication and signaling : CCS 2016;14:13.
35. Heijnen HF, Schiel AE, Fijnheer R, Geuze HJ, Sixma JJ. Activated platelets release two types of membrane vesicles: Microvesicles by surface shedding and exosomes derived from exocytosis of multivesicular bodies and alpha-granules. Blood 1999;94:3791-9.
36. Cocucci E, Racchetti G, Meldolesi J. Shedding microvesicles: Artefacts no more. Trends in cell biology 2009;19:43-51.
37. Muralidharan-Chari V, Clancy J, Plou C, Romao M, Chavrier P, Raposo G, D'Souza-Schorey C. Arf6-regulated shedding of tumor cell-derived plasma membrane microvesicles. Current biology : CB 2009;19:1875-85.
38. Del Conde I, Shrimpton CN, Thiagarajan P, Lopez JA. Tissue-factor-bearing microvesicles arise from lipid rafts and fuse with activated platelets to initiate coagulation. Blood 2005;106:1604-11.
39. Taylor RC, Cullen SP, Martin SJ. Apoptosis: Controlled demolition at the cellular level. Nature reviews Molecular cell biology 2008;9:231-41.
40. Muralidharan-Chari V, Clancy JW, Sedgwick A, D'Souza-Schorey C. Microvesicles: Mediators of extracellular communication during cancer progression. Journal of cell science 2010;123:1603-11.
41. Hessvik NP, Llorente A. Current knowledge on exosome biogenesis and release. Cellular and molecular life sciences : CMLS 2018;75:193-208.
42. Rink J, Ghigo E, Kalaidzidis Y, Zerial M. Rab conversion as a mechanism of progression from early to late endosomes. Cell 2005;122:735-49.
43. Friand V, David G, Zimmermann P. Syntenin and syndecan in the biogenesis of exosomes. Biology of the cell / under the auspices of the European Cell Biology Organization 2015;107:331-41.
44. Colombo M, Raposo G, Thery C. Biogenesis, secretion, and intercellular interactions of exosomes and other extracellular vesicles. Annual review of cell and developmental biology 2014;30:255-89.
45. Keerthikumar S, Chisanga D, Ariyaratne D, Al Saffar H, Anand S, Zhao K, et al. Exocarta: A web-based compendium of exosomal cargo. Journal of molecular biology 2015.
46. Balaj L, Lessard R, Dai L, Cho YJ, Pomeroy SL, Breakefield XO, Skog J. Tumour microvesicles contain retrotransposon elements and amplified oncogene sequences. Nature communications 2011;2:180.
47. Thakur BK, Zhang H, Becker A, Matei I, Huang Y, Costa-Silva B, et al. Double-stranded DNA in exosomes: A novel biomarker in cancer detection. Cell research 2014;24:766-9.
48. O'Brien K, Lowry MC, Corcoran C, Martinez VG, Daly M, Rani S, et al. Mir-134 in extracellular vesicles reduces triple-negative breast cancer aggression and increases drug sensitivity. Oncotarget 2015;6:32774-89.
49. Valadi H, Ekstrom K, Bossios A, Sjostrand M, Lee JJ, Lotvall JO. Exosome-mediated transfer of mrnas and micrornas is a novel mechanism of genetic exchange between cells. Nature cell biology 2007;9:654-9.

50. Janas T, Janas MM, Sapon K, Janas T. Mechanisms of rna loading into exosomes. FEBS letters 2015;589:1391-8.
51. Koppers-Lalic D, Hackenberg M, Bijnsdorp IV, van Eijndhoven MA, Sadek P, Sie D, et al. Nontemplated nucleotide additions distinguish the small rna composition in cells from exosomes. Cell reports 2014;8:1649-58.
52. Didiot MC, Hall LM, Coles AH, Haraszti RA, Godinho BM, Chase K, et al. Exosome-mediated delivery of hydrophobically modified sirna for huntingtin mrna silencing. Molecular therapy : the journal of the American Society of Gene Therapy 2016;24:1836-47.
53. Fevrier B, Raposo G. Exosomes: Endosomal-derived vesicles shipping extracellular messages. Current opinion in cell biology 2004;16:415-21.
54. de Gassart A, Geminard C, Fevrier B, Raposo G, Vidal M. Lipid raft-associated protein sorting in exosomes. Blood 2003;102:4336-44.
55. Andreu Z, Yanez-Mo M. Tetraspanins in extracellular vesicle formation and function. Frontiers in immunology 2014;5:442.
56. Escola JM, Kleijmeer MJ, Stoorvogel W, Griffith JM, Yoshie O, Geuze HJ. Selective enrichment of tetraspan proteins on the internal vesicles of multivesicular endosomes and on exosomes secreted by human b-lymphocytes. The Journal of biological chemistry 1998;273:20121-7.
57. Holleman J, Marchese A. The ubiquitin ligase deltex-3l regulates endosomal sorting of the g protein-coupled receptor cxcr4. Molecular biology of the cell 2014;25:1892-904.
58. van Niel G, Charrin S, Simoes S, Romao M, Rochin L, Saftig P, et al. The tetraspanin cd63 regulates escrt-independent and -dependent endosomal sorting during melanogenesis. Developmental cell 2011;21:708-21.
59. Harris DA, Patel SH, Gucek M, Hendrix A, Westbroek W, Taraska JW. Exosomes released from breast cancer carcinomas stimulate cell movement. PloS one 2015;10:e0117495.
60. Kowal J, Arras G, Colombo M, Jouve M, Morath JP, Primdal-Bengtson B, et al. Proteomic comparison defines novel markers to characterize heterogeneous populations of extracellular vesicle subtypes. Proceedings of the National Academy of Sciences of the United States of America 2016;113:E968-77.
61. Llorente A, Skotland T, Sylvanne T, Kauhanen D, Rog T, Orlowski A, et al. Molecular lipidomics of exosomes released by pc-3 prostate cancer cells. Biochimica et biophysica acta 2013;1831:1302-9.
62. Choi DS, Kim DK, Kim YK, Gho YS. Proteomics, transcriptomics and lipidomics of exosomes and ectosomes. Proteomics 2013;13:1554-71.
63. Skotland T, Sandvig K, Llorente A. Lipids in exosomes: Current knowledge and the way forward. Progress in lipid research 2017;66:30-41.
64. Kucharzewska P, Belting M. Emerging roles of extracellular vesicles in the adaptive response of tumour cells to microenvironmental stress. Journal of extracellular vesicles 2013;2.
65. Lowry MC, Gallagher WM, O'Driscoll L. The role of exosomes in breast cancer. Clin Chem 2015;61:1457-65.
66. Dhani N, Fyles A, Hedley D, Milosevic M. The clinical significance of hypoxia in human cancers. Semin Nucl Med 2015;45:110-21.
67. McDonald PC, Chafe SC, Dedhar S. Overcoming hypoxia-mediated tumor progression: Combinatorial approaches targeting ph regulation, angiogenesis and immune dysfunction. Front Cell Dev Biol 2016;4:27.
68. Pouyssegur J, Dayan F, Mazure NM. Hypoxia signalling in cancer and approaches to enforce tumour regression. Nature 2006;441:437-43.

69. Semenza GL. The hypoxic tumor microenvironment: A driving force for breast cancer progression. Biochimica et biophysica acta 2016;1863:382-91.
70. Wysoczynski M, Ratajczak MZ. Lung cancer secreted microvesicles: Underappreciated modulators of microenvironment in expanding tumors. International journal of cancer Journal international du cancer 2009;125:1595-603.
71. Park JE, Tan HS, Datta A, Lai RC, Zhang H, Meng W, et al. Hypoxic tumor cell modulates its microenvironment to enhance angiogenic and metastatic potential by secretion of proteins and exosomes. Molecular & cellular proteomics : MCP 2010;9:1085-99.
72. Svensson KJ, Kucharzewska P, Christianson HC, Skold S, Lofstedt T, Johansson MC, et al. Hypoxia triggers a proangiogenic pathway involving cancer cell microvesicles and par-2-mediated heparin-binding egf signaling in endothelial cells. Proceedings of the National Academy of Sciences of the United States of America 2011;108:13147-52.
73. Yotsumoto F, Tokunaga E, Oki E, Maehara Y, Yamada H, Nakajima K, et al. Molecular hierarchy of heparin-binding egf-like growth factor-regulated angiogenesis in triple-negative breast cancer. Molecular cancer research : MCR 2013;11:506-17.
74. Huang Z, Feng Y. Exosomes derived from hypoxic colorectal cancer cells promote angiogenesis through wnt4-induced beta-catenin signaling in endothelial cells. Oncology research 2017;25:651-61.
75. Shan Y, You B, Shi S, Shi W, Zhang Z, Zhang Q, et al. Hypoxia-induced matrix metalloproteinase-13 expression in exosomes from nasopharyngeal carcinoma enhances metastases. Cell death & disease 2018;9:382.
76. King HW, Michael MZ, Gleadle JM. Hypoxic enhancement of exosome release by breast cancer cells. BMC Cancer 2012;12:421.
77. Neill T, Jones HR, Crane-Smith Z, Owens RT, Schaefer L, Iozzo RV. Decorin induces rapid secretion of thrombospondin-1 in basal breast carcinoma cells via inhibition of ras homolog gene family, member a/rho-associated coiled-coil containing protein kinase 1. The FEBS journal 2013;280:2353-68.
78. Rong L, Li R, Li S, Luo R. Immunosuppression of breast cancer cells mediated by transforming growth factor-beta in exosomes from cancer cells. Oncology letters 2016;11:500-4.
79. Kalinski P. Regulation of immune responses by prostaglandin e2. J Immunol 2012;188:21-8.
80. Wang X, Luo G, Zhang K, Cao J, Huang C, Jiang T, et al. Hypoxic tumor-derived exosomal mir-301a mediates m2 macrophage polarization via pten/pi3kgamma to promote pancreatic cancer metastasis. Cancer research 2018;78:4586-98.
81. Bos R, van der Groep P, Greijer AE, Shvarts A, Meijer S, Pinedo HM, et al. Levels of hypoxia-inducible factor-1alpha independently predict prognosis in patients with lymph node negative breast carcinoma. Cancer 2003;97:1573-81.
82. Brito LG, Schiavon VF, Andrade JM, Tiezzi DG, Peria FM, Marana HR. Expression of hypoxia-inducible factor 1-alpha and vascular endothelial growth factor-c in locally advanced breast cancer patients. Clinics (Sao Paulo) 2011;66:1313-20.
83. Charpin C, Tavassoli F, Secq V, Giusiano S, Villeret J, Garcia S, et al. Validation of an immunohistochemical signature predictive of 8-year outcome for patients with breast carcinoma. International journal of cancer Journal international du cancer 2012;131:E236-43.
84. Dong M, Wan XB, Yuan ZY, Wei L, Fan XJ, Wang TT, et al. Low expression of beclin 1 and elevated expression of hif-1alpha refine distant metastasis risk and

predict poor prognosis of er-positive, her2-negative breast cancer. Med Oncol 2013;30:355.
85. Peurala E, Koivunen P, Bloigu R, Haapasaari KM, Jukkola-Vuorinen A. Expressions of individual phds associate with good prognostic factors and increased proliferation in breast cancer patients. Breast cancer research and treatment 2012;133:179-88.
86. Rajkovic-Molek K, Mustac E, Hadzisejdic I, Jonjic N. The prognostic importance of nuclear factor kappab and hypoxia-inducible factor 1alpha in relation to the breast cancer subtype and the overall survival. Applied immunohistochemistry & molecular morphology : AIMM / official publication of the Society for Applied Immunohistochemistry 2014;22:464-70.
87. Vleugel MM, Greijer AE, Shvarts A, van der Groep P, van Berkel M, Aarbodem Y, et al. Differential prognostic impact of hypoxia induced and diffuse hif-1alpha expression in invasive breast cancer. Journal of clinical pathology 2005;58:172-7.
88. Wang HX, Qin C, Han FY, Wang XH, Li N. Hif-2alpha as a prognostic marker for breast cancer progression and patient survival. Genetics and molecular research : GMR 2014;13:2817-26.
89. Baba Y, Nosho K, Shima K, Irahara N, Chan AT, Meyerhardt JA, et al. Hif1a overexpression is associated with poor prognosis in a cohort of 731 colorectal cancers. The American journal of pathology 2010;176:2292-301.
90. Cao D, Hou M, Guan YS, Jiang M, Yang Y, Gou HF. Expression of hif-1alpha and vegf in colorectal cancer: Association with clinical outcomes and prognostic implications. BMC Cancer 2009;9:432.
91. Cleven AH, van Engeland M, Wouters BG, de Bruine AP. Stromal expression of hypoxia regulated proteins is an adverse prognostic factor in colorectal carcinomas. Cellular oncology : the official journal of the International Society for Cellular Oncology 2007;29:229-40.
92. Chen J, Li T, Liu Q, Jiao H, Yang W, Liu X, Huo Z. Clinical and prognostic significance of hif-1alpha, pten, cd44v6, and survivin for gastric cancer: A meta-analysis. PloS one 2014;9:e91842.
93. Hashimoto K, Aoyagi K, Isobe T, Kouhuji K, Shirouzu K. Expression of cd133 in the cytoplasm is associated with cancer progression and poor prognosis in gastric cancer. Gastric cancer : official journal of the International Gastric Cancer Association and the Japanese Gastric Cancer Association 2014;17:97-106.
94. Isobe T, Aoyagi K, Koufuji K, Shirouzu K, Kawahara A, Taira T, Kage M. Clinicopathological significance of hypoxia-inducible factor-1 alpha (hif-1alpha) expression in gastric cancer. International journal of clinical oncology 2013;18:293-304.
95. Kolev Y, Uetake H, Takagi Y, Sugihara K. Lactate dehydrogenase-5 (ldh-5) expression in human gastric cancer: Association with hypoxia-inducible factor (hif-1alpha) pathway, angiogenic factors production and poor prognosis. Annals of surgical oncology 2008;15:2336-44.
96. Kubo H, Kitajima Y, Kai K, Nakamura J, Miyake S, Yanagihara K, et al. Regulation and clinical significance of the hypoxia-induced expression of angptl4 in gastric cancer. Oncology letters 2016;11:1026-34.
97. Ma J, Zhang L, Ru GQ, Zhao ZS, Xu WJ. Upregulation of hypoxia inducible factor 1alpha mrna is associated with elevated vascular endothelial growth factor expression and excessive angiogenesis and predicts a poor prognosis in gastric carcinoma. World journal of gastroenterology 2007;13:1680-6.
98. Mizokami K, Kakeji Y, Oda S, Irie K, Yonemura T, Konishi F, Maehara Y. Clinicopathologic significance of hypoxia-inducible factor 1alpha overexpression in gastric carcinomas. Journal of surgical oncology 2006;94:149-54.

99. Liu X, Chen S, Tu J, Cai W, Xu Q. Hsp90 inhibits apoptosis and promotes growth by regulating hif-1alpha abundance in hepatocellular carcinoma. International journal of molecular medicine 2016;37:825-35.
100. Sharma BK, Srinivasan R, Kapil S, Singla B, Chawla YK, Chakraborti A, et al. Angiogenic and anti-angiogenic factor gene transcript level quantitation by quantitative real time pcr in patients with hepatocellular carcinoma. Molecular biology reports 2013;40:5843-52.
101. Xiang ZL, Zeng ZC, Fan J, Tang ZY, He J, Zeng HY, Chang JY. The expression of hif-1alpha in primary hepatocellular carcinoma and its correlation with radiotherapy response and clinical outcome. Molecular biology reports 2012;39:2021-9.
102. Xu W, Kwon JH, Moon YH, Kim YB, Yu YS, Lee N, et al. Influence of preoperative transcatheter arterial chemoembolization on gene expression in the hif-1alpha pathway in patients with hepatocellular carcinoma. Journal of cancer research and clinical oncology 2014;140:1507-15.
103. Zheng SS, Chen XH, Yin X, Zhang BH. Prognostic significance of hif-1alpha expression in hepatocellular carcinoma: A meta-analysis. PloS one 2013;8:e65753.
104. Tsubata Y, Sutani A, Okimoto T, Murakami I, Usuda R, Okumichi T, et al. Comparative analysis of tumor angiogenesis and clinical features of 55 cases of pleomorphic carcinoma and adenocarcinoma of the lung. Anticancer Res 2015;35:389-94.
105. Wang Q, Hu DF, Rui Y, Jiang AB, Liu ZL, Huang LN. Prognosis value of hif-1alpha expression in patients with non-small cell lung cancer. Gene 2014;541:69-74.
106. Wei L, Sun JJ, Cui YC, Jiang SL, Wang XW, Lv LY, et al. Twist may be associated with invasion and metastasis of hypoxic nsclc cells. Tumour Biol 2016;37:9979-87.
107. Wu S, Cheng Z, Yu L, Song W, Tao Y. [expression of cd82/kai1 and hif-1alpha in non-small cell lung cancer and their relationship to vasculogenic mimicry]. Zhongguo Fei Ai Za Zhi 2011;14:918-25.
108. Putra AC, Eguchi H, Lee KL, Yamane Y, Gustine E, Isobe T, et al. The a allele at rs13419896 of epas1 is associated with enhanced expression and poor prognosis for non-small cell lung cancer. PloS one 2015;10:e0134496.
109. Andersen S, Donnem T, Stenvold H, Al-Saad S, Al-Shibli K, Busund LT, Bremnes RM. Overexpression of the hif hydroxylases phd1, phd2, phd3 and fih are individually and collectively unfavorable prognosticators for nsclc survival. PloS one 2011;6:e23847.
110. Andersen S, Eilertsen M, Donnem T, Al-Shibli K, Al-Saad S, Busund LT, Bremnes RM. Diverging prognostic impacts of hypoxic markers according to nsclc histology. Lung Cancer 2011;72:294-302.
111. Li C, Lu HJ, Na FF, Deng L, Xue JX, Wang JW, et al. Prognostic role of hypoxic inducible factor expression in non-small cell lung cancer: A meta-analysis. Asian Pac J Cancer Prev 2013;14:3607-12.
112. Corcoran C, Rani S, O'Brien K, O'Neill A, Prencipe M, Sheikh R, et al. Docetaxel-resistance in prostate cancer: Evaluating associated phenotypic changes and potential for resistance transfer via exosomes. PloS one 2012;7:e50999.
113. Lv MM, Zhu XY, Chen WX, Zhong SL, Hu Q, Ma TF, et al. Exosomes mediate drug resistance transfer in mcf-7 breast cancer cells and a probable mechanism is delivery of p-glycoprotein. Tumour Biol 2014;35:10773-9.
114. Corcoran C, Rani S, O'Driscoll L. Mir-34a is an intracellular and exosomal predictive biomarker for response to docetaxel with clinical relevance to prostate cancer progression. The Prostate 2014;74:1320-34.

115. Samuel P, Fabbri M, Carter DRF. Mechanisms of drug resistance in cancer: The role of extracellular vesicles. Proteomics 2017;17.
116. Namee NM, O'Driscoll L. Extracellular vesicles and anti-cancer drug resistance. Biochimica et biophysica acta Reviews on cancer 2018.
117. Shiozawa K, Shuting J, Yoshioka Y, Ochiya T, Kondo T. Extracellular vesicle-encapsulated microrna-761 enhances pazopanib resistance in synovial sarcoma. Biochemical and biophysical research communications 2018;495:1322-7.
118. Bouvy C, Wannez A, Laloy J, Chatelain C, Dogne JM. Transfer of multidrug resistance among acute myeloid leukemia cells via extracellular vesicles and their microrna cargo. Leukemia research 2017;62:70-6.
119. Kotval JP, Gray LH. Structural changes produced in microspores of tradescantia by alpha-radiation. Journal of genetics 1947;48:135-54.
120. Jella KK, Rani S, O'Driscoll L, McClean B, Byrne HJ, Lyng FM. Exosomes are involved in mediating radiation induced bystander signaling in human keratinocyte cells. Radiation research 2014;181:138-45.
121. Asur RS, Thomas RA, Tucker JD. Chemical induction of the bystander effect in normal human lymphoblastoid cells. Mutation research 2009;676:11-6.
122. Testi S, Azzara A, Giovannini C, Lombardi S, Piaggi S, Facioni MS, Scarpato R. Vincristine-induced bystander effect in human lymphocytes. Mutation research 2016;789:39-47.
123. Samuel P, Mulcahy LA, Furlong F, McCarthy HO, Brooks SA, Fabbri M, et al. Cisplatin induces the release of extracellular vesicles from ovarian cancer cells that can induce invasiveness and drug resistance in bystander cells. Philosophical transactions of the Royal Society of London Series B, Biological sciences 2018;373.
124. Boelens MC, Wu TJ, Nabet BY, Xu B, Qiu Y, Yoon T, et al. Exosome transfer from stromal to breast cancer cells regulates therapy resistance pathways. Cell 2014;159:499-513.
125. Chen WX, Liu XM, Lv MM, Chen L, Zhao JH, Zhong SL, et al. Exosomes from drug-resistant breast cancer cells transmit chemoresistance by a horizontal transfer of micrornas. PloS one 2014;9:e95240.
126. Chen WX, Cai YQ, Lv MM, Chen L, Zhong SL, Ma TF, et al. Exosomes from docetaxel-resistant breast cancer cells alter chemosensitivity by delivering micrornas. Tumour Biol 2014.
127. Wei Y, Lai X, Yu S, Chen S, Ma Y, Zhang Y, et al. Exosomal mir-221/222 enhances tamoxifen resistance in recipient er-positive breast cancer cells. Breast cancer research and treatment 2014;147:423-31.
128. Ciravolo V, Huber V, Ghedini GC, Venturelli E, Bianchi F, Campiglio M, et al. Potential role of her2-overexpressing exosomes in countering trastuzumab-based therapy. Journal of cellular physiology 2012;227:658-67.
129. Bertout JA, Patel SA, Simon MC. The impact of o2 availability on human cancer. Nature reviews Cancer 2008;8:967-75.
130. Breslin S. Investigations of mechanisms of drug-resistance and associated biomarkers in her2-overexpressing breast cancer. PhD thesis, Trinity College Dublin 2015.
131. O'Brien K, Rani S, Corcoran C, Wallace R, Hughes L, Friel AM, et al. Exosomes from triple-negative breast cancer cells can transfer phenotypic traits representing their cells of origin to secondary cells. European journal of cancer 2013;49:1845-59.
132. Van Deun J, Mestdagh P, Agostinis P, Akay O, Anand S, Anckaert J, et al. Ev-track: Transparent reporting and centralizing knowledge in extracellular vesicle research. Nature methods 2017;14:228-32.

133. Lotvall J, Hill AF, Hochberg F, Buzas EI, Di Vizio D, Gardiner C, et al. Minimal experimental requirements for definition of extracellular vesicles and their functions: A position statement from the international society for extracellular vesicles. Journal of extracellular vesicles 2014;3:26913.
134. Witwer KW, Soekmadji C, Hill AF, Wauben MH, Buzas EI, Di Vizio D, et al. Updating the misev minimal requirements for extracellular vesicle studies: Building bridges to reproducibility. Journal of extracellular vesicles 2017;6:1396823.
135. Benjamini Y, Drai D, Elmer G, Kafkafi N, Golani I. Controlling the false discovery rate in behavior genetics research. Behavioural brain research 2001;125:279-84.
136. Chou TC. Drug combination studies and their synergy quantification using the chou-talalay method. Cancer research 2010;70:440-6.
137. Chou TC. Theoretical basis, experimental design, and computerized simulation of synergism and antagonism in drug combination studies. Pharmacological reviews 2006;58:621-81.
138. Novotna A, Krasulova K, Bartonkova I, Korhonova M, Bachleda P, Anzenbacher P, Dvorak Z. Dual effects of ketoconazole cis-enantiomers on cyp3a4 in human hepatocytes and hepg2 cells. PloS one 2014;9:e111286.
139. Li Y, Wang H, Oosterwijk E, Selman Y, Mira JC, Medrano T, et al. Antibody-specific detection of caix in breast and prostate cancers. Biochemical and biophysical research communications 2009;386:488-92.
140. Ames S, Pastorekova S, Becker HM. The proteoglycan-like domain of carbonic anhydrase ix mediates non-catalytic facilitation of lactate transport in cancer cells. Oncotarget 2018;9:27940-57.
141. Chan A, Delaloge S, Holmes FA, Moy B, Iwata H, Harvey VJ, et al. Neratinib after trastuzumab-based adjuvant therapy in patients with her2-positive breast cancer (extenet): A multicentre, randomised, double-blind, placebo-controlled, phase 3 trial. The Lancet Oncology 2016;17:367-77.
142. Hur JY, Kim HJ, Lee JS, Choi CM, Lee JC, Jung MK, et al. Extracellular vesicle-derived DNA for performing egfr genotyping of nsclc patients. Molecular cancer 2018;17:15.
143. Kirouac DC, Du J, Lahdenranta J, Onsum MD, Nielsen UB, Schoeberl B, McDonagh CF. Her2+ cancer cell dependence on pi3k vs. Mapk signaling axes is determined by expression of egfr, erbb3 and cdkn1b. PLoS Comput Biol 2016;12:e1004827.
144. Cancer Genome Atlas N. Comprehensive molecular portraits of human breast tumours. Nature 2012;490:61-70.
145. Baselga J. Targeting the phosphoinositide-3 (pi3) kinase pathway in breast cancer. Oncologist 2011;16 Suppl 1:12-9.
146. O'Neill AK, Niederst MJ, Newton AC. Suppression of survival signalling pathways by the phosphatase phlpp. The FEBS journal 2013;280:572-83.
147. Strotbek M, Schmid S, Sanchez-Gonzalez I, Boerries M, Busch H, Olayioye MA. Mir-181 elevates akt signaling by co-targeting phlpp2 and inpp4b phosphatases in luminal breast cancer. International journal of cancer 2017;140:2310-20.
148. Wen YA, Stevens PD, Gasser ML, Andrei R, Gao T. Downregulation of phlpp expression contributes to hypoxia-induced resistance to chemotherapy in colon cancer cells. Molecular and cellular biology 2013;33:4594-605.
149. Di Luca A, Henry M, Meleady P, O'Connor R. Label-free lc-ms analysis of her2+ breast cancer cell line response to her2 inhibitor treatment. Daru 2015;23:40.
150. Cen X, Liu S, Cheng K. The role of toll-like receptor in inflammation and tumor immunity. Frontiers in pharmacology 2018;9:878.

151. Jia D, Yang W, Li L, Liu H, Tan Y, Ooi S, et al. Beta-catenin and nf-kappab co-activation triggered by tlr3 stimulation facilitates stem cell-like phenotypes in breast cancer. Cell Death Differ 2015;22:298-310.
152. Gonzalez-Reyes S, Marin L, Gonzalez L, Gonzalez LO, del Casar JM, Lamelas ML, et al. Study of tlr3, tlr4 and tlr9 in breast carcinomas and their association with metastasis. BMC Cancer 2010;10:665.
153. Hamilton JA. Colony-stimulating factors in inflammation and autoimmunity. Nature reviews Immunology 2008;8:533-44.
154. Richardsen E, Uglehus RD, Johnsen SH, Busund LT. Macrophage-colony stimulating factor (csf1) predicts breast cancer progression and mortality. Anticancer Res 2015;35:865-74.
155. Aharinejad S, Salama M, Paulus P, Zins K, Berger A, Singer CF. Elevated csf1 serum concentration predicts poor overall survival in women with early breast cancer. Endocr Relat Cancer 2013;20:777-83.
156. Brennan DJ, Jirstrom K, Kronblad A, Millikan RC, Landberg G, Duffy MJ, et al. Ca ix is an independent prognostic marker in premenopausal breast cancer patients with one to three positive lymph nodes and a putative marker of radiation resistance. Clinical cancer research : an official journal of the American Association for Cancer Research 2006;12:6421-31.
157. Kyndi M, Sorensen FB, Knudsen H, Alsner J, Overgaard M, Nielsen HM, et al. Carbonic anhydrase ix and response to postmastectomy radiotherapy in high-risk breast cancer: A subgroup analysis of the dbcg82 b and c trials. Breast Cancer Res 2008;10:R24.
158. Tan EY, Yan M, Campo L, Han C, Takano E, Turley H, et al. The key hypoxia regulated gene caix is upregulated in basal-like breast tumours and is associated with resistance to chemotherapy. British journal of cancer 2009;100:405-11.
159. Ivanova L, Zandberga E, Silina K, Kalnina Z, Abols A, Endzelins E, et al. Prognostic relevance of carbonic anhydrase ix expression is distinct in various subtypes of breast cancer and its silencing suppresses self-renewal capacity of breast cancer cells. Cancer Chemother Pharmacol 2015;75:235-46.
160. Betof AS, Rabbani ZN, Hardee ME, Kim SJ, Broadwater G, Bentley RC, et al. Carbonic anhydrase ix is a predictive marker of doxorubicin resistance in early-stage breast cancer independent of her2 and top2a amplification. British journal of cancer 2012;106:916-22.
161. Hennessy BT, Lu Y, Gonzalez-Angulo AM, Carey MS, Myhre S, Ju Z, et al. A technical assessment of the utility of reverse phase protein arrays for the study of the functional proteome in non-microdissected human breast cancers. Clin Proteomics 2010;6:129-51.
162. Straud S, Zubovych I, De Brabander JK, Roth MG. Inhibition of iron uptake is responsible for differential sensitivity to v-atpase inhibitors in several cancer cell lines. PloS one 2010;5:e11629.
163. Liu Y, Cui Y, Shi M, Zhang Q, Wang Q, Chen X. Deferoxamine promotes mda-mb-231 cell migration and invasion through increased ros-dependent hif-1alpha accumulation. Cellular physiology and biochemistry : international journal of experimental cellular physiology, biochemistry, and pharmacology 2014;33:1036-46.
164. Weis SM, Cheresh DA. Tumor angiogenesis: Molecular pathways and therapeutic targets. Nat Med 2011;17:1359-70.
165. Hardee ME, Dewhirst MW, Agarwal N, Sorg BS. Novel imaging provides new insights into mechanisms of oxygen transport in tumors. Current molecular medicine 2009;9:435-41.

166. Thomlinson RH, Gray LH. The histological structure of some human lung cancers and the possible implications for radiotherapy. British journal of cancer 1955;9:539-49.
167. Walsh JC, Lebedev A, Aten E, Madsen K, Marciano L, Kolb HC. The clinical importance of assessing tumor hypoxia: Relationship of tumor hypoxia to prognosis and therapeutic opportunities. Antioxidants & redox signaling 2014;21:1516-54.
168. Wigerup C, Pahlman S, Bexell D. Therapeutic targeting of hypoxia and hypoxia-inducible factors in cancer. Pharmacology & therapeutics 2016;164:152-69.
169. Swietach P, Hulikova A, Vaughan-Jones RD, Harris AL. New insights into the physiological role of carbonic anhydrase ix in tumour ph regulation. Oncogene 2010;29:6509-21.
170. Webb BA, Chimenti M, Jacobson MP, Barber DL. Dysregulated ph: A perfect storm for cancer progression. Nature reviews Cancer 2011;11:671-7.
171. Parkkila S. Significance of ph regulation and carbonic anhydrases in tumour progression and implications for diagnostic and therapeutic approaches. BJU international 2008;101 Suppl 4:16-21.
172. Sowa T, Menju T, Chen-Yoshikawa TF, Takahashi K, Nishikawa S, Nakanishi T, et al. Hypoxia-inducible factor 1 promotes chemoresistance of lung cancer by inducing carbonic anhydrase ix expression. Cancer medicine 2017;6:288-97.
173. Yang JS, Lin CW, Hsieh YH, Chien MH, Chuang CY, Yang SF. Overexpression of carbonic anhydrase ix induces cell motility by activating matrix metalloproteinase-9 in human oral squamous cell carcinoma cells. Oncotarget 2017;8:83088-99.
174. Matsuyama S, Llopis J, Deveraux QL, Tsien RY, Reed JC. Changes in intramitochondrial and cytosolic ph: Early events that modulate caspase activation during apoptosis. Nature cell biology 2000;2:318-25.
175. Saarnio J, Parkkila S, Parkkila AK, Waheed A, Casey MC, Zhou XY, et al. Immunohistochemistry of carbonic anhydrase isozyme ix (mn/ca ix) in human gut reveals polarized expression in the epithelial cells with the highest proliferative capacity. The journal of histochemistry and cytochemistry : official journal of the Histochemistry Society 1998;46:497-504.
176. van Kuijk SJ, Yaromina A, Houben R, Niemans R, Lambin P, Dubois LJ. Prognostic significance of carbonic anhydrase ix expression in cancer patients: A meta-analysis. Frontiers in oncology 2016;6:69.
177. Zhao Z, Liao G, Li Y, Zhou S, Zou H, Fernando S. Prognostic value of carbonic anhydrase ix immunohistochemical expression in renal cell carcinoma: A meta-analysis of the literature. PloS one 2014;9:e114096.
178. Bartosova M, Parkkila S, Pohlodek K, Karttunen TJ, Galbavy S, Mucha V, et al. Expression of carbonic anhydrase ix in breast is associated with malignant tissues and is related to overexpression of c-erbb2. The Journal of pathology 2002;197:314-21.
179. Beketic-Oreskovic L, Ozretic P, Rabbani ZN, Jackson IL, Sarcevic B, Levanat S, et al. Prognostic significance of carbonic anhydrase ix (ca-ix), endoglin (cd105) and 8-hydroxy-2'-deoxyguanosine (8-ohdg) in breast cancer patients. Pathology oncology research : POR 2011;17:593-603.
180. Pinheiro C, Sousa B, Albergaria A, Paredes J, Dufloth R, Vieira D, et al. Glut1 and caix expression profiles in breast cancer correlate with adverse prognostic factors and mct1 overexpression. Histology and histopathology 2011;26:1279-86.
181. Kaya AO, Gunel N, Benekli M, Akyurek N, Buyukberber S, Tatli H, et al. Hypoxia inducible factor-1 alpha and carbonic anhydrase ix overexpression are associated with poor survival in breast cancer patients. Journal of BUON : official journal of the Balkan Union of Oncology 2012;17:663-8.

182. Schutze D, Milde-Langosch K, Witzel I, Rody A, Karn T, Schmidt M, et al. Relevance of cellular and serum carbonic anhydrase ix in primary breast cancer. Journal of cancer research and clinical oncology 2013;139:747-54.
183. Span PN, Bussink J, Manders P, Beex LV, Sweep CG. Carbonic anhydrase-9 expression levels and prognosis in human breast cancer: Association with treatment outcome. British journal of cancer 2003;89:271-6.
184. Kyndi M, Sorensen FB, Knudsen H, Alsner J, Overgaard M, Nielsen HM, Overgaard J. Carbonic anhydrase ix and response to postmastectomy radiotherapy in high-risk breast cancer: A subgroup analysis of the dbcg82 b and c trials. Breast cancer research : BCR 2008;10:R24.
185. Aomatsu N, Yashiro M, Kashiwagi S, Kawajiri H, Takashima T, Ohsawa M, et al. Carbonic anhydrase 9 is associated with chemosensitivity and prognosis in breast cancer patients treated with taxane and anthracycline. BMC cancer 2014;14:400.
186. Ho D, Huang J, Chapman JW, Leitzel K, Ali SM, Shepherd L, et al. Impact of serum her2, timp-1, and caix on outcome for her2+ metastatic breast cancer patients: Cctg ma.31 (lapatinib vs. Trastuzumab). Breast cancer research and treatment 2017;164:571-80.
187. Reynolds CP, Maurer BJ. Evaluating response to antineoplastic drug combinations in tissue culture models. Methods in molecular medicine 2005;110:173-83.
188. Swietach P, Patiar S, Supuran CT, Harris AL, Vaughan-Jones RD. The role of carbonic anhydrase 9 in regulating extracellular and intracellular ph in three-dimensional tumor cell growths. The Journal of biological chemistry 2009;284:20299-310.
189. Martinez VG, Crown J, Porter RK, O'Driscoll L. Neuromedin u alters bioenergetics and expands the cancer stem cell phenotype in her2-positive breast cancer. International journal of cancer 2017;140:2771-84.
190. Yan H, Yu K, Zhang K, Liu L, Li Y. Efficacy and safety of trastuzumab emtansine (t-dm1) in the treatment of her2-positive metastatic breast cancer (mbc): A meta-analysis of randomized controlled trial. Oncotarget 2017;8:102458-67.
191. Nicolini A, Ferrari P, Duffy MJ. Prognostic and predictive biomarkers in breast cancer: Past, present and future. Seminars in cancer biology 2018;52:56-73.
192. Baran J, Baj-Krzyworzeka M, Weglarczyk K, Szatanek R, Zembala M, Barbasz J, et al. Circulating tumour-derived microvesicles in plasma of gastric cancer patients. Cancer immunology, immunotherapy : CII 2010;59:841-50.
193. Beckham CJ, Olsen J, Yin PN, Wu CH, Ting HJ, Hagen FK, et al. Bladder cancer exosomes contain edil-3/del1 and facilitate cancer progression. The Journal of urology 2014;192:583-92.
194. Li J, Sherman-Baust CA, Tsai-Turton M, Bristow RE, Roden RB, Morin PJ. Claudin-containing exosomes in the peripheral circulation of women with ovarian cancer. BMC cancer 2009;9:244.
195. Worst TS, von Hardenberg J, Gross JC, Erben P, Schnolzer M, Hausser I, et al. Database-augmented mass spectrometry analysis of exosomes identifies claudin 3 as a putative prostate cancer biomarker. Molecular & cellular proteomics : MCP 2017;16:998-1008.
196. Verma M, Lam TK, Hebert E, Divi RL. Extracellular vesicles: Potential applications in cancer diagnosis, prognosis, and epidemiology. BMC clinical pathology 2015;15:6.
197. Sandfeld-Paulsen B, Jakobsen KR, Baek R, Folkersen BH, Rasmussen TR, Meldgaard P, et al. Exosomal proteins as diagnostic biomarkers in lung cancer. Journal of thoracic oncology : official publication of the International Association for the Study of Lung Cancer 2016;11:1701-10.

198. van Niel G, D'Angelo G, Raposo G. Shedding light on the cell biology of extracellular vesicles. Nature reviews Molecular cell biology 2018;19:213-28.
199. Dent R, Trudeau M, Pritchard KI, Hanna WM, Kahn HK, Sawka CA, et al. Triple-negative breast cancer: Clinical features and patterns of recurrence. Clinical cancer research : an official journal of the American Association for Cancer Research 2007;13:4429-34.
200. Foulkes WD, Smith IE, Reis-Filho JS. Triple-negative breast cancer. The New England journal of medicine 2010;363:1938-48.
201. Lehmann BD, Bauer JA, Chen X, Sanders ME, Chakravarthy AB, Shyr Y, Pietenpol JA. Identification of human triple-negative breast cancer subtypes and preclinical models for selection of targeted therapies. The Journal of clinical investigation 2011;121:2750-67.
202. Ring BZ, Hout DR, Morris SW, Lawrence K, Schweitzer BL, Bailey DB, et al. Generation of an algorithm based on minimal gene sets to clinically subtype triple negative breast cancer patients. BMC cancer 2016;16:143.
203. Kameswaran V, Bramswig NC, McKenna LB, Penn M, Schug J, Hand NJ, et al. Epigenetic regulation of the dlk1-meg3 microrna cluster in human type 2 diabetic islets. Cell metabolism 2014;19:135-45.
204. Anders CK, Carey LA. Biology, metastatic patterns, and treatment of patients with triple-negative breast cancer. Clin Breast Cancer 2009;9 Suppl 2:S73-81.
205. Lin NU, Claus E, Sohl J, Razzak AR, Arnaout A, Winer EP. Sites of distant recurrence and clinical outcomes in patients with metastatic triple-negative breast cancer: High incidence of central nervous system metastases. Cancer 2008;113:2638-45.
206. Dent R, Hanna WM, Trudeau M, Rawlinson E, Sun P, Narod SA. Pattern of metastatic spread in triple-negative breast cancer. Breast Cancer Res Treat 2009;115:423-8.
207. Arnedos M, Bihan C, Delaloge S, Andre F. Triple-negative breast cancer: Are we making headway at least? Ther Adv Med Oncol 2012;4:195-210.
208. Andre F, Zielinski CC. Optimal strategies for the treatment of metastatic triple-negative breast cancer with currently approved agents. Ann Oncol 2012;23 Suppl 6:vi46-51.
209. Yadav BS, Sharma SC, Chanana P, Jhamb S. Systemic treatment strategies for triple-negative breast cancer. World journal of clinical oncology 2014;5:125-33.
210. Caldas-Lopes E, Cerchietti L, Ahn JH, Clement CC, Robles AI, Rodina A, et al. Hsp90 inhibitor pu-h71, a multimodal inhibitor of malignancy, induces complete responses in triple-negative breast cancer models. Proc Natl Acad Sci U S A 2009;106:8368-73.
211. Proia DA, Zhang C, Sequeira M, Jimenez JP, He S, Spector N, et al. Preclinical activity profile and therapeutic efficacy of the hsp90 inhibitor ganetespib in triple-negative breast cancer. Clinical cancer research : an official journal of the American Association for Cancer Research 2014;20:413-24.
212. Munster PN, Srethapakdi M, Moasser MM, Rosen N. Inhibition of heat shock protein 90 function by ansamycins causes the morphological and functional differentiation of breast cancer cells. Cancer Res 2001;61:2945-52.
213. Hollingshead M, Alley M, Burger AM, Borgel S, Pacula-Cox C, Fiebig HH, Sausville EA. In vivo antitumor efficacy of 17-dmag (17-dimethylaminoethylamino-17-demethoxygeldanamycin hydrochloride), a water-soluble geldanamycin derivative. Cancer Chemother Pharmacol 2005;56:115-25.
214. Eiseman JL, Lan J, Lagattuta TF, Hamburger DR, Joseph E, Covey JM, Egorin MJ. Pharmacokinetics and pharmacodynamics of 17-demethoxy 17-[[(2-dimethylamino)ethyl]amino]geldanamycin (17dmag, nsc 707545) in c.B-17 scid

mice bearing mda-mb-231 human breast cancer xenografts. Cancer Chemother Pharmacol 2005;55:21-32.
215. Wang C, Pan B, Zhu H, Zhou Y, Mao F, Lin Y, et al. Prognostic value of androgen receptor in triple negative breast cancer: A meta-analysis. Oncotarget 2016;7:46482-91.
216. Traina TA, Miller K, Yardley DA, Eakle J, Schwartzberg LS, O'Shaughnessy J, et al. Enzalutamide for the treatment of androgen receptor-expressing triple-negative breast cancer. Journal of clinical oncology : official journal of the American Society of Clinical Oncology 2018;36:884-90.
217. Cascione L, Gasparini P, Lovat F, Carasi S, Pulvirenti A, Ferro A, et al. Integrated microrna and mrna signatures associated with survival in triple negative breast cancer. PLoS One 2013;8:e55910.
218. Chen K, Rajewsky N. The evolution of gene regulation by transcription factors and micrornas. Nat Rev Genet 2007;8:93-103.
219. Turchinovich A, Weiz L, Langheinz A, Burwinkel B. Characterization of extracellular circulating microrna. Nucleic acids research 2011;39:7223-33.
220. Calin GA, Croce CM. Microrna-cancer connection: The beginning of a new tale. Cancer Res 2006;66:7390-4.
221. Zhang JP, Zeng C, Xu L, Gong J, Fang JH, Zhuang SM. Microrna-148a suppresses the epithelial-mesenchymal transition and metastasis of hepatoma cells by targeting met/snail signaling. Oncogene 2014;33:4069-76.
222. Corcoran C, Friel AM, Duffy MJ, Crown J, O'Driscoll L. Intracellular and extracellular micrornas in breast cancer. Clinical chemistry 2011;57:18-32.
223. Li Y, Zhang M, Chen H, Dong Z, Ganapathy V, Thangaraju M, Huang S. Ratio of mir-196s to hoxc8 messenger rna correlates with breast cancer cell migration and metastasis. Cancer research 2010;70:7894-904.
224. Roy S, Chakravarty D, Cortez V, De Mukhopadhyay K, Bandyopadhyay A, Ahn JM, et al. Significance of pelp1 in er-negative breast cancer metastasis. Molecular cancer research : MCR 2012;10:25-33.
225. Gasparini P, Lovat F, Fassan M, Casadei L, Cascione L, Jacob NK, et al. Protective role of mir-155 in breast cancer through rad51 targeting impairs homologous recombination after irradiation. Proceedings of the National Academy of Sciences of the United States of America 2014;111:4536-41.
226. Valadi H, Ekström K, Bossios A, Sjöstrand M, Lee JJ, Lötvall JO. Exosome-mediated transfer of mrnas and micrornas is a novel mechanism of genetic exchange between cells. Nat Cell Biol 2007;9:654-9.
227. Stoorvogel W. Functional transfer of microrna by exosomes. Blood 2012;119:646-8.
228. Umezu T, Ohyashiki K, Kuroda M, Ohyashiki JH. Leukemia cell to endothelial cell communication via exosomal mirnas. Oncogene 2013;32:2747-55.
229. O'Brien K, Rani S, Corcoran C, Wallace R, Hughes L, Friel AM, et al. Exosomes from triple-negative breast cancer cells can transfer phenotypic traits representing their cells of origin to secondary cells. European Journal of Cancer 2013.
230. Hughes L, Malone C, Chumsri S, Burger AM, McDonnell S. Characterisation of breast cancer cell lines and establishment of a novel isogenic subclone to study migration, invasion and tumourigenicity. Clinical & experimental metastasis 2008;25:549-57.
231. Ben-David U, Siranosian B, Ha G, Tang H, Oren Y, Hinohara K, et al. Genetic and transcriptional evolution alters cancer cell line drug response. Nature 2018;560:325-30.
232. Loibl S, von Minckwitz G, Schneeweiss A, Paepke S, Lehmann A, Rezai M, et al. Pik3ca mutations are associated with lower rates of pathologic complete response

to anti-human epidermal growth factor receptor 2 (her2) therapy in primary her2-overexpressing breast cancer. Journal of clinical oncology : official journal of the American Society of Clinical Oncology 2014;32:3212-20.
233. Vagner T, Spinelli C, Minciacchi VR, Balaj L, Zandian M, Conley A, et al. Large extracellular vesicles carry most of the tumour DNA circulating in prostate cancer patient plasma. Journal of extracellular vesicles 2018;7:1505403.
234. Chamie K, Donin NM, Klopfer P, Bevan P, Fall B, Wilhelm O, et al. Adjuvant weekly girentuximab following nephrectomy for high-risk renal cell carcinoma: The ariser randomized clinical trial. JAMA oncology 2017;3:913-20.
235. Pastorek J, Pastorekova S. Hypoxia-induced carbonic anhydrase ix as a target for cancer therapy: From biology to clinical use. Seminars in cancer biology 2015;31:52-64.
236. Vanchanagiri K, Emmerich D, Bruschke M, Bache M, Seifert F, Csuk R, et al. Synthesis and biological investigation of new carbonic anhydrase ix (caix) inhibitors. Chemico-biological interactions 2018;284:12-23.
237. van Kuijk SJ, Gieling RG, Niemans R, Lieuwes NG, Biemans R, Telfer BA, et al. The sulfamate small molecule caix inhibitor s4 modulates doxorubicin efficacy. PloS one 2016;11:e0161040.

APPENDIX I

APPENDIX I

A. Gene analysis: Sequenom

List of genes analysed in cells and EVs by Sequenom

	Gene	Associated AA change
1.	AKT1	E17K
2.	AKT1	E49K
3.	AKT1	G173R
4.	AKT1	K179M
5.	AKT2	E17K
6.	AKT2	G175R
7.	AKT3	E17K
8.	AKT3	G171R
9.	ALK	L560F
10.	ALK	A877S
11.	ALK	D1091N
12.	ALK	M1166R
13.	ALK	I1171N
14.	ALK	F1174C/S/L/L/I/V
15.	ALK	F1245C/L/V/I
16.	ALK	R1275Q/L
17.	APC	R1114X
18.	APC	E1306X
19.	APC	E1338X
20.	APC	Q1367X
21.	APC	E1379X
22.	APC	Q1429X
23.	APC	R1450X
24.	BRAF	R444Q
25.	BRAF	R462I
26.	BRAF	I463S
27.	BRAF	G464E/V/A/R

28.	BRAF	G466R/E/V/A
29.	BRAF	G469A/E/R/V
30.	BRAF	V471F
31.	BRAF	Y472S
32.	BRAF	E586K
33.	BRAF	D587A/E
34.	BRAF	I592M/V
35.	BRAF	D594E/V/G
36.	BRAF	F595L/L/L/S
37.	BRAF	G596R
38.	BRAF	L597R/R/Q/V
39.	BRAF	T599I
40.	BRAF	V600E/A/G/L/M
41.	BRAF	K601E/N/N
42.	BRAF	S605N
43.	BRAF	G615R
44.	CDK4	R24C/H
45.	CDKN1B	P117S
46.	CDKN2A	R58X
47.	CDKN2A	E61X
48.	CDKN2A	E69X
49.	CDKN2A	R80X
50.	CDKN2A	H83Y
51.	CDKN2A	E88X
52.	CTNNB1	A13T
53.	CTNNB1	A21T
54.	CTNNB1	V22A
55.	CTNNB1	D32A/G/V/H/N/Y
56.	CTNNB1	S33A/P/T
57.	CTNNB1	G34E/V/A/R/R
58.	CTNNB1	I35N/S/T
59.	CTNNB1	H36P/R/Y

60.	CTNNB1	S37A/P/T/C/F/Y
61.	CTNNB1	T41A/P/S/I/N/S
62.	CTNNB1	S45A/P/T/C/F/Y
63.	DDR2	R105S
64.	DDR2	N456S
65.	DDR2	T533K
66.	EGFR	V689M
67.	EGFR	N700D
68.	EGFR	E709A/V/G/K/Q
69.	EGFR	G719A/D/C/S/R
70.	EGFR	S720T/P
71.	EGFR	D761N/Y
72.	EGFR	V769L/M
73.	EGFR	T783A
74.	EGFR	A839T
75.	EGFR	K846R
76.	EGFR	L858M/R
77.	EGFR	L861Q/R
78.	EGFR	G863D
79.	EGFR	H870R
80.	EGFR	E884K
81.	ERBB2	S310F/Y
82.	ERBB2	L755S
83.	ERBB2	G776S/V
84.	ERBB2	D769H
85.	ERBB2	V777A/L/M
86.	ERBB2	V842I
87.	ERBB2	H878Y
88.	FBXO4	S8R
89.	FBXO4	S12L
90.	FBXO4	L23Q
91.	FBXO4	P76T

92.	FBXW7	R465C/H/L
93.	FBXW7	R479G/Q/L
94.	FBXW7	R505C/S/H/L/P
95.	FBXW7	S582L
96.	FGFR1	S125L
97.	FGFR1	P252T
98.	FGFR2	S252W
99.	FGFR2	Y375C
100.	FGFR2	N549K/K
101.	FGFR3	R248C
102.	FGFR3	S249C
103.	FGFR3	G370C
104.	FGFR3	S371C
105.	FGFR3	Y373C
106.	FGFR3	G380R
107.	FGFR3	A391E
108.	FGFR3	K650E/Q/M/T
109.	FGFR3	G697C
110.	GNA11	Q209L/P
111.	GNA11	R183C
112.	GNAS	R201H/S/C
113.	GNAS	Q227H/L/R
114.	GNAQ	Q209L/P/R
115.	HRAS	G12S/R/C/D/A/V
116.	HRAS	G13S/R/C
117.	HRAS	Q61H/H/Q/K/L/P/R
118.	HRAS	E62G
119.	IDH1	G70D
120.	IDH1	R132C/G/S/H/L
121.	IDH1	V178I
122.	IDH2	R172G/W/M/K/S
123.	KIT	M552L

124.	KIT	Y553N
125.	KIT	W557G/R/R
126.	KIT	K558N/R
127.	KIT	V559A/D/G/I
128.	KIT	V560D/A
129.	KIT	G565R
130.	KIT	N566D
131.	KIT	Y568D
132.	KIT	V569G
133.	KIT	P573L
134.	KIT	F584S
135.	KIT	L576P
136.	KIT	E561K
137.	KIT	K642E
138.	KIT	V654A
139.	KIT	T670I
140.	KIT	D716N
141.	KIT	D816E/H/N/Y/G/V/A
142.	KIT	D820E/E/H/Y/A/G/
143.	KIT	N822K/N/K/Y/H
144.	KIT	Y823D/N
145.	KRAS	G12D/A/V/S/R/C
146.	KRAS	G13D/A/V/S/R/C/
147.	KRAS	L19F/F
148.	KRAS	Q22K
149.	KRAS	T58I
150.	KRAS	A59T/G/E
151.	KRAS	G60D
152.	KRAS	Q61E/K/X/H/H/Q/L/P/R
153.	KRAS	A146P/T
154.	MAP2K1	F53C/S
155.	MAP2K1	Q56P

156.	MAP2K1	K57N
157.	MAP2K1	P124L/T/S
158.	MAP2K1	E203K/Q
159.	MAP2K2	E207K/Q
160.	MAP2K2	R388Q
161.	MAP3K13	P373S
162.	MAP3K13	S694L
163.	MAP3K13	R880C
164.	MAP3K13	A882S
165.	MET	E168D
166.	MET	N375S
167.	MET	R970C
168.	MET	T1010I
169.	MET	H1112R/L/Y
170.	MET	H1124D
171.	MET	M1131T
172.	MET	Y1248C/H/D
173.	MET	Y1253D
174.	MET	M1268T
175.	MLH1	V384D
176.	MYC	P57S
177.	MYC	T58A
178.	NCOR1	R108X
179.	NCOR1	Q313X
180.	NCOR1	E379X
181.	NCOR1	I1422S
182.	NCOR1	Q1792X
183.	NRAS	G12D/A/V/S/R/C
184.	NRAS	G13D/A/V/S/R/C
185.	NRAS	A18T
186.	NRAS	Q61E/K/X/H/H/Q/R/P/L
187.	PDGFRA	V561D

188.	PDGFRA	N659K/Y
189.	PDGFRA	D842Y/N/V
190.	PDGFRA	D846Y
191.	PDGFRA	Y849C
192.	PDGFRA	D1071N
193.	PHLPP2	L1016S
194.	PIK3CA	R38H
195.	PIK3CA	Q60K
196.	PIK3CA	R88Q
197.	PIK3CA	K111N
198.	PIK3CA	G118D
199.	PIK3CA	N345K
200.	PIK3CA	S405F
201.	PIK3CA	E418K
202.	PIK3CA	C420R
203.	PIK3CA	E453K
204.	PIK3CA	P539R
205.	PIK3CA	E542K/Q/V/G
206.	PIK3CA	E545D/K/Q/A/V/G
207.	PIK3CA	Q546H/E/K/L/P/R
208.	PIK3CA	C901F
209.	PIK3CA	F909L/L
210.	PIK3CA	M1004I
211.	PIK3CA	G1007R
212.	PIK3CA	Y1021C/H/N
213.	PIK3CA	R1023Q
214.	PIK3CA	T1025A/S/I/T
215.	PIK3CA	A1035T/V
216.	PIK3CA	M1043I/I/I/V
217.	PIK3CA	A1046V
218.	PIK3CA	H1047R/L/Y
219.	PIK3CA	G1049R

220.	PIK3CA	I1058F
221.	PIK3CA	H1065L
222.	PIK3R1	M326I
223.	PIK3R1	G376R
224.	PIK3R1	D560Y
225.	PIK3R1	N564D
226.	PTEN	R130L/P/Q/X
227.	PTEN	R173C/H
228.	PTEN	R233X
229.	PTEN	R335X
230.	PTPN11	A72D/V/T
231.	PTPN11	E69K
232.	PTPN11	E76A/G/V/Q/K
233.	RB1	E137X
234.	RB1	L199X
235.	RB1	R320X
236.	RB1	R358X
237.	RB1	R455X
238.	RB1	R552X
239.	RB1	R556X
240.	RB1	R579X
241.	RB1	C706F
242.	RB1	E748X
243.	RET	C634R/W/Y
244.	RET	A664D
245.	RET	E768D
246.	RET	M918T
247.	SMARCD	Q539X
248.	SMARCD	D391H
249.	SMARCD	Q504X
250.	SOS1	R248H
251.	SOS1	R688Q

252.	SOS1	H888Q
253.	SRC	Q531X
254.	STK11	Q37X
255.	STK11	Q170X
256.	STK11	D194N/Y/V
257.	STK11	G196V
258.	STK11	E199X/K
259.	STK11	P281L
260.	STK11	W332X
261.	STK11	F354L
262.	TBX3	Y163X
263.	TBX3	W197X
264.	TP53	V143A
265.	TP53	R175H/P/L
266.	TP53	C176F
267.	TP53	I195S
268.	TP53	R196X
269.	TP53	R213X/L
270.	TP53	Y220C/S/H/N
271.	TP53	Y234H/N/D/C
272.	TP53	M237I
273.	TP53	G245D/A/S/C/R
274.	TP53	R248Q/P/L/W/G
275.	TP53	R273C/H/P/L/S
276.	TP53	D281G/H/Y
277.	TP53	R282W
278.	TP53	R306X
279.	VHL	P81S
280.	VHL	L85P
281.	VHL	L89H
282.	VHL	L158Q/V
283.	VHL	R161X

284.	VHL	R167W

B. Olink Proseek multiplex loading manual

Load primers to the left and samples to the right on the 96.96 Dynamic Array IFC.

1. Transfer 5 µL by using reverse pipetting from each well in the Primer Plate to the inlets on the left side of the chip in the same manner as described in steps 2-4 for *Sample Plate*.

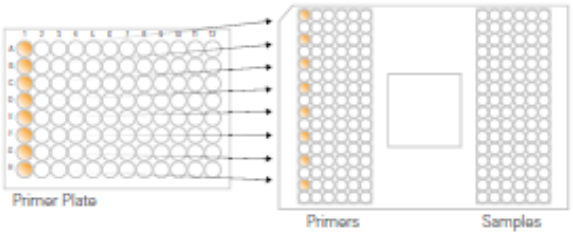

2. Use reverse pipetting. Transfer 5 µL from each well in position 1 A-H (marked in green) to inlets in the first column on the right side of the chip (green). When using an eight-channel pipette every other inlet will be filled according to the image.

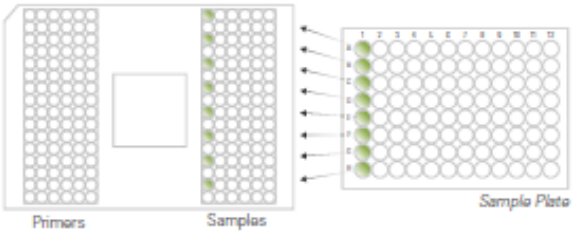

3. Transfer 5 µL from each well in position 2 A-H (blue) to the second column of inlets (blue) according to image. Continue with columns 3-6.

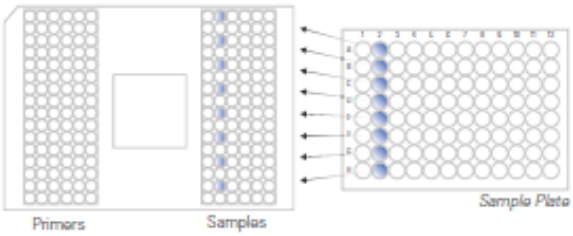

4. Transfer 5 µL from each well in position 7 A-H (red) to inlets in the first column on the right side of the chip (red), start on the second row according to image. Continue with columns 8-12.

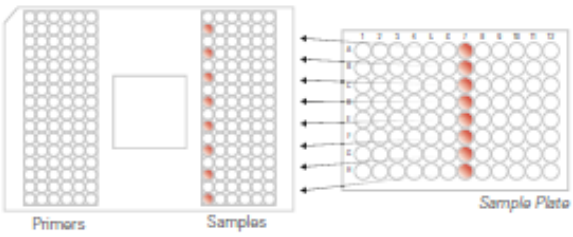

C. Biomarkers in Proseek Multiplex Inflammation

	Protein
1.	Adenosine Deaminase (ADA)
2.	Artemin (ARTN)
3.	Axin-1 (AXIN1)
4.	Beta-nerve growth factor (Beta-NGF)
5.	Brain-derived neurotrophic factor (BDNF)
6.	C-C motif chemokine 19 (CCL19)

7.	C-C motif chemokine 20 (CCL20)
8.	C-X-C motif chemokine 1 (CXCL1)
9.	C-X-C motif chemokine 10 (CXCL10)
10.	C-X-C motif chemokine 11 (CXCL11)
11.	C-X-C motif chemokine 5 (CXCL5)
12.	C-X-C motif chemokine 6 (CXCL6)
13.	C-X-C motif chemokine 9 (CXCL9)
14.	Caspase-8 (CASP-8)
15.	CD40L receptor (CD40)
16.	CUB domain-containing protein 1 (CDCP1)
17.	Cystatin D (CST5)
18.	Eotaxin-1 (CCL11)
19.	Eukaryotic translation initiation factor 4E-binding protein 1 (4E-BP1)
20.	Fibroblast growth factor 19 (FGF-19)
22.	Fibroblast growth factor 21 (FGF-21)
23.	Fibroblast growth factor 23 (FGF-23)
24.	Fibroblast growth factor 5 (FGF-5)
25.	Fms-related tyrosine kinase 3 ligand (Flt3L)
26.	Fractalkine (CX3CL1)
27.	Glial cell line-derived neurotrophic factor (GDNF)
28.	Hepatocyte growth factor (HGF)
29.	Interferon gamma (IFN-gamma)
30.	Interleukin-1 alpha (IL-1 alpha)
31.	Interleukin-10 (IL-10)
32.	Interleukin-10 receptor subunit alpha (IL-10RA)
33.	Interleukin-10 receptor subunit beta (IL-10RB)
34.	Interleukin-12 subunit beta (IL-12B)
35.	Interleukin-13 (IL-13)
36.	Interleukin-15 receptor subunit alpha (IL-15RA)
37.	Interleukin-17A (IL-17A)
38.	Interleukin-17C (IL-17C)
39.	Interleukin-18 (IL-18)

40.	Interleukin-18 receptor 1 (IL-18R1)
41.	Interleukin-2 (IL-2)
42.	Interleukin-2 receptor subunit beta (IL-2RB)
43.	Interleukin-20 (IL-20)
44.	Interleukin-20 receptor subunit alpha (IL-20RA)
45.	Interleukin-22 receptor subunit alpha-1 (IL-22 RA1)
46.	Interleukin-24 (IL-24)
47.	Interleukin-33 (IL-33)
48.	Interleukin-4 (IL-4)
49.	Interleukin-5 (IL-5)
50.	Interleukin-6 (IL-6)
51.	Interleukin-7 (IL-7)
52.	Interleukin-8 (IL-8)
53.	Latency-associated peptide transforming growth factor beta-1 (LTBP1)
54.	Leukemia inhibitory factor (LIF)
55.	Leukemia inhibitory factor receptor (LIF-R)
56.	Macrophage colony-stimulating factor 1 (CSF-1)
57.	Matrix metalloproteinase-1 (MMP-1)
58.	Matrix metalloproteinase-10 (MMP-10)
59.	Monocyte chemotactic protein 1 (MCP-1)
60.	Monocyte chemotactic protein 2 (MCP-2)
61.	Monocyte chemotactic protein 3 (MCP-3)
62.	Monocyte chemotactic protein 4 (MCP-4)
63.	Natural killer cell receptor 2B4 (CD244)
64.	Neurotrophin-3 (NT-3)
65.	Neurturin (NRTN)
66.	Oncostatin-M (OSM)
67.	Osteoprotegerin (OPG)
68.	Programmed cell death 1 ligand 1 (PD-L1)
69.	Protein S100-A12 (EN-RAGE)
70.	Delta and Notch-like epidermal growth factor-related receptor (Q8NFT8)
71.	Signaling lymphocytic activation molecule (SLAMF1)

72.	SIR2-like protein 2 (SIRT2)
73.	STAM-binding protein (STAMPB)
74.	Stem cell factor (SCF)
75.	Sulfotransferase 1A1 (ST1A1)
76.	T cell surface glycoprotein CD6 isoform (CD6)
77.	T-cell surface glycoprotein CD5 (CD5)
78.	Thymic stromal lymphopoietin (TSLP)
79.	TNF-beta (TNFB)
80.	TNF-related activation-induced cytokine (TRANCE)
81.	TNF-related apoptosis-inducing ligand (TRAIL)
82.	Transforming growth factor alpha (TGF-alpha)
83.	Tumour necrosis factor (Ligand) superfamily, member 12 ()
84.	Tumour necrosis factor (TNF)
85.	Tumour necrosis factor ligand superfamily member 14 (TNFSF14)
86.	Tumour necrosis factor receptor superfamily member 9 (TNFRSF9)
87.	Urokinase-type plasminogen activator (uPA)
88.	Vascular endothelial growth factor A (VEGF-A)

D. Biomarkers in Proseek Multiplex Oncology II

	Protein
1.	5'-nucleotidase (5'-NT)
2.	A disintegrin and metalloproteinase with thrombospondin motifs 15 (ADAM-TS 15)
3.	Alpha-taxilin (TXLNA)
4.	Amphiregulin (AR)
5.	Annexin A1 (ANXA1)
6.	C-type lectin domain family 4 member K (CD207)
7.	C-X-C motif chemokine 13 (CXCL13)
8.	Carbonic anhydrase IX (CAIX)
9.	Carboxypeptidase E (CPE)
10.	Carcinoembryonic antigen (CEA)

11.	Carcinoembryonic antigen-related cell adhesion molecule 1 (CEACAM1)
12.	Cathepsin L2 (CTSV)
13.	CD160 antigen (CD160)
14.	CD27 antigen (CD27)
15.	CD48 antigen (CD48)
16.	CD70 antigen (CD70)
17.	Cornulin (CRNN)
18.	Cyclin-dependent kinase inhibitor 1 (CDKN1A)
19.	Delta-like protein 1 (DLL1)
20.	Disintegrin and metalloproteinase domain-containing protein 8 (ADAM8)
22.	Endothelial cell-specific molecule 1 (ESM-1)
23.	Ephrin type-A receptor 2 (EPHA2)
24.	Fas antigen ligand (FasL)
25.	FAS-associated death domain protein (FADD)
26.	Fc receptor-like B (FCRLB)
27.	Fibroblast growth factor-binding protein 1 (FGF-BP1)
28.	Folate receptor alpha (FR-alpha)
29.	Folate receptor gamma (FR-gamma)
30.	Furin (FUR)
31.	Galectin-1 (Gal-1)
32.	Glypican-1 (GPC1)
33.	Granzyme B (GZMB)
34.	Granzyme H (GZMH)
35.	Hepatocyte growth factor (HGF)
36.	ICOS ligand (ICOSLG)
37.	Insulin-like growth factor 1 receptor (IGF1R)
38.	Integrin alpha-V (ITGAV)
39.	Integrin beta-5 (ITGB5)
40.	Interferon gamma receptor 1 (IFN-gamma-R1)
41.	Interleukin-6 (IL-6)
42.	Kallikrein-11 (hK11)

43.	Kallikrein-13 (KLK13)
44.	Kallikrein-14 (hK14)
45.	Kallikrein-8 (hK8)
46.	Ly6/PLAUR domain-containing protein 3 (LYPD3)
47.	Melanoma-derived growth regulatory protein (MIA)
48.	Mesothelin (MSLN)
49.	Methionine aminopeptidase 2 (MetAP 2)
50.	MHC class I polypeptide-related sequence A/B (MIC-A/B)
51.	Midkine (MK)
52.	Mothers against decapentaplegic homolog 5 (MAD homolog 5)
53.	Mucin-16 (MUC-16)
54.	Nectin-4 (PVRL4)
55.	Pancreatic prohormone (PPY)
56.	Podocalyxin (PODXL)
57.	Pro-epidermal growth factor (EGF)
58.	Protein CYR61 (CYR61)
59.	Protein S100-A11 (S100A11)
60.	Protein S100-A4 (S100A4)
61.	Proto-oncogene tyrosine-protein kinase receptor Ret (RET)
62.	R-spondin-3 (RSPO3)
63.	Receptor tyrosine-protein kinase erbB-2 (ErbB2/HER2)
64.	Receptor tyrosine-protein kinase erbB-3 (ErbB3/HER3)
65.	Receptor tyrosine-protein kinase erbB-4 (ErbB4/HER4)
66.	Secretory carrier-associated membrane protein 3 (SCAMP3)
67.	Seizure 6-like protein (SEZ6L)
68.	SPARC (SPARC)
69.	Stem cell factor (SCF)
70.	Syndecan-1 (SYND1)
71.	T-cell leukemia / lymphoma protein 1A (TCL1A)
72.	T-lymphocyte surface antigen Ly-9 (LY9)
73.	TGF-beta receptor type-2 (TGFR-2)
74.	Tissue factor pathway inhibitor 2 (TFPI-2)

75.	TNF-related apoptosis-inducing ligand (TRAIL)
76.	Toll-like receptor 3 (TLR3)
77.	Transforming growth factor alpha (TGF-alpha)
78.	Transmembrane glycoprotein NMB (GPNMB)
79.	Tumour necrosis factor ligand superfamily member 13 (TNFSF13)
80.	Tumour necrosis factor receptor superfamily member 19 (TNFRSF19)
81.	Tumour necrosis factor receptor superfamily member 4 (TNFRSF4)
82.	Tumour necrosis factor receptor superfamily member 6B (TNFRSF6B)
83.	Tyrosine-protein kinase ABL1 (ABL1)
84.	Tyrosine-protein kinase Lyn (LYN)
85.	Vascular endothelial growth factor A (VEGF-A)
86.	Vascular endothelial growth factor receptor 2 (VEGFR-2)
87.	Vascular endothelial growth factor receptor 3 (VEGFR-3)
88.	VEGF-co regulated chemokine 1 (CXL17)
89.	Vimentin (VIM)
90.	WAP four-disulfide core domain protein 2 (WFDC2)
91.	Wnt inhibitory factor 1 (WIF-1)
92.	WNT1-inducible-signaling pathway protein 1 (WISP-1)
93.	Xaa-Pro aminopeptidase 2 (XPNPEP2)

E. Chapter five appendix: The relevance of CAIX as a predictive biomarker in HER2+ breast cancer patients

i. Quantification of total protein in patient plasma specimens

To ensure that protein levels were not indicative of response prior to CAIX determination, total plasma protein levels were assessed. There was no significant difference in protein level when comparing post-treatment plasma specimens (32.44±0.5µg/mL) to pre-treatment specimens (32.28±0.3µg/mL) (Figure E.1) (*p-value*=0.4393), All outliers that were present in the data are shown in graphs (white data points) but are removed from statistical analysis.

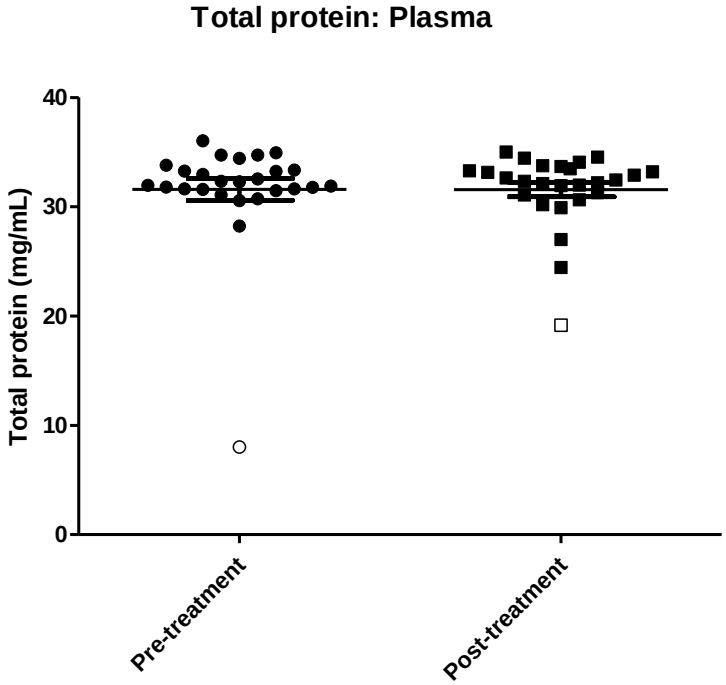

Figure E.1: Total protein per mL of plasma: pre-treatment and post-treatment
Total plasma protein levels assessed in pre-treatment specimens and post-treatment specimens. No significant differences were observed (Student's t-test). Outlier values (white data point) as determined by Grubbs test were included in the figure but excluded from statistical analysis.

ii. EV quantification (plasma specimens)

When investigating EV quantities per treatment arm, there were no significant differences between pre- (31.53±11.8µg/mL) and post-treatment specimens for TCH (30.19±6.2µg/mL) (Figure E.2 (A.)), TCL (pre-treatment 38.16±5.9µg/mL and post-

treatment 24.44±11.3µg/mL) (Figure E.2 (B.)) or TCHL (pre-treatment 23±9.1µg/mL and post-treatment 10.51±6.9µg/mL) (Figure E.2 (C.). EV quantities were compared between treatment arms for pre-treatment (TCH 31.53±11.8µg/mL, TCL 53.67±5.9µg/mL, TCHL 23±9.1µg/mL) (Figure E.3 (A.)) and post-treatment (TCH 30.19±6.2µg/mL, TCL 24.44±11.3µg/mL, TCHL 10.51±6.9µg/mL) (Figure E.3 (B.)). There were no significant differences in EV quantities for treatment arms.

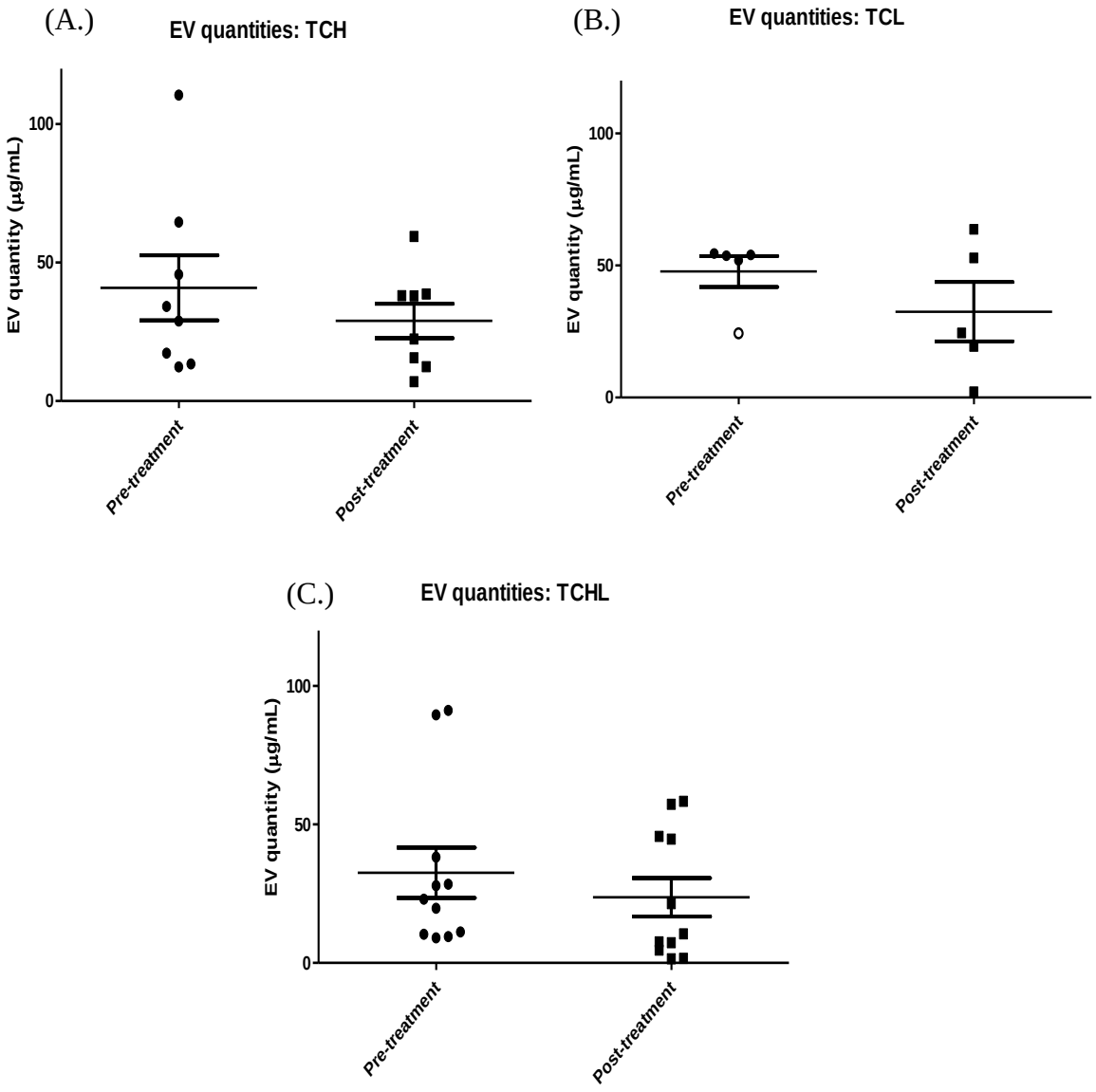

Figure E.2: EV quantities (treatment arms)
The quantity of EVs was evaluated by treatment arm. There were no significant differences in EV quantities between pre- and post-treatment specimens for the TCH arm (A.), TCL arm (B.) and the TCHL arm (C.). Outlier value (white data point) as determined by Grubbs test was included in the figure but excluded from statistical analysis (Student's t-test).

(A.)

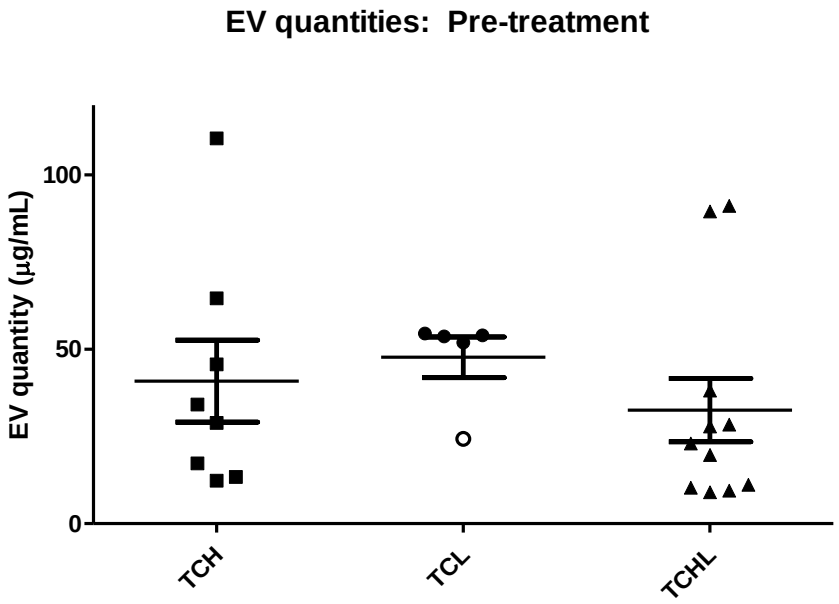

(B.)

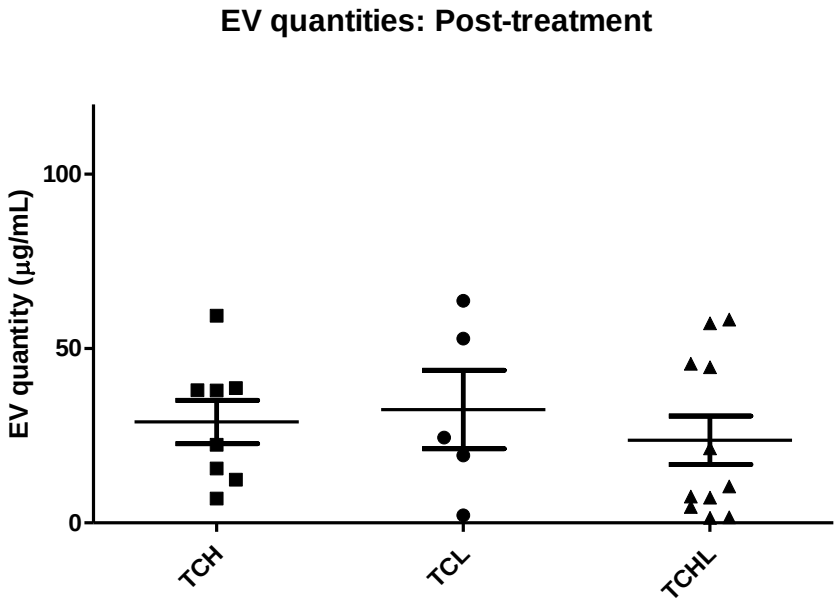

Figure E.3: EV quantities in treatment arms (pre-treatment and post-treatment)
The quantity of EVs in each treatment arm for pre- and post-treatment specimens was determined. There were no significant differences in EV quantities between treatment arms in pre-treatment specimens (A.) or post-treatment specimens (B.). Outlier value (white data point) as determined by Grubbs test was included in the figure but excluded from statistical analysis (*ANOVA*).

iii. Quantification of CAIX: Plasma specimen EV surface

CAIX quantity was unchanged when comparing treatment responses for pre-treatment EV samples (Figure E.4 (A.)) and post-treatment EV samples (Figure E.4 (B.)). When stratifying by treatment response, there were no significant differences in CAIX between pre- and post-treatment samples for CR, PR or NoR (Figure E.5 (A.), (B.) and (C.)). CAIX

quantities were determined in all pre- and post-treatment samples per treatment arm (TCH, TCL and TCHL), no significant differences were observed (Figure E.6 (A.), (B.) and (C.)). When quantifying CAIX levels in EV suspension for each treatment arm for pre-treatment (Figure E.7 (A.)) and post-treatment (Figure E.7 (B.)), there were no significant differences between the arms.

(A.) (B.)

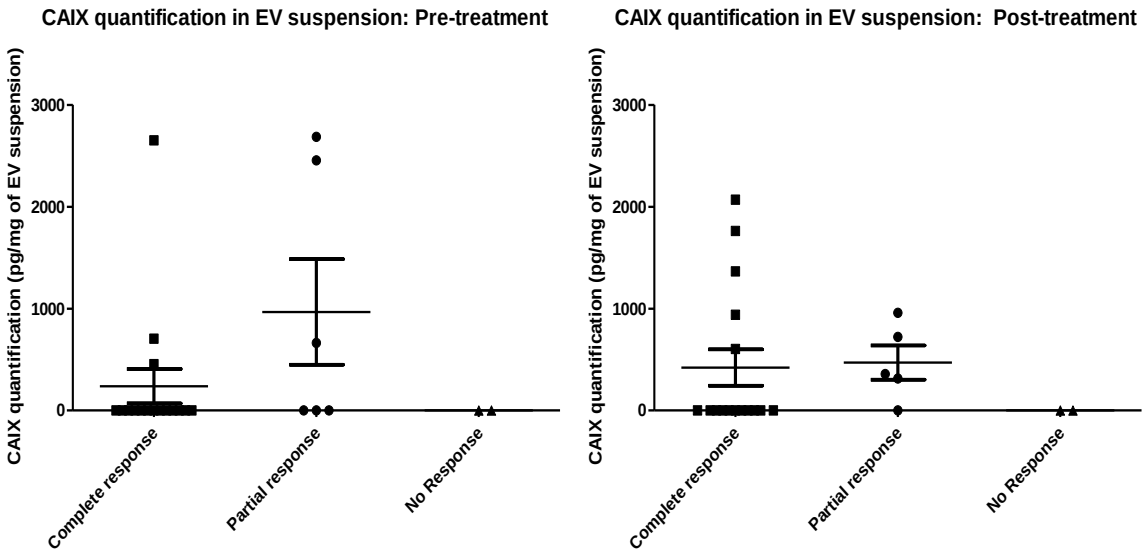

Figure E.4: CAIX quantification: EV suspension pre-treatment and post-treatment (treatment response)

CAIX quantification in EV suspension for all treatment responses for pre-treatment samples (A.) and post-treatment samples (B.). There were no significant differences. Statistical analysis could not be performed for non-responder samples (n=2). (*ANOVA*).

(A.) (B.)

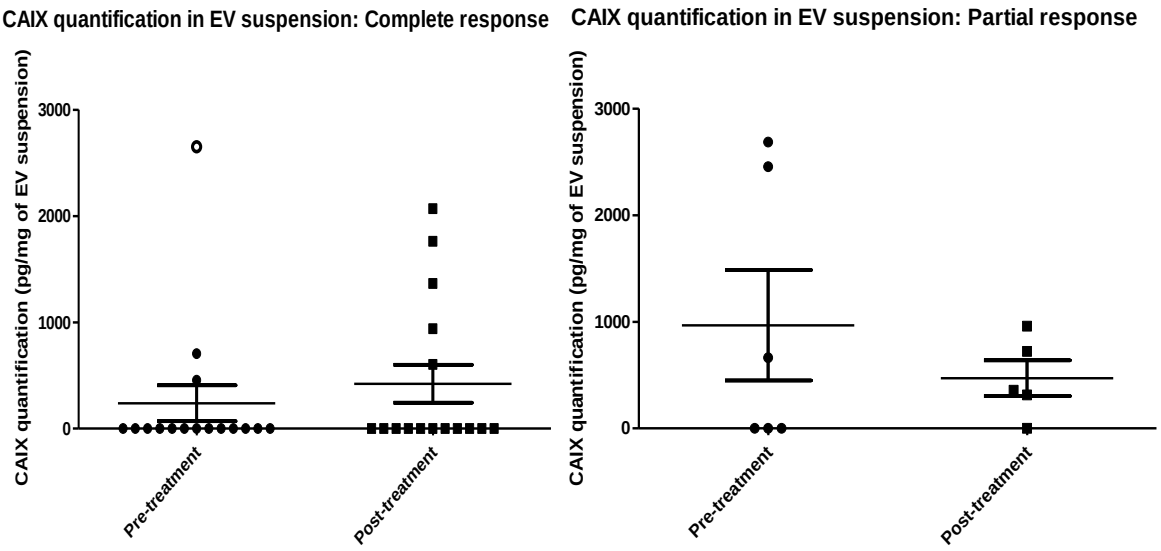

(C.)

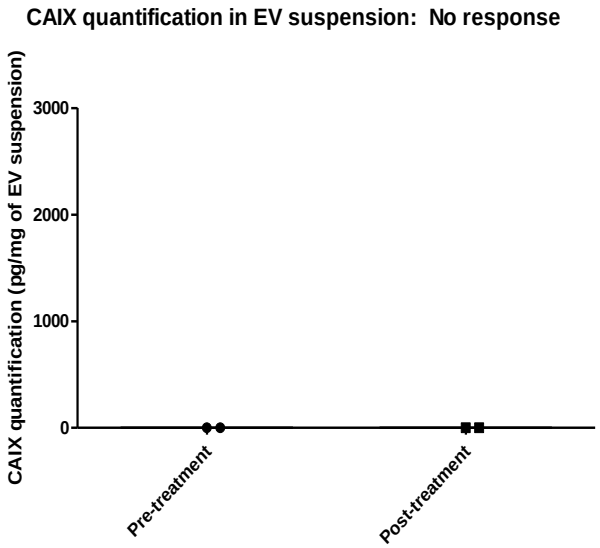

Figure E.5: CAIX quantification: EV suspension (treatment response)
CAIX quantification in EV suspension for all pre- and post-treatment samples for complete response (A.), partial response (B.) and no response (C.). There were no significant differences. Statistical analysis could not be performed for non-responder samples (n=2). Outlier value (white data point) as determined by Grubbs test was included in the figure but excluded from statistical analysis. (Student's t-test).

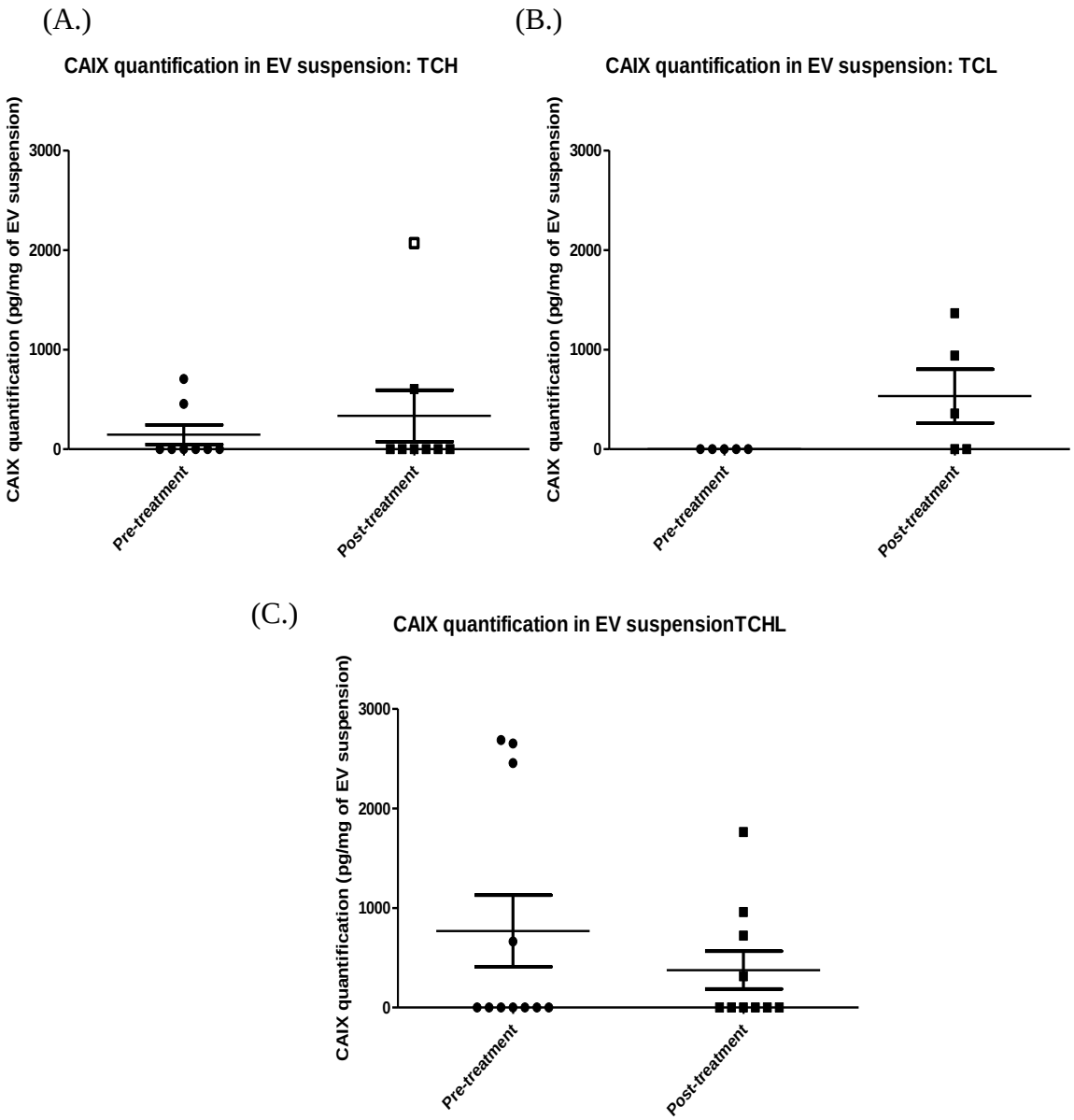

Figure E.6: CAIX quantification: EV suspension (treatment arms)
CAIX quantification in EV suspension for all pre- and post-treatment samples, stratified by treatment arms; TCH (A.), TCL (B.) and TCHL (C.). There were no significant differences. Outlier value (white data point) as determined by Grubbs test was included in the figure but excluded from statistical analysis. (Student's t-test).

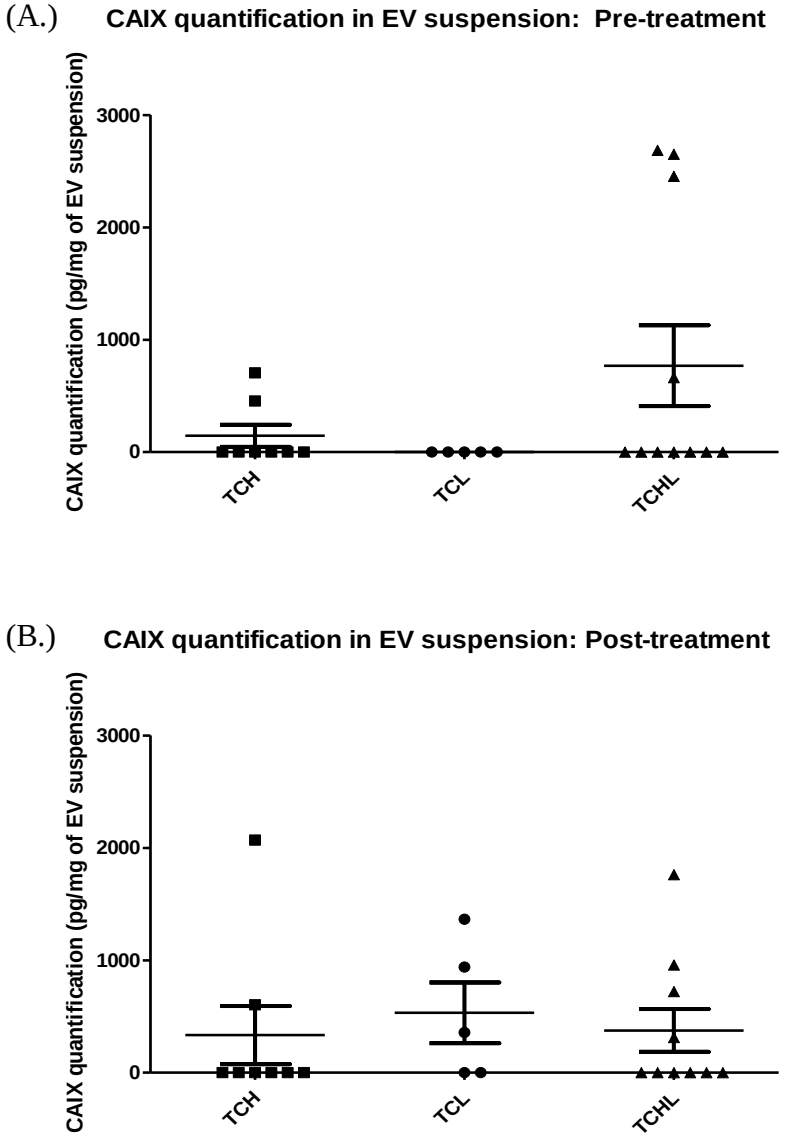

Figure E.7: CAIX quantification EV suspension treatment arms (pre-treatment and post-treatment)
CAIX quantification in EV suspension for treatment arms in pre-treatment samples (A.) and post-treatment samples (B.). There were no significant differences. (*ANOVA*).

iv. Associated discussion

Total protein quantification was analysed in all plasma specimens. There were no significant differences in protein quantity between pre- and post-treatment specimens, between treatment responses (CR, PR and NoR) or between the treatment arms (TCH, TCL and TCHL). This ensured that protein quantity was not indicative of response to therapies and was not altered between pre- and post-treatment samples. Thus, CAIX protein levels were analysed using ELISA and normalised to total protein content in all plasma specimens.

APPENDIX II: Research Outputs

APPENDIX II

Publications, achievements and presentations

A. Publications

Research Articles:

- Breslin S*, **Lowry MC***, O'Driscoll L. Neratinib-resistance and cross-resistance to other HER2-targeted drugs due to increased activity of metabolism enzyme cytochrome P4503A4. British Journal of Cancer. 2017 Feb 28; 116(5):620-625.
- O'Brien K*, **Lowry MC***, Corcoran C, Martinez VG, Daly M, Rani S, Gallagher WM, Radomski MW, MacLeod RA, O'Driscoll L. miR-134 in extracellular vesicles reduces triple-negative breast cancer aggression and increases drug sensitivity. Oncotarget. 2015 Oct 20; 6(32):32774-89.

* These authors contributed equally to this work.

Reviews:

- **Lowry MC**, O'Driscoll L. Can hi-jacking hypoxia inhibit extracellular vesicles in cancer? Review. Drug Discovery Today. 2018 Jun 23 (6):1267-1273.
- **Lowry MC**, Gallagher WM, O'Driscoll L. The role of Exosomes in Breast Cancer. Review. Clinical Chemistry. 2015 Dec; 61(12):1457-65.

Published abstracts:

- **Lowry MC**, Breslin S, O'Driscoll L. Investigating the roles of macrophage colony-stimulating factor (CSF1) and carbonic anhydrase 9 (CAIX) in neratinib-resistant HER2+ breast cancer cell lines and extracellular vesicles. ISEV 2018 abstract book. Journal of Extraceullular Vesicles. Published April 2018. Page 23. DOI: 10.1080/20013078.2018.1461450.
- **Lowry MC**, Breslin S, Toomey S, Hennessy BT, O'Driscoll L. Insights into the mechanisms of neratinib-resistance: investigating a possible role for extracellular vesicles in HER2-overexpressing breast cancer. ISEV 2017 abstract book. Journal

of Extraceullular Vesicles. Published April 2018. Page 163. DOI: 10.1080/20013078.2017.1310414.

- Conlon NT, **Lowry MC**, Breslin S, O'Driscoll L, Eustace AJ, Crown J, O'Donovan N, Colins DM. Src inhibition overcomes neratinib-resistance in HER2-positive breast cancer. AACR 2018 abstract book .Experimental and Molecular Therapeutics. Abstract 1834. Published July 2018. DOI: 10.1158/1538-7445.AM2018-1834.

Manuscripts in press:

- **Lowry MC** contributing author. Minimal Information for Studies of Extracellular Vesicles 2018 (MISEV2018): a position statement of the International Society for Extracellular Vesicles and update of the MISEV2014 guidelines. Journal of Extracellular Vesicles. (*In press).*

Manuscripts in preparation

- CAIX plays a role in the mechanism of neratinib-resistance in HER2+ breast cancer.

  Michelle C. Lowry, Susan Breslin, Neil T. Conlon, Denis M. Collins, Crown J, Alex J. Eustace, Lorraine O'Driscoll.

- Mechanically stimulated Osteocytes regulate Human Skeletal Stem Cell Recruitment and Differentiation via Extracellular Vesicle Communication
  Kian F. Eichholz, Ian Woods, Nian Shen, Gillian P. Johnson, Michele Corrigan, Marie-Noelle Labour, Kieran Wynne, **Michelle C. Lowry**, Lorraine O'Driscoll, David A. Hoey.

B. Awards and other

- Awarded the Irish Cancer Society Researcher of the year 2017. Awarded gold medal.

- Awarded an ISEV 2017 Junior Member Scholarship (registration waiver of €629.86).

- Awarded a Trinity Trust Travel grant (€1042) to travel to ISEV 2017 in Toronto, Canada.
- Awarded a ME-HaD travel grant (€900) to attend Extracellular vesicle training, Siena, Italy (Jan 2015).

C. Outreach work

- Media request. Promoting the Pink Ribbon Walk launch on a radio interview for Clare FM. October 2017.
- Oral lay presentation. Pink Ribbon Walk Launch, Killaloe, Co. Clare. To drug or not to drug? What treatments works best for breast cancer patients? October 2017.
- Oral lay presentation to staff of the Irish Cancer Society. Drug resistance: How some breast cancer cells can change to survive treatments. October 2017.

D. International and national conference presentations

Oral presentations:

- **Lowry MC**, Breslin S, Conlon NT, Collins D, Eustace A, Crown J, Maher S, O'Sullivan J, O'Driscoll L. Investigating the role of CAIX in the mechanisms of HER2-targeted drug resistance in breast cancer cells and extracellular vesicles. Breast-Predict showcase, UCD, Dublin. 17th October 2018.
- **Lowry MC**, Breslin S, O'Driscoll L. Investigating the roles of CSF-1 and CAIX in neratinib-resistant HER2+ breast cancer cell lines and extracellular vesicles International Society for Extracellular Vesicles (ISEV) Conference 2018, Barcelona, Spain (2nd-6th May 2018). Oral with poster presentation.
- **Lowry MC**, Breslin S, Toomey S, Hennessy BT, O'Driscoll. Investigating the mechanisms of neratinib-resistance in HER2-overexpressing breast cancer. Irish Association of Pharmacologist Annual Conference 2016, Royal College of Surgeons, Dublin 2. (30th November 2017).
- **Lowry MC**, Breslin S, Toomey S, Hennessy BT, O'Driscoll L. Insights into the mechanisms of neratinib-resistance: investigating a possible role for extracellular vesicles in HER2-overexpressing breast cancer. International Society for

Extracellular Vesicles (ISEV) Conference 2017, Toronto, Canada (17th-22nd May 2017).

- **Lowry MC**, O'Brien K, Corcoran C, Martinez VG, Daly M, Rani S, Gallagher WM, Radomski MW, MacLeod RAF, O'Driscoll L. miR-134 in Breast Cancer-derived Extracellular Vesicles. Irish Association of Pharmacologist Annual Conference 2016, Royal College of Surgeons, Dublin 2 (30th November 2016).
- **MC Lowry**, K O'Brien, C Corcoran, VG Martinez, M Daly, S Rani, WM Gallagher, MW Radomski, RAF MacLeod, L O'Driscoll. Extracellular vesicle studies identify the potential diagnostic relevance of miR-134 both as a biomarker for triple negative breast cancer and as a potential therapeutic option. Cancer conference, Trinity Biomedical Sciences Institute (18th October 2016).
- Shortlisted for TCD Thesis-in-3 competition. Presentation at TCD Probe 2016 (30th September 2016).
- **MC Lowry**, K O'Brien, C Corcoran, VG Martinez, M Daly, S Rani, WM Gallagher, MW Radomski, RAF MacLeod, L O'Driscoll. miR-134 in extracellular vesicles reduces TNBC aggression and increases drug sensitivity. BREAST-PREDICT Midway Point Research Showcase, University College Dublin, Dublin 4 (31st March 2016).

Poster presentations:

- **Lowry MC**, Breslin S, Toomey S, Hennessy BT, O'Driscoll L. Investigation of mechanisms of neratinib-resistance in HER2-overexpressing Breast Cancer. Irish Association for Cancer Research (IACR) conference, Kilkenny (22-24th February 2017).
- **MC Lowry**, K O'Brien, C Corcoran, VG Martinez, M Daly, S Rani, WM Gallagher, MW Radomski, RAF MacLeod, L O'Driscoll. miR-134 in breast cancer-derived extracellular vesicles: potential biomarker and therapeutic option. Faculty of Health Sciences Research Day, Trinity Biomedical Sciences Institute (September 15th 2016).
- **MC Lowry**, K O'Brien, C Corcoran, VG Martinez, M Daly, S Rani, WM Gallagher, MW Radomski, RAF MacLeod, L O'Driscoll. Extracellular vesicle studies identify miR-134 as a potential biomarker and novel therapeutic target for

breast cancer. Irish Association for Cancer Research (IACR) conference, Limerick (24-26th February 2016). Poster Shortlisted for prize (unable to attend conference).

- **MC Lowry**, K O'Brien, C Corcoran, VG Martinez, M Daly, S Rani, WM Gallagher, MW Radomski, RAF MacLeod, L O'Driscoll. miR-134 in extracellular vesicles reduces TNBC aggression and increases drug sensitivity. The 2nd UK extracellular vesicle forum, Cardiff, Wales (15th December 2015).